UNIVERSITÀ POLITECNICA DELLE MARCHE

Facoltà di Medicina e Chirurgia

Corso di Dottorato in Salute dell'Uomo

Cytosolic nucleic acids as new markers of senescence and hyperglycemia-induced inflammation

Dottoranda:

Deborah Ramini

Docente Tutor:

Prof.ssa Fabiola Olivieri

XXXIII ciclo

Triennio 2017/2020

SUMMARY

Aging is characterized by a gradual functional decline resulting from a complex interaction between genetic, epigenetic, stochastic factors and the rate of aging is recognized as the most important risk factor for the development of the most common age-related diseases (ARDs). Research on aging process is currently focused on understanding the molecular mechanisms underlying age-related features accompanying on one hand, the onset of ARDs and on the other hand, the chances to reach a successful aging. A chronic, systemic, low-grade, age-related pro-inflammatory status, called "Inflammaging" is correlated with ARDs development. The two main culprits of inflammaging are the repeated stimulation of immune system over time and the increased burden of senescent cells. Senescent cells are able to modify the microenvironment acquiring a senescence-associated secretory phenotype (SASP). In patients affected by ADRs, the rate of aging process in increased, as well as the burden of senescent cells with SASP.

In this scenario, a better understanding of the molecular mechanisms that promote cellular senescence is of basic and clinical relevance. A number of mechanisms promoting senescence have been well characterized. Increasing evidence suggest that nuclear DNA fragility and a sub-functional DNA damage response (DDR) is associated with an increase release of nucleic acids in cytoplasm, including RNA:DNA hybrids. However, only few studies have tempted to assess the pro- or anti-inflammatory effects of this misplaced nucleic acid pool in different cellular models.

In this framework, we have analysed the cytoplasmic pool of misplaced nucleic acids in a model of human endothelial cells (HUVECs), in two prototypical stress conditions related to inflammaging, such as "replicative cell senescence" and "hyperglycemic condition".

A significant increased amount of misplaced nucleic acids was observed in the cytoplasm of senescent cells compared to the younger ones, and in young cells cultured for 1-week in hyperglycemic condition compared to young cells cultured in normoglycemic medium. The cytosolic pool of misplaced nucleic acids is composed of dsDNA, including micronuclei, bubbles and telomere sequences, dsRNA and hybrids. A reduced expression of RNaseH2, the enzyme involved in the degradation of RNA moiety of RNA:DNA hybrids was observed in senescent cells compared to the younger ones and in young cells treated with hyperglycemic medium. The amounts of mis-incorporated ribonucleotides, biomarkers of genome instability, were inversely related to RNaseH2 expression level, suggesting that both "senescence" and "hyperglycemic condition" are associated with increased genomic instability.

Since the presence of nucleic acids in cytoplasm can activate a number of cytosolic receptors inducing the antiviral response, characterized by increased release of IFN-1, we analysed cGAS/STING/IRF3 axis and IFN-1 expression in "senescence" and "hyperglycemic condition". Surprisingly, a strong reduction of cGAS expression was observed in senescent cells in normo and hyperglycemic conditions, in association with the absence of IFN-1 modulation, whereas the expression of proinflammatory cytokines, such as IL-1beta, IL-6 and IL-8 was significantly increased. Overall, our results suggest an imbalance between antiviral and proinflammatory response in senescent cells and in young cells under hyperglycemic conditions.

Increasing evidence suggest that senescent cells have an enhanced susceptibility to viral infections. We hypothesized that such imbalance between antiviral and proinflammatory responses could be, almost in part, a direct consequence of their ability "to tolerate" a high cytosolic nucleic acids load.

Overall, our results pave the way to explain why old subjects, especially the elderly patients affected by diabetes, are more susceptible to adverse outcomes of infectious diseases.

1 INTRODUCTION

1.1 Aging process

Despite a standardized definition of "aging" has still to be achieved, there is a clear awareness on the pathophysiological role of increasing age in modulating human organ and system functions and on its role as the major risk factor for the development of the common ARDs. Aging is therefore a complex and dynamic phenotype, resulting from the continuous interaction between genetic make-up and environmental factors. As a consequence, the spectrum of possible aging phenotypes varies from successful aging (*e.g.* centenary and over 100-year-old subjects) to un-successful aging, characterized by disabilities and increased risk of develop diseases and to die.

Not only in animals but also in humans, syndromes related to premature aging can be induced by specific genetic mutations or by the accumulation of cellular and molecular modifications resulting from the exposure to a plethora of both endogenous and exogenous damages. Extensive efforts were devoted to identifying the main hallmarks of aging, that should have the following characteristics:

1. should occur during normal aging;
2. the experimental induction of these mechanisms should accelerate the rate of the aging process;
3. the attenuation of these mechanisms should delay the physiological senescence process and thus slow down the rate of aging.

Based on the above mentioned criteria, nine key mechanisms have been yet identified and characterized, such as: genomic instability, telomere attrition, epigenetic alterations, loss of proteostasis, deregulated nutrient-sensing, mitochondrial dysfunction, cellular senescence, stem cell exhaustion, and altered intercellular communication (López-Otín et al., 2013).

Among them, “cellular senescence” was extensively investigated in the contexts of aging process and ARDs development, but the molecular mechanisms underpinning this cellular condition were not completely clarified.

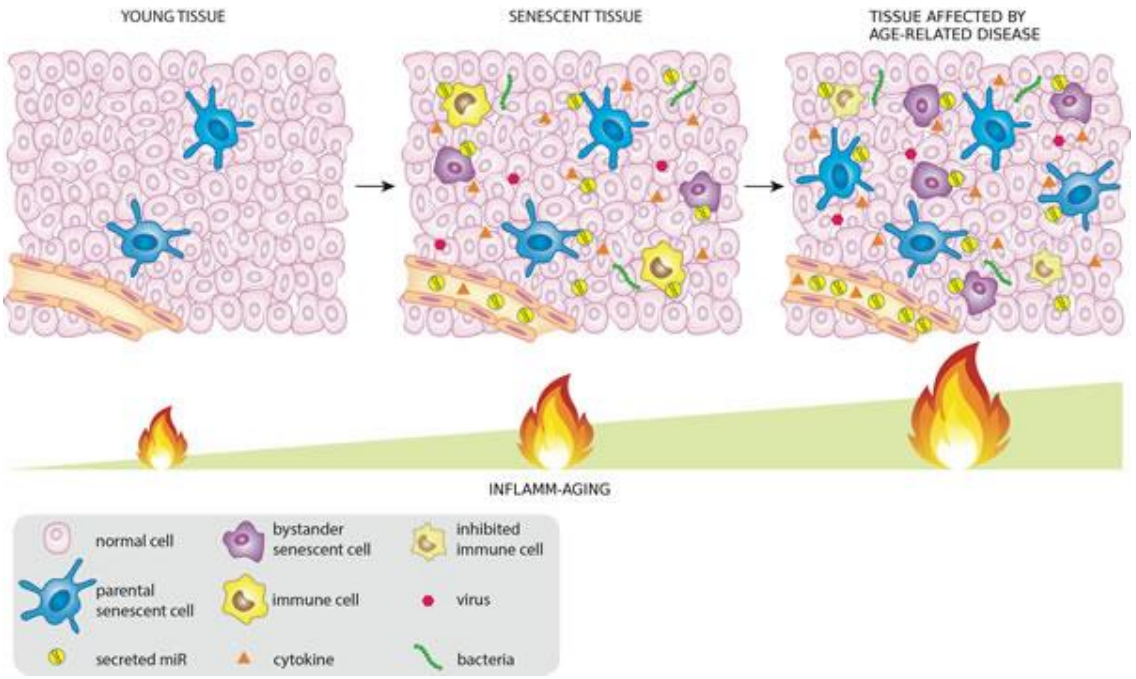

Figure 1. Senescent cells accumulation in age and age-related disease *(Olivieri F. et al., 2015).*

1.2 Cellular senescence

The definition of "cellular senescence" dates to 1965 when it was demonstrated that normal cells have a limited replicative capacity (Hayflick; in 1965). Extensive studies on this issue suggested that this phenomenon could explain, almost in part, human aging at the cellular level. The numerous studies aimed at characterizing senescent phenotype (Suram A. et al., 2012; Chen J.H. et al., 2004; Courtois-Cox S. et al., Braig M. et al., 2005; Haigis K.M. and Sweet-Cordero A., 2011) showed that cellular senescence was basically characterized by the progressive loss of replicative capacity, as a result of two fundamental processes, such as:

1. repeated cellular divisions (replicative cellular senescence)
2. exposure to potentially dangerous/stressogenous stimuli (stress-induced cellular senescence)

The acquisition of senescent phenotype was well studied *in vitro*, whereas *in vivo* it is more complex to quantify the number of senescent cells and to identify the roles played by senescent cells.

Even if senescent cells are characterized by a stable arrest of the cell cycle, they show stereotyped phenotypic changes and an increased metabolic activity (Campisi J. and d'Adda di Fagagna F., 2007; Collado et al., 2007; Kuilman et al., 2010). Senescent cells increase the expression and release of numerous pro-inflammatory factors, including growth factors, proteases, cytokines and chemokines, which have potent autocrine and paracrine activities (Coppé et al., 2010), thus acquiring a phenotype known as senescence associated secretory phenotype (SASP). SASP can modify the microenvironment, since the intracellular signals induced by the response to DNA damage (DDR) in senescent cells, converge on the activation of nuclear factor NF-kB, which in turn activates the transcription program for a numerous pro-inflammatory cytokines, such as IL-1, IL-6, TNF-alpha, chemokines, metalloproteases and others nuclear factors, i.e. CCA AT/enhancer–binding protein beta (C/EPBβ) (Passos J.F. et al., 2010; Kuiman T. et al., 2010; Kuiman T. et al., 2008; Acosta J.C. et al., 2010).

NF-kB pathway is the key signalling in the activation of innate immune responses. Innate immunity is the first line of defense against a plethora of non-self and modified-self antigens. Innate immunity is activated by a limited set of receptors, defined as pattern recognition receptors (PRRs), that sense molecular patterns associated to pathogens, also known as pathogen-associated molecular patterns (PAMPs) and damage-associated molecular patterns (DAMPs) (Janeway C.A. and Medzhitov R., 2002).

Probably the release of pro-inflammatory signals by senescent cells have the function of activate immune cells involved in the clearance of senescent cells (Campisi J. and d'Adda di Fagagna F., 2007; Xue W. et al., 2007; Krizhanovsky V. et al., 2008). However, the accumulation of senescent cells during aging, observed in the tissues of animal models and in humans,

suggests that with aging the immune system's ability to eliminate senescent cells is reduced, a phenomenon named as “immunosenescence” (Franceschi et al., 2000; Shaw et al., 2010; Hall B.M. et al., 2016).

The relationship between aging and cell senescence is reinforced by the evidence that some hallmarks of aging are also involved in the induction of cellular senescence (McHugh and Gil, 2018). Telomeres shortening, genomic instability, DNA damages epigenetic modifications, alterations in protein metabolism, mitochondrial dysfunction, increased levels of ROS (reactive oxygen species), lysosomal dysfunctions, among others can be considered as features of aging and cellular senescence (Collin G. et al., 2018).

The increased activity of lysosomal SA–β-galactosidase (β-gal) (Dimri et al., 1995), which partly reflects the expansion of the lysosomal compartment, giving rise to an increase in β-gal activity that can be measured at suboptimal pH 6 (Kurz et al., 2000), is the well characterized biomarker of cellular senescence. In addition, distinctive enlarged flat morphology was also identified as senescence feature (Campisi J. et al., 2011; Rodier F. and Campisi J., 2011; De Cecco M. et al., 2011). In addition, senescent cells reorganize chromatin, with a substantial increase in hetero-chromatin, associated with extensive changes in gene expression and accumulation of SA heterochromatic foci (SAHF) (Salminen et al., 2012). These foci contain activated DDR proteins, including phospho-ATM and phosphorylated ATM/ataxia telangiectasia and Rad3 related (ATR) substrates (d’Adda di Fagagna et al., 2003). This leads to the local phosphorylation of multiple ATM substrates in the chromatin surrounding the DNA lesion, usually including a variant of histone H2AX, γH2AX.

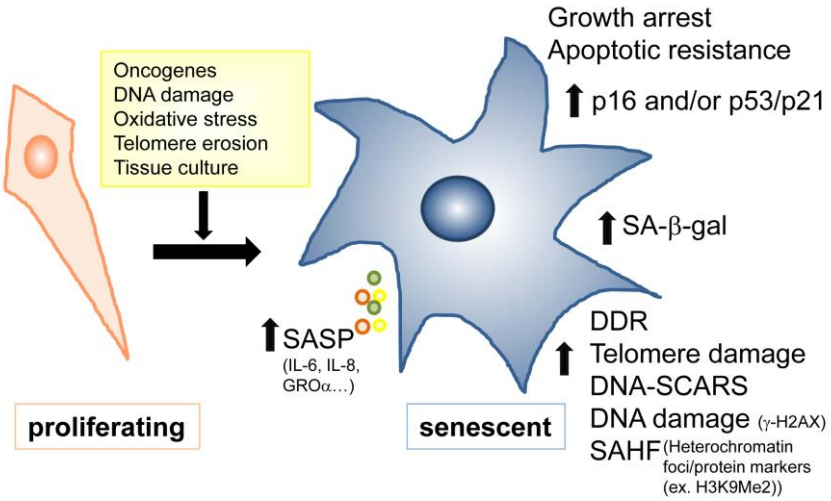

Figure 2. Cellular senescence characterization

Recent evidences suggest that also an increase cytoplasmic DNA can be correlated with cellular senescence (Franceschi C. and Campisi J., 2014). In fact, the accumulation of cytoplasmic DNA could play a role in promoting SASP, thus contributing to propagate aging signals locally and systemically (Bonafè M. et al., 2012). Nevertheless, cytoplasmic DNA accumulates even in the absence of senescence, for example in cells that are not yet in the replication phase, reinforcing the hypothesis that it is a more generalized phenomenon (Paulsen T. et al. 2018).

The physiological role of cytoplasmatic sensors for nucleic acid is to detect viral DNA and/or RNA and activate the antiviral response, characterized by increased release of interferon (IFN) type 1. Very low constitutive levels of IFN1 are produced in the absence of infections (Lienenklaus S. et al., 2009). This implies that, in order to prevent the accumulation of cytoplasmic DNA and maintain its levels below a certain threshold value, an efficient clearance of misplaced DNA is needed (Dempsey A. and Bowie A.G., 2015). The best characterized mechanism of cytoplasmic DNA degradation is based on the combined activity of DNase2 and TREX1, enzymes that degrade cytoplasmic DNA both single-stranded and double-stranded with a 3' excess. A recent study showed that in senescent cells the reduced levels of expression of DNase2/TREX1 would result in an accumulation of cytoplasmic DNA molecules capable of

activating DNA sensors, such as cGAS and STING, thus leading to the activation of antiviral response (Takahashi A. et al., 2018).

The presence of misplaced nucleic acid pool in cytoplasm has been proven in several cells from accelerated aging syndromes i.e. Ataxia Telangiectasia (Härtlova A. et al., 2015), Werner syndrome (Marabitti V. et al., 2019) and Amyotrophic Lateral Sclerosis (ALS; Giannini M. et al., 2020).

Different mechanisms could be involved in the accumulation of misplaced nucleic acids during physiological and pathological aging. Nuclear DNA, through mechanisms not yet well delineated, could be released into the cytosol, acting as DAMPS, thus activating DNA sensing receptors such as cGAS/STING pathway (Loo T.M. et al., 2020; Glück S. et al., 2017; Yang H. et al., 2017).

Recently, it has been shown that cGAS/STING axis is also activated by RNA:DNA hybrid (Mankan A.K. et al., 2014), an R-loop/triple helix structures in which the nascent RNA strand is complexed into the DNA duplex as soon as it is generated by the RNA polymerase (Aguilera A. and García-Muse T., 2012; Costantino L. and Koshland D., 2018; Crossley M.P. et al., 2019).

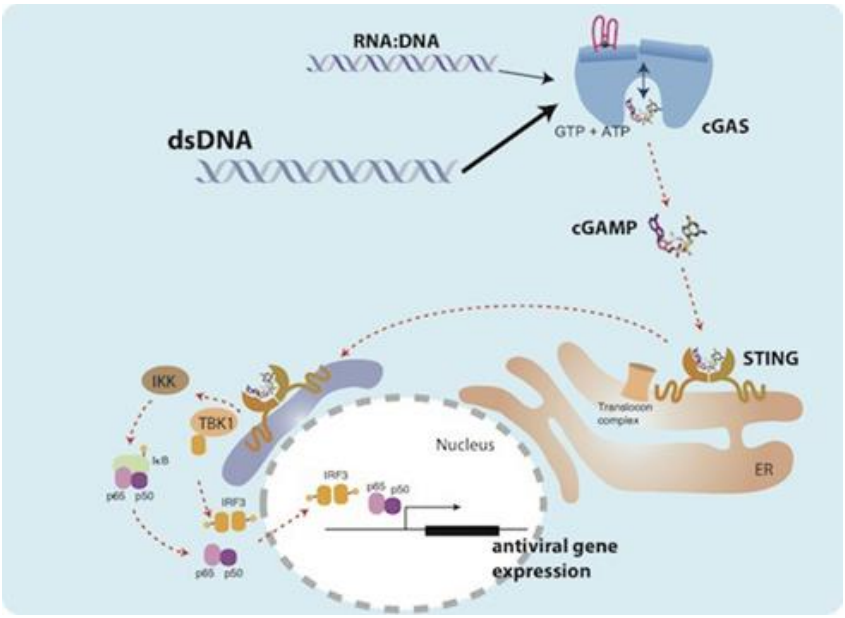

Figure 3. RNA:DNA hybrids activates cGAS/STING pathway *(Mankan Arun K. et al., 2014).*

Cytoplasmic DNA could be modified, as the result a variety of oxidative stress-related mechanisms such as inflammation (Radak Z. and Boldogh I., 2010). A substantial amount of cytoplasmic DNA with modified guanosine can derive from mitochondrial DNA (mtDNA), released as a result of mitochondrial dysfunction. MtDNA is considered a marker of cellular senescence, reinforcing the notion that mitochondrial alterations constitute the greatest source of oxidative stress within cells (Shimada K. et al., 2012). Oxidized DNA, enriched in 8-oxoguanine instead of guanine, has also been shown to be resistant to degradation by DNase2/TREX1.

Further data on the biochemical characteristics of cytoplasmic DNA are provided by studies on pathologies in which the IFN pathway is constitutively activated, demonstrating the crucial role of RNase H2 in the control of innate immunity (Crow Y.J. et al., 2015). RNase H2 degrades the RNA component in RNA:DNA hybrids and allows the TREX/DNase2 complex to degrade the remaining single-stranded DNA molecule. Instead, RNA:DNA hybrids are resistant to DNase activity, thus emerging as resistant and powerful cytoplasmic activation of the immune response (Shen Y.J et al., 2015: Koo C.X. et al., 2015).

Regarding the origin of cytoplasmatic hybrids, a number of hypothesis were suggested. RNA:DNA hybrids can result from the loss of genomic regions where one RNA molecule and complementary single-strand DNA forms a stable triple helix called R-loop in which the other strand of DNA is displaced (Santos-Pereira J.M. and Aguilera A., 2015). They can also derive from mtDNA released by dysfunctional or stressed mitochondria or from telomere sequences (Pohjoismaki J.L. et al., 2010).

However, the study of hybrid sequences is a recent issue, due to the technical challenges. Increasing studies are currently ongoing due to the recent commercialization of the antibody hybridoma S9.6 antibody, capable of recognize the specific structure of RNA:DNA hybrids (Zhang et al., 2015). The S9.6 antibody recognizes RNA:DNA hybrids with a subnanomolar

affinity, making it a broadly used tool to detect and study RNA:DNA hybrids. However, S9.6 also binds double-stranded RNA *in vitro* with significant affinity.

This discovery gave the opportunity to study and identify hybrid sequences in the cell cytoplasm and evaluate their possible contribution to a number of mechanisms including cell senescence and development and progression of all diseases associated with aging.

1.3 Cellular senescence and hyperglycemic damage

1.3.1 Endothelial cellular senescence

All cell types can acquire a senescent phenotype characterized by SASP, contributing to the increase inflammatory condition and loss of all tissues and organs functionality.

Endothelial cells represent a cell type with wide diffusion in all tissues. There are approximately 2–10 trillion ($2–10 \times 10^{12}$) endothelial cells in the human body and they form the endothelial surface of 500 m^2 of blood vessels. Endothelial senescence, associated with endothelial dysfunction represents to date, one of the main risk factors for the development of the most common ARDs (Olivieri F. et al., 2015).

Endothelial dysfunction is a pathological state of the endothelium and can be defined as an aberration of the normal endothelial function of vascular relaxation, blood clotting and immune function. In general, impaired endothelium-dependent vasodilation can result from the imbalance between vasodilating and vasoconstricting substances produced by or acting on the endothelium.

1.3.2 Endothelial senescence induced by hyperglycemic condition

Glucose is a major source of energy in our body, and a number of homeostatic mechanisms are activated to maintain stable the glucose levels in blood. However, the increase of glycemia over a specific threshold, condition clinically defined as diabetes, even if in absence of evident clinical effects on the short term, can cause serious long-term complications. Endothelial cells absorb

glucose from the blood through the insulin-independent glucose transporter 1 (GLUT1). Therefore, the endothelial cells are particularly sensible to variation of glycemic conditions, especially to hyperglycemic injury. Hyperglycemia is associated with the activation of various ROS-producing pathways and increased oxidant production was described in endothelial cells (Giacco F. and Brownlee M., 2010; Quijano C. et al., 2007). Oxidants play a significant role in the destruction of nitric oxide and other signaling molecules and result in impaired vasoreactivity (De Vriese A.S. et al., 2000; Coppey L. J. et al., 2001; Haj-Yehia A. I. et al., 1999). Hyperglycemia induced an increased amount of ROS, thus stimulating the production of inflammatory cytokines, which characterizes the early stages of the injury, activating endothelial function (Ceriello A. and Testa R., 2009). Oxidative stress also induces DNA damage and triggers endothelial cell senescence that have an impact on vascular function in the later stages of the injury (Maeda M. et al., 2015). In fact, it has been shown that in age-related pathologies such as diabetes and cardiovascular disease (CVD), a slowdown in the turnover of stem cells together with cellular senescence characterizes later hyperglycemic damage stages (Loomans C.J.M. et al., 2004; Rogers S.C. et al., 2013).

Hyperglycemia has different effects on different cell types. Mesangial cells in the kidney, neurons and Schwann cells in peripheral nerves have hyperglycemia-dipendent dysfunction but only a subset of endothelial cells, microvascular and arterial endothelial cells show impairment (Brownlee M., 2005). Differences in the pressure, blood flow or vessel function, protein and RNA expression patterns, including the non-coding RNA, *i.e.* miRNA, expression profiles, and the different responses of microvascular and macrovascular endothelial cells to various metabolic stimuli may be attributed to this difference (McCall M.N. et al., 2011). Another difference could be due to the inability of endothelial cells and mesangial cells to decrease the transport rate during glucose uptake (Heilig C.W. et al., 1995, Kaiser N. et al., 1993).

1.3.3 Mitochondrial dysfunction in hyperglycemic condition

Glucose overload causes an increase in mitochondrial membrane potential due to increased production of reactive oxygen species (ROS). Endothelial cells can express uncoupling protein 2 (UCP2) that create proton leak across the inner mitochondrial membrane, uncoupling oxidative phosphorylation from ATP synthesis and decreasing the amount of ATP generated in the mitochondria. As result it dissipates energy in the form of heat and protect against mitochondrial hyperpolarization. These transport channels are regulated by oxidative stress: high levels of oxygen species open the channels on the contrary low levels result in its closure (Mailloux R.J. and Harper M.E., 2011; Mailloux R.J. and Harper M.E., 2012). While in venous endothelial cells the efficiency of this regulation mechanism has been demonstrated, in the microvascular endothelial cells the expression of UCP2 does not appear to increase in response to mitochondrial hyperpolarization caused by increased glucose concentration (Gerö D.s and Szabo C., 2016).

In *vitro* experiments have shown that the damage induced by hyperglycemia is not immediate, in fact it takes days to induce a significant increase in the mitochondrial membrane potential and oxidant production (Gerö D.s and Szabo C., 2016; Davidson S.M. and Yellon D.M. 2006). Concentrations including 20–30 mmol/L can damage cells after several weeks or within a few months (Engerman R. et al., 1977). It has also been shown that hyper/hypo-blood glucose conditions reduce the replication capacity of endothelial cells and after several replication steps can also induce senescence (Rogers S.C. et al., 2013). On the contrary, patients with type 2 diabetes develop vascular complications even after years from confirmed diagnosis (American Diabetes Association, 2019) although retinopathy and nephropathy were often present (in 10–37% of patients) at the time of clinical diagnosis or within the first year after diagnosis (Cheng A.Y.Y. and Leiter L.A., 2010).

Glucose-induced endothelial damage is not only caused by constantly high glucose concentration but also by transiently elevated glucose levels. In experimental models, damage induced by intermittent high glucose is comparable or more severe than the injury induced by constantly high glucose concentration. Glycemic swings caused at least as severe tissue damage as constant hyperglycemia and persistence of high-glucose memory was postulated in cells and animals that were exposed to normoglycemic conditions following hyperglycemic exposure (Horváth E.M. et al., 2009; Ihnat M.A. et al., 2007a; Ihnat M.A. et al., 2007b). Thus, the endothelial cell continues to produce ROS because their pathways are kept active even after the restoration of normoglycemic conditions. In fact, even when endothelial cells return to basal glucose concentrations, they continue to produce ROS and activate poly (ADP-ribose) polymerase (PARP; Ihnat M.A. et al., 2007b). Thus, led to the thought that endothelial cells should have glucose memory. To date we do not know what its duration is, but the implication of inflammatory pathways and the persistence of the response to damage not limited to the life cycle of a single cell but also to generations of subsequent cells, suggests a lasting nature.

Oxidative stress is the key feature of the changes induced by hyperglycemia, and "metabolic memory" is another term referring to these characteristic metabolic changes (Ihnat M.A. et al., 2007a).

1.3.4 Hyperglycemic perturbation of endothelial cells metabolism

Endothelial cells use glucose as a source for ATP production through glycolysis. Glycolytic flux exceeds the rate of oxidative phosphorylation (OXPHOS) by two orders of magnitude in endothelial cells in vitro and similar ratio is suspected in vivo (Krützfeldt A. et al., 1990; Harjes U. et al., 2012). Thus, excess glucose is not converted to glycogen for storage in endothelial cells but is pushed toward glycolysis (Noyman I. et al., 2002). The combined action between hyperglycemia and increased ROS production also produces the inhibit endothelial nitric-oxide (NO) synthase (eNOS) activity, which leads to vascular dysfunction (Cosentino F. et al., 1997).

The activity of the enzyme is strictly regulated by the amount of ROS present in the cell, determined by both the rate of formation and the detoxify ability of the cell. If superoxide anions accumulate in the cell, an imbalance between NO and O_2^- may occur and inactivation of NO by O_2^- may contribute to vascular dysfunction as reduction of available NO leads to impaired endothelium-dependent relaxation (McVeigh G.E. et al., 1992).

Glutamine is another energy source for endothelial cell. Through glutaminolysis, GTP is produced and later converted to ATP. Further five ATP molecules from NADH+ and FADH2 are synthetized via oxidative phosphorylation OXPHOS. Glutamine is the most abundant amino acid in the plasma and represents an energy resource for the endothelial cell if glycolytic output is low. In addition, each glutaminolysis strep occurs in the mitochondria via tricarboxylic acid (TCA) cycle or OXPHOS, this implies that mitochondrial impairment may affect the energy efficacy of glutaminolysis (Goveia J. et al., 2014). Perturbations in TCA cycle flux have been widely demonstrated in diabetic subjects, where it has been observed that the metabolic change associated with the hyperglycemic condition does not only affect carbohydrate and lipid metabolism but also the catabolism of proteins and amino acids (Sas K.M. et al., 2015).

The high glycolytic input and low OXPHOS capacity may gradually block the main metabolic steps and shunt the metabolism to alternative pathways such as methylglyoxal, hexosamine and polyol pathways.

Dihydroxyacetone phosphate (DHAP) is diverted to the methylglyoxal pathway and leads to protein kinase C (PKC) activation, and fructose-6-phosphate (F6P) increases the flux through the hexosamine pathway and excess glucose enters the polyol pathway when converted to sorbitol (Goveia J. et al., 2014; Brownlee M., 2001). Moreover, suppressed expression of the gluconeogenetic enzyme glucose-6-phosphate dehydrogenase (G6PDH) prevents shunting of glucose to the pentose phosphate pathway that further increases the glycolytic load (Leopold J.A. et al., 2003; Zhang Z. et al., 2012). All these alterations involve an overexpression of ROS and

the generation of advanced glycation end products (AGEs), the products of nonenzymatic glycation and oxidation of proteins and lipids that accumulate in diabetes. AGEs signal through the receptor of AGE (RAGE), a cell surface receptor that is also activated by HMGB1 (high-mobility group box 1) and S100 proteins (Ramasamy R. et al.,2011; Scavello F. et al., 2019) activates transcription factor NF-kB and controls several inflammatory genes, thus links hyperglycemia to inflammation.

Conditions of hyperglycemia in endothelial tissue implies a long-lasting suppression of two enzymes involved in the metabolic balance between glycolysis and OXPHOS, Sirtuin 1 (SIRT1) and MP-activated protein kinase (AMPK). Thus, it results in enhanced glycolysis, inhibition of gluconeogenesis and decreased mitochondrial biogenesis and OXPHOS, states that remain unchanged even after the restoration of the normoglycemic conditions (Zheng Z. et al., 2012; Houtkooper R.H. et al., 2012).

One further molecule that possibly takes part in the maintenance of oxidative stress in hyperglycemic endothelial cells is 66-kDa Src homology 2 domain-containing protein (p66SHC; Camici G.G. et al., 2007). p66SHC is a redox enzyme associated with heat shock protein (Hsp70) and is predominantly present in the mitochondria intermembrane space. Its depletion on diabetic animal models involves a diminution of oxidative stress while hyperglycemia induces its expression. Under these conditions, the molecule is phosphorylated, and this involves its translocation from the cytoplasm to the mitochondria, where the production of hydrogen peroxide (H_2O_2) increases and transferring electrons of the transport chain to molecular oxygen. The activity of p66SHC is also regulated by acetylation: it is a direct target of SIRT1 and diminished SIRT1 activity increases the acetylation and activity of p66SHC in hyperglycemia (Kumar S. et al., 2017).

Many studies have been carried out to understand exactly whether superoxide itself or the steps leading to its increased production result in oxidative damage, but the issue remains

controversial. To date, in fact, we do not know whether the high TCA flux and elevated glycolytic dysfunctional state in hyperglycemia a cause of mitochondrial ROS production or of dysfunctional OXPHOS a consequence are (Nishikawa T. et al., 2000). However, various pharmacological interventions aimed at reducing ROS production have yielded expected results, not all substances used to increase the flux through the electron transport chain to reduce the accumulation of glycolytic worked. All studies, however, agree in recognizing mitochondrial superoxide generated by the electron transport chain is responsible for the initiation of hyperglycemic endothelial damage (Brownlee M., 2005; Nishikawa T. et al., 2000).

1.3.5 Mitochondrial ROS generation

Ros production in the mitochondria can take place:

1. nonenzymatically via multiple respiratory complexes in the electron transport chain;
2. enzymatically via the mitochondrial xanthine oxidase (Murphy M.P., 2009; Turrens J.F., 2003; Rus D.A. et al., 2007).

The nonenzymatic production of superoxide occurs when a single electron is directly transferred to oxygen by prosthetic groups of the respiratory complexes or by reduced coenzymes that act as soluble electron carriers.

The leak of electrons during the various phases of transport chain and its oxygen binding is a potential source of di superoxide in hyperglycemia. The electron transport chain may produce superoxide by multiple mechanisms but electron leakage before Complex III is suspected to represent the main source of superoxide in hyperglycemic endothelial cells (Brownlee M., 2005; Nishikawa T. et al., 2000). Complexes I and III can produce large quantities of ROS under specific conditions. Complex I may produce superoxide by two mechanisms:

1. the reduced flavin mononucleotide (FMN) can transfer electrons to oxygen instead of CoQ when the NADH/NAD+ ratio is high

2. by reverse electron transfer (RET) from the CoQ binding site if there is high electron supply from Complex II and the electrons are forced back to Complex I instead of proceeding to Complex III (Murphy M.P., 2009; Treberg J.R. et al., 2012).

In complex III, ROS can be produced by semiquinone anionic state of CoQ (semiubiquinone) that directly reacting with oxygen instead of completing the Q-cycle (Murphy M.P., 2009; Bleier L. and Dröse S., 2013).

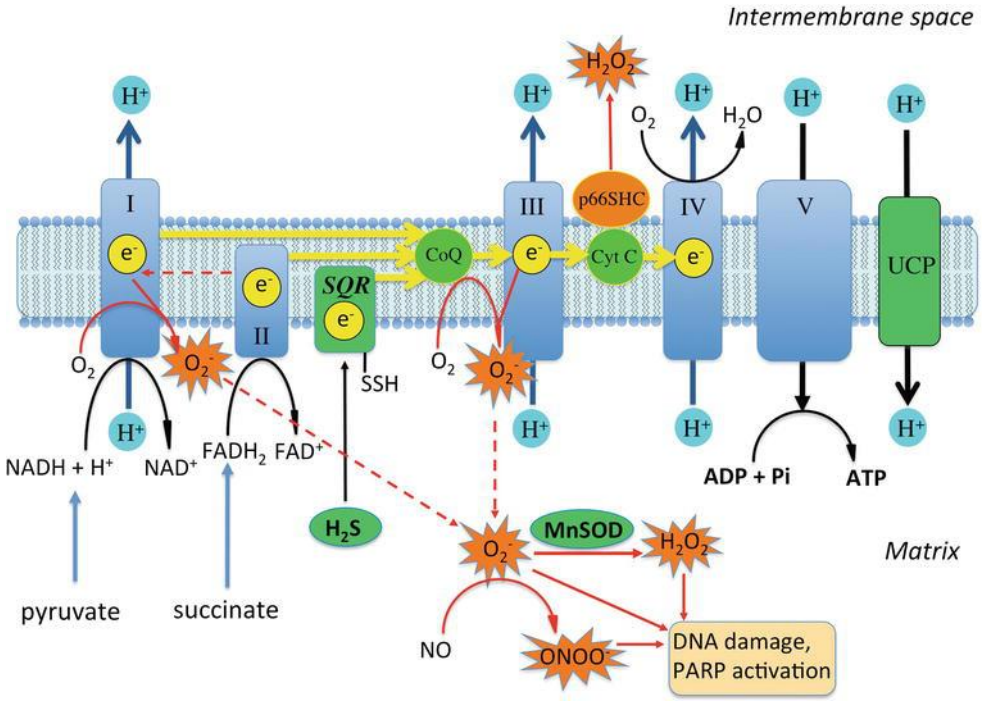

Figure 4. Oxidant production by the mitochondrial electron transport chain *(Gerö D., 2018).*
CoQ: coenzyme Q, ubiquinone; Cyt C: cytochrome C; FAD+/FADH2 : flavin adenine dinucleotide; H2 O2 : hydrogen peroxide; MnSOD: manganese-dependent superoxide dismutase; NO•: nitric oxide; O2 •−: superoxide, ONOO•−: peroxynitrite; PARP: poly(ADP-ribose) polymerase; p66SHC: 66-kDa Src homology 2 domain-containing protein; SQR: sulfide:quinone oxidoreductase and UCP: uncoupling protein.

Superoxide can be produced by enzymes interacting with NADH or CoQ respectively in the mitochondrial matrix and inner membrane. These include:

1. α-ketoglutarate dehydrogenase that may produce superoxide if its substrate (α-ketoglutarate) concentration and the NADH/NAD+ ratio increase in the matrix;
2. α-glycerophosphate dehydrogenase may produce superoxide partly via RET and Complex II, which transfer electrons from succinate to CoQ (Murphy M.P., 2009).

In endothelial cells cultured in hyperglycemic condition, superoxide has been shown to be increased by reduced CoQ pool, before it gives electrons to complex III (Brownlee M., 2001; Nishikawa T. et al., 2000). The high electron donor input from glycolysis and the TCA cycle may increase the membrane potential and inhibit the electron transfer at Complex III, thus increase the concentration of reduced and free radical intermediates of CoQ. The failure to transport electrons to molecular oxygen in fact involves a longer period of CoQ intermediates in the lipid double layer and their binding to Complex III or via RET through Complex I. Superoxide generation is also promoted by the increased and proton concentration gradient through the inner membrane (Korshunov S.S. et al., 1997; Gerö D. and Szabo C., 2016; Suzuki K. et al., 2011].

1.3.6 Cell damaging responses to ROS production in hyperglycemia

Hyperglycemia-induced mitochondrial superoxide production is a functional change of the respiratory chain and membrane potential. These changes are reversible: normalization of the membrane potential suppresses the ROS production in endothelial cells (Brownlee M., 2005; Gerö D. and Szabo C., 2016; Nishikawa T. et al., 2000; Suzuki K. et al., 2011; Gerö D. et al., 2016). Moreover, overexpression of either uncoupling protein 1 (UCP1) or uncoupling protein 2 (UCP2) normalizes the membrane potential and reduces the ROS production (Brownlee M., 2005; Gerö D. and Szabo C., 2016; Nishikawa T. et al., 2000) in hyperpolarized mitochondrial membranes.

The mitochondrial matrix also has antioxidant enzymes, superoxide dismutase 2 (SOD2) that converts superoxide to H_2O_2 which is subsequently converted to water by glutathione peroxidase and catalase. It represents the most important antioxidant protein in mitochondria. Overexpression of SOD2 prevents hyperglycemic injury in endothelial cells, confirming that the respiratory chain is the source of oxidants in hyperglycemia (Brownlee M., 2005; Nishikawa T. et al., 2000).

Hydrogen sulfide (H_2S), is an inorganic molecule that acts as an endogenous electron donor. It reduces the mitochondrial potential and promote ATP synthesis, but hyperglycemia reduces the mitochondrial H_2S pool and the plasma concentration of H_2S, (Suzuki K. et al., 2011; Jain S.K. et al., 2010; Suzuki K. Et al., 2017). The above-mentioned reactions represent the preliminary stage of the damage caused by hyperglycemia. These damage responses are accompanied by mitochondria morphological changes. Hyperglycemia stimulates the fission of mitochondria that can reduce the mitochondrial membrane potential but also helps dissociate the respiratory complexes and decrease the chance of assembly of various proteins within a complex (Wang W. et al., 2012; Yu Ti. Et al., 2011; Yu Ti. Et al., 2006; Makino A., et al., 2010; Shenouda S.M. et al., 2011). Mitochondrial ROS production results in DNA damage in the mitochondria that activates the mitochondrial DNA repair enzymes (Larsen N.B. et al., 2005). PARP1 adds ADP-ribose polymers (PARs) to the mitochondrial base excision repair (BER) enzymes, exo/endonuclease G (EXOG) and DNA polymerase gamma (Polγ) and activates the mitochondrial DNA repair (Szczesny B. et al., 2014). However, the activation of mitochondrial PARP1 is inversely proportional to nuclear one and may decrease the DNA repair and slow down the mitochondrial biogenesis.

Oxidative stress causes oxidative damage to nuclear DNA as well as its rupture and subsequent activation of nuclear PARP1 leading to ATP depletion and necrosis or apoptosis (Gerö D. and Szabó C., 2008).

There are further changes in the cellular metabolism that reduce the ATP output. High extracellular glucose immediately stimulates glucose uptake, but at the same time reduce the expression of GLUT1 resulting in diminished glucose uptake, and it may contribute to the low ATP output (Alpert E. et al., 2005; Cohen G. et al., 2007). The reduction of glyceraldehyde-3-phosphate dehydrogenase (GAPDH) activity and the promotion of anaerobic glucose metabolism is also a consequence of hyperglycemic stimulus in endothelial cells, finalized to

reduce the ATP generation in the cells and block the anaerobic compensation for the diminished mitochondrial activity. Finally, oxidative stress will induce DNA strand breaks in the mitochondria and promote mutations and senescence of endothelial cells. Accelerated aging of endothelial cells and the lack of endothelial progenitor cells decrease the functional endothelial cell pool in hyperglycemia (Jarajapu Y.P.R. and Grant M.B., 2010).

1.4 Misplaced nucleic acids in cellular senescence and hyperglycemic conditions

DNA damage has been postulated to be a major cause of cellular aging and cumulative damages may generate misplaced nucleic acids leading to persistent inflammation in senescent cells. Unrepaired or persistent double-stranded breaks (DSBs) can be found in senescent cells (Le et al., 2010) and aged human and animal tissues (Rube et al., 2011; Sedelnikova et al., 2004; Wang et al., 2009). The nuclei of senescent cells also undergo dramatic chromatin changes with increased fragments budding. Nucleic acids are a well-recognized class of molecules that can activate the innate immune response. For example, accumulation of mitochondrial and nuclear DNA in cytoplasm and/or extracellular space is a powerful stimulus for inflammaging (Storci G. et al. 2018). Proper DNA replication and repair are crucial aspects for maintaining genomic stability and to reduce inflammatory and antiviral responses. In fact, misplaced nucleic acids can activate the type 1 IFN pathway. Notably, the overactivation of this pathway contributes to the phenotype of the progeria in murine model causes cognitive decline (Yu Q. et al. 2015; Baruch K. Et al. 2014).

A wide variety of nucleic acids molecules can contribute to cytoplasmic pool, such as dsDNA, dsRNA and molecules that hybridize with complementary RNA, leading to the formation of RNA:DNA hybrids.

1.4.1 RNA:DNA hybrids (R-loop)

R-loops have been described for the first time in 1976 and they consist of a three stranded structure composed of a RNA:DNA hybrid and a ssDNA (Thomas M.et al.1976). These triple helix structures are mainly formed during transcription in areas rich in guanidine residues present in the RNA filament. According to this most accepted model (thread back model), the nascent RNA must thread back into the DNA duplex upstream from the complex (Deepankar R. and Lieber M.R., 2009). An alternative model proposes R-loop might form as a continuous extension from the short RNA-DNA duplex within the transcription complex, by conceding an elongation of the RNA:DNA hybrid (Belotserkovskii B.P. et al., 2018). However, this co-transcriptional model for R-loop formation does not explain why hybrids are elevated in mutants that affect RNA post-transcriptionally, like RNA export and degradation (Costantino L. and Koshland D., 2015). A post-transcription formation of RNA:DNA is one of the hypothesized explanations in which RNA increases its stasis in the nucleus and then hybridize homologous DNA even after transcription is completed. Indeed, the formation of R-loop *in trans* involves RNA transcription in a locus other than the one where hybridization with complementary DNA takes place (Wahba L. et al., 2013).

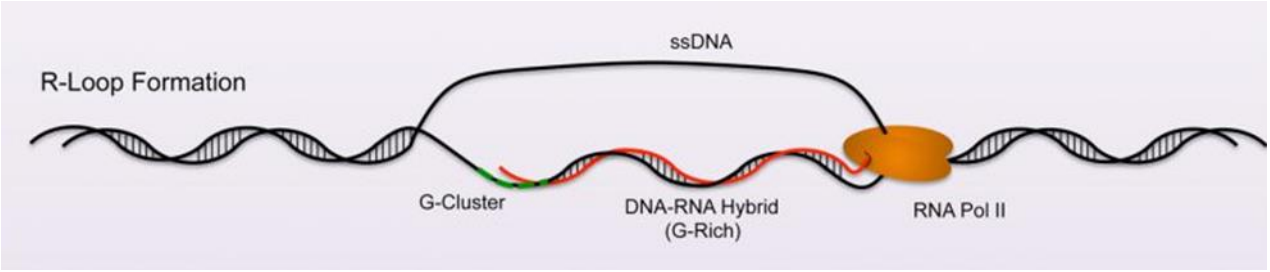

Figure 5. R-loop structure *(Allison D.F. and Wang G.G., 2019).*

There are also conditions that can favour hybrids formation. The presence of negative supercoiling, as well as the presence of distortions in the non-template DNA filament slows down the passage of trailing fork of the transcription bubble, increasing the possibility of

annealing between neo-synthetized RNA and DNA (Allison D.F. and Wang G.G., 2019). Once they are formed, R-loops are very stable since RNA:DNA interactions are stronger than those between DNA:DNA (Roberts R.W. and Crothers D.M., 1992).

Hybrids make up 5% of the human genome and are involved in many physiological processes such as transcription and DNA replication where RNA primers, synthesized by DNA polymerase α, are used by DNA polymerase δ to polymerize mature Okazaki fragment (Strzyz P., 2016). Hybrids are present at the switch (S) region during immunoglobulin class switching recombination and at DNA damage/repair sites (García-Muse T. and Aguilera A., 2019). Moreover, these structures are fundamental for mitochondrial DNA replication (Xu B. and Clayton D.A., 2017) and are also binding sites for telomerase, during the telomere elongation process (Graff M. et al. 2017). There are hybrids that are not R-loop considerate because they don't have a misplaced DNA strand. They are constituted by incorporation of ribonucleotides monophosphates (rNMPs) into genomic DNA during DNA replication and represent the site for nonhomologous end-joining (NHEJ) and homology recombination (HR) repair systems (Cerritelli S.M. and Crouch R.J., 2016).

R-loops also have a different role in regulating transcription (Santos-Pereira J.M. and Aguilera A., 2015). It has been shown that the co-transcriptional formation of R loop in downstream CpG island promoter regions promote gene expression by the inhibition of DNA methyltransferases (Ginno P.A. et al., 2012) and they also can facilitate the binding of transcription factors to regulatory elements on DNA (Boque-Sastre R., 2015).

R-loop are also associated to epigenetic modifications and chromatin remodeling. At promoter regions, R-loops associate with higher levels of histone marks characteristic of active transcription (H3K4me1, H3K4me3, H3 acetylation) and transcription elongation (H3K36me3; Sanz Lionel A., et al., 2016; Chédin F., 2016). It has been showed that R loops are tightly linked

to histone H3 S10 phosphorylation (H3S10P), a mark of chromatin condensation (Castellano-Pozo M. et al., 2013; García-Pichardo D. et al., 2017).

They can also activate the protective histone H3K4 or demethylation complexes (Chen P.B. et al., 2015; Chong S.Y. et al., 2020).

1.4.2 RNA:DNA hybrids threat genome stability

Although R-loops are important for many cellular processes, these nucleic acid species can also lead to genome instability and DNA damage. ssDNA is more exposed to the action of nucleases, genotoxics and transcription-associated mutagenesis (TAM) or transcription-associated recombination (TAR; Skourti-Stathaki K. and Proudfoot N.J., 2014). However, the mechanism leading from an R-loop to genomic instability remains largely unknown. One of the proposed mechanisms provides that the ssDNA may be subject to spontaneous deamination of dC to dU, leading to DSBs and recombination (Aguilera A., 2002; Li X. and Manley J.L., 2006; Aguilera A. and Garcia-Muse T., 2012). Another mechanism provides that this replacement will be carried out by activation-induced deaminase (AID) protein, that selectively binds R-loop causing DNA rapture. This mutation can be maintained in subsequent replication cycles or resolved by base excision repair (BER). The uracil removal creates a distortion or a site without nucleobases which may cause DSB or the pairing of any other nitrogen base, respectively (Su X.A. and Freudenreich C.H., 2017). Genetic stress and changes or mutations in gene expression of proteins involved in the regulation of R-loops could threat genome integrity due to their accumulation. The mechanism by which the accumulation of R-loops involves a blockage of the replication fork, due to RNA polymerase (RNAP) block causing it to stall, has been well characterized. The RNAP might pause or stall when encountering an RNA-DNA hybrid within an R-loop. This involves creating a synthesized DSB and formation of common fragile sites (CFS; Sanchez A. et al., 2020). In contrast to the collision-mediated mechanism, an R-loop "intrinsic" mechanism is also proposed. Studies *in vitro* suggest that transcription can also become

blocked by R-loop formation in the wake of the RNAP, in other words transcription blocking can occur even when the R-loop is behind RNA polymerase. An explanation for this intrinsic R-loop mediated blockage is that the hybridization between the nascent RNA and the DNA template strand within an R-loop could destabilize the transcription complex; for example, by partial disruption of interactions between the nascent RNA and the RNAP, or by deformations within the transcription complex similar to those caused by hairpin formation within the nascent RNA (Belotserkovskii B.P. et al., 2013; Artsimovitch I. and Belogurov G.A., 2018; Kang J.Y. et al., 2018).

R-loop can act as a transcription termination in eukaryotes, in fact during transcription of most eukaryotic genes part of the nascent RNA is cleaved and becomes involved in other transactions. The site of cleavage is usually defined by a polyadenylation (poly A) signal sequence within the nascent RNA. An R-loop-prone (G-rich) sequence immediately forms from the poly A cleavage site causes transcription termination, thus the formation of R-loops in transcriptional pause regions is essential in causing Pol II to pause downstream of the poly(A) site prior to termination (Skourti-Stathaki K. et al., 2011).

1.4.3 Enzymatic degradation of RNA:DNA hybrids

By establishing the ability of RNA:DNA hybrids to cause genomic stability (Halász L. et al., 2017), the researchers began to study the molecular mechanisms through which their accumulation is controlled. Enzymes involved in the homeostatic control of RNA:DNA hybrids can act both by avoiding the formation of RNA:DNA hybrids during transcription or degrading and solving formed hybrids.

The most relevant enzymes able to modulate hybrids content in cells are:

1) **ribonucleases H** (RNases H), enzyme that hydrolyse the RNA portion of RNA:DNA hybrids (Stein H. and Hausen P., 1969). There are two types of RNase H, RNase H1 presents two isoforms that are localized in the nucleus and mitochondria (Cerritelli S.M. et al., 2003)

confirming the presence of RNA:DNA hybrids at the mitochondrial level in human and mouse models. (Lima W.F. et al., 2016; Posse V. et al., 2019) and RNase H2 with more nuclear activity than RNase H1 (Hyjek M. et al., 2019). Mutations in any these of subunits cause the Aicardi–Goutieres syndrome, a neuroinflammatory disease associated with the chronic activation of the immune system in response to an excessive accumulation of nucleic acids hybrids (Crow Y.J. et al., 2006). Very recently, RNase H2 was also shown to regulate RNA:DNA hybrid levels at telomeres (Graf M. et al., 2017) and to recruit HR proteins (BRCA1/BRCA2/RAD51) in the resolution of the DSB. Specifically, RNase H2 mediates BRAC1 and BRAC2 localization to DSBs in the S/G2 cell-cycle phase, and controls RNA:DNA hybrid levels through Fanconi Anemia (FA) mediated DSB repair pathway (D'Alessandro G. et al., 2018; Ceccaldi R. et al., 2016).

2) **DEAD/DEXH-box RNA and Senataxin,** enzymes with helicase activity, able to unwind dsRNA and dsDNA as well as noncanonical polynucleotide structures, such as G-quadruplex and R-loop structures in ATP-dependent way (Chakraborty P. and Grosse F., 2011). Human senataxin (SETX), the mammalian Sen1 homolog, was initially identified when mutations causing ataxia oculomotor apraxia 2 (AOA2) and amyotrophic lateral sclerosis type 4 (ALS4) were mapped to the senataxin gene (James P.A. and Talbot K., 2006; Palau F. and Espinós C., 2006). The enzyme is involved in the resolution of R-loops in transcription termination systems. It has been shown that the depletion of senataxin in Hela cells involves R-loops stabilization downstream of the poly(A) signal, preventing nascent RNA degradation and efficient termination (Skourti-Stathaki K. et al., 2011). ChIP experiments followed by high throughput sequencing (ChIP-seq), they also showed that senataxin is recruited at DSBs when they occur in transcriptionally active loci where it removes RNA:DNA hybrids forming *in cis* regulating γH2AX signaling, to promote Rad51 loading and to avoid abnormal re-joining of distant DNA ends (Cohen S. et al., 2018);

3) **THO/TREX (DNase III) complex,** that binds ssRNA to initiate mRNP maturation, and these interactions prohibit R-loop formation (Li X. and James L.M., 2005; Gómez-González B. et al., 2011; Allison D.F. and Wang G.G., 2019). Biogenesis of messenger ribonucleo-protein particles (mRNP) also prevents R-loop accumulation. During mRNP biogenesis, RNA-binding proteins (RBP) interact with nascent mRNA to promote mRNA processing and export from the nucleus. Human depletion of THO/TREX complex implies impairs transcription elongation and mRNA export and increases instability associated with DNA breaks, leading to hyper-recombination and γH2AX and 53BP1 foci accumulation (Domínguez-Sánchez M.S. et al., 2011). The mechanism of action of the complex is not yet clear, but recent studies have proposed that human THO interacts with the Sin3A histone deacetylase complex to suppress co-transcriptional R-loops, DNA damage, and replication impairment (Salas-Armenteros I. et al., 2017).

4) **Topoisomerase TOP1 and TOP2,** a class of enzymes that releases the supercoiling and torsional tension of DNA introduced during the DNA replication and transcription by transiently cleaving and rejoining one strand of the DNA duplex (El Hage A. et al., 2010; Promonet A. et al., 2020). Topoisomerase 1 (TOP1) and Topoisomerase 2 (TOP2) have both been shown to relieve torsional stress and prevent R-loop accumulation at the rDNA locus (El Hage A. et al., 2010). Moreover, topoisomerase 3B (TOP3B) reduces R-loop formation at highly expressed genes like the protooncogene MYC (Yang Y. et al., 2014).

1.4.4 RNA:DNA hybrids and immune system activation

The PRR able to sense PAMP and DAMP, can be activated by different types of molecules, including nucleic acids. It has been shown that TLR9, a member of TLR able to detect nucleic acids and cGAS-STING axis are able to bind also RNA:DNA hybrids and trigger the antiviral response, characterized mainly by the production of type I IFN (Samuel C.E., 2001; Mankan A.K. et al., 2014; Rigby R.E. et al., 2014). TLR9 resides in the endolysosome where it is transported

by the chaperon protein UNC93B1 (protein unc-93 homolog B1; Kim Y. et al., 2008). Once TLR9 reaches endolysosome it undergoes a proteolytic cleavage of the ectodomain by proteases and, therefore, the full-length TLR9 is only found in the endoplasmic reticulum. This cleavage is fundamental since it increases binding to unmethylated CpG motifs and allows the recruitment of the myeloid differentiation primary response 88 (Myd88), starting the signal transduction. Myd88 is an adaptor protein that leads to the nuclear ttransfer of NF-κB, or interferon response factor IRF-1, IRF-5, and IRF-7 (McKelvey K.J. et al., 2011; Ewald S.E. et al., 2008; Park B. et al., 2008).

More recent is the discovery of cGAS, a cytoplasmic sensor of nucleic acids, able to induce a type I IFN response (Sun L. et al., 2013) following its specific non-sequence bond with dsDNA or RNA:DNA hybrids (Ma R. et al., 2020; Luecke S. et al., 2017).

cGAS uses ATP and GTP to synthesize a cyclic dinucleotide (CDN) molecule, known as cGAMP, as the second messenger for the activation of STING which is in the endoplasmic reticulum (Ishikawa H. and Barber G.N., 2008). Once activated, STING activates two protein kinases, IKK and TBK1, which activate the transcription factors NF-κB and IRF3, respectively. As previously described in the TLR9 signalling cascade, NF-kB and IRF3 translocate inside the nucleus in order to promote the expression of type I IFNs and other cytokines (Gao D. et al., 2015). An aberrant accumulation of endogenous nucleic acids has been observed in senescent cells or in cells of patients affected by age-related diseases (Lan Y.Y. et al., 2019; Yang H. et al., 2017; Gentili M. and Manel N., 2016; Dou Z. et al., 2017).

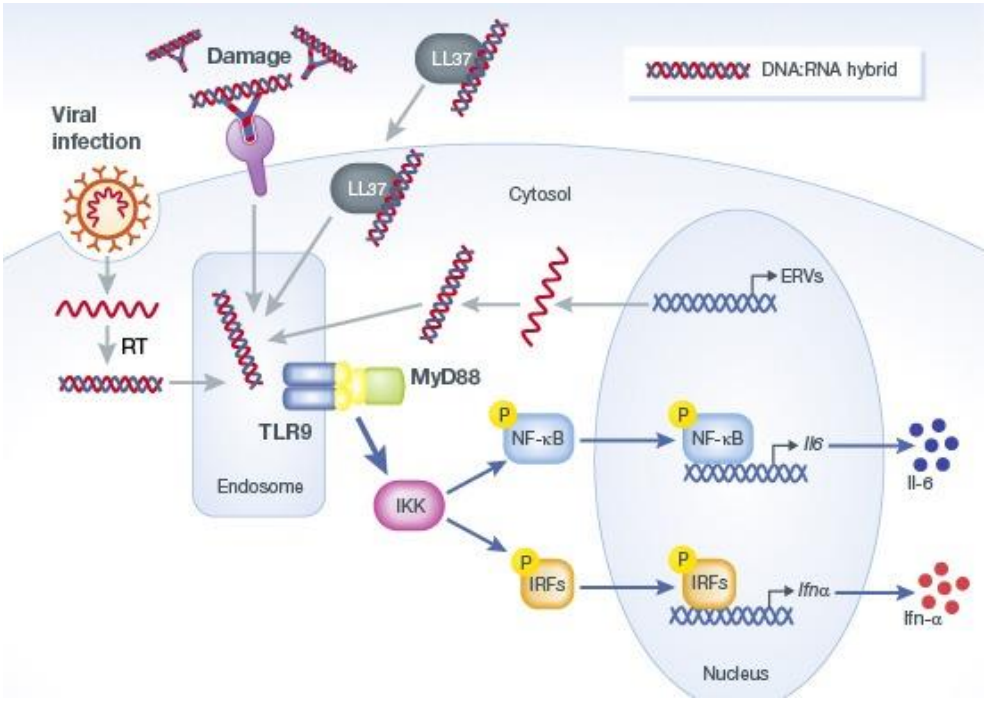

Figure 6. TLR9 pathway activation *(Rigby R.E. et al., 2014).*

2 AIM OF WORK

Research on aging process is focuses on understanding the cellular and molecular mechanisms underlying the key functional changes that yields the onset of persistent inflammation, *i.e.* inflammaging. In this context, the ceaseless stimulation of the innate immune system over time and the increased burden of "molecular garbage" have been proposed as major triggers. Along these accumulating molecules of nucleic acids have been regarded as major players. Moreover, these phenomena may occur systemically at cellular level, in particular in senescent cells. Indeed, the accumulation of senescent cells during aging, observed in the tissues of animal models and in humans, suggests that with aging the immune system's ability to eliminate senescent cells is reduced and this may fuel inflammaging.

In this scenario, a better understanding of the molecular mechanisms that activate the innate immune responses in senescent cells and under stress condition, *i.e*. hyperglycemia, could help to disentangle the mechanisms underlying the development of ARDs, including T2DM.

In this framework, with the aims to better clarify the molecular culprits of inflammaging and to identify potential new biomarkers of ARDs, we have analysed the cytoplasmic pool of misplaced nucleic acids in a model of human endothelial cells (HUVECs), in two prototypical stress-conditions, both related to the rate of the aging process, such as "replicative cell senescence" and "hyperglycemic condition".

3.1 Characterisation of HUVEC senescence

HUVEC senescence was characterised by analysing a number of well-established senescence biomarkers in non-senescent (control, ctr) and senescent (sen) cells. Compared with ctr cells (cPD=4), sen cells (cPD=11) were characterised by: 1) growth arrest which was documented by reduced cPD (**Figure 7a**); 2) progressive telomere shortening (**Figure 7b**); 3) increased SA β-gal activity (**Figure 7c**); 4) up-regulation of the cell cycle regulator p16 both at the transcriptional (CDKN2A) and at the protein level (InK4A; **Figure 7d**); 5) significant hypo-expression of SIRT1 protein (**Figure 7e**); 6) significant hyper-expression of mRNAs coding for the pro-inflammatory SASP components interleukin *IL-6, IL-1β* and *IL-8* (**Figure 7f**); 7) significant hyper-expression of miR-146a-5p (**Figure7g**); 8) significant increase of phospho-histone H2AX (pH2A.X), a biomarker of persistent DNA damage (**Figure 7h**).

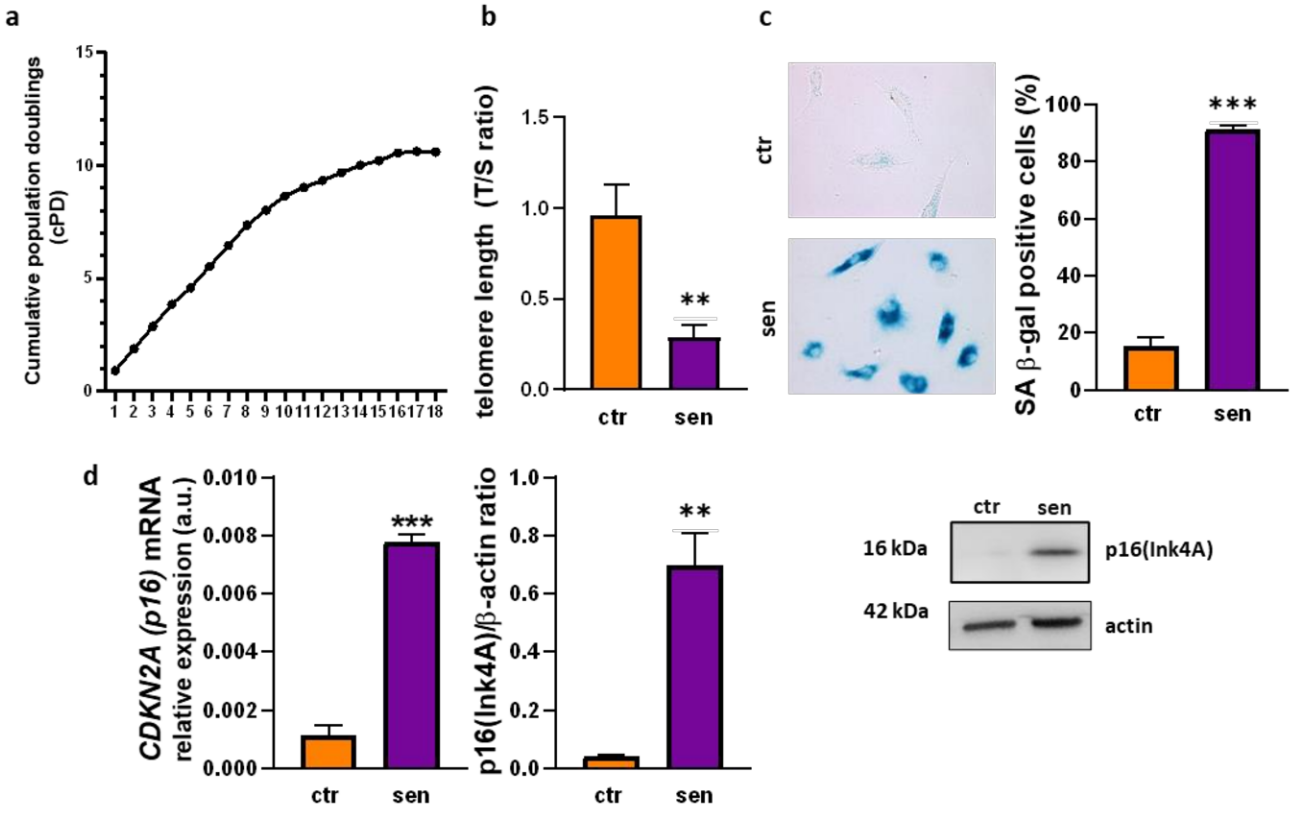

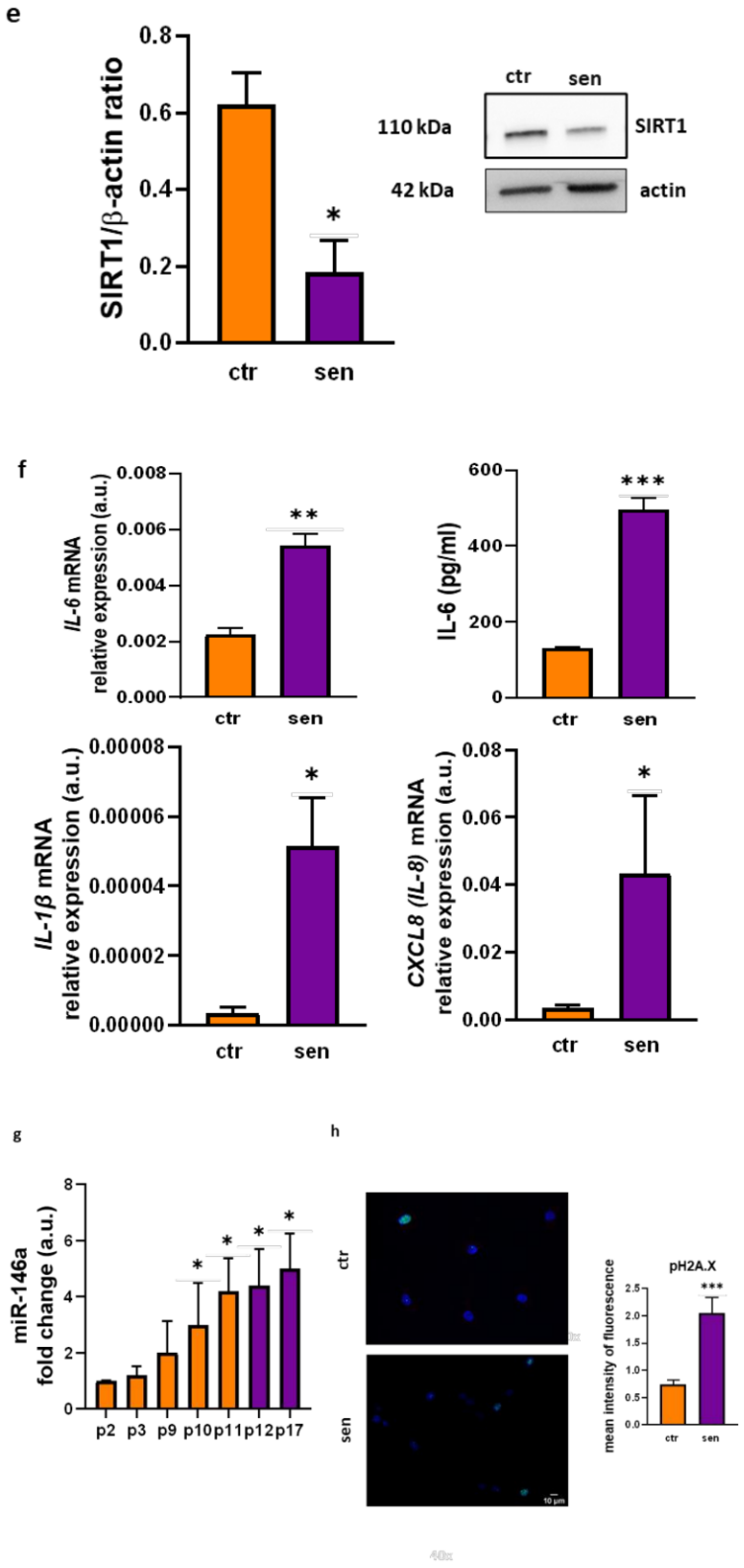

Figure 7. Characterisation of replicative senescence in human umbilical vein endothelial cells (HUVECs). *(a) Cumulative population doubling (cPD) curves. (b) Telomere/single copy gene ratio (T/S) in DNA from HUVECs at different passages. (c) Representative positivity and quantification of the SA β-Gal staining in control (ctr, < 20%) and senescent (sen, > 80%) cells. (d) mRNA relative expression and western blot densitometric analysis of p16(Ink4a) in ctr and sen cells. Protein expression values are reported as p16(Ink4)/β-actin ratio. (e) Western blot densitometric analysis of SIRT1 in ctr and sen cells. Protein expression values are reported as SIRT1/β-actin ratio (f) mRNA relative expression of interleukin IL-6, (IL)-1β, IL-8. (g) MiR-146a expression (fold increase vs P2 considered as 1). (h) Immunofluorescence staining of phospho-histone H2AX (pH2AX) in ctr and sen cells. For qPCR, western blot and immunofluorescence analysis data from three independent experiments are represented as mean ± SD.*, p ≤ 0.05; **, p < 0.01; ***, p < 0.001 from paired t-tests.*

3.2 Hyperglycemia induces senescence in HUVEC cells

Ctr and sen HUVEC cells were cultured for 1 week in 25 mM glucose medium, a concentration 5-folds higher than that present in normoglycemic medium (5.5 mM). The kinetic of telomere shortening was analyzed in ctr cells to assess whether week-long hyperglycemic stress was able to induce the senescent phenotype in young cells (ctr). Significant telomere shortening was observed at day 7; after 6 days of culture in hyperglycemic medium ctr cells exhibit a telomere attrition comparable to that of sen cells (**Figure 8a**).

The replicative capacity of ctr cells cultured in hyperglycemia was not increased compared to that of ctr cells cultured in normoglycemic medium, suggesting that telomere shortening was due to the hyperglycemic condition "per se" rather than to an increase in the proliferation rate (ctr NG, PD=2.5±0.4; ctr HG, PD=2.2±0.3).

The detection of telomere DNA sequences through FISH technique showed, as expected, the presence inside the nucleus, of a number of telomere sequences; surprisingly it was observed also a cytoplasmic localization of some telomere sequences in ctr cells treated with hyperglycemia (**Figure 8b**). Ctr cells cultured in hyperglycemia showed increased levels of a number of senescence biomarkers, such as: SA β-gal activity (**Figure 8c**), cell cycle regulator p16 both at the transcriptional (CDKN2A) and at the protein level (InK4A; **Figure 8d**), *IL-6* levels, both as mRNA and as protein released in the culture medium and *IL-8* as mRNA (**Figure 8e**), H2AX histone phosphorylation (**Figure 8f**). These results strongly suggest that ctr cells cultured 1 week in hyperglycemic medium acquire phenotypes similar to those of senescent cells.

Notably, sen cells cultured 1 week in hyperglycemic medium showed no significant increase in any of the analyzed senescence biomarkers.

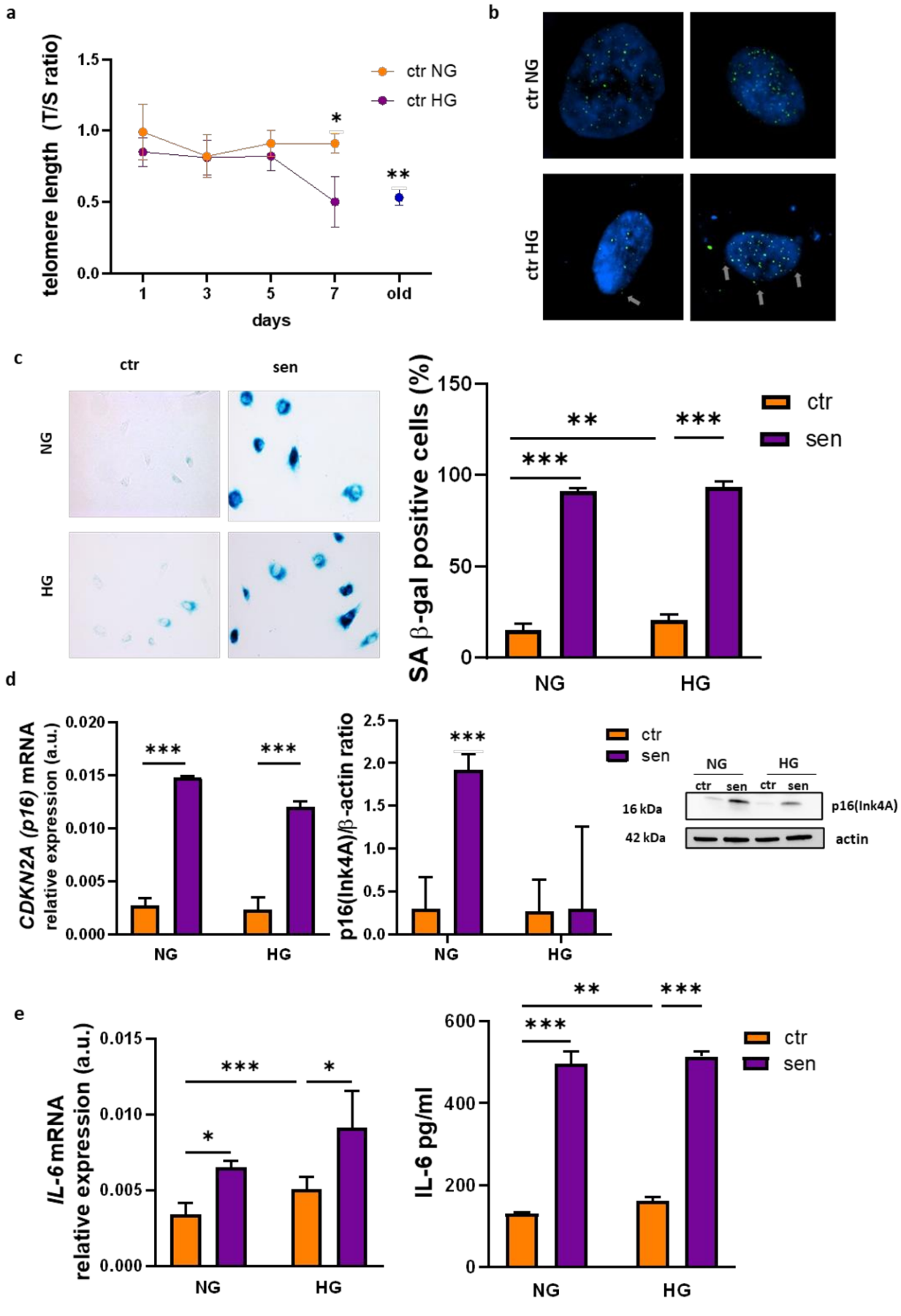
a
telomere length (T/S ratio)
1.5
1.0
0.5
0.0
1
3
5
7
old
days
ctr NG
ctr HG
*
**
b
ctr NG
ctr HG
c
ctr
sen
NG
HG
SA β-gal positive cells (%)
150
100
50
0
**
***
***
ctr
sen
NG
HG
d
CDKN2A (p16) mRNA
relative expression (a.u.)
0.020
0.015
0.010
0.005
0.000
***
***
NG
HG
p16(Ink4A)/β-actin ratio
2.5
2.0
1.5
1.0
0.5
0.0
***
NG
HG
ctr
sen
NG
HG
ctr
sen
ctr
sen
16 kDa
42 kDa
p16(Ink4A)
actin
e
IL-6 mRNA
relative expression (a.u.)
0.015
0.010
0.005
0.000
***
*
*
NG
HG
IL-6 pg/ml
600
400
200
0
**
***
***
NG
HG
ctr
sen

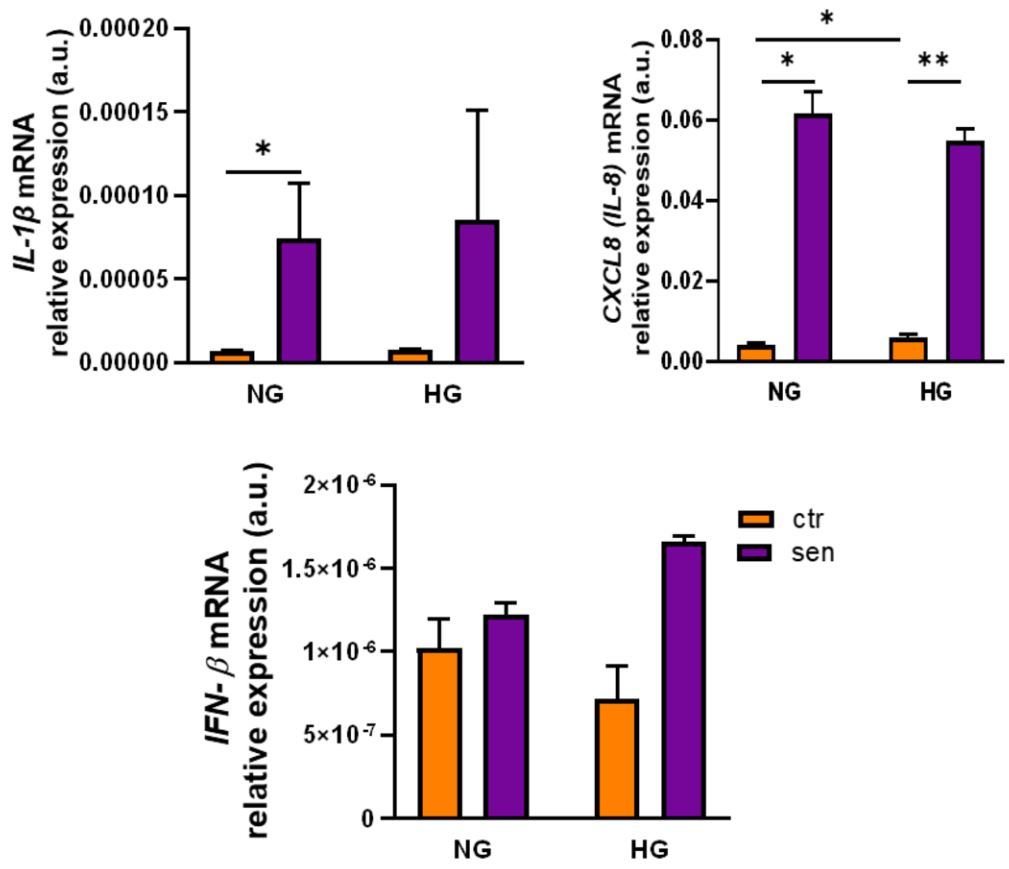

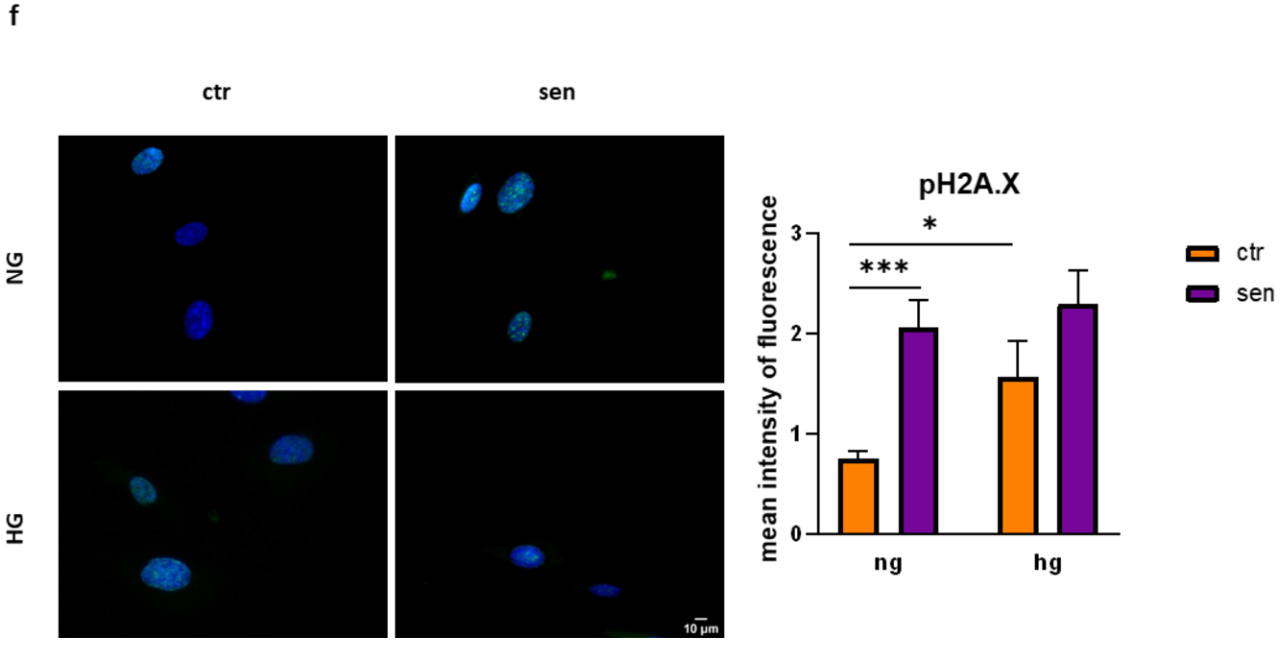

Figure 8. Hyperglycemia effects induced in ctr and sen human umbilical vein endothelial cells (HUVECs). *(a) Telomere/single copy gene ratio (T/S) in DNA from ctr HUVECs in hyperglycemic condition at different days of treatment (b) Telomere FISH images of ctr NG and HG conditions, green: telomere signals, blue: chromatin DNA. (c) Representative positivity and quantification of the SA β-Gal staining in ctr and sen cells in normoglycemic and hyperglycemic conditions. (d) mRNA relative expression and western blot densitometric analysis of p16(Ink4a) in ctr and sen cells. Protein expression values are reported as p16(Ink4)/β-actin ratio. (e) mRNA relative expression of interleukin IL-6, (IL)-1β, IL-8 and IFN-β. (f) Immunofluorescence staining of phospho-histone H2AX (pH2AX) in ctr and sen cells. For qPCR, western blot and immunofluorescence analysis data from three independent experiments are represented as mean ± SD.*, p ≤ 0.05; **, p < 0.01; ***, p < 0.001 from paired t-tests.*

3.3 Accumulation of cytoplasmatic nucleic acids in ctr and sen cells in normo- and hyper-glycemic conditions

Based on a number of studies showing increased DNA damage in different types of senescent cells (*i.e.* endothelial cells, fibroblasts, immune cells), and the increasing evidence suggesting a cytosolic nucleic acid accumulation under stress conditions (*i.e.* UV treatment), we hypothesized that hyperglycemia and senescence could be two stress conditions able to induce an increased amount of cytosolic nucleic acids. To verify our hypothesis we analysed through immunofluorescence (IF) double-stranded DNA (dsDNA), double-stranded RNA (dsRNA), and hybrids (RNA:DNA) in ctr and sen cells cultured under normo- and hyper-glycemic conditions. Significant increased levels of cytosolic dsDNA were observed in normoglycemic sen *vs* ctr cells, and in ctr HG *vs* NG cells (**Figure 9a**). Immunofluorescence images confirmed the 2-folds increase of dsDNA sequences in NG sen *vs* ctr cells, and 1.6-folds increase in HG sen *vs* NG cells (**Figure 9a1**). Moreover, increased amounts of chromatin micronuclei and bubbles were observed in the same conditions (**Figure 9b** shows representative images).

Hybrids (RNA:DNA) were detected using Ab S9.6, which is able also to detect dsRNAs. We observed increased fluorescence signals in NG sen *vs* ctr cells, and in both ctr and sen HG *vs* NG cells (**Figure 9c** shows representative images). Since S9.6 antibody can detect also dsRNAs, to disentangle the S9.6 IF signals related to hybrid sequences detectable in the cytoplasm, we treated cells with RNase III enzymes (that degrades specifically dsRNA) and with RNase T1 (that degrades ssRNA) (**Figure 9c**). After RNase III and RNase T1 treatments, immunofluorescence images confirmed the persistence of increased levels of hybrid sequences in NG sen *vs* ctr cells, and in HG sen *vs* ctr cells (**Figure 9c**).

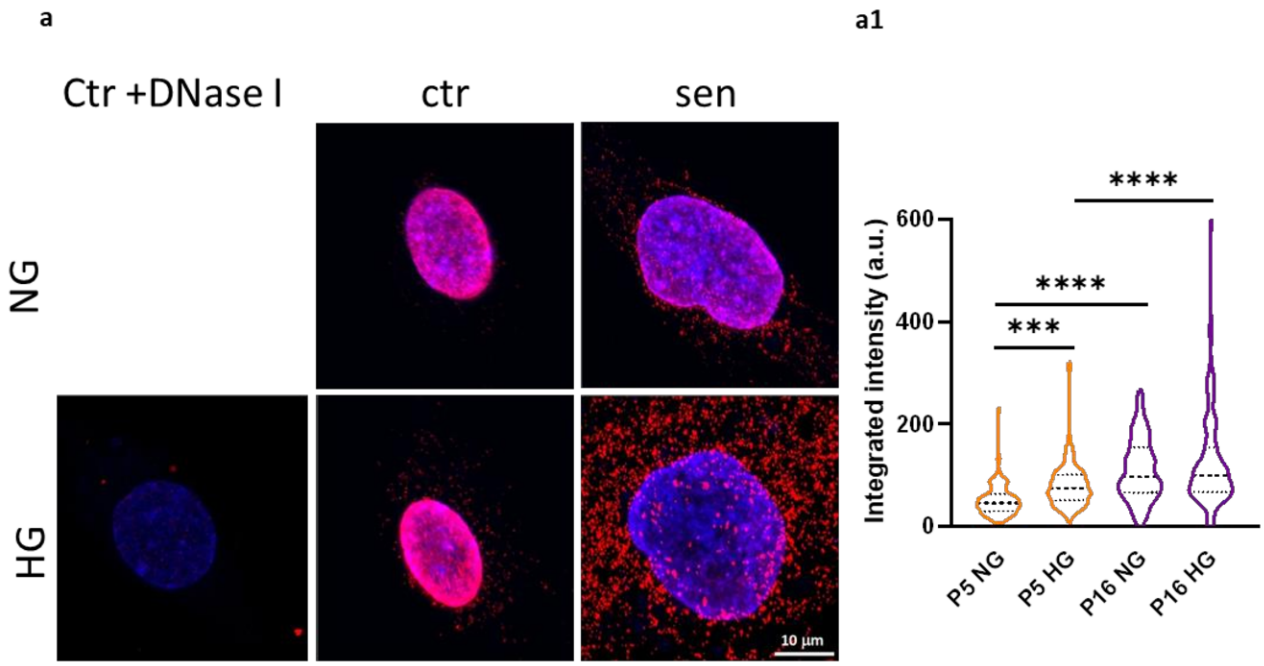
a
Ctr +DNase I
ctr
sen
NG
HG
10 µm
a1
Integrated intensity (a.u.)
600
400
200
0
****
****
***
P5 NG
P5 HG
P16 NG
P16 HG

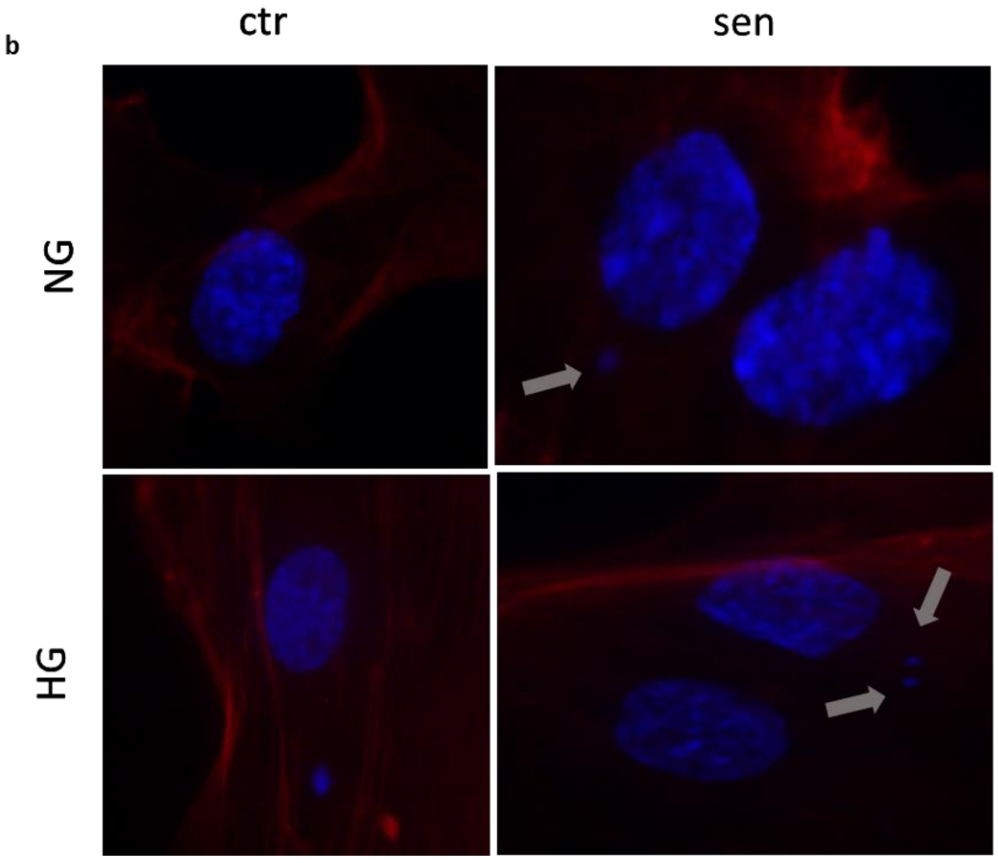
b
ctr
sen
NG
HG

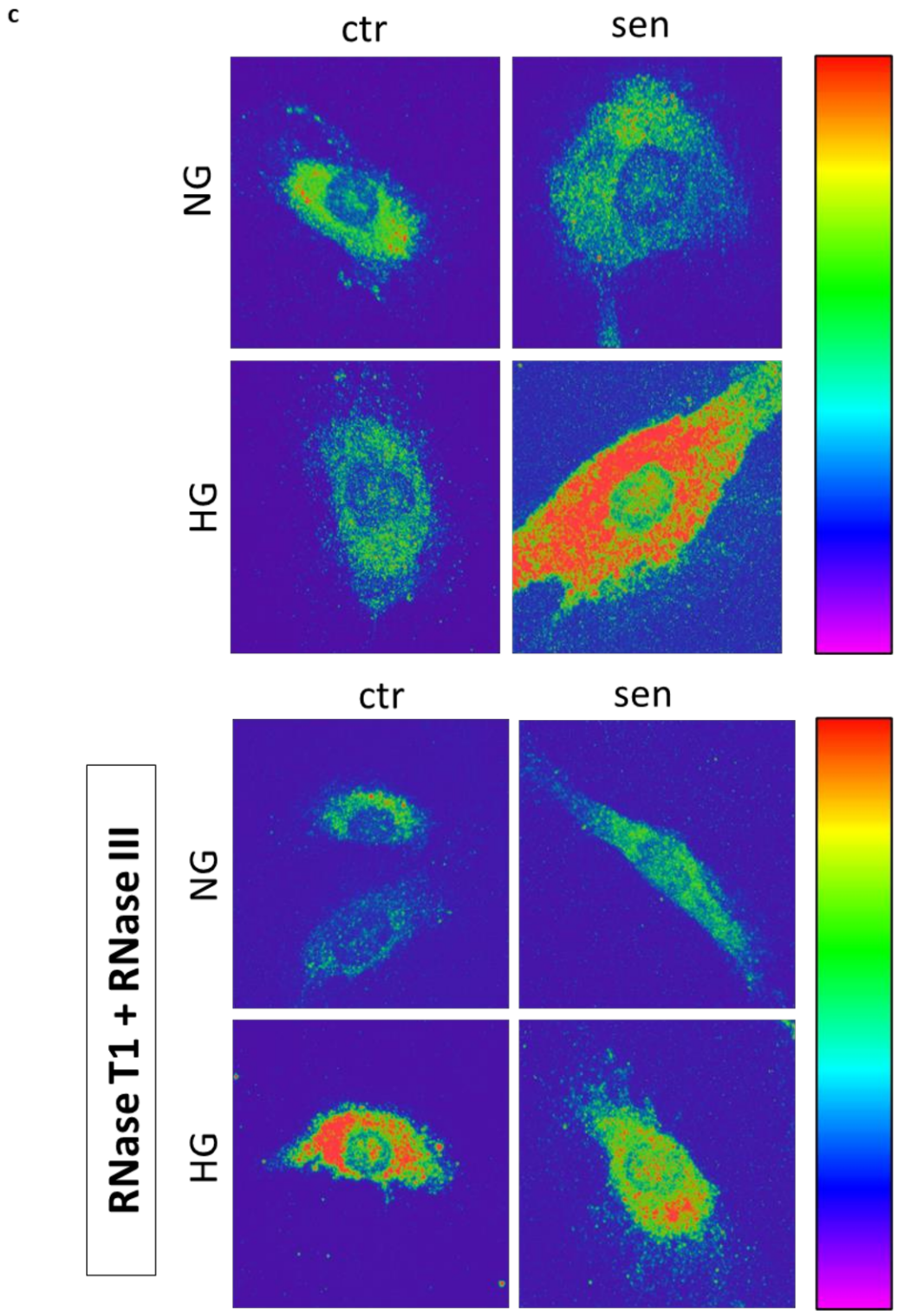

Figure 9. Senescence and hyperglycemia cause cytoplasmatic accumulation of nucleic acids in human umbilical vein endothelial cells (HUVECs). *(a) IF staining and (a1) quantitation of anti-dsDNA (red) in ctr and sen, NG and HG cells. (b) Representative images of cytosolic presence of bubbles stained with HOECHST (blue) in ctr and sen NG, HG conditions. (c) SIM (structured Illumination Microscopy) analysis of RNA:DNA hybrids (S9.6 antibody) in NG, HG ctr and sen cells with/without RNase T1 and RNase III treatment. Data from n = 3 independent experiments are represented as mean ± SEM. *, p < 0.05; **, p < 0.01; ***, p < 0.001 from one-way ANOVA followed by Tukey's multiple comparison test for pairwise comparisons.*

3.4 Senescence and hyperglycemic conditions are associated with reduced expression of RNase H2 and consequent misincorporation of ribonucleotide in genomic DNA

Since RNaseH2 plays crucial role in the post-transcriptional modulation of RNA:DNA sequences, degrading the RNA component of the hybrid, we treated ctr and sen cells with the aim to identify possible inverse relationships between hybrid sequences and RnaseH2 enzyme. RNaseH2 expression levels were significantly downregulated in sen *vs* ctr cells both in NG and in HG conditions (**Figure 10a**). These data seem to be in accordance with the accumulation of hybrid sequences into the cytoplasm of the senescent cells in normo- and hyper-glycemic conditions.

Since RNase H2 identifies DNA damages and initiates the ribonucleotide excision repair (RER), resulting in error-free removal of mis-incorporated ribonucleotides, we treated DNA purified from ctr cells, both in NG and HG conditions, and from NG sen was treated with 0.3M NaOH at 55 °C to cleave DNA at the positions of ribonucleotides and sized by electrophoresis on a denaturing agarose gel. As represented in **figure 10b**, significant increased misincorporation of ribonucleotides were observed in NG sen *vs* ctr, and in ctr, HG *vs* NG (**Figure 10b**).

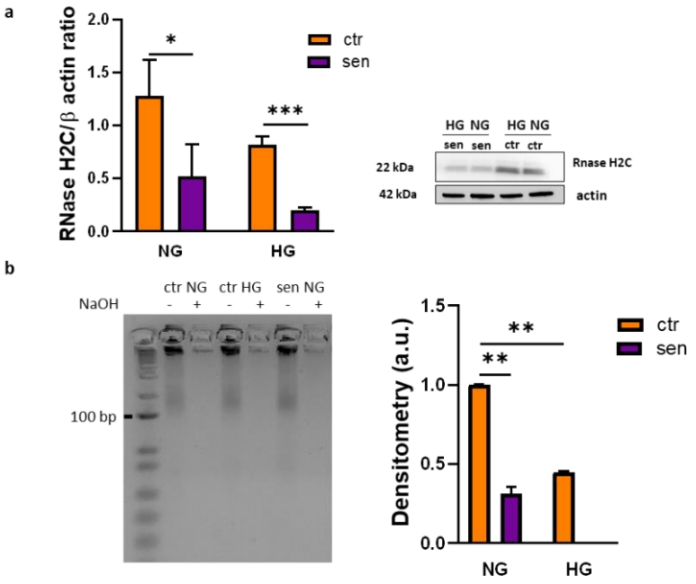

Figure 10. Senescence and hyperglycemic conditions cause reduced expression of RNase H2 and consequent misincorporation of ribonucleotide in genomic DNA *(a)Western blot densitometric analysis of RNase H2C in ctr and sen cells in normoglycemic and hyperglycemic conditions. Protein expression values are reported as RNase H2C/β-actin ratio. (b) Alkaline gel electrophoresis of 1 µg of DNA from HUVECs cells. Lanes: marker, (1) ctr NG, (2) ctr NG + NaOH 0.3 M, (3) ctr HG (4) ctr HG +*

NaOH 0.3 M, (5) sen NG, (6) sen NG + NaOH 0.3 M. Data from n = 3 independent experiments are represented as mean ± SD (fold increase vs CTR NG considered as 1)., p ≤ 0.05; **, p < 0.01; ***, p < 0.001 from paired t-tests.*

3.5 Molecular characterization of nucleic acid sensing cytoplasmatic pathways in ctr and sen cells in normo- and hyper-glycemic conditions.

cGAS, STING and IRF3 molecules belong to the IFN type1 pathway activated by cytoplasmatic nucleic acids. cGAS can recognize both dsDNA and RNA:DNA hybrid sequences. We observed a significant decreased of cGAS in sen *vs* ctr, both in NG and HG conditions (**Figure 11a**). Notably, sen cells in HG showed significant decreased cGAS expression compared to sen in NG.

STING levels were not significantly modulated by senescence nor by hyperglycemia (**Figure 11a1**). IRF3 levels were not significantly different between ctr and sen but, as observed for cGAS, sen cells in HG showed significant decreased expression compared to sen in NG (**Figure 11b**).

We also analysed the expression levels of TLR4, involved in responses to proteins-antigens, and TLR9, involved in the responses to nucleic-acids-antigens. As expected, we observed significant increased expression of TLR9 in NG sen *vs* ctr and in HG sen *vs* ctr (**Figure 11c**).

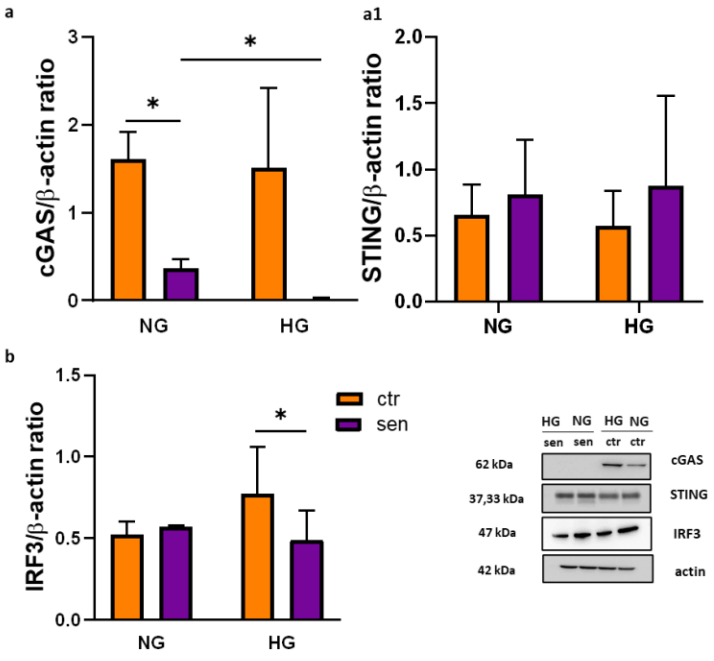

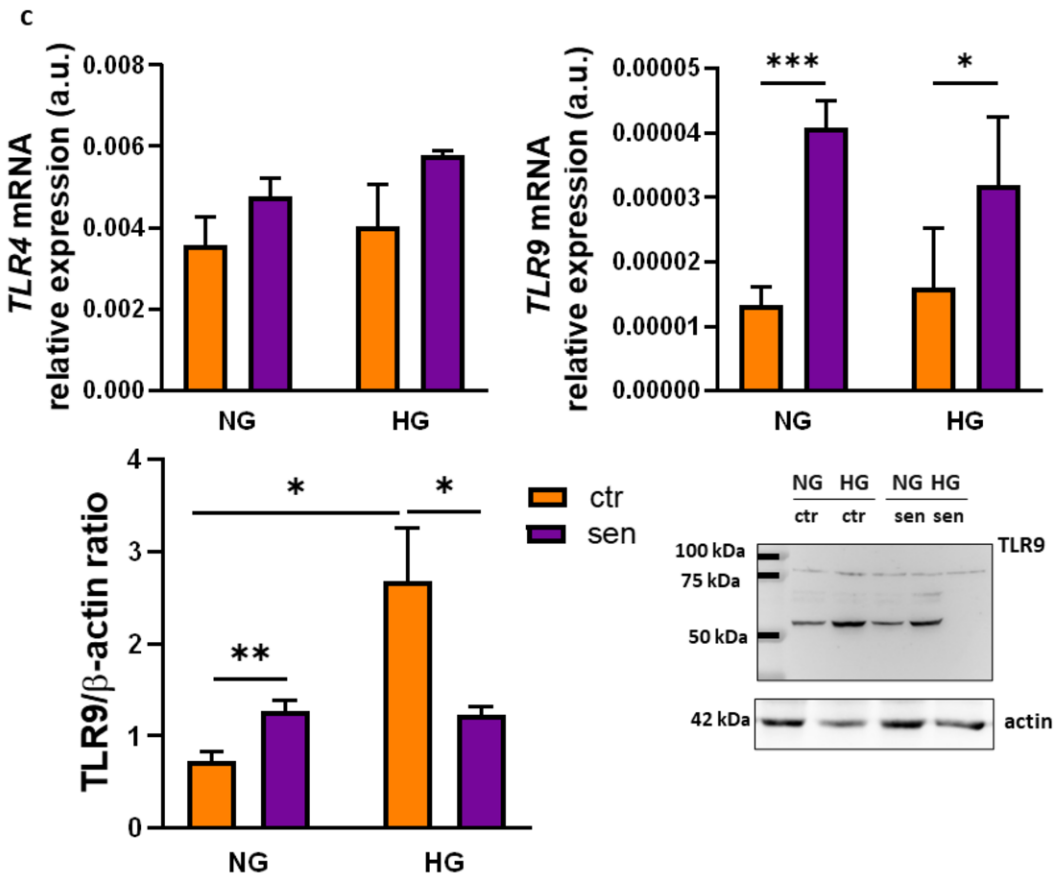

Figure11. Senescence and hyperglycemia innate immune pathways activation. *Western blot densitometric analysis of (a) cGAS, (a1) STING and (b) IRF3 in NG, HG ctr and sen cells. Protein expression values are reported as protein/β-actin ratio. (c) mRNA relative expression of TLR4, TLR9 and western blot densitometric analysis of TLR9 in NG, HG ctr and sen cells. Protein expression values are reported as tlr9/β-actin ratio. For qPCR and western blot analysis data from three independent experiments are represented as mean ± SD.*, p ≤ 0.05; **, p < 0.01; ***, p < 0.001 from paired t-tests.*

4 DISCUSSION

The accumulation of senescent cells is considered a key hallmark of aging process and is believed to be one of the main risk factors for the development of the most common age-related diseases, including type two diabetes (T2DM). Senescent cells acquire a senescence associated pro-inflammatory secretory phenotype (SASP), characterized by increased release of soluble factors (pro-inflammatory cytokines and chemokines), growth factors and extracellular matrix (ECM) remodelling enzymes (Coppè J.P. et al., 2008; 2010; Song P. et al., 2020), thus contributing to maintain a systemic age-related proinflammatory status, named about 20 years ago as "inflammaging" (Franceschi C. et al., 2000) and recently defined as "senoinflammation" (Tchkonia T. et al., 2013; Chung H.Y. et al., 2019). Increasing evidence suggest that different stress conditions can converge on the induction of SASP; primarily the activation of a DNA damage response (DDR), triggered by genomic lesions, one of the first molecular mechanisms associated with cellular senescence (Rodier F. et al., 2009; Sulli G. et al., 2012; Olivieri F. et al., 2015). In this scenario, a better understanding of the molecular mechanisms that activate SASP in senescent cells and under stress condition, *i.e.* hyperglycemia, could help to disentangle the mechanisms underlying the development of ARDs, including T2DM.

Using HUVEC cells, human endothelial cells able to undergo replicative senescence *in vitro*, we analysed the modulation of some well-recognized senescence biomarkers and of potential innovative biomarkers, such as misplaced nucleic acids (dsDNA, dsRNA, ssRNA and RNA:DNA hybrids), in "senescence" and/or in "hyperglycemic condition", considered as an *in vitro* model of T2DM.

One of the most relevant results is the significant increased level of all the analysed senescence-associated biomarkers in young cells cultured for 1-week in hyperglycemic medium. This result suggests that the acquisition of the senescent phenotype, observed in about 3 months of culture

in normoglycemic medium, can be acquired in only 1 week when young cells are cultured in a medium with 5-folds increased glucose level. Our results suggest that the accelerated rate of aging observed in diabetic patients could be due, almost in part, to the ability of hyperglycemic condition to increase the rate of senescence, thus promoting an increased burden of senescent cells.

The most innovative result of this research is the observation that senescent cells have a significant increased amount of misplaced nucleic acids in cytoplasm compared to the younger ones, as well as young cells cultured for 1-week in hyperglycemic condition compared to young cells cultured in normoglycemic medium. We searched to identify the different types of misplaced nucleic acids in these cells, showing the presence of dsDNA, including micronuclei, bubbles and telomere sequences, of dsRNA and of hybrids. With the aim to identify the causes of this increased amount of misplaced nucleic acids, we treated the cells with RNase H2, an enzyme able to identify DNA damages and initiates the ribonucleotide excision repair (RER), resulting in error-free removal of mis-incorporated ribonucleotides. We observed reduced RNaseH2 expression in senescent cells compared to the younger ones and in young cells treated with hyperglycemic medium. The amounts of misincorporated ribonucleotides were inversely related to the amount of RNase H2, suggesting that both “senescence” and “hyperglycemic condition” are associated with increased genomic instability, marked by the increased amount of misincorporated ribonucleotides.

Our results are in accordance with recent evidence suggesting that mis-spliced, intron-retained mRNAs can be an unexplored source of endogenous dsRNA. Therefore, alternative splicing is emerging as a critical contributor to senescence and aging. Spliceosomal perturbation, induced by pharmacologic and genetic inhibition of spliceosomal genes, is able to trigger cells to enter senescence, up-regulating the transcription factor Sp1 (Kwon S.M. et al., 2021).

DsRNA-sensing pathways could respond to global aberrations of RNA splicing (Bowling E.A. et al., 2021).

Eukaryotic cells express a number of cytoplasmic nucleic acids receptor to sense microbial and viral DNA and RNA. However, these sensors can also be activated by endogenous DNA and RNA, including extranuclear chromatin resulting from genotoxic stress and DNA released from mitochondria, placing this signalling as important axis in autoimmunity, sterile inflammatory responses and cellular senescence. The cGAS-STING-IRF3 signalling axis, is the key signalling for cytoplasmic nucleic acids detection and IFN type 1 expression involved in antiviral response.

Therefore, we analysed this signalling in "senescence" and "hyperglycemic condition". Surprisingly, the expression of the cGAS-STING-IRF3 as well as the expression of IFN-1 were not significantly increased in such stress conditions, whereas the release of proinflammatory cytokines, such as *IL-1β, IL-6* and *IL-8* was significantly increased.

These results suggest an imbalance between antiviral response and proinflammatory response in senescent cells and in young cells under hyperglycemic conditions.

Notably, the elderly population is very susceptible to infection by the single-stranded RNA influenza virus (IV) infection and the reactivation of the double stranded DNA varicella zoster virus (VZV) (Wilhelm M. et al., 2018). Besides the reduced efficacy of the immune response, the increased susceptibility to viral infection could be fuelled by an enhanced viral replication in senescent cells. Recent evidence showed that primary human bronchial epithelial cells or human dermal fibroblasts undergoing replicative senescence present increased susceptibility to both IV and VZV as assessed by increased viral gene expression and virus titres compared to non-senescent cells (Kim J.A. et al., 2016).

The enhanced susceptibility of senescent cells to viral infections may be a direct consequence of their ability to resist apoptosis and tolerate a high cytosolic nucleic acids load.

Our results suggest that endothelial senescent cells end young cell under hypeglycemic condition tolerate an increased load of misplaced-nucleic acids compared to younger cells. A strong reduction of cGAS expression was observed in senescent HUVEC cells in normo and hyperglycemic conditions, in association with the absence of IFN 1 modulation.

Overall, when cells encounter stress conditions, such as senescence and hyperglycemic condition, the cytoplasmic load of nucleic acid increase, whereas the cytosolic sensors of this misplaced nucleic acids are not responsive to such stimulation, a condition that resembles a "tolerance status". Such tolerant cells could be more susceptible to viral infections. These results could explain, almost in part, why old subjects, especially elderly patients affected by T2DM, with an increased burden of senescent cells, are more susceptible to adverse outcomes of infectious diseases, including SarS-Cov-2 infections (Bonafè M. et al., 2020).

Hepatocytes do not produce type-I IFNs in response to synthetic dsDNA or HBV infection because hepatocytes lack the cGAS/STING pathway (Pan S. et al., 2018). This may also be considered a reasonable explanation for HBV's ability to specifically adapt in hepatocyte cells and may contribute to these cells' weak capacity to eliminate HBV infection.

The current knowledge on the crosstalk between cellular senescence and infection is still in its infancy, but it highlights that senescence can exert a dual role in infection, either enhancing susceptibility to infection by promoting immunosenescence and favouring microbial or viral replication within the host cells (Humphreys D. et al., 2020). In this framework, to better clarify the origin of misplaced endogenous nucleic acids in senescent cells and in cells under hyperglycemic condition, cold help to understand the "increased tolerance" of such cells also to potential microbial or viral infections.

Further studies will help to disentangle this complex issue.

5 MATERIALS AND METHODS

5.1 Cell line and cell culture

HUVECs (Human Umbilical Vein Endothelial cells) derived from donor pools were purchased from Clonetics (Lonza, Basel, Switzerland) and cultured in EGM-2, endothelial growth medium (CC-3162, Lonza, Walkersville, MD USA). Briefly, fresh cells were seeded in T25 flasks (Corning Costar, Sigma Aldrich, St. Louis MO, USA) and sub-cultured when they reached 70–80% confluence at a density of 5000/cm2 in humidified atmosphere of 5% CO2 at 37°C. The medium was changed at 48 h intervals. All cells tested were negative for mycoplasma infection. The passages of trypsinization and cell count are repeated until replicative senescence, in this way the replication senescence curve is obtained. Each step calculates population doubling (PD) which is given by the formula: (log10 F – log10 I)/log102 where I represents the number of plated cells and F the number of viable cells counted the following passage (F) and Cumulative population doubling (CPD) was calculated as the sum of all PD changes. When the value of I is equal to or less than the value of F, the cells are in replicative block and reach the plateau phase of the growth curve. In the experiments carried out, replicative senescence was obtained from 18 replication cycles.

5.2 Cell cultures in hyperglycemic conditions

The condition of hyperglycemia was obtained by adding to the culture medium (5.5 mM) the glucose necessary to reach the concentration of 25 mM, concentrations employed had been applied in earlier studies by other authors (Karbach S. et al., 2012; Haspula D. et al., 2019; Chen X. et al., 2019). The properly cultivated cells after 3 washes in Phosphate Buffer Saline (PBS) 1X, were maintained in hyperglycemic conditions for a week. Hyperglycemic and control conditions have been worked in parallel.

5.3 Analysis of senescence biomarkers

5.3.1 Lysosomal SA–β-galactosidase activity

The percentage of senescent cells has been evaluated using Senescence Detection Kit (Catalog #K320-BioVision Inc., Milpitas, CA, USA), which detects the activity of the enzyme β-galactosidase to pH 6. Young, pre-senescent and quiescent cells have reduced enzymatic activity, while in senescent cells activity increases. The kit involves the use of an organic compound X-Gal, consisting of a galactose molecule bound by a replaced indole, which reacting with the enzyme, is split producing galactose and 5-bromo-4-chloro-3-hydroxylysis. The latter is then oxidized to 5,5'-dibromo-4,4'-dichloro-indigo, an insoluble blue molecule. Cultured cells are seeded in a 12 wells plate and then the medium is removed. After a washing in PBS 1X, 1 ml of "Fixative Solution" is added and 15 minutes later two more washes were carried out and 1 ml of "β-Galactosidase Staining Solution" is added at room temperature. It was left to incubate at 37 °C overnight and proceeds with the display under an optical microscope. The percentage of β-gal-positive cells was determined by counting at least 500 cells per well. Cells were divided into young (SA-β-Gal < 10 %) and senescent (SA-β-Gal > 50%).

5.3.2 Telomere length

The telomere is the terminal region of a highly repeated DNA chromosome that protects the end of the chromosome itself from deterioration or fusion with neighbouring chromosomes. In vertebrates, the sequence of nucleotides in telomeres is TTAGGG. This TTAGGG sequence repeats about 2500 times in humans. It was thought to be a non-coding region, but recent discoveries have shown that it produces a long non-coding RNA transcribed TERRA (telomeric repeat-containing RNA), which are hypothesized to be involved in regulating telomerase. Telomere plays a decisive role in avoiding loss of information during chromosomal duplication, as DNA polymerase is unable to replicate the chromosome until its termination. DNA was

extracted from young and senescent HUVEC cell pellets derived from three independent experiments via RNA/DNA Purification kit, cat. No. 48700 Norgen Biotek Corporation Thorold, ON, Canada. Telomere length is measured as a T/S ratio where T indicates the telomere and S the single copy gene 36B4 via the RT-PCR described by Cawthton (Cawthton R.M., 2012), using 5 µl of sample containing 15 ng of DNA and 10 µl of master mix for each sample. First you create a calibration line with serial dilutions of genomic DNA (human genomic DNA, Roche, Germany) from 10.08 ng to 0.13 ng (dilution factor 1.68) contained in a volume of 5 µl.

The telomeres primers sequences are:

tel1: GGTTTTTGAGGTGAGGGTGAGGGTGAGGGTGAGGGT

Tel2: TCCCGACTATCCCTATCCCTATCCCTATCCCTATCCCTA

Those of the single copy *36B4* gene are:

Fw: CAGCAAGTGGGAAGGTGTAATCC

Rv: CCCATTCTATCATCAACGGGTACAA

Master mix used is Sso Advanced Universal Syber-green supermix cat. No. 172-5271, BioRad, Inc, USA. Two mixes are prepared, one for the telomere and the other for the single copy gene. The telomeric mix contains: 7.5 µl Master Mix, 0.27 µl tel1 primer (270 nM), 0.9 µl tel2 primer (900 nM) and 1.33 µl H2O. 36B4 mix contains: 7.5 µl Master Mix, 0.3 µl Fw primer (10 nM), 0.3 µl Rv primer (10 nM), 1.6 µl H2O. The thermal profile is: one cycle at 95°C for 3 minutes followed by 40 cycles consisting of two steps: at 95°C for 15 seconds and 60°C for 30 seconds. The samples were analyzed in duplicate and the respective Ct reported as T/S ratio.

5.3.3 p16, IL-1β, IL-6, IL-8 and IFN1B mRNA expression level

Total RNA from young and senescent HUVECs in the conditions of normo and hyperglycemia was isolated using the Norgen Biotek Kit (#37500, Thorold, ON, Canada), according to the manufacturer's instructions. RNA was stored at −80 °C until use. For mRNA genes expression 1 µg of purified RNA is reverse-transcribed following the protocol PrimeScript™ RT Reagent Kit

with gDNA Eraser (cat. NO. RR047A, Takara Bio Inc.). The retrotranscription reaction providers the preparation of a Master Mix consisting of the Reverse transcriptase enzyme (PrimeScript RT Enzyme Mix I), RT primer Mix, 5X PrimeScript Buffer and RNase Free H2O. The reaction requires a first step at 37°C for 15 minutes followed by 5 minutes at 85°C. The cDNA is stored at 4°C for 24 hours or -20°C for longer storage. qPCR reactions were conducted in a Rotor Gene Q 5plex HRM apparatus (Qiagen, Germany) in a 10 µl total reaction volume using TB Green Premix Ex Taq II (Tli Rnase H Plus; cat. NO. RR420 A, Takara Bio Inc.) according to the manufacturer's instructions. Each reaction was run in triplicate and always included a no-template control. The mRNA expression of the genes of interest was calculated using *β-actin* as reference gene, using the 2−DDCt method.

The primers sequences (written 5'-3') were:

p16, Fw: CATAGATGCCGCGGAAGGT, Rv: CTAAGTTTCCCGAGGTTTCTCAGA;

IL-1β, Fw: CCAGCTACGAATCTCCGACC, Rv: TGGGGTGGAAAGGTTTGGA;

IL-6, Fw: CCAGCTACGAATCTCCGACC, Rv: CATGGCCACAACAATGACG;

IL-8, Fw: TCTGCAGCTCTGTGTGTGAAGG, Rv: TGGGGTGGAAAGGTTTGGA;

β-actin, Fw: TGCTATCCCTGTACGCCTCT, Rv: GTGGTGGTGAAGCTGTAGCC;

IFN1, Fw: TGCTCTCCTGTTGTGCTTCT; Rv: CATAGATGGTCAATGCGGCG

Primer concentration was 10 nM.

5.3.4 Immunofluorescence analysis of H2A.X

Cells are tripsinized and seeded on polylysine coated and autoclaved coverslips. Cells were washed twice with PBS and then fixed in 4% paraformaldehyde in PBS for 1 h at 4°C. After three washes in blocking buffer (5% BSA, 0.3% Tryton X-100 in PBS) they were incubated with anti-Phospho-Histone H2A.X (Ser139) antibody (dilution 1:200 in blocking buffer, #9718, Cell Signaling, USA) overnight at 4°C. Secondary antibody incubation was performed at room temperature for 1 hour (Alexa Fluor® 488-conjugated AffiniPure Goat anti-rabbit IgG, Cat. NO.

111-545-003, Jackson Immunoresearch Laboratories Inc., USA). After a wash in PBS, cells were stained with nuclear HOECHST 33,342 (cat. no. H-3570; Molecular Probes, USA) at 1:5000 dilution in PBS for 15 min and coverslipped with Vectashield mounting medium (H-1200, Vector Laboratories). At least 100 nuclei have been assessed for each condition and each replicate using the using the CellProfiler image analysis software, version 3.1.9 (McQuin C. et al., 2018).

5.4 Protein extraction and immunoblotting

Cells were washed twice in cold phosphate buffered saline (PBS). Total protein was extracted using RIPA buffer (150 mM NaCl, 10 mM Tris, pH 7.2, 0.1 % SDS, 1.0 % Triton X-100, 5 mM EDTA, pH 8.0) containing a protease inhibitor cocktail (Roche Applied Science, Indianapolis, IN, USA). Once lysed, it centrifuges at 1400g by 30' at 4 °C and takes the supernatant containing the proteins that is stored in ice. Protein concentration was determined using Bradford Reagent (Sigma-Aldrich, Milano, Italy). Total protein extracts (30 μg) were separated by SDS-PAGE and transferred to nitrocellulose membranes (Whatman, Germany). Membranes were blocked in phosphate-buffered saline (PBS) with 0.1% Tween 20 (PBS-T) containing 5% fat-free dry milk for 1 h and then incubated overnight at 4°C with primary antibodies targeting p16(Ink4a) (1:200; sc-377412, Santa Cruz Biotechnology), SIRT1 (1:1000; ab12193, Abcam), cGAS (1:1000; clone D1D3G #15102, Cell Signaling), STING (1:1000; clone D2P2F, #13647, Cell Signaling) IRF-3 (1:2000; Cat. NO. GTX133768, GeneTex), TLR-9 (1:1000; clone 26C593.2, Cat. NO. NBP2-24729, Novus Biologicals), RNase H2C (1:500; Cat. NO. 16518-1-AP, Proteintech). Subsequently they were incubated with a secondary antibody conjugated to horseradish peroxidase (HRP)-conjugated antibody (Vector, USA) for 1 h at room temperature.

Immunoreactive proteins were visualized using ECL Plus chemiluminescence substrate (GE Healthcare, Pittsburgh, PA, USA); the autoradiographic films thus obtained were quantified

using ImageJ2 software (Rueden C.T. et al., 2017). Membranes were incubated with anti β-actin diluted 1:3000 (# 3700, Cell Signaling) as normalizer. Independent samples t-test was used to analyse the differences between samples. p values < 0.05 were considered significant.

5.5 Cytoplasmic hybrids detection by immunofluorescence

Controls and hyperglycemic treated cells, were tripsinized and seeded on polylysine coated and autoclaved coverslips. Cells were washed twice with PBS and then fixed in 4% paraformaldehyde in PBS for 1 h at 4°C. After three washes in blocking buffer (5% BSA, 0.3% Tryton X-100 in PBS) they were incubated with anti-DNA-RNA hybrid antibody (dilution 1:100; clone S9.6, Cat. No. MABE1095, MerckMillipore, CA, USA), overnight at 4°C. Cells were washed in staining buffer (TBST with 0.1% BSA (A9647-50G, Sigma)) and incubated with secondary Alexa Fluor™ 568 goat anti-mouse IgG (H+L; dilution 1:2000, Cat. NO. A11031, Invitrogen) at room temperature in staining buffer for 1 h in wet room.

After a wash in PBS, cells were stained with nuclear HOECHST 33342 (cat. no. H-3570; Molecular Probes, USA) at 1:5000 dilution in PBS for 5 min, coverslipped with Vectashield mounting medium (H-1200, Vector Laboratories) and viewed in a fluorescence microscope. At least 200 nuclei have been assessed for each condition and each replicate using the using the CellProfiler image analysis software, version 3.1.9 (McQuin C. et al., 2018).

5.5.1 RNase III and RNase T1 enzymatic treatment

Formaldehyde-fixed samples were washed once with PBS, and then incubated in permeabilization buffer (PBS with 0.1% Triton X-100) for 10 minutes. Samples were then incubated in staining buffer (TBST with 0.1% BSA) for 10 minutes with rocking. Enzymatic treatments were done in staining buffer supplemented with 3 mM magnesium chloride with 1:200 dilutions of RNase T1 (EN0541, Thermo Fisher), RNase III (ShortCut RNase III, M0245S, New England Biolabs) and incubated with rocking for 1 hour. Samples were subsequently

washed with staining buffer for 10 minutes with rocking and incubated overnight with primary antibody.

5.6 Cytoplasmic dsDNA detection by immunofluorescence

Cells were seeded and fixed as describe above. Immunofluorescence was performed according to the manufacturer's instructions. Briefly, cells were incubating with 0.3% Triton X-100 solution in PBS 1X with rocking. After three PBS washes for 5 min, cells were incubated with 1% BSA, in PBST for 30 min to block unspecific binding of the antibody. The incubation of Anti-dsDNA antibody (1:100, cat. NO. ab27156, clone 35I9 DNA, Abcam, UK) was performed in 1% BSA in PBST in a humidified chamber for 1 h overnight at 4°C. Cells were washed in PBS and incubated with secondary anti-mouse Alexa Fluor™ 568 goat anti-mouse IgG (H+L; dilution 1:2000, Cat. NO. A11031, Invitrogen, Life Technologies Corporation), at room temperature in 1% BSA in PBST for 1 h. The nuclear chromatin was stained with HOECHST 33,342 (cat. no. H-3570; Molecular Probes, USA) at 1:5000 dilution in PBS for 15 min. At least 200 nuclei have been assessed for each condition and each replicate using the using the CellProfiler image analysis software, version 3.1.9 (McQuin C. et al., 2018).

5.7 Visualization of cytoplasmatic telomere sequences by fluorescent in situ hybridization (FISH)

A probe was used to detect the presence of telomere DNA at the cytoplasmic level, capable of tying the CCATTG telomere sequence and emitting fluorescence, Telomere PNA Fisch kit/Fitc (Dako, cat, NO. K5325, Agilent, CA, USA). The cells were fixed on slides by methanol passages for 10 minutes and acetone for 1 minute. The slides were treated following the procedure recommended by the product datasheet.

5.8 Statistical analysis

Data are presented as the mean ± SD from three replicates. All data were processed by SPSS software (version 22.0). Student's t test and one-way analysis of variance were used to determine the statistical differences among different treatments. A P-value <0.05 was considered statistically significant.

6 REFERENCES

Aguilera Andrés, Tatiana García-Muse. «R Loops: From Transcription Byproducts to Threats to Genome Stability». Molecular Cell 46, n. 2 (2012): 115–24. https://doi.org/10.1016/j.molcel.2012.04.009.

Aguilera Andrés. «The Connection between Transcription and Genomic Instability». The EMBO Journal 21, n. 3 (2002): 195–201. https://doi.org/10.1093/emboj/21.3.195.

Allison David F. and Gang Greg Wang. «R-Loops: Formation, Function, and Relevance to Cell Stress». Cell Stress 3, n. 2 (2019): 38–46. https://doi.org/10.15698/cst2019.02.175.

Alpert E., A. Gruzman, Y. Riahi, R. Blejter, P. Aharoni, G. Weisinger, J. Eckel, N. Kaiser, e S. Sasson. «Delayed Autoregulation of Glucose Transport in Vascular Endothelial Cells». Diabetologia 48, n. 4 (2005): 752–55. https://doi.org/10.1007/s00125-005-1681-y.

American Diabetes Association. «2. Classification and Diagnosis of Diabetes: Standards of Medical Care in Diabetes-2019». Diabetes Care 42, n. Suppl 1 (2019): S13–28. https://doi.org/10.2337/dc19-S002.

Artsimovitch Irina, e Georgiy A. Belogurov. «Uneven Braking Spins RNA Polymerase into a Pause». Molecular Cell 69, n. 5 (2018): 723–25. https://doi.org/10.1016/j.molcel.2018.02.013.

Baruch Kuti, Aleksandra Deczkowska, Eyal David, Joseph M. Castellano, Omer Miller, Alexander Kertser, Tamara Berkutzki, et al. «Aging. Aging-Induced Type I Interferon Response at the Choroid Plexus Negatively Affects Brain Function». Science (New York, N.Y.) 346, n. 6205 (2014): 89–93. https://doi.org/10.1126/science.1252945.

Baz-Martínez, Maite, Sabela Da Silva-Álvarez, Estefanía Rodríguez, Jorge Guerra, Ahmed El Motiam, Anxo Vidal, Tomás García-Caballero, et al. «Cell senescence is an antiviral defense mechanism». Scientific Reports 6 (2016). https://doi.org/10.1038/srep37007.

Belotserkovskii Boris P., Alexander J. Neil, Syed Shayon Saleh, Jane Hae Soo Shin, Sergei M. Mirkin, e Philip C. Hanawalt. «Transcription Blockage by Homopurine DNA Sequences: Role of Sequence Composition and Single-Strand Breaks». Nucleic Acids Research 41, n. 3 (2013): 1817–28. https://doi.org/10.1093/nar/gks1333.

Belotserkovskii Boris P., Silvia Tornaletti, Alicia D. D'Souza, e Philip C. Hanawalt. «R-Loop Generation during Transcription: Formation, Processing and Cellular Outcomes». DNA Repair 71 (2018): 69–81. https://doi.org/10.1016/j.dnarep.2018.08.009.

Bleier Lea and Stefan Dröse. «Superoxide Generation by Complex III: From Mechanistic Rationales to Functional Consequences». Biochimica Et Biophysica Acta 1827, n. 11–12 (2013): 1320–31. https://doi.org/10.1016/j.bbabio.2012.12.002.

Bonafè Massimiliano, Gianluca Storci, e Claudio Franceschi. «Inflamm-Aging of the Stem Cell Niche: Breast Cancer as a Paradigmatic Example: Breakdown of the Multi-Shell Cytokine Network Fuels Cancer in Aged People».

BioEssays: News and Reviews in Molecular, Cellular and Developmental Biology 34, n. 1 (2012): 40–49. https://doi.org/10.1002/bies.201100104.

Bonafè Massimiliano, Francesco Prattichizzo, Angelica Giuliani, Gianluca Storci, Jacopo Sabbatinelli, Fabiola Olivieri. « Inflamm-aging: Why older men are the most susceptible to SARS-CoV-2 complicated outcomes» Cytokine Growth Factor Rev.2020 Jun; 53:33-37. doi:10.1016/j.cytogfr.2020.04.005. Epub 2020 May 3.

Boque-Sastre Raquel, Marta Soler, Cristina Oliveira-Mateos, Anna Portela, Catia Moutinho, Sergi Sayols, Alberto Villanueva, Manel Esteller, e Sonia Guil. «Head-to-Head Antisense Transcription and R-Loop Formation Promotes Transcriptional Activation». Proceedings of the National Academy of Sciences of the United States of America 112, n. 18 (2015): 5785–90. https://doi.org/10.1073/pnas.1421197112.

Bowling EA, Wang JH, Gong F, Wu W, Neill NJ, Kim IS, Tyagi S, Orellana M, Kurley SJ, Dominguez-Vidaña R, Chung HC, Hsu TY, Dubrulle J, Saltzman AB, Li H, Meena JK, Canlas GM, Chamakuri S, Singh S, Simon LM, Olson CM, Dobrolecki LE, Lewis MT, Zhang B, Golding I, Rosen JM, Young DW, Malovannaya A, Stossi F, Miles G, Ellis MJ, Yu L, Buonamici S, Lin CY, Karlin KL, Zhang XH, Westbrook TF. Spliceosome-targeted therapies trigger an antiviral immune response in triple-negative breast cancer. Cell. 2021 Jan 21;184(2):384-403.e21. doi: 10.1016/j.cell.2020.12.031

Brégnard Christelle, Monsef Benkirane, e Nadine Laguette. «DNA Damage Repair Machinery and HIV Escape from Innate Immune Sensing». Frontiers in Microbiology 5 (2014): 176. https://doi.org/10.3389/fmicb.2014.00176.

Brownlee M. «Biochemistry and Molecular Cell Biology of Diabetic Complications». Nature 414, n. 6865 (2001): 813–20. https://doi.org/10.1038/414813a.

Brownlee Michael. «The Pathobiology of Diabetic Complications: A Unifying Mechanism». Diabetes 54, n. 6 (2005): 1615–25. https://doi.org/10.2337/diabetes.54.6.1615.

Camici Giovanni G., Marzia Schiavoni, Pietro Francia, Markus Bachschmid, Ines Martin-Padura, Martin Hersberger, Felix C. Tanner, et al. «Genetic Deletion of P66(Shc) Adaptor Protein Prevents Hyperglycemia-Induced Endothelial Dysfunction and Oxidative Stress». Proceedings of the National Academy of Sciences of the United States of America 104, n. 12 (2007): 5217–22. https://doi.org/10.1073/pnas.0609656104.

Castellano-Pozo Maikel, José M. Santos-Pereira, Ana G. Rondón, Sonia Barroso, Eloisa Andújar, Mónica Pérez-Alegre, Tatiana García-Muse, e Andrés Aguilera. «R Loops Are Linked to Histone H3 S10 Phosphorylation and Chromatin Condensation». Molecular Cell 52, n. 4 (2013): 583–90. https://doi.org/10.1016/j.molcel.2013.10.006.

Ceccaldi Raphael, Prabha Sarangi, e Alan D. D'Andrea. «The Fanconi Anaemia Pathway: New Players and New Functions». Nature Reviews. Molecular Cell Biology 17, n. 6 (2016): 337–49. https://doi.org/10.1038/nrm.2016.48.

Ceriello Antonio and Roberto Testa. «Antioxidant Anti-Inflammatory Treatment in Type 2 Diabetes». Diabetes Care 32 Suppl 2 (2009): S232-236. https://doi.org/10.2337/dc09-S316.

Cerritelli Susana M., e Robert J. Crouch. «The Balancing Act of Ribonucleotides in DNA». Trends in Biochemical Sciences 41, n. 5 (2016): 434–45. https://doi.org/10.1016/j.tibs.2016.02.005.

Cerritelli Susana M., Ella G. Frolova, Chiguang Feng, Alexander Grinberg, Paul E. Love, e Robert J. Crouch. «Failure to Produce Mitochondrial DNA Results in Embryonic Lethality in Rnaseh1 Null Mice». Molecular Cell 11, n. 3 (2003): 807–15. https://doi.org/10.1016/s1097-2765(03)00088-1.

Chakraborty Prasun, e Frank Grosse. «Human DHX9 Helicase Preferentially Unwinds RNA-Containing Displacement Loops (R-Loops) and G-Quadruplexes». DNA Repair 10, n. 6 (2011): 654–65. https://doi.org/10.1016/j.dnarep.2011.04.013.

Chédin Frédéric. «Nascent Connections: R-Loops and Chromatin Patterning». Trends in Genetics: TIG 32, n. 12 (2016): 828–38. https://doi.org/10.1016/j.tig.2016.10.002.

Chen Poshen B., Hsiuyi V. Chen, Diwash Acharya, Oliver J. Rando, e Thomas G. Fazzio. «R Loops Regulate Promoter-Proximal Chromatin Architecture and Cellular Differentiation». Nature Structural & Molecular Biology 22, n. 12 (2015): 999–1007. https://doi.org/10.1038/nsmb.3122.

Chen Xiangyuan, Qichao Wu, Hui Jiang, Jiaqiang Wang, Yanjun Zhao, Yajun Xu, Minmin Zhu. «SET8 is involved in the regulation of hyperglycemic memory in human umbilical endothelial cells». Acta Biochim Biophys Sin (Shanghai). 2018 Jul 1;50(7):635-642. doi: 10.1093/abbs/gmy051.

Cheng Alice Y. Y. and Lawrence A. Leiter. «Glucose Lowering and Cardiovascular Disease: What Do We Know and What Should We Do?» European Journal of Cardiovascular Prevention and Rehabilitation: Official Journal of the European Society of Cardiology, Working Groups on Epidemiology & Prevention and Cardiac Rehabilitation and Exercise Physiology 17 Suppl 1 (2010): S25-31. https://doi.org/10.1097/01.hjr.0000368194.32356.5f.

Chong Shin Yen, Sam Cutler, Jing-Jer Lin, Cheng-Hung Tsai, Huai-Kuang Tsai, Sue Biggins, Toshio Tsukiyama, Yi-Chen Lo, e Cheng-Fu Kao. «H3K4 Methylation at Active Genes Mitigates Transcription-Replication Conflicts during Replication Stress». Nature Communications 11, n. 1 (2020): 809. https://doi.org/10.1038/s41467-020-14595-4.

Chow Jonathan, Kate M. Franz, e Jonathan C. Kagan. «PRRs Are Watching You: Localization of Innate Sensing and Signaling Regulators». Virology 479–480 (2015): 104–9. https://doi.org/10.1016/j.virol.2015.02.051.

Chung Hae Young, Dae Hyun Kim, Eun Kyeong Lee, Ki Wung Chung, Sangwoon Chung, Bonggi Lee, Arnold Y Seo, Jae Heun Chung, Young Suk Jung, Eunok Im, Jaewon Lee, Nam Deuk Kim, Yeon Ja Choi, Dong Soon Im, Byung Pal Yu. «Redefining Chronic Inflammation in Aging and Age-Related Diseases: Proposal of the Senoinflammation Concept». Aging Dis. 2019 Apr 1;10(2):367-382. doi: 10.14336/AD.2018.0324. eCollection 2019 Apr.

Cohen G., Y. Riahi, E. Alpert, A. Gruzman, e S. Sasson. «The Roles of Hyperglycaemia and Oxidative Stress in the Rise and Collapse of the Natural Protective Mechanism against Vascular Endothelial Cell Dysfunction in Diabetes». Archives of Physiology and Biochemistry 113, n. 4–5 (2007): 259–67. https://doi.org/10.1080/13813450701783513.

Cohen Sarah, Nadine Puget, Yea-Lih Lin, Thomas Clouaire, Marion Aguirrebengoa, Vincent Rocher, Philippe Pasero, Yvan Canitrot, e Gaëlle Legube. «Senataxin Resolves RNA:DNA Hybrids Forming at DNA Double-Strand Breaks to Prevent Translocations». Nature Communications 9, n. 1 (2018): 533. https://doi.org/10.1038/s41467-018-02894-w.

Coppé J.P., Patil C.K., Rodier F, Sun Y, Muñoz DP, Goldstein J, Nelson PS, Desprez PY, Campisi J. Senescence-associated secretory phenotypes reveal cell-nonautonomous functions of oncogenic RAS and the p53 tumor suppressor. PLoS Biol. 2008 Dec 2;6(12):2853-68. doi: 10.1371/journal.pbio.0060301

Coppe J.P., Desprez P.Y,. Krtolica A, Campisi J. The senescence-associated secretory phenotype: the dark side of tumor suppression. Annu. Rev. Pathol., 5 (2010) pp. 99-118

Coppey L. J., J. S. Gellett, E. P. Davidson, J. A. Dunlap, D. D. Lund, e M. A. Yorek. «Effect of Antioxidant Treatment of Streptozotocin-Induced Diabetic Rats on Endoneurial Blood Flow, Motor Nerve Conduction Velocity, and Vascular Reactivity of Epineurial Arterioles of the Sciatic Nerve». Diabetes 50, n. 8 (2001): 1927–37. https://doi.org/10.2337/diabetes.50.8.1927.

Cosentino F., K. Hishikawa, Z. S. Katusic, e T. F. Lüscher. «High Glucose Increases Nitric Oxide Synthase Expression and Superoxide Anion Generation in Human Aortic Endothelial Cells». Circulation 96, n. 1 (1997): 25–28. https://doi.org/10.1161/01.cir.96.1.25.

Costantino Lorenzo, Douglas Koshland. «Genome-Wide Map of R-Loop-Induced Damage Reveals How a Subset of R-Loops Contributes to Genomic Instability». Molecular Cell 71, n. 4 (2018): 487-497.e3. https://doi.org/10.1016/j.molcel.2018.06.037.

Costantino Lorenzo, e Douglas Koshland. «The Yin and Yang of R-Loop Biology». Current Opinion in Cell Biology 34 (2015): 39–45. https://doi.org/10.1016/j.ceb.2015.04.008.

Cristini Agnese, Matthias Groh, Maiken S. Kristiansen, e Natalia Gromak. «RNA/DNA Hybrid Interactome Identifies DXH9 as a Molecular Player in Transcriptional Termination and R-Loop-Associated DNA Damage». Cell Reports 23, n. 6 (2018): 1891–1905. https://doi.org/10.1016/j.celrep.2018.04.025.

Crossley Madzia P., Michael Bocek, e Karlene A. Cimprich. «R-Loops as Cellular Regulators and Genomic Threats». Molecular Cell 73, n. 3 (2019): 398–411. https://doi.org/10.1016/j.molcel.2019.01.024.

Crow Yanick J., Andrea Leitch, Bruce E. Hayward, Anna Garner, Rekha Parmar, Elen Griffith, Manir Ali, et al. «Mutations in Genes Encoding Ribonuclease H2 Subunits Cause Aicardi-Goutières Syndrome and Mimic Congenital Viral Brain Infection». Nature Genetics 38, n. 8 (2006): 910–16. https://doi.org/10.1038/ng1842.

D'Alessandro Giuseppina, Donna Rose Whelan, Sean Michael Howard, Valerio Vitelli, Xavier Renaudin, Marek Adamowicz, Fabio Iannelli, et al. «BRCA2 Controls DNA:RNA Hybrid Level at DSBs by Mediating RNase H2 Recruitment». Nature Communications 9, n. 1 (2018): 5376.

Davidson Sean M. and Derek M. Yellon. «Does Hyperglycemia Reduce Proliferation or Increase Apoptosis?» American Journal of Physiology. Heart and Circulatory Physiology 291, n. 3 (2006): H1486; author reply H1487. https://doi.org/10.1152/ajpheart.00301.2006.

De Vriese A. S., T. J. Verbeuren, J. Van de Voorde, N. H. Lameire, e P. M. Vanhoutte. «Endothelial Dysfunction in Diabetes». British Journal of Pharmacology 130, n. 5 (2000): 963–74. https://doi.org/10.1038/sj.bjp.0703393.

Dempsey Alan, e Andrew G. Bowie. «Innate Immune Recognition of DNA: A Recent History». Virology 479–480 (2015): 146–52. https://doi.org/10.1016/j.virol.2015.03.013.

Dou Zhixun, Kanad Ghosh, Maria Grazia Vizioli, Jiajun Zhu, Payel Sen, Kirk J. Wangensteen, Johayra Simithy, et al. «Cytoplasmic Chromatin Triggers Inflammation in Senescence and Cancer». Nature 550, n. 7676 (2017): 402–6. https://doi.org/10.1038/nature24050.

El Hage Aziz, Sarah L. French, Ann L. Beyer, e David Tollervey. «Loss of Topoisomerase I Leads to R-Loop-Mediated Transcriptional Blocks during Ribosomal RNA Synthesis». Genes & Development 24, n. 14 (2010): 1546–58. https://doi.org/10.1101/gad.573310.

Engerman R., J. M. Bloodworth, e S. Nelson. «Relationship of Microvascular Disease in Diabetes to Metabolic Control». Diabetes 26, n. 8 (1977): 760–69. https://doi.org/10.2337/diab.26.8.760.

Ewald Sarah E., Bettina L. Lee, Laura Lau, Katherine E. Wickliffe, Guo-Ping Shi, Harold A. Chapman, e Gregory M. Barton. «The Ectodomain of Toll-like Receptor 9 Is Cleaved to Generate a Functional Receptor». Nature 456, n. 7222 (2008): 658–62. https://doi.org/10.1038/nature07405.

Fane, Mitchell, e Ashani T. Weeraratna. «How the Ageing Microenvironment Influences Tumour Progression». Nature Reviews. Cancer 20, n. 2 (2020): 89–106. https://doi.org/10.1038/s41568-019-0222-9.

Fuller-Pace Frances V. «DEAD Box RNA Helicase Functions in Cancer». RNA Biology 10, n. 1 (2013): 121–32. https://doi.org/10.4161/rna.23312.

Gao Daxing, Tuo Li, Xiao-Dong Li, Xiang Chen, Quan-Zhen Li, Mary Wight-Carter, e Zhijian J. Chen. «Activation of Cyclic GMP-AMP Synthase by Self-DNA Causes Autoimmune Diseases». Proceedings of the National Academy of Sciences of the United States of America 112, n. 42 (2015): E5699-5705. https://doi.org/10.1073/pnas.1516465112.

García-Muse Tatiana, e Andrés Aguilera. «R Loops: From Physiological to Pathological Roles». Cell 179, n. 3 (2019): 604–18. https://doi.org/10.1016/j.cell.2019.08.055.

García-Pichardo Desiré, Juan C. Cañas, María L. García-Rubio, Belén Gómez-González, Ana G. Rondón, e Andrés Aguilera. «Histone Mutants Separate R Loop Formation from Genome Instability Induction». Molecular Cell 66, n. 5 (2017): 597-609.e5. https://doi.org/10.1016/j.molcel.2017.05.014.

Gentili Matteo and Nicolas Manel. «CGAS-STING Do It Again: Pivotal Role in RNase H2 Genetic Disease». The EMBO Journal 35, n. 8 (2016): 796–97. https://doi.org/10.15252/embj.201694226.

Gerö Domokos and Csaba Szabo. «Glucocorticoids Suppress Mitochondrial Oxidant Production via Upregulation of Uncoupling Protein 2 in Hyperglycemic Endothelial Cells». PloS One 11, n. 4 (2016): e0154813. https://doi.org/10.1371/journal.pone.0154813.

Gerö Domokos and Csaba Szabó. «Poly(ADP-Ribose) Polymerase: A New Therapeutic Target?» Current Opinion in Anaesthesiology 21, n. 2 (2008): 111–21. https://doi.org/10.1097/ACO.0b013e3282f63c15.

Gerő Domokos, Roberta Torregrossa, Alexis Perry, Alicia Waters, Sophie Le-Trionnaire, Jacqueline L. Whatmore, Mark Wood, e Matthew Whiteman. «The Novel Mitochondria-Targeted Hydrogen Sulfide (H2S) Donors AP123 and AP39 Protect against Hyperglycemic Injury in Microvascular Endothelial Cells in Vitro». Pharmacological Research 113, n. Pt A (2016): 186–98. https://doi.org/10.1016/j.phrs.2016.08.019.

Gerő Domokos. Hyperglycemia-Induced Endothelial Dysfunction. Endothelial Dysfunction - Old Concepts and New Challenges. (2018): doi:10.5772/intechopen.71433

Giacco Ferdinando and Michael Brownlee. «Oxidative Stress and Diabetic Complications». Circulation Research 107, n. 9 (2010): 1058–70. https://doi.org/10.1161/CIRCRESAHA.110.223545.

Giannini Marta, Aleix Bayona-Feliu, Daisy Sproviero, Sonia I. Barroso, Cristina Cereda, e Andrés Aguilera. «TDP-43 Mutations Link Amyotrophic Lateral Sclerosis with R-Loop Homeostasis and R Loop-Mediated DNA Damage». PLoS Genetics 16, n. 12 (2020): e1009260. https://doi.org/10.1371/journal.pgen.1009260.

Ginno Paul A., Paul L. Lott, Holly C. Christensen, Ian Korf, e Frédéric Chédin. «R-Loop Formation Is a Distinctive Characteristic of Unmethylated Human CpG Island Promoters». Molecular Cell 45, n. 6 (2012): 814–25. https://doi.org/10.1016/j.molcel.2012.01.017.

Glück Selene, Baptiste Guey, Muhammet Fatih Gulen, Katharina Wolter, Tae-Won Kang, Niklas Arndt Schmacke, Anne Bridgeman, Jan Rehwinkel, Lars Zender, e Andrea Ablasser. «Innate Immune Sensing of Cytosolic Chromatin Fragments through CGAS Promotes Senescence». Nature Cell Biology 19, n. 9 (2017): 1061–70. https://doi.org/10.1038/ncb3586.

Gómez-González Belén, María García-Rubio, Rodrigo Bermejo, Hélène Gaillard, Katsuhiko Shirahige, Antonio Marín, Marco Foiani, e Andrés Aguilera. «Genome-Wide Function of THO/TREX in Active Genes Prevents R-Loop-Dependent Replication Obstacles». The EMBO Journal 30, n. 15 (2011): 3106–19. https://doi.org/10.1038/emboj.2011.206.

Goveia Jermaine, Peter Stapor, Peter Carmeliet. «Principles of Targeting Endothelial Cell Metabolism to Treat Angiogenesis and Endothelial Cell Dysfunction in Disease». EMBO Molecular Medicine 6, n. 9 (2014): 1105–20. https://doi.org/10.15252/emmm.201404156.

Graf Marco, Diego Bonetti, Arianna Lockhart, Kamar Serhal, Vanessa Kellner, André Maicher, Pascale Jolivet, Maria Teresa Teixeira, e Brian Luke. «Telomere Length Determines TERRA and R-Loop Regulation through the Cell Cycle». Cell 170, n. 1 (2017): 72-85.e14. https://doi.org/10.1016/j.cell.2017.06.006.

Guedes Guilherme, James C. Tsai, e Nils A. Loewen. «Glaucoma and Aging». Current Aging Science 4, n. 2 (2011): 110–17. https://doi.org/10.2174/1874609811104020110.

Haj-Yehia A. I., T. Nassar, P. Assaf, H. Nassar, e E. E. Anggård. «Effects of the Superoxide Dismutase-Mimic Compound TEMPOL on Oxidant Stress-Mediated Endothelial Dysfunction». Antioxidants & Redox Signaling 1, n. 2 (1999): 221–32. https://doi.org/10.1089/ars.1999.1.2-221.

Halász László, Zsolt Karányi, Beáta Boros-Oláh, Tímea Kuik-Rózsa, Éva Sipos, Éva Nagy, Ágnes Mosolygó-L, et al. «RNA-DNA Hybrid (R-Loop) Immunoprecipitation Mapping: An Analytical Workflow to Evaluate Inherent Biases». Genome Research 27, n. 6 (2017): 1063–73. https://doi.org/10.1101/gr.219394.116.

Harjes U., K. Bensaad, e A. L. Harris. «Endothelial Cell Metabolism and Implications for Cancer Therapy». British Journal of Cancer 107, n. 8 (2012): 1207–12. https://doi.org/10.1038/bjc.2012.398.

Härtlova Anetta, Saskia F. Erttmann, Faizal Am Raffi, Anja M. Schmalz, Ulrike Resch, Sharath Anugula, Stefan Lienenklaus, et al. «DNA Damage Primes the Type I Interferon System via the Cytosolic DNA Sensor STING to Promote Anti-Microbial Innate Immunity». Immunity 42, n. 2 (2015): 332–43. https://doi.org/10.1016/j.immuni.2015.01.012.

Haspula Dhanush, Andrew K Vallejos, Timothy M Moore, Namrata Tomar, Ranjan K Dash, Brian R Hoffmann. «Influence of a Hyperglycemic Microenvironment on a Diabetic Versus Healthy Rat Vascular Endothelium Reveals Distinguishable Mechanistic and Phenotypic Responses». Front Physiol. 2019 May 10;10:558. doi: 10.3389/fphys.2019.00558. eCollection 2019.

Heilig C. W., L. A. Concepcion, B. L. Riser, S. O. Freytag, M. Zhu, e P. Cortes. «Overexpression of Glucose Transporters in Rat Mesangial Cells Cultured in a Normal Glucose Milieu Mimics the Diabetic Phenotype». The Journal of Clinical Investigation 96, n. 4 (1995): 1802–14. https://doi.org/10.1172/JCI118226.

Hodroj Dana, Bénédicte Recolin, Kamar Serhal, Susan Martinez, Nikolay Tsanov, Raghida Abou Merhi, e Domenico Maiorano. «An ATR-Dependent Function for the Ddx19 RNA Helicase in Nuclear R-Loop Metabolism». The EMBO Journal 36, n. 9 (2017): 1182–98. https://doi.org/10.15252/embj.201695131.

Horváth E. M., R. Benko, L. Kiss, M. Murányi, T. Pék, K. Fekete, T. Bárány, A. Somlai, A. Csordás, e C. Szabo. «Rapid "glycaemic Swings" Induce Nitrosative Stress, Activate Poly(ADP-Ribose) Polymerase and Impair Endothelial Function in a Rat Model of Diabetes Mellitus». Diabetologia 52, n. 5 (2009): 952–61. https://doi.org/10.1007/s00125-009-1304-0.

Houtkooper Riekelt H., Eija Pirinen, e Johan Auwerx. «Sirtuins as Regulators of Metabolism and Healthspan». Nature Reviews. Molecular Cell Biology 13, n. 4 (2012): 225–38. https://doi.org/10.1038/nrm3293.

Humphreys D, ElGhazaly M, Frisan T. Senescence and Host-Pathogen Interactions. Cells. 2020 Jul 21;9(7):1747. doi: 10.3390/cells9071747.

Hyjek Malwina, Małgorzata Figiel, e Marcin Nowotny. «RNases H: Structure and Mechanism». DNA Repair 84 (2019): 102672. https://doi.org/10.1016/j.dnarep.2019.102672.

Ihnat M. A., J. E. Thorpe, C. D. Kamat, C. Szabó, D. E. Green, L. A. Warnke, Z. Lacza, et al. «Reactive Oxygen Species Mediate a Cellular "memory" of High Glucose Stress Signalling». Diabetologia 50, n. 7 (2007): 1523–31. https://doi.org/10.1007/s00125-007-0684-2.

Ihnat M. A., J. E. Thorpe, e A. Ceriello. «Hypothesis: The "Metabolic Memory", the New Challenge of Diabetes». Diabetic Medicine: A Journal of the British Diabetic Association 24, n. 6 (2007): 582–86. https://doi.org/10.1111/j.1464-5491.2007.02138.x.

Ishikawa Hiroki and Glen N. Barber. «STING Is an Endoplasmic Reticulum Adaptor That Facilitates Innate Immune Signalling». Nature 455, n. 7213 (2008): 674–78. https://doi.org/10.1038/nature07317.

Jain Sushil K., Rebeca Bull, Justin L. Rains, Pat F. Bass, Steven N. Levine, Sudha Reddy, Robert McVie, e Joseph A. Bocchini. «Low Levels of Hydrogen Sulfide in the Blood of Diabetes Patients and Streptozotocin-Treated Rats Causes Vascular Inflammation?» Antioxidants & Redox Signaling 12, n. 11 (2010): 1333–37. https://doi.org/10.1089/ars.2009.2956.

James Paul A., e Kevin Talbot. «The Molecular Genetics of Non-ALS Motor Neuron Diseases». Biochimica Et Biophysica Acta 1762, n. 11–12 (2006): 986–1000. https://doi.org/10.1016/j.bbadis.2006.04.003.

Janeway Charles A. and Ruslan Medzhitov. «Innate Immune Recognition». Annual Review of Immunology 20 (2002): 197–216. https://doi.org/10.1146/annurev.immunol.20.083001.084359.

Jarajapu Yagna P. R. and Maria B. Grant. «The Promise of Cell-Based Therapies for Diabetic Complications: Challenges and Solutions». Circulation Research 106, n. 5 (2010): 854–69. https://doi.org/10.1161/CIRCRESAHA.109.213140.

Kaiser N., S. Sasson, E. P. Feener, N. Boukobza-Vardi, S. Higashi, D. E. Moller, S. Davidheiser, R. J. Przybylski, e G. L. King. «Differential Regulation of Glucose Transport and Transporters by Glucose in Vascular Endothelial and Smooth Muscle Cells». Diabetes 42, n. 1 (1993): 80–89. https://doi.org/10.2337/diab.42.1.80.

Kang Jin Young, Tatiana V. Mishanina, Michael J. Bellecourt, Rachel Anne Mooney, Seth A. Darst, e Robert Landick. «RNA Polymerase Accommodates a Pause RNA Hairpin by Global Conformational Rearrangements That Prolong Pausing». Molecular Cell 69, n. 5 (2018): 802-815.e5. https://doi.org/10.1016/j.molcel.2018.01.018.

Karbach Susanne, Thomas Jansen, Sven Horke, Tjebo Heeren, Alexander Scholz, Meike Coldewey, Angelica Karpi, Michael Hausding, Swenja Kröller-Schön, Matthias Oelze, Thomas Münzel, Andreas Daiber. «Hyperglycemia and oxidative stress in cultured endothelial cells--a comparison of primary endothelial cells with an immortalized endothelial cell line». J Diabetes Complications. May-Jun 2012;26(3):155-62. doi: 10.1016/j.jdiacomp.2012.03.011. Epub 2012 Apr 20.

Kim Sangin, Nalae Kang, Su Hyung Park, James Wells, Taejoo Hwang, Eunjin Ryu, Byung-Gyu Kim, et al. «ATAD5 Restricts R-Loop Formation through PCNA Unloading and RNA Helicase Maintenance at the Replication Fork». Nucleic Acids Research 48, n. 13 (2020): 7218–38. https://doi.org/10.1093/nar/gkaa501.

Kim You-Me, Melanie M. Brinkmann, Marie-Eve Paquet, e Hidde L. Ploegh. «UNC93B1 Delivers Nucleotide-Sensing Toll-like Receptors to Endolysosomes». Nature 452, n. 7184 (2008): 234–38. https://doi.org/10.1038/nature06726.

Kim, J.A.; Seong, R.K.; Shin, O.S. Enhanced Viral Replication by Cellular Replicative Senescence. Immune Netw. 2016, 16, 286–295.

Koo Christine Xing'er, Kouji Kobiyama, Yu J. Shen, Nina LeBert, Shandar Ahmad, Muznah Khatoo, Taiki Aoshi, Stephan Gasser, e Ken J. Ishii. «RNA Polymerase III Regulates Cytosolic RNA:DNA Hybrids and Intracellular MicroRNA Expression». The Journal of Biological Chemistry 290, n. 12 (2015): 7463–73. https://doi.org/10.1074/jbc.M115.636365.

Korshunov S. S., V. P. Skulachev, e A. A. Starkov. «High Protonic Potential Actuates a Mechanism of Production of Reactive Oxygen Species in Mitochondria». FEBS Letters 416, n. 1 (1997): 15–18. https://doi.org/10.1016/s0014-5793(97)01159-9.

Krützfeldt A., R. Spahr, S. Mertens, B. Siegmund, e H. M. Piper. «Metabolism of Exogenous Substrates by Coronary Endothelial Cells in Culture». Journal of Molecular and Cellular Cardiology 22, n. 12 (1990): 1393–1404. https://doi.org/10.1016/0022-2828(90)90984-a.

Kumar Santosh, Young-Rae Kim, Ajit Vikram, Asma Naqvi, Qiuxia Li, Modar Kassan, Vikas Kumar, et al. «Sirtuin1-Regulated Lysine Acetylation of P66Shc Governs Diabetes-Induced Vascular Oxidative Stress and Endothelial Dysfunction». Proceedings of the National Academy of Sciences of the United States of America 114, n. 7 (2017): 1714–19. https://doi.org/10.1073/pnas.1614112114.

Kwon SM, Min S, Jeoun UW, Sim MS, Jung GH, Hong SM, Jee BA, Woo HG, Lee C, Yoon G. Global spliceosome activity regulates entry into cellular senescence. FASEB J. 2021 Jan;35(1):e21204. doi: 10.1096/fj.202000395RR.

Lan Yuk Yuen, James M. Heather, Thomas Eisenhaure, Christopher Stuart Garris, David Lieb, Raktima Raychowdhury, e Nir Hacohen. «Extranuclear DNA Accumulates in Aged Cells and Contributes to Senescence and Inflammation». Aging Cell 18, n. 2 (2019): e12901. https://doi.org/10.1111/acel.12901.

Larsen Nicolai Balle, Merete Rasmussen, e Lene Juel Rasmussen. «Nuclear and Mitochondrial DNA Repair: Similar Pathways? » Mitochondrion 5, n. 2 (2005): 89–108. https://doi.org/10.1016/j.mito.2005.02.002.

Leopold Jane A., Ying-Yi Zhang, Anne W. Scribner, Robert C. Stanton, e Joseph Loscalzo. «Glucose-6-Phosphate Dehydrogenase Overexpression Decreases Endothelial Cell Oxidant Stress and Increases Bioavailable Nitric Oxide». Arteriosclerosis, Thrombosis, and Vascular Biology 23, n. 3 (2003): 411–17. https://doi.org/10.1161/01.ATV.0000056744.26901.BA.

Li Lei, Devon R. Germain, Ho-Yin Poon, Matthew R. Hildebrandt, Elizabeth A. Monckton, Darin McDonald, Michael J. Hendzel, e Roseline Godbout. «DEAD Box 1 Facilitates Removal of RNA and Homologous Recombination at DNA Double-Strand Breaks». Molecular and Cellular Biology 36, n. 22 (2016): 2794–2810. https://doi.org/10.1128/MCB.00415-16.

Li Xialu, e James L. Manley. «Cotranscriptional Processes and Their Influence on Genome Stability». Genes & Development 20, n. 14 (2006): 1838–47. https://doi.org/10.1101/gad.1438306.

Li Xialu, e James L. Manley. «Inactivation of the SR Protein Splicing Factor ASF/SF2 Results in Genomic Instability». Cell 122, n. 3 (2005): 365–78. https://doi.org/10.1016/j.cell.2005.06.008.

Lienenklaus Stefan, Marius Cornitescu, Natalia Zietara, Marcin Łyszkiewicz, Nelson Gekara, Jadwiga Jabłónska, Frank Edenhofer, et al. «Novel Reporter Mouse Reveals Constitutive and Inflammatory Expression of IFN-Beta in Vivo». Journal of Immunology (Baltimore, Md.: 1950) 183, n. 5 (2009): 3229–36. https://doi.org/10.4049/jimmunol.0804277.

Lima Walt F., Heather M. Murray, Sagar S. Damle, Christopher E. Hart, Gene Hung, Cheryl Li De Hoyos, Xue-Hai Liang, e Stanley T. Crooke. «Viable RNaseH1 Knockout Mice Show RNaseH1 Is Essential for R Loop Processing, Mitochondrial and Liver Function». Nucleic Acids Research 44, n. 11 (2016): 5299–5312. https://doi.org/10.1093/nar/gkw350.

Loo Tze Mun, Kenichi Miyata, Yoko Tanaka, e Akiko Takahashi. «Cellular Senescence and Senescence-Associated Secretory Phenotype via the CGAS-STING Signaling Pathway in Cancer». Cancer Science 111, n. 2 (2020): 304–11. https://doi.org/10.1111/cas.14266.

Loomans Cindy J. M., Eelco J. P. de Koning, Frank J. T. Staal, Maarten B. Rookmaaker, Caroline Verseyden, Hetty C. de Boer, Marianne C. Verhaar, Branko Braam, Ton J. Rabelink, e Anton-Jan van Zonneveld. «Endothelial Progenitor Cell Dysfunction: A Novel Concept in the Pathogenesis of Vascular Complications of Type 1 Diabetes». Diabetes 53, n. 1 (2004): 195–99. https://doi.org/10.2337/diabetes.53.1.195.

López-Otín, Carlos, Maria A. Blasco, Linda Partridge, Manuel Serrano, e Guido Kroemer. «The Hallmarks of Aging». Cell 153, n. 6 (2013): 1194–1217. https://doi.org/10.1016/j.cell.2013.05.039.

Luecke Stefanie, Andreas Holleufer, Maria H. Christensen, Kasper L. Jønsson, Gerardo A. Boni, Lambert K. Sørensen, Mogens Johannsen, Martin R. Jakobsen, Rune Hartmann, e Søren R. Paludan. «CGAS Is Activated by DNA in a Length-Dependent Manner». EMBO Reports 18, n. 10 (2017): 1707–15. https://doi.org/10.15252/embr.201744017.

Ma Ruihua, Tatiana P. Ortiz Serrano, Jennifer Davis, Andrew D. Prigge, e Karen M. Ridge. «The CGAS-STING Pathway: The Role of Self-DNA Sensing in Inflammatory Lung Disease». FASEB Journal: Official Publication of the Federation of American Societies for Experimental Biology 34, n. 10 (2020): 13156–70. https://doi.org/10.1096/fj.202001607R.

Maeda Morihiko, Toshio Hayashi, Natsumi Mizuno, Yuichi Hattori, e Masafumi Kuzuya. «Intermittent High Glucose Implements Stress-Induced Senescence in Human Vascular Endothelial Cells: Role of Superoxide Production by NADPH Oxidase». PloS One 10, n. 4 (2015): e0123169. https://doi.org/10.1371/journal.pone.0123169.

Mailloux Ryan J. and Mary-Ellen Harper. «Uncoupling Proteins and the Control of Mitochondrial Reactive Oxygen Species Production». Free Radical Biology & Medicine 51, n. 6 (15 settembre 2011): 1106–15. https://doi.org/10.1016/j.freeradbiomed.2011.06.022.

Makino A., B. T. Scott, e W. H. Dillmann. «Mitochondrial Fragmentation and Superoxide Anion Production in Coronary Endothelial Cells from a Mouse Model of Type 1 Diabetes». Diabetologia 53, n. 8 (2010): 1783–94. https://doi.org/10.1007/s00125-010-1770-4.

Mankan Arun K, Tobias Schmidt, Dhruv Chauhan, Marion Goldeck, Klara Höning, Moritz Gaidt, Andrew V Kubarenko, Liudmila Andreeva, Karl-Peter Hopfner, e Veit Hornung. «Cytosolic RNA:DNA hybrids activate the cGAS–STING axis». The EMBO Journal 33, n. 24 (2014): 2937–46. https://doi.org/10.15252/embj.201488726.

Marabitti Veronica, Giorgia Lillo, Eva Malacaria, Valentina Palermo, Massimo Sanchez, Pietro Pichierri, e Annapaola Franchitto. «ATM Pathway Activation Limits R-Loop-Associated Genomic Instability in Werner Syndrome Cells». Nucleic Acids Research 47, n. 7 (2019): 3485–3502. https://doi.org/10.1093/nar/gkz025.

Matsui Misaki, Ryo Sakasai, Masako Abe, Yusuke Kimura, Shoki Kajita, Wakana Torii, Yoko Katsuki, et al. «USP42 Enhances Homologous Recombination Repair by Promoting R-Loop Resolution with a DNA-RNA Helicase DHX9». Oncogenesis 9, n. 6 (2020): 60. https://doi.org/10.1038/s41389-020-00244-4.

McCall Matthew N., Oliver A. Kent, Jianshi Yu, Karen Fox-Talbot, Ari L. Zaiman, e Marc K. Halushka. «MicroRNA Profiling of Diverse Endothelial Cell Types». BMC Medical Genomics 4 (2011): 78. https://doi.org/10.1186/1755-8794-4-78.

McHugh Domhnall, e Jesús Gil. «Senescence and Aging: Causes, Consequences, and Therapeutic Avenues». The Journal of Cell Biology 217, n. 1 (2018): 65–77. https://doi.org/10.1083/jcb.201708092.

McKelvey Kelly J., John Highton, e Paul A. Hessian. «Cell-Specific Expression of TLR9 Isoforms in Inflammation». Journal of Autoimmunity 36, n. 1 (2011): 76–86. https://doi.org/10.1016/j.jaut.2010.11.001.

McQuin Claire, Allen Goodman, Vasiliy Chernyshev, Lee Kamentsky, Beth A. Cimini, Kyle W. Karhohs, Minh Doan, et al. «CellProfiler 3.0: Next-Generation Image Processing for Biology». PLOS Biology 16, n. 7 (2018): e2005970. https://doi.org/10.1371/journal.pbio.2005970.

McVeigh G. E., G. M. Brennan, G. D. Johnston, B. J. McDermott, L. T. McGrath, W. R. Henry, J. W. Andrews, e J. R. Hayes. «Impaired Endothelium-Dependent and Independent Vasodilation in Patients with Type 2 (Non-Insulin-Dependent) Diabetes Mellitus». Diabetologia 35, n. 8 (1992): 771–76. https://doi.org/10.1007/BF00429099.

Medzhitov Ruslan. «Recognition of Microorganisms and Activation of the Immune Response». Nature 449, n. 7164 (2007): 819–26. https://doi.org/10.1038/nature06246.

Mersaoui Sofiane Y., Zhenbao Yu, Yan Coulombe, Martin Karam, Franciele F. Busatto, Jean-Yves Masson, e Stéphane Richard. «Arginine Methylation of the DDX5 Helicase RGG/RG Motif by PRMT5 Regulates Resolution of RNA:DNA Hybrids». The EMBO Journal 38, n. 15 (2019): e100986. https://doi.org/10.15252/embj.2018100986.

Minamino T., Miyauchi H., Yoshida T., Ishida Y., Yoshida H., Komuro I. Endothelial cell senescence in human atherosclerosis: role of telomere in endothelial dysfunction. Circulation, 105 (2002), pp. 1541-

Morales Julio C., Patricia Richard, Praveen L. Patidar, Edward A. Motea, Tuyen T. Dang, James L. Manley, e David A. Boothman. «XRN2 Links Transcription Termination to DNA Damage and Replication Stress». PLoS Genetics 12, n. 7 (2016): e1006107. https://doi.org/10.1371/journal.pgen.1006107.

Murphy Michael P. «How Mitochondria Produce Reactive Oxygen Species». The Biochemical Journal 417, n. 1 (2009): 1–13. https://doi.org/10.1042/BJ20081386.

Nishikawa T., D. Edelstein, X. L. Du, S. Yamagishi, T. Matsumura, Y. Kaneda, M. A. Yorek, et al. «Normalizing Mitochondrial Superoxide Production Blocks Three Pathways of Hyperglycaemic Damage». Nature 404, n. 6779 (2000): 787–90. https://doi.org/10.1038/35008121.

North Brian J., e David A. Sinclair. «The Intersection between Aging and Cardiovascular Disease». Circulation Research 110, n. 8 (2012): 1097–1108. https://doi.org/10.1161/CIRCRESAHA.111.246876.

Noyman I., M. Marikovsky, S. Sasson, A. H. Stark, K. Bernath, R. Seger, e Z. Madar. «Hyperglycemia Reduces Nitric Oxide Synthase and Glycogen Synthase Activity in Endothelial Cells». Nitric Oxide: Biology and Chemistry 7, n. 3 (2002): 187–93. https://doi.org/10.1016/s1089-8603(02)00106-4.

Okamoto Yusuke, Masako Abe, Akiko Itaya, Junya Tomida, Masamichi Ishiai, Akifumi Takaori-Kondo, Masato Taoka, Toshiaki Isobe, e Minoru Takata. «FANCD2 Protects Genome Stability by Recruiting RNA Processing Enzymes to Resolve R-Loops during Mild Replication Stress». The FEBS Journal 286, n. 1 (2019): 139–50. https://doi.org/10.1111/febs.14700.

Olivieri F, Capri M, Bonafè M, Morsiani C, Jung HJ, Spazzafumo L, Viña J, Suh Y. Circulating miRNAs and miRNA shuttles as biomarkers: Perspective trajectories of healthy and unhealthy aging. Mech Aging Dev. (2017). 165(Pt B):162-170. doi: 10.1016/j.mad.2016.12.004.

Olivieri Fabiola, Francesco Prattichizzo, Johannes Grillari, e Carmela R. Balistreri. «Cellular Senescence and Inflammaging in Age-Related Diseases». Mediators of Inflammation 2018 (2018): 9076485. https://doi.org/10.1155/2018/9076485.

Palau Francesc, e Carmen Espinós. «Autosomal Recessive Cerebellar Ataxias». Orphanet Journal of Rare Diseases 1 (2006): 47. https://doi.org/10.1186/1750-1172-1-47.

Pan S, Liu X, Ma Y, Cao Y, He B. Herpes simplex virus 1 g134. 5 protein inhibits STING activation that restricts viral replication. J Virol. 2018;92:e01015–18.

Park Boyoun, Melanie M. Brinkmann, Eric Spooner, Clarissa C. Lee, You-Me Kim, e Hidde L. Ploegh. «Proteolytic Cleavage in an Endolysosomal Compartment Is Required for Activation of Toll-like Receptor 9». Nature Immunology 9, n. 12 (2008): 1407–14. https://doi.org/10.1038/ni.1669.

Park Su Hyung, Nalae Kang, Eunho Song, Minwoo Wie, Eun A. Lee, Sunyoung Hwang, Deokjae Lee, et al. «ATAD5 Promotes Replication Restart by Regulating RAD51 and PCNA in Response to Replication Stress». Nature Communications 10, n. 1 (2019): 5718. https://doi.org/10.1038/s41467-019-13667-4.

Paulsen Teressa, Pankaj Kumar, M. Murat Koseoglu, e Anindya Dutta. «Discoveries of Extrachromosomal Circles of DNA in Normal and Tumor Cells». Trends in Genetics: TIG 34, n. 4 (2018): 270–78. https://doi.org/10.1016/j.tig.2017.12.010.

Pfeiffer Verena, Jérôme Crittin, Larissa Grolimund, e Joachim Lingner. «The THO Complex Component Thp2 Counteracts Telomeric R-Loops and Telomere Shortening». The EMBO Journal 32, n. 21 (2013): 2861–71. https://doi.org/10.1038/emboj.2013.217.

Pohjoismäki Jaakko L. O., J. Bradley Holmes, Stuart R. Wood, Ming-Yao Yang, Takehiro Yasukawa, Aurelio Reyes, Laura J. Bailey, et al. «Mammalian Mitochondrial DNA Replication Intermediates Are Essentially Duplex but Contain Extensive Tracts of RNA/DNA Hybrid». Journal of Molecular Biology 397, n. 5 (2010): 1144–55. https://doi.org/10.1016/j.jmb.2010.02.029.

Popp H.D., Susanne Brendel, Wolf-Karsten Hofmann, e Alice Fabarius. «Immunofluorescence Microscopy of γH2AX and 53BP1 for Analyzing the Formation and Repair of DNA Double-Strand Breaks». *Journal of Visualized Experiments: JoVE*, n. 129 (3 novembre 2017). https://doi.org/10.3791/56617.

Posse Viktor, Ali Al-Behadili, Jay P. Uhler, Anders R. Clausen, Aurelio Reyes, Massimo Zeviani, Maria Falkenberg, e Claes M. Gustafsson. «RNase H1 Directs Origin-Specific Initiation of DNA Replication in Human Mitochondria». PLoS Genetics 15, n. 1 (2019): e1007781. https://doi.org/10.1371/journal.pgen.1007781.

Promonet Alexy, Ismaël Padioleau, Yaqun Liu, Lionel Sanz, Anna Biernacka, Anne-Lyne Schmitz, Magdalena Skrzypczak, et al. «Topoisomerase 1 Prevents Replication Stress at R-Loop-Enriched Transcription Termination Sites». Nature Communications 11, n. 1 (2020): 3940. https://doi.org/10.1038/s41467-020-17858-2.

Quijano Celia, Laura Castro, Gonzalo Peluffo, Valeria Valez, e Rafael Radi. «Enhanced Mitochondrial Superoxide in Hyperglycemic Endothelial Cells: Direct Measurements and Formation of Hydrogen Peroxide and Peroxynitrite». American Journal of Physiology. Heart and Circulatory Physiology 293, n. 6 (2007): H3404-3414. https://doi.org/10.1152/ajpheart.00761.2007.

Radak Zsolt, e Istvan Boldogh. «8-Oxo-7,8-Dihydroguanine: Links to Gene Expression, Aging, and Defense against Oxidative Stress». Free Radical Biology & Medicine 49, n. 4 (2010): 587–96. https://doi.org/10.1016/j.freeradbiomed.2010.05.008.

Ramasamy Ravichandran, Shi Fang Yan, e Ann Marie Schmidt. «Receptor for AGE (RAGE): Signaling Mechanisms in the Pathogenesis of Diabetes and Its Complications». Annals of the New York Academy of Sciences 1243 (2011): 88–102.

Reijns Martin A. M., Doryen Bubeck, Lucien C. D. Gibson, Stephen C. Graham, George S. Baillie, E. Yvonne Jones, e Andrew P. Jackson. «The Structure of the Human RNase H2 Complex Defines Key Interaction Interfaces Relevant to Enzyme Function and Human Disease». The Journal of Biological Chemistry 286, n. 12 (2011): 10530–39. https://doi.org/10.1074/jbc.M110.177394.

Rigby Rachel E., Lauren M. Webb, Karen J. Mackenzie, Yue Li, Andrea Leitch, Martin A. M. Reijns, Rachel J. Lundie, et al. «RNA:DNA Hybrids Are a Novel Molecular Pattern Sensed by TLR9». The EMBO Journal 33, n. 6 (2014): 542–58. https://doi.org/10.1002/embj.201386117.

Roberts R. W., e D. M. Crothers. «Stability and Properties of Double and Triple Helices: Dramatic Effects of RNA or DNA Backbone Composition». Science (New York, N.Y.) 258, n. 5087 (1992): 1463–66. https://doi.org/10.1126/science.1279808.

Rodier Francis, Jean-Philippe Coppé, Christopher K Patil, Wieteke A M Hoeijmakers, Denise P Muñoz, Saba R Raza, Adam Freund, Eric Campeau, Albert R Davalos, Judith Campisi. «Persistent DNA damage signalling triggers senescence-associated inflammatory cytokine secretion». Nat Cell Biol. 2009 Aug;11(8):973-9.doi: 10.1038/ncb1909. Epub 2009 Jul 13.

Roers Axel, Björn Hiller, e Veit Hornung. «Recognition of Endogenous Nucleic Acids by the Innate Immune System». Immunity 44, n. 4 (2016): 739–54. https://doi.org/10.1016/j.immuni.2016.04.002.

Rogers Steven C., Xiaomin Zhang, Gohar Azhar, Shaoke Luo, e Jeanne Y. Wei. «Exposure to High or Low Glucose Levels Accelerates the Appearance of Markers of Endothelial Cell Senescence and Induces Dysregulation of Nitric Oxide Synthase». The Journals of Gerontology. Series A, Biological Sciences and Medical Sciences 68, n. 12 (2013): 1469–81. https://doi.org/10.1093/gerona/glt033.

Roy Deepankar, e Michael R. Lieber. «G Clustering Is Important for the Initiation of Transcription-Induced R-Loops in Vitro, Whereas High G Density without Clustering Is Sufficient Thereafter». Molecular and Cellular Biology 29, n. 11 (2009): 3124–33. https://doi.org/10.1128/MCB.00139-09.

Royall Donald R., Safa Al-Rubaye, Ram Bishnoi, e Raymond F. Palmer. «Serum protein mediators of dementia and aging proper». Aging (Albany NY) 8, n. 12 (2016): 3241–54. https://doi.org/10.18632/aging.101091.

Rueden Curtis T., Johannes Schindelin, Mark C. Hiner, Barry E. DeZonia, Alison E. Walter, Ellen T. Arena, e Kevin W. Eliceiri. «ImageJ2: ImageJ for the next Generation of Scientific Image Data». BMC Bioinformatics 18, n. 1 (2017): 529. https://doi.org/10.1186/s12859-017-1934-z.

Rus Diana A., Juan Sastre, José Viña, e Federico V. Pallardó. «Induction of Mitochondrial Xanthine Oxidase Activity during Apoptosis in the Rat Mammary Gland». Frontiers in Bioscience: A Journal and Virtual Library 12 (2007): 1184–89. https://doi.org/10.2741/2136.

Salas-Armenteros Irene, Carmen Pérez-Calero, Aleix Bayona-Feliu, Emanuela Tumini, Rosa Luna, e Andrés Aguilera. «Human THO-Sin3A Interaction Reveals New Mechanisms to Prevent R-Loops That Cause Genome Instability». The EMBO Journal 36, n. 23 (2017): 3532–47. https://doi.org/10.15252/embj.201797208.

Samuel C. E. «Antiviral Actions of Interferons». Clinical Microbiology Reviews 14, n. 4 (2001): 778–809, table of contents. https://doi.org/10.1128/CMR.14.4.778-809.2001.

Sanchez Anthony, Angelo de Vivo, Peter Tonzi, Jeonghyeon Kim, Tony T. Huang, e Younghoon Kee. «Transcription-Replication Conflicts as a Source of Common Fragile Site Instability Caused by BMI1-RNF2 Deficiency». PLoS Genetics 16, n. 3 (2020): e1008524. https://doi.org/10.1371/journal.pgen.1008524.

Santos-Pereira José M., e Andrés Aguilera. «R Loops: New Modulators of Genome Dynamics and Function». Nature Reviews. Genetics 16, n. 10 (2015): 583–97. https://doi.org/10.1038/nrg3961.

Sanz Lionel A., Stella R. Hartono, Yoong Wearn Lim, Sandra Steyaert, Aparna Rajpurkar, Paul A. Ginno, Xiaoqin Xu, e Frédéric Chédin. «Prevalent, Dynamic, and Conserved R-Loop Structures Associate with Specific Epigenomic Signatures in Mammals». Molecular Cell 63, n. 1 (2016): 167–78. https://doi.org/10.1016/j.molcel.2016.05.032.

Sas Kelli M., Alla Karnovsky, George Michailidis, e Subramaniam Pennathur. «Metabolomics and Diabetes: Analytical and Computational Approaches». Diabetes 64, n. 3 (2015): 718–32. https://doi.org/10.2337/db14-0509.

Scavello Francesco, Filippo Zeni, Calogero C. Tedesco, Emanuela Mensà, Fabrizio Veglia, Antonio Domenico Procopio, Anna Rita Bonfigli, Fabiola Olivieri, e Angela Raucci. «Modulation of Soluble Receptor for Advanced Glycation End-Products (RAGE) Isoforms and Their Ligands in Healthy Aging». Aging 11, n. 6 (2019): 1648–63. https://doi.org/10.18632/aging.101860.

Seoane Rocío, Santiago Vidal, Yanis Hichem Bouzaher, Ahmed El Motiam, e Carmen Rivas. «The Interaction of Viruses with the Cellular Senescence Response». Biology 9, n. 12 (2020): 455. https://doi.org/10.3390/biology9120455.

Shen Yu J., Nina Le Bert, Anuja A. Chitre, Christine Xing'Er Koo, Xing H. Nga, Samantha S. W. Ho, Muznah Khatoo, Nikki Y. Tan, Ken J. Ishii, e Stephan Gasser. «Genome-Derived Cytosolic DNA Mediates Type I Interferon-Dependent Rejection of B Cell Lymphoma Cells». Cell Reports 11, n. 3 (2015): 460–73. https://doi.org/10.1016/j.celrep.2015.03.041.

Shenouda Sherene M., Michael E. Widlansky, Kai Chen, Guoquan Xu, Monika Holbrook, Corey E. Tabit, Naomi M. Hamburg, et al. «Altered Mitochondrial Dynamics Contributes to Endothelial Dysfunction in Diabetes Mellitus». Circulation 124, n. 4 (2011): 444–53. https://doi.org/10.1161/CIRCULATIONAHA.110.014506.

Shimada Kenichi, Timothy R. Crother, Justin Karlin, Jargalsaikhan Dagvadorj, Norika Chiba, Shuang Chen, V. Krishnan Ramanujan, et al. «Oxidized Mitochondrial DNA Activates the NLRP3 Inflammasome during Apoptosis». Immunity 36, n. 3 (2012): 401–14. https://doi.org/10.1016/j.immuni.2012.01.009.

Skourti-Stathaki Konstantina, e Nicholas J. Proudfoot. «A Double-Edged Sword: R Loops as Threats to Genome Integrity and Powerful Regulators of Gene Expression». Genes & Development 28, n. 13 (2014): 1384–96. https://doi.org/10.1101/gad.242990.114.

Skourti-Stathaki Konstantina, Nicholas J. Proudfoot, e Natalia Gromak. «Human Senataxin Resolves RNA/DNA Hybrids Formed at Transcriptional Pause Sites to Promote Xrn2-Dependent Termination». Molecular Cell 42, n. 6 (2011): 794–805. https://doi.org/10.1016/j.molcel.2011.04.026.

Song Chenlin, Agnes Hotz-Wagenblatt, Renate Voit, e Ingrid Grummt. «SIRT7 and the DEAD-Box Helicase DDX21 Cooperate to Resolve Genomic R Loops and Safeguard Genome Stability». Genes & Development 31, n. 13 (2017): 1370–81. https://doi.org/10.1101/gad.300624.117.

Song Ping, Junqing An, Ming-Hui Zou. «Immune Clearance of Senescent Cells to Combat Ageing and Chronic Diseases». Cells. Mar 10 2020;9(3):671. doi: 10.3390/cells9030671.

Sparks Justin L., Hyongi Chon, Susana M. Cerritelli, Thomas A. Kunkel, Erik Johansson, Robert J. Crouch, e Peter M. Burgers. «RNase H2-Initiated Ribonucleotide Excision Repair». Molecular Cell 47, n. 6 (2012): 980–86. https://doi.org/10.1016/j.molcel.2012.06.035.

Spazzafumo Liana, Fabiola Olivieri, Angela Marie Abbatecola, Gastone Castellani, Daniela Monti, Rosamaria Lisa, Roberta Galeazzi, et al. «Remodelling of Biological Parameters during Human Ageing: Evidence for Complex Regulation in Longevity and in Type 2 Diabetes». Age (Dordrecht, Netherlands) 35, n. 2 (2013): 419–29. https://doi.org/10.1007/s11357-011-9348-8.

Sridhara Sreerama Chaitanya, Sílvia Carvalho, Ana Rita Grosso, Lina Marcela Gallego-Paez, Maria Carmo-Fonseca, e Sérgio Fernandes de Almeida. «Transcription Dynamics Prevent RNA-Mediated Genomic Instability through SRPK2-Dependent DDX23 Phosphorylation». Cell Reports 18, n. 2 (2017): 334–43. https://doi.org/10.1016/j.celrep.2016.12.050.

Stein H., e Hausen P. «Enzyme from Calf Thymus Degrading the RNA Moiety of DNA-RNA Hybrids: Effect on DNA-Dependent RNA Polymerase». Science (New York, N.Y.) 166, n. 3903 (1969): 393–95. https://doi.org/10.1126/science.166.3903.393.

Stern Shlomo, Behar Solomon, e Gottlieb Shmuel. «Aging and Diseases of the Heart». Circulation 108, n. 14 (2003): e99–101. https://doi.org/10.1161/01.CIR.0000086898.96021.B9.

Storci Gianluca, Maria Giulia Bacalini, Francesca Bonifazi, Paolo Garagnani, Sabrina De Carolis, Stefano Salvioli, Fabiola Olivieri, e Massimiliano Bonafè. «Ribosomal DNA Instability: An Evolutionary Conserved Fuel for Inflammaging». Ageing Research Reviews 58 (2020): 101018. https://doi.org/10.1016/j.arr.2020.101018.

Storci Gianluca, Sabrina De Carolis, Fabiola Olivieri, e Massimiliano Bonafè. «Changes in the Biochemical Taste of Cytoplasmic and Cell-Free DNA Are Major Fuels for Inflamm-Aging». Seminars in Immunology 40 (2018): 6–16. https://doi.org/10.1016/j.smim.2018.08.003.

Straub Rainer H., Maurizio Cutolo, e Roberto Pacifici. «Evolutionary Medicine and Bone Loss in Chronic Inflammatory Diseases--A Theory of Inflammation-Related Osteopenia». Seminars in Arthritis and Rheumatism 45, n. 2 (2015): 220–28. https://doi.org/10.1016/j.semarthrit.2015.04.014.

Strzyz Paulina. «DNA Repair: RNA-DNA Hybrids: A Double-Edged Sword in Genomic Stability». Nature Reviews. Molecular Cell Biology 17, n. 12 (2016): 740. https://doi.org/10.1038/nrm.2016.155.

Sulli Gabriele, Raffaella Di Micco, Fabrizio d'Adda di Fagagna. «Crosstalk between chromatin state and DNA damage response in cellular senescence and cancer». Nat Rev Cancer. 2012 Oct;12(10):709-20. doi: 10.1038/nrc3344. Epub 2012 Sep 6.

Su Xiaofeng A., e Catherine H. Freudenreich. «Cytosine Deamination and Base Excision Repair Cause R-Loop-Induced CAG Repeat Fragility and Instability in Saccharomyces Cerevisiae». Proceedings of the National Academy of Sciences of the United States of America 114, n. 40 (2017): E8392–8401. https://doi.org/10.1073/pnas.1711283114.

Sun Lijun, Jiaxi Wu, Fenghe Du, Xiang Chen, e Zhijian J. Chen. «Cyclic GMP-AMP Synthase Is a Cytosolic DNA Sensor That Activates the Type I Interferon Pathway». Science (New York, N.Y.) 339, n. 6121 (2013): 786–91. https://doi.org/10.1126/science.1232458.

Suzuki Kunihiro, Gabor Olah, Katalin Modis, Ciro Coletta, Gabriella Kulp, Domokos Gerö, Petra Szoleczky, et al. «Hydrogen Sulfide Replacement Therapy Protects the Vascular Endothelium in Hyperglycemia by Preserving Mitochondrial Function». Proceedings of the National Academy of Sciences of the United States of America 108, n. 33 (2011): 13829–34. https://doi.org/10.1073/pnas.1105121108.

Suzuki Kunihiro, Masaaki Sagara, Chie Aoki, Seiichi Tanaka, e Yoshimasa Aso. «Clinical Implication of Plasma Hydrogen Sulfide Levels in Japanese Patients with Type 2 Diabetes». Internal Medicine (Tokyo, Japan) 56, n. 1 (2017): 17–21. https://doi.org/10.2169/internalmedicine.56.7403.

Szczesny Bartosz, Attila Brunyanszki, Gabor Olah, Sankar Mitra, e Csaba Szabo. «Opposing Roles of Mitochondrial and Nuclear PARP1 in the Regulation of Mitochondrial and Nuclear DNA Integrity: Implications for the Regulation of Mitochondrial Function». Nucleic Acids Research 42, n. 21 (2014): 13161–73. https://doi.org/10.1093/nar/gku1089.

Takahashi Akiko, Tze Mun Loo, Ryo Okada, Fumitaka Kamachi, Yoshihiro Watanabe, Masahiro Wakita, Sugiko Watanabe, et al. «Downregulation of Cytoplasmic DNases Is Implicated in Cytoplasmic DNA Accumulation and SASP in Senescent Cells». Nature Communications 9, n. 1 (2018): 1249. https://doi.org/10.1038/s41467-018-03555-8.

Taniguchi Noboru, Yasuhiko Kawakami, Ikuro Maruyama, e Martin Lotz. «HMGB Proteins and Arthritis». Human Cell 31, n. 1 (2018): 1–9. https://doi.org/10.1007/s13577-017-0182-x.

Tanner N. K., e P. Linder. «DExD/H Box RNA Helicases: From Generic Motors to Specific Dissociation Functions». Molecular Cell 8, n. 2 (2001): 251–62. https://doi.org/10.1016/s1097-2765(01)00329-x.

Tchkonia Tamara, Yi Zhu, Jan van Deursen, Judith Campisi, James L Kirkland. «Cellular senescence and the senescent secretory phenotype: therapeutic opportunities». J Clin Invest. 2013 Mar;123(3):966-72. doi: 10.1172/JCI64098. Epub 2013 Mar 1.

Thomas M., R. L. White, e R. W. Davis. «Hybridization of RNA to Double-Stranded DNA: Formation of R-Loops». Proceedings of the National Academy of Sciences of the United States of America 73, n. 7 (1976): 2294–98. https://doi.org/10.1073/pnas.73.7.2294.

Treberg Jason R., Casey L. Quinlan, e Martin D. Brand. «Evidence for Two Sites of Superoxide Production by Mitochondrial NADH-Ubiquinone Oxidoreductase (Complex I) ». The Journal of Biological Chemistry 286, n. 31 (2011): 27103–10. https://doi.org/10.1074/jbc.M111.252502.

Turrens Julio F. «Mitochondrial Formation of Reactive Oxygen Species». The Journal of Physiology 552, n. Pt 2 (2003): 335–44. https://doi.org/10.1113/jphysiol.2003.049478.

Vanoosthuyse Vincent. «Strengths and Weaknesses of the Current Strategies to Map and Characterize R-Loops». *Non-Coding RNA* 4, n. 2 (2018). https://doi.org/10.3390/ncrna4020009.

Wahba Lamia, Steven K. Gore, e Douglas Koshland. «The Homologous Recombination Machinery Modulates the Formation of RNA-DNA Hybrids and Associated Chromosome Instability». ELife 2 (2013): e00505. https://doi.org/10.7554/eLife.00505.

Wang Wenjian, Yin Wang, Jianyin Long, Jinrong Wang, Sandra B. Haudek, Paul Overbeek, Benny H. J. Chang, Paul T. Schumacker, e Farhad R. Danesh. «Mitochondrial Fission Triggered by Hyperglycemia Is Mediated by ROCK1 Activation in Podocytes and Endothelial Cells». Cell Metabolism 15, n. 2 (2012): 186–200. https://doi.org/10.1016/j.cmet.2012.01.009.

Wilhelm, M. Influenza in Older Patients: A Call to Action and Recent Updates for Vaccinations. Am. J.

Manag. Care 2018, 24 (Suppl. 2), S15–S24

Yang Hui, Hanze Wang, Junyao Ren, Qi Chen, e Zhijian J. Chen. «CGAS Is Essential for Cellular Senescence». Proceedings of the National Academy of Sciences of the United States of America 114, n. 23 (2017): E4612–20. https://doi.org/10.1073/pnas.1705499114.

Yang Yanzhong, Kevin M. McBride, Sean Hensley, Yue Lu, Frederic Chedin, e Mark T. Bedford. «Arginine Methylation Facilitates the Recruitment of TOP3B to Chromatin to Prevent R Loop Accumulation». Molecular Cell 53, n. 3 (2014): 484–97. https://doi.org/10.1016/j.molcel.2014.01.011.

Yu Qiujing, Yuliya V. Katlinskaya, Christopher J. Carbone, Bin Zhao, Kanstantsin V. Katlinski, Hui Zheng, Manti Guha, et al. «DNA-Damage-Induced Type I Interferon Promotes Senescence and Inhibits Stem Cell Function». Cell Reports 11, n. 5 (2015): 785–97. https://doi.org/10.1016/j.celrep.2015.03.069.

Yu Tianzheng, Bong Sook Jhun, e Yisang Yoon. «High-Glucose Stimulation Increases Reactive Oxygen Species Production through the Calcium and Mitogen-Activated Protein Kinase-Mediated Activation of Mitochondrial Fission». Antioxidants & Redox Signaling 14, n. 3 (2011): 425–37. https://doi.org/10.1089/ars.2010.3284.

Yu Tianzheng, James L. Robotham, e Yisang Yoon. «Increased Production of Reactive Oxygen Species in Hyperglycemic Conditions Requires Dynamic Change of Mitochondrial Morphology». Proceedings of the National Academy of Sciences of the United States of America 103, n. 8 (2006): 2653–58. https://doi.org/10.1073/pnas.0511154103.

Zank, Daniel C., Marta Bueno, Ana L. Mora, e Mauricio Rojas. «Idiopathic Pulmonary Fibrosis: Aging, Mitochondrial Dysfunction, and Cellular Bioenergetics». Frontiers in Medicine 5 (2018): 10. https://doi.org/10.3389/fmed.2018.00010.

Zhang ZZ, Pannunzio NR, Hsieh CL, Yu K, Lieber MR. Complexities due to single-stranded RNA during antibody detection of genomic rna:dna hybrids. BMC Res Notes. 2015 Apr 8;8:127. doi: 10.1186/s13104-015-1092-1.

Zhang Zhaoyun, Zhihong Yang, Bo Zhu, Ji Hu, Chong Wee Liew, Yingyi Zhang, Jane A. Leopold, Diane E. Handy, Joseph Loscalzo, e Robert C. Stanton. «Increasing Glucose 6-Phosphate Dehydrogenase Activity Restores Redox Balance in Vascular Endothelial Cells Exposed to High Glucose». PloS One 7, n. 11 (2012): e49128. https://doi.org/10.1371/journal.pone.0049128.

Zheng Zhi, Haibing Chen, Jun Li, Tao Li, Bingqing Zheng, Ying Zheng, Huiyi Jin, Ying He, Qing Gu, e Xun Xu. «Sirtuin 1-Mediated Cellular Metabolic Memory of High Glucose via the LKB1/AMPK/ROS Pathway and Therapeutic Effects of Metformin». Diabetes 61, n. 1 (2012): 217–28. https://doi.org/10.2337/db11-0416.

7 PUBLICATIONS

Research Paper

Diagnostic performance of new and classic CSF biomarkers in age-related dementias

Francesca Marchegiani[1], Giulia Matacchione[2], Deborah Ramini[2], Fiorella Marcheselli[1], Rina Recchioni[1], Tiziana Casoli[3], Elisa Mercuri[2], Marco Lazzarini[2], Belinda Giorgetti[3], Valentina Cameriere[4], Susy Paolini[4], Lucia Paciaroni[4], Tommaso Rossi[4], Roberta Galeazzi[5], Rosamaria Lisa[6], Anna Rita Bonfigli[6], Antonio Domenico Procopio[1,2], Maria De Luca[7], Giuseppe Pelliccioni[4,*], Fabiola Olivieri[1,2,*]

[1]Center of Clinical Pathology and Innovative Therapy, IRCCS INRCA, Ancona, Italy
[2]Department of Clinical and Molecular Sciences, DISCLIMO, Università Politecnica delle Marche, Ancona, Italy
[3]Center for Neurobiology of Aging, IRCCS INRCA, Ancona, Italy
[4]Neurology Unit, IRCCS INRCA, Ancona, Italy
[5]Clinical Laboratory and Molecular Diagnostics, IRCCS INRCA, Ancona, Italy
[6]Scientific Direction, IRCCS INRCA, Ancona, Italy
[7]Department of Nutrition Sciences, University of Alabama at Birmingham, Birmingham, AL 35294, USA
[*]Equal contribution

Correspondence to: Giulia Matacchione, Deborah Ramini; **email:** g.matacchione@pm.univpm.it, debby.ramini@gmail.com
Keywords: neurofilament-light, microRNAs, age-related dementias, CSF
Received: March 18, 2019 **Accepted:** April 14, 2019 **Published:** April 27, 2019

ABSTRACT

The identification of diagnostic-prognostic biomarkers of dementia has become a global priority due to the prevalence of neurodegenerative diseases in aging populations. The objective of this study was to assess the diagnostic performance of cerebrospinal fluid (CSF) biomarkers across patients affected by either Alzheimer's disease (AD), tauopathies other than AD (TP), or vascular dementia (VD), and cognitively normal subjects (CNS). One hundred fifty-three patients were recruited and tested for classical AD CSF biomarkers- Amyloid-ß42 and tau proteins - and novel candidate biomarkers - neurofilament (NF-) light and microRNA (miR) -21, -125b, -146a, and -222.

All dementia patients had significantly higher concentrations of NF-light compared to CNS, with the TP group displaying the highest NF-light values. A significant inverse correlation was also observed between NF-light and cognitive impairment. Of the four miRNAs analyzed, miR-222 levels were significantly increased in VD patients compared to both CNS and AD. In addition, while NF-light showed a better diagnostic performance than miR-222 and classical AD biomarkers in differentiating TP and VD from CNS, classical AD biomarkers revealed higher performance in discriminating AD from non-AD disorders.

Overall, our results suggest that CSF NF-light and miR-222 are promising biomarkers that may help to diagnose non-AD disorders.

INTRODUCTION

The constant rate of increase in global life expectancy and the consequent rise in the average age of the population have been accompanied by a significant surge in the incidence of the most common age-related diseases (ARDs), including neurodegenerative diseases [1]. The economic costs and social burden associated with neurodegenerative diseases have motivated efforts to identify innovative biomarkers for accurate and timely diagnosis and effective treatments. Neurodegenerative diseases include Alzheimer's disease (AD), the most common form of dementia, and non-Alzheimer's diseases (NAD), a group of disorders that account for approximately 30-40 per cent of dementias worldwide [2]. Among NAD, Lewy Bodies (DLB), vascular (VD) and frontotemporal dementia (FTD) are the most prevalent types of dementia.

AD diagnosis is currently based on clinical evaluation, neuropsychological testing, neuro-imaging techniques, and cerebrospinal fluid (CSF) classical biomarkers [3-6]. Three core CSF biomarkers, *e.g.* Amyloid-ß42 (Aß42), total tau (t-tau) and phosphorylated tau (p-tau) proteins, have been included in the diagnostic criteria of AD, and could be relevant for differential diagnosis [3]. A recent Cochrane review suggested that they have a better sensitivity than specificity, performing best in ruling out AD [5].

Tau is a microtubule-associated protein involved in microtubule assembly and stabilization that can form

Table 1. Clinical and anthropometric characteristics of the studied subjects.

	CNS (n. 43)	*AD (n. 70)*	*TP (n. 23)*	*VD (n. 17)*
Age (yrs)	66.9±12.0	77.0±7.7*	68.6±8.3	79.4±6.2*
Gender Male N (%)	21 (48.8%)	26 (37.1%)	12 (52.2%)	8 (47.1%)
Aß42 (pg/ml)	657.0 (143.0-1238.0)	384.5 (113.0-877.0) *	713.0 (194.0-1006.0)	645.0 (394.0-1107.0)
T-tau (pg/ml)	178.0 (57.0-2358.0)	447.0 (117.0-2693.0) *	247.0 (90.0-774.0)	305.0 (66.0-673.0)
P-tau (pg/ml)	35.0 (6.0-81.0)	64.0 (21.0-194.0) *	48 (2.0-112.0)	44.0 (25.0-91.0)
MMSE	25.3±3.1	14.9±6.3 *	18.2±7.7 *	20.3±7.8 *
IATI	1.4 (0.3-3.1)	0.5 (0.1-1.7) *	1.1 (0.3-2.1) *	1.3 (0.5-2.2)
NF-light (pg/ml)	796.7 (81.3-1584.3)	1332.7 (424.7-5730.1) **	2071.0 (400.5-7864.9) **	1603.2 (370.1-6295.7) $^{++}$
MiR-21	324.7±215.1	369.7±236.9	304.9±139.3	286.1±177.5
MiR-125b	171.8±165.5	166.6±151.2	129.1±122.1	167.0±199.9
MiR-146a	14.8±15.1	14.4±11.2	16.5±19.5	16.4±18.9
MiR-222	11.2±12.1	13.8±13.8	23. ±58.8	40.6±64.0^{++}

Data are reported as mean ± SD or as median (Interquartile Range) as appropriate. Aß42: beta-amyloid (1-42) peptide. T-tau: Tau protein. P-tau: threonine-181 hyperphosphorylated tau protein. MMSE: Mini Mental State Evaluation. IATI: Innotest Amyloid Tau Index. CNS: cognitively normal subjects. AD: Alzheimer's diseases. TP: the TP group was composed of 3 patients with progressive supranuclear palsy (PSP), 19 patients with frontotemporal dementia (FTD) and 3 patients with corticobasal degeneration (CBD). VD: vascular dementia. *$p<0.05$ *vs*. CNS group; $^{++}$ $p<0.01$ *vs.* CNS and AD group; ** $p< 0.01$ *vs.* CNS.

filamentous deposits that are hallmarks of several neurodegenerative diseases collectively referred to as tauopathies (TP). TPs include AD and non-AD diseases, such as FTD and progressive supranuclear palsy (PSP) [6].

The onset of clinical symptoms and signs is a late occurrence in the natural history of dementia since the neurodegenerative processes start decades before the characteristic clinical manifestations [7,8]. To date, there is no single test that can diagnose the different types of dementia and the identification of innovative diagnostic biomarkers that can contribute to distinguish AD from NAD is needed.

New molecules, such as neurofilament light (NF-light) and microRNAs, have been proposed as promising biomarkers for neurodegenerative diseases. Neurofilaments are the major cytoskeletal constituents of neuronal cells, involved in axonal caliber maintenance and morpho-functional integrity [8-10]. NF-light levels are correlated with axonal degeneration, suggesting a potential diagnostic relevance for AD [11,12]. Increased NF-light levels have been observed in a large number of neurodegenerative diseases and conditions, including multiple sclerosis (MS) [13,14], amyotrophic lateral sclerosis (ALS) [15], AD [12], subcortical vascular disease [16], FTD [17,18], various central nervous system infections [19], and chronic experimental autoimmune encephalomyelitis [20].

Circulating microRNAs (miRNAs), which are short single-strand RNA molecules that are involved in gene expression modulation, have been linked to a number of ARDs, including neurodegenerative diseases. Four miRNAs, miR-21, miR-125b, miR-146a, and miR-222, were previously associated with AD diagnosis [21–23]. Moreover, two of them, miR-21 and miR-146a, were found to be involved in the modulation of the inflammatory process, which in turn is currently believed to underlie the neurodegeneration processes [24]. These miRNAs were defined as “inflammamiRs” [25].

The aim of this study was to compare the diagnostic performance of classical and novel CSF biomarkers across patients affected by AD and NAD, such as TP and VD, and cognitively normal subjects (CNS).

RESULTS

The biochemical, clinical and anthropometric characteristics of the studied subjects are reported in Table 1. The proportion between genders among groups was not significantly different. TP patients have mean age similar to that of CNS, whereas AD and VD patients were significantly older than CNS.

With respect to classical AD CSF biomarkers, AD patients showed the characteristic profiles characterized by low levels of Aß42 and high levels of t- and p-tau, whereas the CNS group had high levels of Aß42 and low levels of t- and p- tau. NAD patients showed intermediate profiles.

A significant increasing trend from CNS to AD and NAD was observed for NF-light concentration levels. Specifically, the TP group was characterized by the highest NF-light value (Table 1 and Fig. 1A).

When gender-stratified analyses were performed, NF-light levels were significantly higher in males than in females in both AD and NAD (TP and VD groups) (Fig. 1B).

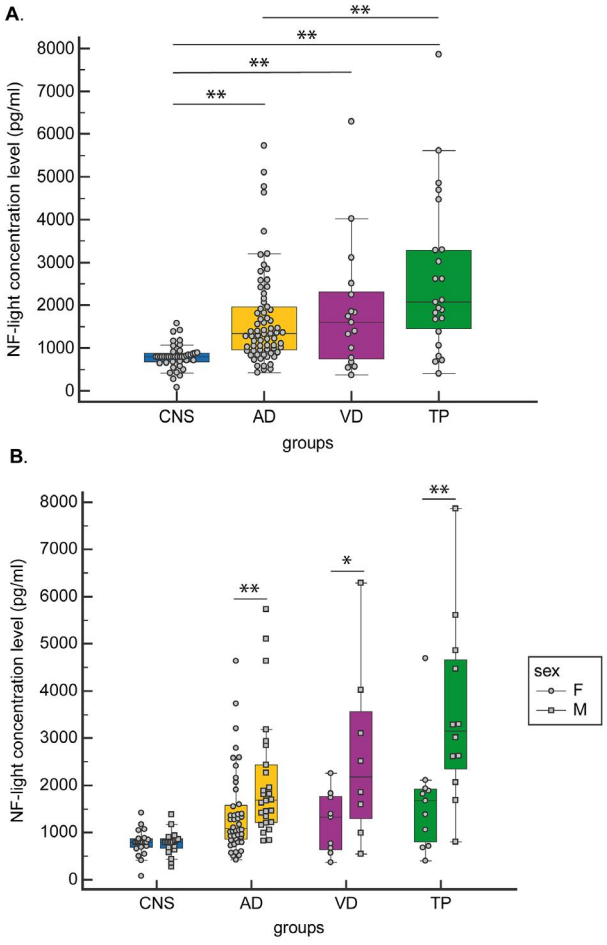

Figure 1. CSF NF-light concentration levels. (**A**) in CNS, AD, VD and TP and (**B**) in CNS, AD, VD and TP grouped by gender. Data are presented as median (Interquartile Range). *$p<0.05$; **$p<0.01$.

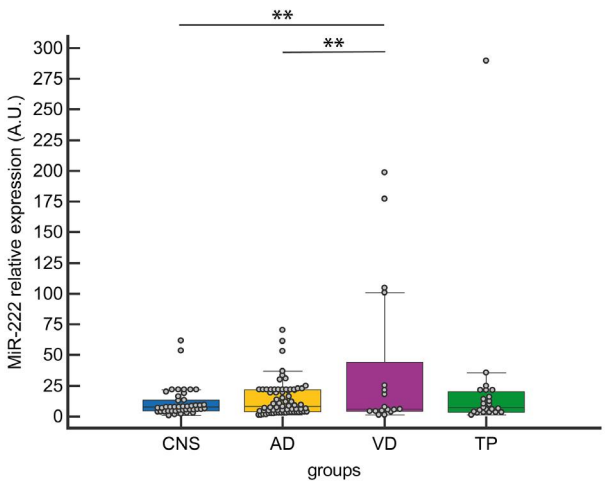

Figure 2. CSF miR-222 expression levels in CNS, AD, VD and TP. Data are presented as median [interquartile range]; ***p<0.01*

Among the four selected miRNAs, miR-222 CSF levels were significantly increased in VD compared to both AD and CNS (Fig. 2).

One-way analysis of covariance (ANCOVA) adjusted for age and gender confirmed a statistically significant difference among CNS, AD, TP and VD patients in the levels of NF-light (F =13.07 (3, 141), p <0.001) and miR-222 (F= 5.51 (3, 141), p=0.001), (Wilk's Lambda, F= 9.20 (3, 141), p <0.001). These results were still significant after adjusting for Aß42, t-tau, and p- tau.

The diagnostic performance of each biomarker was than assessed using ROC curve analysis. NF-light concentrations performed better than miR-222 levels in discriminating VD from CNS (ROC analysis: The diagnostic performance of each biomarker was than assessed using ROC curve analysis. NF-light concentrations performed better than miR-222 levels in discriminating VD from CNS (ROC analysis: AUC=0.746) (Fig. 3A), but neither NF-light nor miR-222 were able to distinguish between AD and VD (Fig. 3B).

On the other hand, the performance of NF-light levels in discriminating AD from CNS was similar to that of classical AD biomarkers (ROC analysis: AUC=0.830, AD *vs.* CNS) (Fig. 4A), whereas a better performance than Aß42, t- and p-tau and IATI (a parameter combining

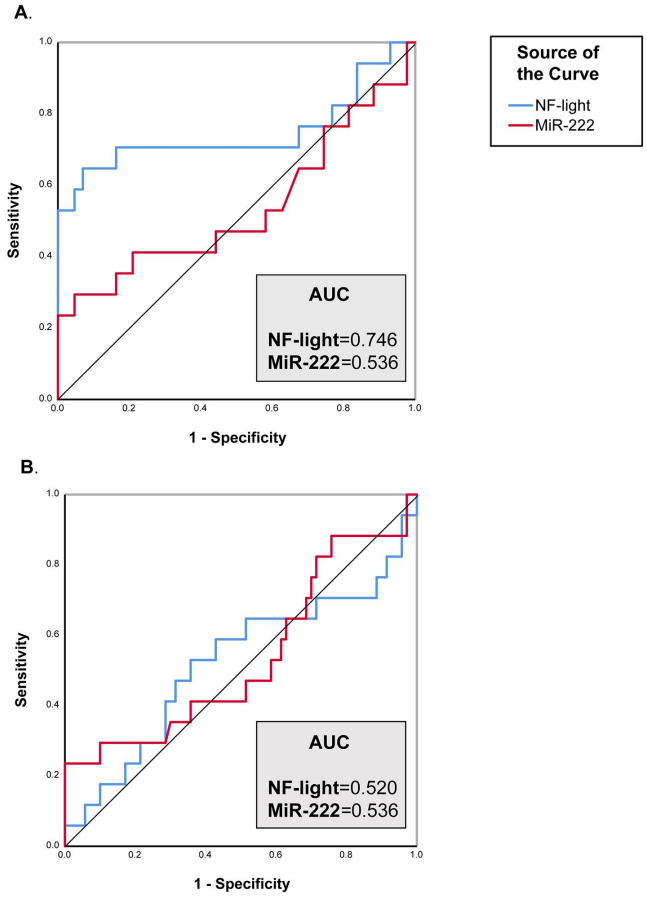

Figure 3. ROC curve analysis of NF-Light and miR-222. (**A**) CNS *vs.* VD. (**B**) AD *vs.* VD. AUC= Area Under the Curve.

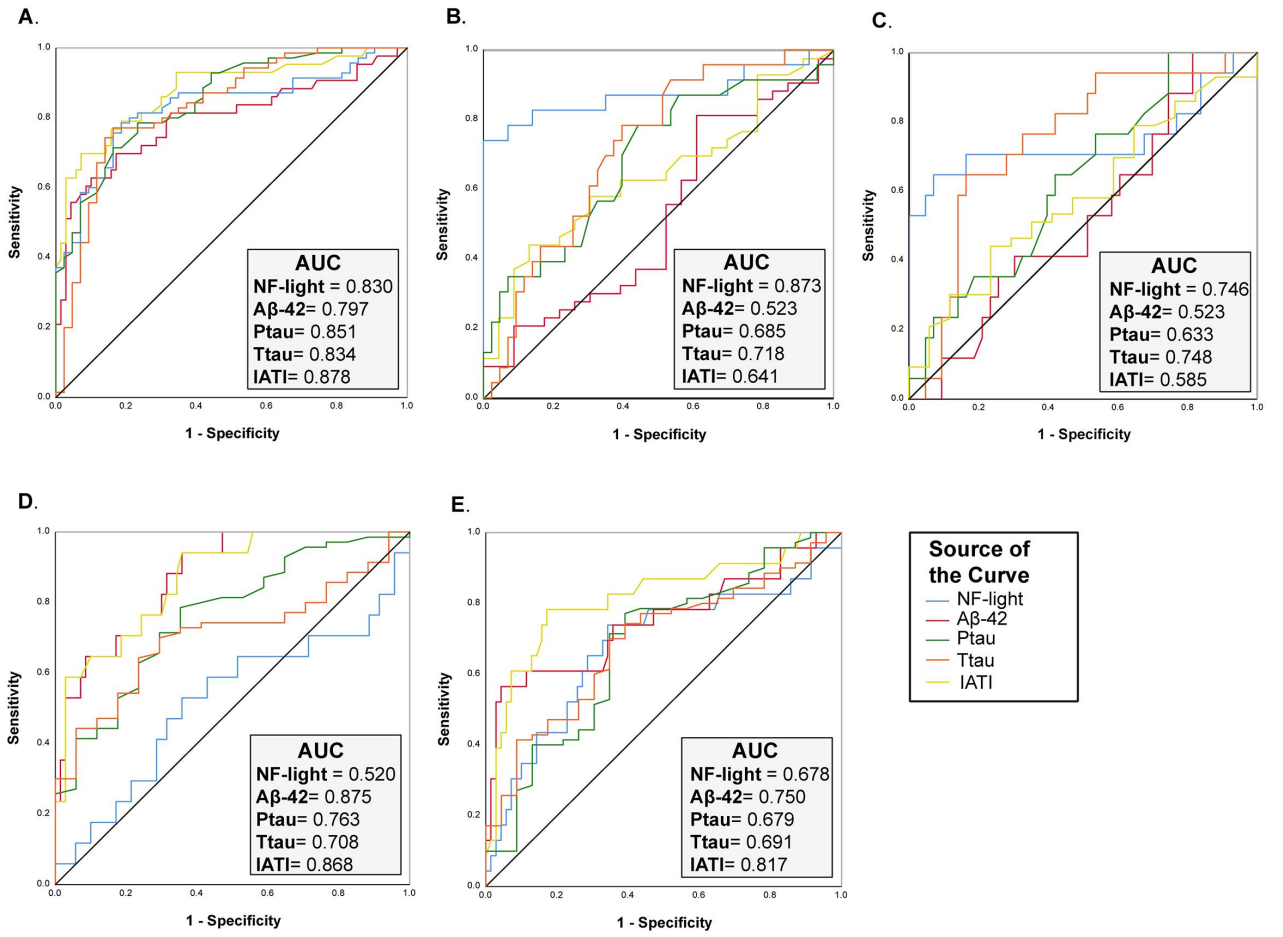

Figure 4. ROC curve analysis of NF-Light and classical AD biomarkers. (**A**) CNS *vs.* AD. (**B**) CNS *vs.* TP. (**C**) CNS *vs.* VD. (**D**) AD *vs.* VD and (**E**) AD *vs.* TP. AUC= Area Under the Curve.

Aß42 and t-tau) was observed in differentiating TP patients from CNS (ROC analysis: AUC=0.873, TP *vs.* CNS) (Fig. 4B). Furthermore, IATI had the best performance in differentiating between AD and NAD (ROC analysis: AUC=0.868, AD *vs.* VD and AUC=0.817, AD *vs.* TP) (Fig. 4D-E).

Significant correlations were observed between NF-light and t-tau, p-tau and IATI (Table 2).

Finally, a significant inverse correlation was observed between NF-light levels and the Mini-Mental State Examination (MMSE) score (Table 2).

DISCUSSION

The confidence in AD diagnosis is highly enhanced by the quantification of classical biomarkers in CSF. However, the diagnostic relevance of these biomarkers in non-AD dementia and in differentiating between AD and non-AD is still under investigation. In addition, the identification of additional CSF biomarkers of dementia may help to improve the CSF biomarker-based classification. To this end, our results showed that CSF NF-light levels increased in all analyzed groups of patients with dementia compared to CNS. The TP group was characterized by the highest NF-light values, which, in turn, showed a better diagnostic performance than classical AD biomarkers in distinguishing TP from CNS. A notable finding of our study is that NF-light levels were strongly correlated with t-tau and p-tau, which confirms previous data [26]. This relationship is not surprising since t- and p-tau as well as NF-light are proteins belonging to the neuronal cytoskeleton and their increased levels in CSF are indicative of neuronal damages. The tau protein is mainly associated with the microtubules of the cortical axons; therefore, the value of t-tau in CSF is proportional to axonal damage. On the other hand, the axonal damage, in general, is an event common to all neurodegenerative diseases. Indeed, increases of t-tau are also detectable in VD, Lewy body dementia, FTD dementias and Creutzfeldt-Jacob disease

Table 2. Correlation between classical and innovative (NF-light and miR-222) neurodegenerative biomarkers.

	NF-light		*MiR-222*	
	Spearman's rho coefficient	***P value***	***Spearman's rho coefficient***	***P value***
Aß42	*-0.031*	*0.692*	*-0.011*	*0.888*
T-tau	***0.360***	***< 0.001***	*-0.077*	*0.319*
P-tau	***0.262***	***0.001***	*-0.016*	*0.838*
IATI	***-0.210***	***0.006***	*0.040*	*0.603*
MMSE	***-0.210***	***0.022***	*0.026*	*0.786*

Aß42: beta-amyloid (1-42) peptide. T-tau: Tau protein. P-tau: threonine-181 hyperphosphorylated tau protein. MMSE: Mini Mental State Evaluation. IATI: Innotest Amyloid Tau Index.

[27,28]. Given that the tau protein is expressed mainly in the axons of cortical neurons, an increase in CSF reflects a neuronal damage of cortical neurons [29]. Nevertheless, the increase in CSF t-tau levels remains a finding rather non-specific, since other pathologies, besides AD, are responsible for most of the cortical neuronal damage, *i.e.* Creutzfeld's-Jacob disease [30]. NF-light as representative of axonal injury, axonal pathology, and/or axonal dysfunction has been observed in various models of mouse [26-31]. Moreover, results from this study showed a significant inverse correlation between NF-light and the MMSE score, the best-known screening tool for providing an overall measure of cognitive impairment in clinical and research field [32]. However, as seen previously [33], CSF NF-light levels demonstrated worse diagnostic performance in discriminating between AD and non-AD dementia, suggesting that NF-light is a biomarker of neurodegeneration not specific for AD dementia

On the other hand, IATI, a parameter combining Aß42 and t-tau that, had the best performance in discriminating between AD and non-AD dementia. This result is in contrast with findings from a recent Cochrane systematic review on the clinical impact of CSF t-tau and p-tau for the diagnosis of Alzheimer's and other dementias in people with mild cognitive impairment (MCI), which reported that the classical AD biomarkers showed better potential in ruling out AD rather than in ruling in [5]. Despite the large number of patients analysed in the above-mentioned systematic review, the diagnostic clinical utility of these biomarkers was not defined. Indeed, an increase in their levels is not a guarantee of a progression of MCI into dementia, suggesting that further efforts should be devoted to search for more specific and informative biomarkers.

Regarding miRNAs levels as diagnostic biomarkers of dementia, our study showed a significant increase of CSF miR-222 levels in VD patients, suggesting a potential role in supporting the diagnosis of vascular dementia. MiR-222 was previously defined as an anti-angiogenic miR, upregulated in vascular walls with neointimal lesion formation [34–36]. Notably, circulating miR-222 levels were recently proposed as promising and independent biomarkers for the risk of acute ischemic stroke [37]. However, miR-222 performed worse than NF-light in distinguishing VD from CNS. The diagnostic relevance previously hypothesized for miR-21, miR-146a, and miR-125b CSF expression levels was not confirmed in our study [21–23]. Methodological bias, lack of standardization procedures, or different inclusion-exclusion criteria for enrolled patients could explain these non-concordant results.

The main limitation of our study is the small number of recruited patients. This is due to the fact that an invasive procedure is needed to collect CSF samples. Even if CSF biomarkers levels reflect the neuropathological alterations better than peripheral blood, applying routinely the invasive procedure needed for CSF collection in elderly patients can be difficult [38]. Therefore, the main effort in the future will be to measure NF-light in serum or plasma and compare the diagnostic performance of this

innovative biomarker in CSF and in peripheral blood samples.

Overall, our results suggest that, although the non-specificity of NF-light CSF levels for the different types of dementia, CSF NF-light could be useful in supporting the diagnosis of non-AD dementia in combination with imaging and clinical data.

MATERIALS AND METHODS

Participants

One hundred fifty-three patients (67 males and 86 females) were consecutively admitted to the Neurology Unit of the Geriatric Hospital, IRCCS INRCA, of Ancona. The period of recruitment was from July 20, 2010 to July 17, 2017. Participants with CSF sample available were included in the study. The Institutional Review Board of INRCA approved the study protocol and all study participants, or their next of kin, provided written informed consent in the case of relevant cognitive impairment. All recruited subjects were between 38 and 90 years of age.

Based on the cognitive assessments and clinical diagnosis, the patients were grouped into the following diagnostic categories: 70 AD, 23 TP, 17 VD, and 43 defined as CNS. The TP group was composed of: 3 patients with PSP, 19 FTD, and 3 patients with corticobasal degeneration (CBD). Tauopathies and vascular dementia are classified as NAD.

All the participants underwent physical, neurological and neuropsychological assessments, including laboratory tests, brain imaging and the MMSE evaluation. MMSE values were recoded as: 24-30 = no cognitive impairment, 19-23= mild cognitive impairment, 10-18 = moderate cognitive impairment and < 9 = severe cognitive impairment.

The diagnosis of dementia was made according to consensus criteria (AD: [3,39,40]; PSP: [41]; FTD: [42,43]; VD: [44,45]; CBD: [46]).

CNS were enrolled by Neurology Unit of the Geriatric Hospital, IRCCS INRCA, of Ancona. They did not meet criteria for mild cognitive impairment [47] and did not have any signs of inflammatory or neurodegenerative disorders, or family history of neurodegenerative disease.

For the purpose of this study, patients with unidentified neurodegenerative disease or patients with different various diagnoses (*e.g.* psychiatric disorders, traumatic brain injury, alcoholism, metabolic encephalopathy) defined according to international criteria, were excluded.

Cerebrospinal fluid collection and analysis

CSF was obtained by lumbar puncture in the L3/L4 or L4/L5 intervertebral space. CSF samples were collected in polypropylene vials and centrifuged at 2000 x g for 10 min to pellet residual cells and other insoluble material, then the supernatant was aliquoted and stored at -80 °C until use for biomarker determination. The CSF levels of Aß42, t-tau, and p-tau were determined using commercially available ELISA kits (Fujirebio Inc., Japan) according to the manufacturer's instructions. Assay performance was monitored using internal and external quality control samples. All analyses were performed by the same investigators who were blinded to patients' demographic, clinical, and cognitive data. The cutoff values of the CSF biomarkers considered as biochemical evidence of AD were determined in samples ran in the same laboratory as the CSF samples [48] and were Aß42 < 500 pg/ml, t-tau > 350 pg/ml, and p-tau > 50 pg/ml. The IATI parameter was calculated as follows: Aβ42 / (240 + 1.18 × t-tau).

The CSF NF-Light concentrations were measured using a commercial ELISA kit (IBL, Hamburg, Germany) as described by the manufacturer. All samples were ran in duplicate and the mean value was considered for the analysis. Samples with an intra-assay coefficient of variation below 10.0% were included in this study. The lower limit of quantification is 32 pg/ml and the upper limit is 10000 pg/ml.

RNA isolation

Total RNA was isolated from CSF sample (100µl) using Total RNA Purification Kit (product #17200) by Norgen Biotek Corporation (Thorold, ON, Canada), according to the manufacturer's specific recommendations. RNA was stored at − 80°C until use.

Quantitative RT-PCR of mature miRNAs

MiRNA relative expression was measured as reported in [49].

Statistical analysis

Baseline characteristics were determined using descriptive statistics. Mean ± standard deviation (SD) or median (interquartile range (IQR)) were reported for continuous variables. To assess the normal distribution of the data, a Kolmogorov-Smirnov test was performed and non-normally distributed data were log10 transformed. Absolute frequencies or percentages were described for categorical variables. ANCOVA followed by Bonferroni's post-hoc test for multiple comparisons was used to compare the mean differences in clinical variables

after adjustment for age and sex. Associations between the variables were tested using Spearman correlation test.

To assess the diagnostic performance of each biomarker in distinguishing CNS from AD and NAD, a receiver operating characteristic (ROC) curve analysis was performed, and areas under the curve (AUC) were compared.

All tests were two-sided, and significance was set at $p< 0.05$. Statistical analyses were performed using IBM SPSS (IBM Corp, Armonk, NY, USA) version 25.0.

CONFLICTS OF INTEREST

All authors disclose no conflicts of interest.

FUNDING

This study was partially supported by Ricerca Corrente funding from Italian Ministry of Health to IRCCS INRCA and by grants from UNIVPM to FO.

REFERENCES

1. Fulop T, Witkowski JM, Olivieri F, Larbi A. The integration of inflammaging in age-related diseases. Semin Immunol. 2018; 40:17–35. https://doi.org/10.1016/j.smim.2018.09.003

2. Dening T, Sandilyan MB. Dementia: definitions and types. Nurs Stand. 2015; 29:37–42. https://doi.org/10.7748/ns.29.37.37.e9405

3. Dubois B, Feldman HH, Jacova C, Dekosky ST, Barberger-Gateau P, Cummings J, Delacourte A, Galasko D, Gauthier S, Jicha G, Meguro K, O'brien J, Pasquier F, et al. Research criteria for the diagnosis of Alzheimer's disease: revising the NINCDS-ADRDA criteria. Lancet Neurol. 2007; 6:734–46. https://doi.org/10.1016/S1474-4422(07)70178-3

4. Mattsson N, Blennow K, Zetterberg H. CSF biomarkers: pinpointing Alzheimer pathogenesis. Ann N Y Acad Sci. 2009; 1180:28–35. https://doi.org/10.1111/j.1749-6632.2009.04944.x

5. Ritchie C, Smailagic N, Noel-Storr AH, Ukoumunne O, Ladds EC, Martin S. CSF tau and the CSF tau/ABeta ratio for the diagnosis of Alzheimer's disease dementia and other dementias in people with mild cognitive impairment (MCI). Cochrane Database Syst Rev. 2017; 3:CD010803.

6. Yamada K. Extracellular Tau and its potential role in the propagation of Tau pathology. Front Neurosci. 2017; 11:667. https://doi.org/10.3389/fnins.2017.00667

7. Holtzman DM, Morris JC, Goate AM. Alzheimer's disease: the challenge of the second century. Sci Transl Med. 2011; 3:77sr1. https://doi.org/10.1126/scitranslmed.3002369

8. Bateman RJ, Xiong C, Benzinger TL, Fagan AM, Goate A, Fox NC, Marcus DS, Cairns NJ, Xie X, Blazey TM, Holtzman DM, Santacruz A, Buckles V, et al, and Dominantly Inherited Alzheimer Network. Clinical and biomarker changes in dominantly inherited Alzheimer's disease. N Engl J Med. 2012; 367:795–804. https://doi.org/10.1056/NEJMoa1202753

9. Lee MK, Cleveland DW. Neurofilament function and dysfunction: involvement in axonal growth and neuronal disease. Curr Opin Cell Biol. 1994; 6:34–40. https://doi.org/10.1016/0955-0674(94)90113-9

10. Yuan A, Rao MV, Veeranna, Nixon RA. Neurofilaments at a glance. J Cell Sci. 2012; 125:3257–63. https://doi.org/10.1242/jcs.104729

11. Olsson B, Lautner R, Andreasson U, Öhrfelt A, Portelius E, Bjerke M, Hölttä M, Rosén C, Olsson C, Strobel G, Wu E, Dakin K, Petzold M, et al. CSF and blood biomarkers for the diagnosis of Alzheimer's disease: a systematic review and meta-analysis. Lancet Neurol. 2016; 15:673–84. https://doi.org/10.1016/S1474-4422(16)00070-3

12. Zetterberg H, Skillbäck T, Mattsson N, Trojanowski JQ, Portelius E, Shaw LM, Weiner MW, Blennow K, and Alzheimer's Disease Neuroimaging Initiative. Association of cerebrospinal fluid neurofilament light concentration with Alzheimer Disease progression. JAMA Neurol. 2016; 73:60–67. https://doi.org/10.1001/jamaneurol.2015.3037

13. Teunissen CE, Khalil M. Neurofilaments as biomarkers in multiple sclerosis. Mult Scler. 2012; 18:552–56. https://doi.org/10.1177/1352458512443092

14. Khalil M, Salzer J. CSF neurofilament light: A universal risk biomarker in multiple sclerosis? Neurology. 2016; 87:1068–69. https://doi.org/10.1212/WNL.0000000000003107

15. Gaiani A, Martinelli I, Bello L, Querin G, Puthenparampil M, Ruggero S, Toffanin E, Cagnin A, Briani C, Pegoraro E, Sorarù G. Diagnostic and prognostic biomarkers in Amyotrophic Lateral Sclerosis: neurofilament light chain levels in definite subtypes of disease. JAMA Neurol. 2017; 74:525–32. https://doi.org/10.1001/jamaneurol.2016.5398

16. Sjögren M, Blomberg M, Jonsson M, Wahlund LO, Edman A, Lind K, Rosengren L, Blennow K, Wallin A. Neurofilament protein in cerebrospinal fluid: a marker of white matter changes. J Neurosci Res. 2001; 66:510–16. https://doi.org/10.1002/jnr.1242

17. Sjögren M, Rosengren L, Minthon L, Davidsson P, Blennow K, Wallin A. Cytoskeleton proteins in CSF distinguish frontotemporal dementia from AD. Neurology. 2000; 54:1960–64. https://doi.org/10.1212/WNL.54.10.1960

18. Skillbäck T, Farahmand B, Bartlett JW, Rosén C, Mattsson N, Nägga K, Kilander L, Religa D, Wimo A, Winblad B, Rosengren L, Schott JM, Blennow K, et al. CSF neurofilament light differs in neurodegenerative diseases and predicts severity and survival. Neurology. 2014; 83:1945–53. https://doi.org/10.1212/WNL.0000000000001015

19. Mattsson N, Bremell D, Anckarsäter R, Blennow K, Anckarsäter H, Zetterberg H, Hagberg L. Neuroinflammation in Lyme neuroborreliosis affects amyloid metabolism. BMC Neurol. 2010; 10:51. https://doi.org/10.1186/1471-2377-10-51

20. Norgren N, Edelstam A, Stigbrand T. Cerebrospinal fluid levels of neurofilament light in chronic experimental autoimmune encephalomyelitis. Brain Res Bull. 2005; 67:264–68. https://doi.org/10.1016/j.brainresbull.2005.06.031

21. Kiko T, Nakagawa K, Tsuduki T, Furukawa K, Arai H, Miyazawa T. MicroRNAs in plasma and cerebrospinal fluid as potential markers for Alzheimer's disease. J Alzheimers Dis. 2014; 39:253–59. https://doi.org/10.3233/JAD-130932

22. Jin Y, Tu Q, Liu M. MicroRNA 125b regulates Alzheimer's disease through SphK1 regulation. Mol Med Rep. 2018; 18:2373–80. https://doi.org/10.3892/mmr.2018.9156

23. Dangla-Valls A, Molinuevo JL, Altirriba J, Sánchez-Valle R, Alcolea D, Fortea J, Rami L, Balasa M, Muñoz-García C, Ezquerra M, Fernández-Santiago R, Lleó A, Lladó A, Antonell A. CSF microRNA profiling in Alzheimer's Disease: a screening and validation study. Mol Neurobiol. 2017; 54:6647–54. https://doi.org/10.1007/s12035-016-0106-x

24. Fiebich BL, Batista CR, Saliba SW, Yousif NM, de Oliveira AC. Role of Microglia TLRs in Neurodegeneration. Front Cell Neurosci. 2018; 12:329. https://doi.org/10.3389/fncel.2018.00329

25. Olivieri F, Rippo MR, Procopio AD, Fazioli F. Circulating inflamma-miRs in aging and age-related diseases. Front Genet. 2013; 4:121. https://doi.org/10.3389/fgene.2013.00121

26. Bacioglu M, Maia LF, Preische O, Schelle J, Apel A, Kaeser SA, Schweighauser M, Eninger T, Lambert M, Pilotto A, Shimshek DR, Neumann U, Kahle PJ, et al. Neurofilament light chain in blood and CSF as marker of disease progression in mouse models and in neurodegenerative diseases. Neuron. 2016; 91:56–66. https://doi.org/10.1016/j.neuron.2016.05.018

27. Frankfort SV, Tulner LR, van Campen JP, Verbeek MM, Jansen RW, Beijnen JH. Amyloid beta protein and tau in cerebrospinal fluid and plasma as biomarkers for dementia: a review of recent literature. Curr Clin Pharmacol. 2008; 3:123–31. https://doi.org/10.2174/157488408784293723

28. Buerger K, Otto M, Teipel SJ, Zinkowski R, Blennow K, DeBernardis J, Kerkman D, Schröder J, Schönknecht P, Cepek L, McCulloch C, Möller HJ, Wiltfang J, et al. Dissociation between CSF total tau and tau protein phosphorylated at threonine 231 in Creutzfeldt-Jakob disease. Neurobiol Aging. 2006; 27:10–15. https://doi.org/10.1016/j.neurobiolaging.2004.12.003

29. Blennow K, Hampel H. CSF markers for incipient Alzheimer's disease. Lancet Neurol. 2003; 2:605–13. https://doi.org/10.1016/S1474-4422(03)00530-1

30. Otto M, Wiltfang J, Tumani H, Zerr I, Lantsch M, Kornhuber J, Weber T, Kretzschmar HA, Poser S. Elevated levels of tau-protein in cerebrospinal fluid of patients with Creutzfeldt-Jakob disease. Neurosci Lett. 1997; 225:210–12. https://doi.org/10.1016/S0304-3940(97)00215-2

31. Petzold A. Neurofilament phosphoforms: surrogate markers for axonal injury, degeneration and loss. J Neurol Sci. 2005; 233:183–98. https://doi.org/10.1016/j.jns.2005.03.015

32. Arevalo-Rodriguez I, Smailagic N, Roqué I Figuls M, Ciapponi A, Sanchez-Perez E, Giannakou A, Pedraza OL, Bonfill Cosp X, Cullum S. Mini-Mental State Examination (MMSE) for the detection of Alzheimer's disease and other dementias in people with mild cognitive impairment (MCI). Cochrane Database Syst Rev. 2015; 3:CD010783. https://doi.org/10.1002/14651858.CD010783.pub2

33. Mattsson N, Andreasson U, Zetterberg H, Blennow K, and Alzheimer's Disease Neuroimaging Initiative. Association of plasma neurofilament light with neurodegeneration in patients with Alzheimer Disease. JAMA Neurol. 2017; 74:557–66. https://doi.org/10.1001/jamaneurol.2016.6117

34. Ji R, Cheng Y, Yue J, Yang J, Liu X, Chen H, Dean DB, Zhang C. MicroRNA expression signature and antisense-mediated depletion reveal an essential role of MicroRNA in vascular neointimal lesion formation. Circ Res. 2007; 100:1579–88. https://doi.org/10.1161/CIRCRESAHA.106.141986

35. Ahmed FW, Bakhashab S, Bastaman IT, Crossland RE, Glanville M, Weaver JU. Anti-Angiogenic miR-222, miR-195, and miR-21a plasma levels in T1DM are improved

by metformin therapy, thus elucidating its cardioprotective effect: the MERIT Study. Int J Mol Sci. 2018; 19:3242. https://doi.org/10.3390/ijms19103242

36. Mensà E, Recchioni R, Marcheselli F, Giuliodori K, Consales V, Molinelli E, Prattichizzo F, Rippo MR, Campanati A, Procopio AD, Olivieri F, Offidani AM. MiR-146a-5p correlates with clinical efficacy in patients with psoriasis treated with the tumour necrosis factor-alpha inhibitor adalimumab. Br J Dermatol. 2018; 179:787–89. https://doi.org/10.1111/bjd.16659

37. Jin F, Xing J. Circulating pro-angiogenic and anti-angiogenic microRNA expressions in patients with acute ischemic stroke and their association with disease severity. Neurol Sci. 2017; 38:2015–23. https://doi.org/10.1007/s10072-017-3071-x

38. Irwin DJ, Trojanowski JQ, Grossman M. Cerebrospinal fluid biomarkers for differentiation of frontotemporal lobar degeneration from Alzheimer's disease. Front Aging Neurosci. 2013; 5:6. https://doi.org/10.3389/fnagi.2013.00006

39. Jack CR Jr, Albert MS, Knopman DS, McKhann GM, Sperling RA, Carrillo MC, Thies B, Phelps CH. Introduction to the recommendations from the National Institute on Aging-Alzheimer's Association workgroups on diagnostic guidelines for Alzheimer's disease. Alzheimers Dement. 2011; 7:257–62. https://doi.org/10.1016/j.jalz.2011.03.004

40. McKhann GM, Knopman DS, Chertkow H, Hyman BT, Jack CR Jr, Kawas CH, Klunk WE, Koroshetz WJ, Manly JJ, Mayeux R, Mohs RC, Morris JC, Rossor MN, et al. The diagnosis of dementia due to Alzheimer's disease: recommendations from the National Institute on Aging-Alzheimer's Association workgroups on diagnostic guidelines for Alzheimer's disease. Alzheimers Dement. 2011; 7:263–69. https://doi.org/10.1016/j.jalz.2011.03.005

41. Litvan I, Agid Y, Calne D, Campbell G, Dubois B, Duvoisin RC, Goetz CG, Golbe LI, Grafman J, Growdon JH, Hallett M, Jankovic J, Quinn NP, et al. Clinical research criteria for the diagnosis of progressive supranuclear palsy (Steele-Richardson-Olszewski syndrome): report of the NINDS-SPSP international workshop. Neurology. 1996; 47:1–9. https://doi.org/10.1212/WNL.47.1.1

42. Neary D, Snowden JS, Gustafson L, Passant U, Stuss D, Black S, Freedman M, Kertesz A, Robert PH, Albert M, Boone K, Miller BL, Cummings J, Benson DF. Frontotemporal lobar degeneration: a consensus on clinical diagnostic criteria. Neurology. 1998; 51:1546–54. https://doi.org/10.1212/WNL.51.6.1546

43. Rascovsky K, Hodges JR, Knopman D, Mendez MF, Kramer JH, Neuhaus J, van Swieten JC, Seelaar H, Dopper EG, Onyike CU, Hillis AE, Josephs KA, Boeve BF, et al. Sensitivity of revised diagnostic criteria for the behavioural variant of frontotemporal dementia. Brain. 2011; 134:2456–77. https://doi.org/10.1093/brain/awr179

44. Román GC, Tatemichi TK, Erkinjuntti T, Cummings JL, Masdeu JC, Garcia JH, Amaducci L, Orgogozo JM, Brun A, Hofman A, Moody DM, O'Brien MD, Yamaguchi T, et al. Vascular dementia: diagnostic criteria for research studies. Report of the NINDS-AIREN International Workshop. Neurology. 1993; 43:250–60. https://doi.org/10.1212/WNL.43.2.250

45. Sachdev P, Kalaria R, O'Brien J, Skoog I, Alladi S, Black SE, Blacker D, Blazer DG, Chen C, Chui H, Ganguli M, Jellinger K, Jeste DV, et al, and Internationlal Society for Vascular Behavioral and Cognitive Disorders. Diagnostic criteria for vascular cognitive disorders: a VASCOG statement. Alzheimer Dis Assoc Disord. 2014; 28:206–18. https://doi.org/10.1097/WAD.0000000000000034

46. Armstrong MJ, Litvan I, Lang AE, Bak TH, Bhatia KP, Borroni B, Boxer AL, Dickson DW, Grossman M, Hallett M, Josephs KA, Kertesz A, Lee SE, et al. Criteria for the diagnosis of corticobasal degeneration. Neurology. 2013; 80:496–503. https://doi.org/10.1212/WNL.0b013e31827f0fd1

47. Albert MS, DeKosky ST, Dickson D, Dubois B, Feldman HH, Fox NC, Gamst A, Holtzman DM, Jagust WJ, Petersen RC, Snyder PJ, Carrillo MC, Thies B, Phelps CH. The diagnosis of mild cognitive impairment due to Alzheimer's disease: recommendations from the National Institute on Aging-Alzheimer's Association workgroups on diagnostic guidelines for Alzheimer's disease. Alzheimers Dement. 2011; 7:270–79. https://doi.org/10.1016/j.jalz.2011.03.008

48. Tabaraud F, Leman JP, Milor AM, Roussie JM, Barrière G, Tartary M, Boutros-Toni F, Rigaud M. Alzheimer CSF biomarkers in routine clinical setting. Acta Neurol Scand. 2012; 125:416–23. https://doi.org/10.1111/j.1600-0404.2011.01592.x

49. Giuliani A, Cirilli I, Prattichizzo F, Mensà E, Fulgenzi G, Sabbatinelli J, Graciotti L, Olivieri F, Procopio AD, Tiano L, Rippo MR. The mitomiR/Bcl-2 axis affects mitochondrial function and autophagic vacuole formation in senescent endothelial cells. Aging (Albany NY). 2018; 10:2855–73. https://doi.org/10.18632/aging.101591

Ageing Research Reviews 50 (2019) 27–42

Contents lists available at ScienceDirect

Ageing Research Reviews

journal homepage: www.elsevier.com/locate/arr

Review

The telomere world and aging: Analytical challenges and future perspectives

Emanuela Mensà[a], Silvia Latini[a], Deborah Ramini[a], Gianluca Storci[b,c], Massimiliano Bonafè[b,c,d], Fabiola Olivieri[a,e,*]

[a] Department of Clinical and Molecular Sciences, DISCLIMO, Università Politecnica delle Marche, Ancona, Italy
[b] Department of Experimental, Diagnostic and Specialty Medicine, University of Bologna, Bologna, Italy
[c] Interdepartmental Centre "L. Galvani" (CIG), University of Bologna, Bologna, Italy
[d] Istituto Scientifico Romagnolo per lo Studio e la Cura dei Tumori (IRST), IRCCS, Biosciences Laboratory, Meldola, Italy
[e] Center of Clinical Pathology and Innovative Therapy, IRCCS INRCA, Ancona, Italy

ARTICLE INFO

Keywords:
Telomere length
TERRA
Telomerase activity
Aging

ABSTRACT

Telomeres, the terminal nucleoprotein structures of eukaryotic chromosomes, play pleiotropic functions in cellular and organismal aging. Telomere length (TL) varies throughout life due to the influence of genetic factors and to a complex balancing between "shortening" and "elongation" signals. Telomerase, the only enzyme that can elongate a telomeric DNA chain, and telomeric repeat-containing RNA (TERRA), a long non-coding RNA involved in looping maintenance, play key roles in TL during life. Despite recent advances in the knowledge of TL, TERRA and telomerase activity (TA) biology and their measurement techniques, the experimental and theoretical issues involved raise a number of problems that should carefully be considered by researchers approaching the "telomere world". The increasing use of such parameters – hailed as promising clinically relevant biomarkers – has failed to be paralleled by the development of automated and standardized measurement technology. Consequently, associating given TL values to specific pathological conditions involves on the one hand technological issues and on the other clinical-biological issues related to the planning of clinically relevant association studies. Addressing these issues would help avoid major biases in association studies involving TL and a number of outcomes, especially those focusing on psychological and bio-behavioral variables. The main challenge in telomere research is the development of accurate and reliable measurement methods to achieve simple and sensitive TL, TERRA, and TA detection. The discovery of the localization of telomeres and TERRA in cellular and extracellular compartments had added an additional layer of complexity to the measurement of these age-related biomarkers. Since combined analysis of TL, TERRA and TA may well provide more exhaustive clinical information than a single parameter, we feel it is important for researchers in the various fields to become familiar with their most common measurement techniques and to be aware of the respective merits and drawbacks of these approaches.

1. Introduction

Telomeres, the terminal nucleoprotein structures of eukaryotic chromosomes, have a key role in protecting chromosomal DNA ends (Blackburn, 1990). Mounting evidence suggests that they play pleiotropic functions that are not simply related to the maintenance of chromosome homeostasis, but also to the regulation of gene expression and the modulation of stress-related signaling pathways (Blackburn, 2005). Telomere length (TL) is species-specific and heritable (Chiang et al., 2010); therefore, its value at any time depends on genetic characteristics and on the balance between "shortening" and "elongation" signals (Honig et al., 2015). Shortening signals come from a variety of stressors like repeated cell division, nuclease activation, oxidative damage, DNA replication, and transcriptional stress (Blackburn et al., 2015). Elongation signals are capable of activating telomerase or alternative lengthening of telomeres (ALT); the latter mechanism relies on recombination-mediated telomere elongation and can be induced by telomere-specific DNA damage (Hu et al., 2016). Telomerase is an RNA-protein complex that extends telomeric DNA at the 3′ ends of chromosomes through telomerase reverse transcriptase (TERT) and integral template-containing telomerase RNA (TER) (Jiang et al., 2018). Telomerase is responsible for the preservation of replicative potential in most eukaryotic cells and is involved in pleiotropic functions that range from TL maintenance and genome stability to tissue renewal and

* Corresponding author at: Department of Clinical and Molecular Sciences (DISCLIMO), Università Politecnica delle Marche, Via Conca 70, Ancona, Italy.
E-mail address: f.olivieri@univpm.it (F. Olivieri).

https://doi.org/10.1016/j.arr.2019.01.004
Received 31 August 2018; Received in revised form 15 November 2018; Accepted 3 January 2019
Available online 04 January 2019
1568-1637/

mitochondrial protection (Li et al., 2018a, 2018b). TL is a marker of the metabolic activity and pluripotency state of embryonic stem cells (Wang et al., 2017a). In embryonic cell lines telomerase is activated and keeps TL constant; in adult stem cells its limited activity and provides only partial compensation for telomere shortening (TS); and in somatic cells it is usually not activated. As a result, during somatic cellular and organismal aging shortening outpaces elongation. Telomeres that have reached a critical length become dysfunctional and activate a DNA damage response which leads to a senescence phenotype characterized by reduced proliferative ability and the acquisition of a secretory proinflammatory phenotype (SASP) (d'Adda di Fagagna et al., 2003).

TL has long been known to be critically involved in cellular aging as a consequence of replication and/or the action of a wide range of stressors, but is also being extensively investigated in relation to organismal aging. Although cell senescence does not necessarily equate with aging of an organism, TS has been observed in both conditions (reviewed in Zhu et al., 2018), and TL has been investigated as a biomarker of aging *per se* and as a risk factor for the development and progression of the most common age-related diseases (ARDs) (Jose et al., 2017).

Recent insights into telomere biology and function indicate that telomeric repeat-containing RNA (TERRA), a long non-coding RNA, is involved in the telomere looping maintenance mechanism (Graf et al., 2017). An inverse correlation has been documented between TL and TERRA both *in vitro* and *in vivo*. According to two hypotheses that have been advanced to explain it, TERRA transcription could facilitate 5′-3′ nuclease activity at the chromosome ends (Pfeiffer and Lingner, 2012), or TS could induce TERRA expression to coordinate telomerase molecule recruitment and activity at the shortest telomeres (Cusanelli et al., 2013).

Notably, telomere DNA, TERRA, and telomerase are not independent molecules; in fact, their structures and temporal relationships are closely regulated by complexes such as shelterin, small nucleolar RNAs (snoRNAs), and small nucleolar ribonucleoproteins (snoRNPs), besides the transcription machinery (Blasco et al., 1999; Gomez et al., 2012). Even though the latter molecules are capable of affecting endpoint TL, the present work focuses on telomeres, TERRA, and telomerase activity (TA).

Despite recent advances, there are a number of outstanding issues related to the knowledge and measurement technology of TL, TERRA, and TA. The most important are: i) the accuracy of the methods employed to measure TL, TERRA, and TA in biomedical research; ii) their strengths and weaknesses; iii) the scope for their improvement; iv) the chemical-clinical variables to be correlated with TL in association studies of aging and ARDs; and v) the need for human longitudinal studies to evaluate the ability of specific approaches (pharmaceutical, nutraceutical) to reverse TS during aging.

Addressing these issues would help avoid major biases in association studies addressing TL and a wide range of outcomes (Montpetit et al., 2014).

This work describes the analytical caveats and criticisms regarding the various TL, TERRA, and TA measurement methods. Since not all protocols are appropriate (or recommended) for epidemiological and longitudinal ARD studies, and some approaches may be applicable only to tumor tissue, the paper focuses on the methods that are suitable for clinical and epidemiological applications.

We will also describe and discuss the localization of telomere and telomere-related sequences in the cellular and extracellular compartment, since localization adds an additional layer of complexity to telomere, TERRA, and TA measurement.

2. Localization of telomere and telomere-related sequences

Recent studies have highlighted a number of possible localizations of telomeric sequences, including the cellular and extracellular compartment (Fig. 1). In cells, telomere sequences can be detected in the nucleus, the chromosome ends and interstitial loci (Smith et al., 2018), and the cytoplasm (Cohen et al., 2010; Zhang et al., 2017a). Localizations in the extracellular compartment include exosomes (Li et al., 2008; Zinkova et al., 2017).

An increased number of telomeric sequences has been described in the cytoplasm of stressed cells in physiological as well as pathological conditions (Kuttler and Mai, 2007; Byrd et al., 2016). Telomeric circles (t-circles or c-circles) are extrachromosomal duplex or single-stranded circular DNA molecules composed of (CCCTAA)(n) sequences. Integration of t-circles in telomere repeats at the chromosome ends results in telomere elongation; circular DNA forms can also be involved in the rapid elongation of DNA ends in rolling-circle replication processes (Nabetani and Ishikawa, 2011).

T-circles, which can be found in human immortalized and cancer cells, rely on ALT pathways or high TA (Tokutake et al., 1998). In fact, in cells showing high TA, extrachromosomal telomeric DNA circles can be excised from the overextended chromosomal ends and released outside the nucleus (Pickett et al., 2009). T-circles have been detected in blood from patients with ALT + tumors; their analysis may have clinical value for their diagnosis and management (Henson et al., 2009). Importantly, t-circles are also found in healthy tissue (Tomaska et al., 2009).

Recent evidence indicates that telomeric sequences are also found in cell-free (cf)-DNA, including biofluids such as plasma and serum (Zinkova et al., 2017). Most of the DNA found in such biofluids is associated to nanovesicles, mainly exosomes, (Fernando et al., 2017; Németh et al., 2017).

TERRA, the long non-coding RNA molecules deriving from transcription of telomeric/subtelomeric regions, is enriched with 5′-(UUAGGG)-3′ repetitions that are complementary to AATCCC, the strand opposite to TTAGGG sequences. TERRA can therefore combine with AATCCC strands, generating three-stranded nucleic acid structures that contain a DNA:RNA hybrid molecule and a displaced DNA strand (Balk et al., 2014). These structures are localized at the level of R-loops and are involved in telomere homeostasis (Toubiana and Selig, 2018). In contrast, UUTCCC molecules, the RNA sequence complementary to TTAGGG, are not related to telomere DNA:RNA hybrids in human cells.

Notably, cf-TERRA – which is shorter (measuring about 200 nt) and more stable than TERRA associated to telomeric DNA in the nucleus – has also been detected in extracellular vesicles. These characteristics suggest that some extrachromosomal telomere-related sequences may be RNA and/or DNA:RNA hybrids (Wang and Lieberman, 2016) (see Fig. 1).

In eukaryotic cells, telomeres and TERRA can fold into G-quadruplexes (G4s), which are characterized by four G combined through non-canonical Hoogsten hydrogen bonding to generate planar structures called tetrads (Martadinata et al., 2011; Wang et al., 2018a) (see Fig. 1). Two or more tetrads can overlap and interact with each other *via* π-stacking, generating stable G4s. Experimental studies and bioinformatics predictions support the view that G4s are involved in several cellular functions such as telomeric DNA elongation, recombination, and transcription, and RNA post-transcriptional mechanisms (Cammas and Millevoi, 2017).

Whereas the location of telomere sequences and TERRA in the nucleus is well known, it is more difficult to describe the cytoplasmic localization of telomere repeats and TERRA.

It has been hypothesized that a cytoplasmic location of TAGGG may exert a suppressive effect on innate immune cells due to their ability to form G4s (Gursel et al., 2003). Colocalization of CpG DNA with toll-like receptor (TLR) 9 in endosomal vesicles is disrupted by TTAGGG telomeric repetitive elements, although cell binding and uptake remain unchanged, suggesting that specific host-derived molecules can downregulate the innate immune response elicited by a TLR ligand.

While cytoplasmic (cy-) or cf-telomeric sequences seem to restrain inflammation, TERRA found in extracellular fractions can stimulate innate immune signaling (Wang et al., 2015). TERRA can be activated

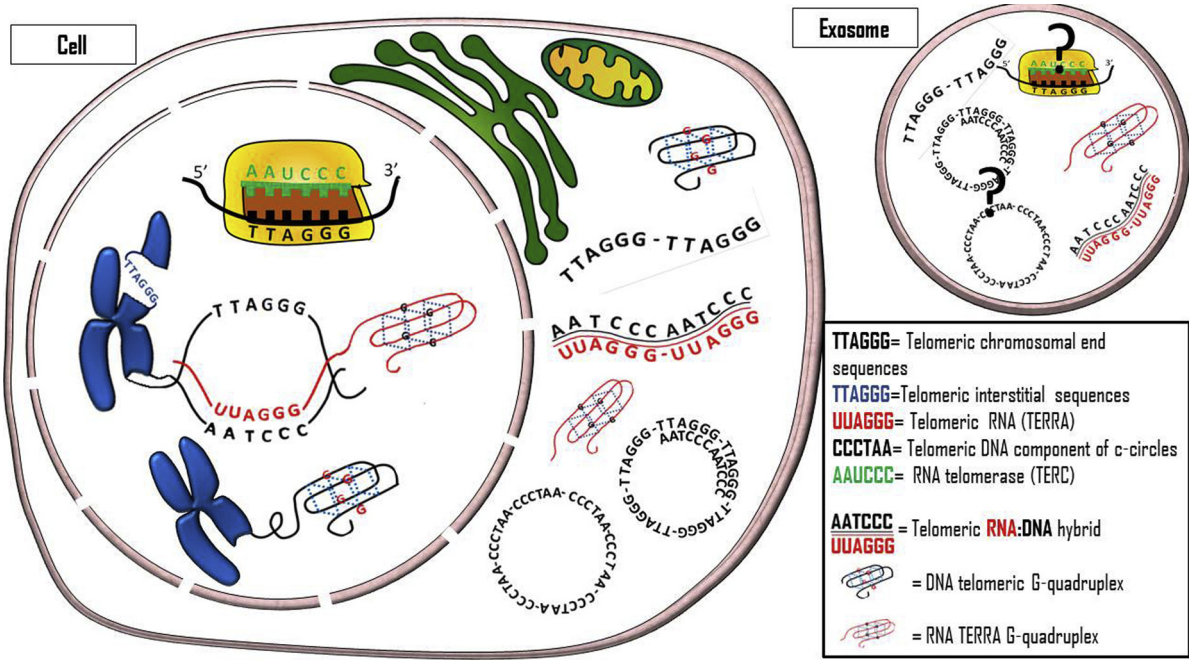

Fig. 1. Telomere-related molecules in cells (nucleus and cytoplasm) and exosomes.
Telomeric sequences can have a number of possible localizations not only in cells (nucleus and cytoplasm) but also in nanovesicles.
DNA, TERRA, DNA:RNA hybrids, and telomerase are not independent molecules: their structures and temporal relationships are closely regulated by key complexes such as shelterin and snoRNPs, besides the transcription machinery. However, these important parameters cannot be depicted here.

through a p53-response element embedded in a retrotransposon-like repeat found in human subtelomeres. TERRA secretion in extracellular vesicles serves as a danger signal, inducing the production of inflammatory cytokines in neighboring cells (Wang et al., 2017c). These findings suggest that TERRA may be part of the innate immune response to viral infection and that exosomes containing cf-TERRA carry a telomere-associated molecular pattern and telomere-specific alarmin from dysfunctional telomeres to the extracellular environment to elicit an inflammatory response (Wang and Lieberman, 2016).

Recently, we have hypothesized that telomeric sequences may be important components of the cy- and cf-DNA payload and that changes in a variety of biochemical features of cy- and cf-DNA (*e.g.* the proportion of DNA hybridized with RNA and the amount of 5-methyl-deoxy-cytosine and 8-oxo-deoxy-guanosine) can affect the ability of these DNA pools to ignite the innate immune system (Storci et al., 2018).

Notably, the localization of telomeric sequences in the cellular and extracellular compartment adds a further layer of complexity to telomere measurement, because different extraction/separation procedures may affect their reciprocal amounts (Komosa et al., 2015).

3. Telomeres and aging

A number of epidemiological studies have found a significant association linking telomere attrition, aging, and several biological outcomes including morbidity and mortality (Gorenjak et al., 2018; Gao et al., 2018). Short leukocyte TL (LTL) has been identified as an independent risk factor for functional decline in elderly European populations (Montiel Rojas et al., 2018) and has been found to be associated to altered fatty acid metabolism and increased oxidative stress in human aging (Zierer et al., 2016). Epidemiological studies provide support for a putative effect of dietary components and exercise on TL and the aging process (Mundstock et al., 2015a; Freitas-Simoes et al., 2018). An association has also been reported between telomere attrition and body mass index gain, suggesting potential pathways linking adiposity and aging outcomes (Müezzinler et al., 2016; Wulaningsih et al., 2018). However, these associations have been described in works performed with different methodological approaches, of which few were prospective; adequately powered randomized controlled trials are therefore warranted. For all these reasons, the causal relationships between important functional parameters and TL remain an open question (Mundstock et al., 2015b; Pérez et al., 2017).

Recent evidence suggests that TL may not be a useful clinical marker of functional aging in older adult populations, whereas it may play a crucial role in longitudinal studies involving young and middle-aged populations (Brown et al., 2018). Since the trajectories of aging begin to diverge as early as in young adulthood (Belsky et al., 2015), it is critical to assess the contribution of telomere-related variations to the diverse aging pathways. Although telomeres shorten during aging, different cell types may have a diverse telomere attrition rate (TAR), *i.e.* a different rate of tissue and organ aging. A yearly TAR of ~25 base pairs during aging has been reported in blood leukocytes, mononuclear cells, and isolated T and B lymphocytes (Müezzinler et al., 2013), whereas high interindividual TAR variation has been described in some longitudinal studies (Chen et al., 2011; Lin et al., 2015).

The marked heterogeneity of health outcomes seen in older individuals suggests that although “chronological” age is a major risk factor for functional impairment, “biological” age may be a more accurate predictor of the rate of aging (Lowsky et al., 2014). TL is currently the most extensively investigated biological age predictor, although new predictors, *e.g.* the epigenetic clock, are emerging (Jylhävä et al., 2017). Mounting evidence suggests that the various biological age predictors may reflect different aspects of the aging process, even though links between the various biomarkers are likely (Vetter et al., 2018). At present, the most stimulating area in telomere research is the study of how progressive TS induces epigenetic alterations and changes in gene expression associated to human healthy and unhealthy aging (Shay, 2018). In this scenario, combinations of the diverse predictors may shed light on the complexity of the aging process and help to improve the estimation of aging trajectories. Composite scores integrating molecular and physiological data have been proposed to measure biological aging in humans (Khan et al., 2017; Belsky et al.,

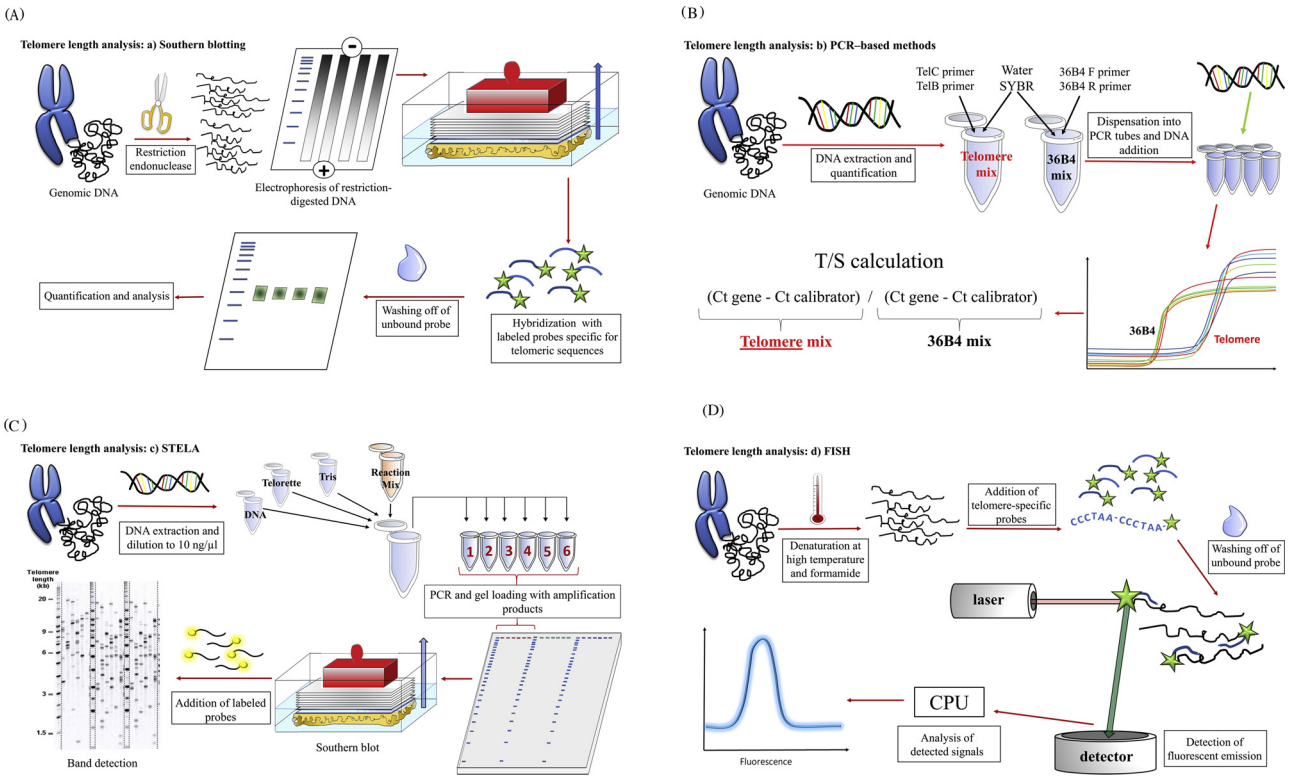

Fig. 2. Most commonly used techniques employed to measure TL.
Schematic representation of the most common techniques employed to measure TL: 2a) Southern blotting-RTF; 2b) PCR-based methods; 2c) STELA; 2d) FISH.

2018).

Growing evidence also suggests that the association of LTL to functional impairment, *i.e.* frailty, may be driven by the unfavorable effect of having short telomeres, rather than reflect a linear dose-response relationship. Short telomeres, rather than TL *per se*, may thus be an informative biomarker of aging and ARDs (Montiel Rojas et al., 2018; Haapanen et al., 2018). Several findings indicate that short telomeres precede the clinical manifestation of the most common ARDs, such as type 2 diabetes and atherosclerotic disease (Toupance et al., 2017).

Overall, even though the factors involved in TAR and the pleiotropic roles of telomeres are not entirely clear, TL is being widely used as a biomarker of the aging process, and intense effort is being devoted to translating TL values into information that can be employed in clinical practice (Hastings et al., 2017). However, translation from the bench to the beside is being hampered by a number of biological factors, including the dependence of TL on genetic, epigenetic, environmental and behavioral factors, as well as by technical aspects such as pre-analytical issues and poor standardization of TL measurement techniques (Danese and Lippi, 2018). With regard to the latter question, since current measurement methods have been developed for use in molecular biology laboratories, reliable and robust TL estimation requires a high level of technical understanding and competence. Since researchers involved in areas other than cell biology, including physiology, psychology, evolution and ecology, have become interested in telomere biology and dynamics (Nussey et al., 2014; Conklin et al., 2018), we feel it is important for all those who work in these varied fields to become familiar with the most common TL measurement techniques and to be aware of their respective advantages and drawbacks.

4. Measurement of telomere length: analytical caveats

A variety of techniques are employed to measure TL; they include: i) Southern blot analysis of terminal restriction fragments (TRFs), which measures the length distribution and average TL in biological samples; ii) fluorescence *in situ* hybridization (FISH), including Q-FISH and flow-FISH; iii) polymerase chain reaction (PCR)-based methods like quantitative (q)PCR, Single TElomere Length Analysis (STELA), and Telomere Shortest Length Assay (TeSLA); and iv) whole genome sequencing (WGS)-based techniques.

Although Southern blotting is the gold standard technique for TL measurement, the methods used most frequently in clinical and epidemiological studies are qPCR and FISH. Since the correlations among Southern blotting, FISH, and qPCR data from different laboratories can show different strength, laboratory-specific internal validation is clearly essential (Khincha et al., 2017).

The most commonly used matrix for TL measurement is still venous blood, although less invasive DNA collection methods are increasingly used. However, too little is known about how TL values relate in different samples. A recent study of three matrices – whole venous blood, finger-prick dried blood spot (DBS) and saliva – has shown that DBS and saliva are viable alternatives to invasive venous blood draws (Stout et al., 2017). Notably, TL values were higher in saliva than in whole blood or DBS.

Notably, all TL measurement techniques have been developed at a time when telomeric sequences were believed to be measureable only in the nucleus of eukaryotic cells. Now that TL has been found to provide much more complex biological information, it would be useful to distinguish between TL measured in the nucleus and in the other intra- and extracellular compartments. The difficulty of applying some of the techniques devised for the nucleus to sequences found in extra-chromosomal compartments suggests the need for novel technical approaches.

Since all TL measurement methods suffer from considerable weaknesses, several analytical caveats must be resolved before they can be put to routine use (Tarik et al., 2018; Lai et al., 2017, 2018).

The most commonly used methods and their technical drawbacks

are briefly reviewed below and depicted in Fig. 2 (**2a,** Southern blotting- TRF**; 2b,** PCR-based methods; **2c,** STELA; **2d** FISH).

4.1. Terminal restriction fragment (TRF) technique

This is a modified Southern blotting approach that measures the TL range in a cell population using the TRF length distribution expressed in kilobases (Fig. 2a) (Harley et al., 1990; Ouellette et al., 2000). It is one of the earliest TL assessment tools and has become the gold standard in telomere biology. DNA is extracted, digested, resolved by gel electrophoresis, transferred to a membrane, hybridized with labeled probes, and quantified. Though precise and highly accurate, it requires a considerable amount of intact genomic DNA and provides only an average TL for a population of cells (Kimura et al., 2010). The use of this time-consuming, expensive, and labor-intensive technique, which also requires high DNA concentrations, is therefore generally limited to studies involving limited number of samples. Southern blot analysis has recently been proposed to monitor the addition of telomeric sequences to single, newly generated telomeres *in vivo* (Bonetti and Longhese, 2018).

4.2. qPCR technique

qPCR is widely used in epidemiological studies, because it quickly provides mean relative TL (RTL) and requires small amounts of DNA (about 20 ng/reaction) (Fig. 2b). Introduced by Cawthon (2009), it achieves telomeric DNA detection through fluorescent signals (T) using partially mismatched primers. Telomeric DNA is normalized to a single-copy housekeeping gene (S) amplified in the same sample, and the T/S ratio is computed as a measure of RTL. A successive, improved version, Monochrome Multiplex Real-Time PCR (MMQPCR), requires a smaller amount of DNA. Amplification of both telomeric DNA and the single-copy gene in the same well of a plate reduce variability compared with monoplex PCR. Since the use of single-copy genes does not ensure optimal data normalization in cancer DNA, new primer sets have been developed to obtain a more precise evaluation of RTL (Dahlgren et al., 2018).

The chief drawback of measuring TL by qPCR is primer design. The repetitive nature of telomeres involves that primers can crosslink, giving rise to dimers and non-specific PCR signal. The problem can be overcome using samples with a good initial amount of template, since low template concentrations may generate non-specific signal. However, intra- and intersample variability can be high, and the wide range of the coefficient of variation described by a number of studies suggests limited reproducibility (Martin-Ruiz et al., 2015). Moreover, certain methodological conditions are known to affect TL measurement. For instance, some PCR master mixes can influence result specificity and consistency (Jiménez and Forero, 2018). Given the availability of different PCR mixes, the presence of stabilizers for the newly synthesized double-stranded DNA should carefully be checked (Wang et al., 2004). Another limitation of qPCR is that it provides a relative value (RTL) *per* genome rather than an absolute value in kilobases. This is a problem, given the limited number of comparative studies that have been conducted to validate qPCR with the gold standard Southern blotting. Although significant positive correlations have been reported between TL measured by qPCR and Southern blotting, experimental discrepancies do impact TL analysis, requiring optimization of PCR conditions (Tarik et al., 2018). Notably, the difficulty of comparing RTL values entails that only trends can be compared between studies.

Despite these important caveats, TL measurement by PCR is the most widely used method in epidemiological studies, and blood and saliva are the most common matrices in studies of large numbers of samples. The Genetic Epidemiology Research on Adult Health and Aging (GERA) has analyzed TL in 110,266 DNA specimens extracted from saliva (Lapham et al., 2015) using a novel high-throughput robotic system for TL and informatics analysis. Samples were run in triplicate along with control samples; within-sample variability was limited by employing thresholds to eliminate outlying measurements. Interestingly about 99% of samples passed all quality control measures. Another common matrix used for TL measurement by qPCR is leukocytes. LTL analyzed in 12,199 adults participating in two population-based prospective cohort studies in Europe (ESTHER) and the United States (Nurses' Health Study) was found to be associated to all-cause, cardiovascular disease (CVD), and cancer mortality (Mons et al., 2017).

Notably, DNA extraction methods have a pronounced influence on TL values, which in some circumstances can result in spurious or lost associations in epidemiological studies (Raschenberger et al., 2016). A recent meta-analysis of LTL and all-cause mortality suggests that the accuracy of the TL measurement technique used affects risk assessment (Wang et al., 2018b). Whereas qPCR provides reliable TL analysis in blood and saliva, this is not true of cancer cell DNA, because use of single-copy genes in conditions of genomic instability, which is typical of cancer cells, may affect the accuracy of normalization. Dedicated primer sets have recently been developed to achieve RTL measurement in cancer cells (Dahlgren et al., 2018).

The discovery of cf-DNA/RNA has raised the problem of detecting telomeric sequences in samples, such as microvesicles and exosomes, that contain very diluted template sequences, since in these cases qPCR efficiency may also be reduced. Moreover, no single-copy genes have yet been validated for cf-telomere estimation.

A more detailed description is required for STELA (Fig. 2c), which allows assessing the length of a chromosome subset, and TeSLA, which enables TL measurement in the subset of the shortest telomeres, *i.e.* those induced by sudden TS due not to cell replication but to breaks resulting from the action of stressors (Lai et al., 2017). TeSLA has been developed to overcome the problems posed by telomere repeat sequences (TRSs) in detecting abrupt TS in a single chromosome. STELA is labor-intensive and unsuitable for testing large numbers of samples. However, STELA data may have prognostic implications in the clinical assessment of disease cells, *e.g.* to predict clinical outcome in patients with chronic lymphocytic leukemia (Lin et al., 2014) or myelodysplastic syndrome (Williams et al., 2017).

4.3. Probe-based non-PCR methods

Probe-based TL assays, which involve the use of probes for telomeres (T) and a reference gene (R) for a given DNA sample, may provide a cost-effective approach to measure TL in extracted DNA samples (Kibriya et al., 2014). A novel, accurate, high-throughput, pooled-sample multiplex Luminex assay suitable for large-scale studies has recently been described (Jasmine et al., 2018).

4.4. Fluorescence in-situ hybridization (FISH) techniques: Q-FISH and flow-FISH

Q-FISH is a molecular cytogenetic method that can be employed to obtain information from metaphase or interphase cells, depending on the sequence of the fluorochrome-conjugated probe used. FISH methods can be used to measure TL in subsets of cells separated from fresh blood or from tissues (Fig. 2d) (Perner et al., 2003). Whereas the telomeres of each chromosome arm can provide heterogeneous staining results due to a different number of telomeric repeats, those found on the two sister chromatids generally display nearly identical intensities. The use of telomeric probes allows probe binding to its target to be identified by a distinct fluorescent signal within the cell nucleus. Synthetic DNA/RNA analogs capable of binding to DNA/RNA in a sequence-specific manner have been proved to yield more sensitive and specific TL measurements than DNA probes (Marchesini et al., 2016).

Since correct interpretation of the fluorescence signal requires a fluorescence microscope, FISH techniques require expensive equipment that may not be available at all laboratories.

Flow-FISH, first described in 1998 (Rufer et al., 1998), utilizes the

quantitative properties of telomere-specific probe retention to quantify median fluorescence in a population of cells *via* use of a flow cytometer instead of a fluorescence microscope. TL measurement by flow-FISH can have clinical relevance in specific clinical indications and selected settings, *e.g.* patients with mutations in some inherited genes (Alder et al., 2018). Flow-FISH has demonstrated excellent diagnostic sensitivity in measuring TL in patients with short telomere syndrome (STS). STSs are accelerated aging syndromes caused by heritable gene mutations which result in TS. For instance, RTL measurement by qPCR is not optimal to diagnose dyskeratosis congenital, an STS characterized by inherited bone marrow failure and cancer susceptibility caused by germline mutations in telomere biology genes (Gadalla et al., 2016); in these patients LTL analysis by flow-FISH is the recommended molecular diagnostic test (Gutierrez-Rodrigues et al., 2014). Flow-FISH can also be applied to measure TL in stored samples.

4.5. Whole genome sequence (WGS)-based technique

WGS-based TL measurement supplies reliable sequencing reads from telomeres **(**Castle et al., 2010; Parker et al., 2012**)**. However, their standard alignment to the reference sequence provides limited information on the region of origin, due to the repetitive nature of telomeric regions and to the fact that in the human reference sequence the ends of most chromosomes are simply stretches of Ns, which stand for unknown nucleotides. Methods have been developed to measure average TL from whole genome or exome shotgun sequence data (Ding et al., 2014) and to provide simultaneous TL measurement and global transcriptome analysis in the same cell (Wang et al., 2017a). The chief challenge for using next-generation sequences (NGSs) to measure TL is the need for bioinformatics expertise and softwares to decipher massive datasets. Several bioinformatics tools that adopt different approaches to identify, quantify, and normalize telomeric reads – like Motif_counter, TelSeq, Computel, qMotif, and Telomerecat – have been designed to determine telomere content and TL from NGS data (Lee et al., 2017; Farmery et al., 2018). Direct comparison of these WGS-based telomere measurement tools has shown that their best motifs all yielded similar performances when used to measure telomere content (Lee et al., 2017). In contrast, calculations using the best motif for TelSeq and Computel, the two tools that produce a TL estimate, were significantly lower and did not correlate well with TL measurements by TRF analysis (Lee et al., 2017).

Other important factors that should be considered when comparing WGS-based telomere measurement techniques are tool accessibility, ease of tool use, the time required to analyze one sample, and multithreading ability (Lee et al., 2017).

Telomere Dysfunction-Induced Foci (TIF) (Takai et al., 2003; de Lange, 2002; Karlseder et al., 1999) and Extrachromosomal DNA (Tokutake et al., 1998; Cohen and Méchali, 2002; Cesare and Griffith, 2004; Henson et al., 2009; Schvartzman et al., 2013; Komosa et al., 2015; Moye et al., 2015; Henson et al., 2017) analysis are not quantitative techniques and are not optimized for epidemiological studies. Separation of extrachromosomal DNA depends on sample preparation, DNA/RNA extraction procedures, and DNAse or RNase treatment, according to the compartment being assessed.

4.6. TL heterogeneity

TL heterogeneity has been detected in various cell types, including stem and cancer cells and can directly influence the frequency with which chromosomes undergo telomeric fusion and subsequent breakage-fusion-bridge cycles (Londoño-Vallejo, 2004). Single-cell analysis technology has recently been developed and effectively employed to investigate TL heterogeneity. Single-cell analysis of TL, *i.e.* STELA, where each amplicon is derived from a single telomeric molecule from a single cell, can disclose the full detail of TL distribution. Notably, STELA measures TL within the length ranges observed in senescent cells **(**Garcia-Martin et al., 2017), providing a new tool to explore the relationship between TL and the aging process.

5. TERRA and aging

The role of TERRA has been an outstanding issue in telomere biology for the past decade, mainly due to lack of knowledge of its loci. New insights suggest that TERRA molecules can be transcribed from nearly all telomeres in mammalian cells, always in centromere to telomere direction; they also suggest the involvement of subtelomeric regions – transcriptionally active genomic regions that give rise to long non-coding RNAs whose size ranges from 100 to 9 kb according to the position of the transcription starting site (Diman and Decottignies, 2018). These transcripts often display a cap structure added at the 5′ end, and only 7% of these transcripts are polyadenylated (Oliva-Rico and Herrera, 2017).

Cf-TERRA sequences have also been detected in human blood and serum, especially as exosome-associated molecules: the secretory phenotype characterized by release of cf-TERRA has been called TASP (TERRA-associated secretory phenotype) (Wang et al., 2015). Since high TERRA levels may be detected in human tumor tissue, they may prove to be innovative cancer biomarkers (Arora et al., 2014).

Notably, TERRA forms RNA:DNA hybrids at the chromosome ends and can fold into G-quadruplexes (Balk et al., 2014). Experimental evidence has shown that TERRA can also form higher-order structures based on parallel G4 units (Martadinata et al., 2011).

A mounting number of human diseases are being associated to abnormal G4 RNA regulation, suggesting the potential relevance of G4s to human health. Recent work supports the notion that G4s in the promoter regions of oncogene and telomere DNA could be therapeutic targets in cancer patients (Kaulage et al., 2018).

5.1. Measurement of TERRA: analytical caveats

The major problem in TERRA measurement is that transcription can start from the subtelomeric regions of all chromosomes. A number of primers specific for different subtelomeric regions have been used, including primers matching the 1q, 2q, 3p, 7p, 10p, 10q, 12q 13q, 14q, 15q, 17p,17q, 18p, XqYq, and XpYp chromosome, (Feretzaki and Lingner, 2017; Wang et al., 2015). However, some loci seem to be more involved in TERRA transcription than others. Chromosomes 20q and Xp have been suggested to be the main TERRA loci in human cells (Montero et al., 2016).

The techniques used most commonly to quantify TERRA sequences are briefly described below and are depicted in Fig. 3 **(3a,** RT-PCR; **3b,** Northern blotting; **3c,** RNA dot blotting; and **3d,** G-quadruplex detection with specific antibodies).

5.1.1. RT-qPCR

RT-qPCR is currently the fastest and most practical quantitative analysis technique for TERRA measurement.

The initial reverse transcription that yields cDNA can require a different amount of starting RNA, depending on the sample (Feretzaki and Lingner, 2017). DNAse treatment is required after RNA extraction (Iglesias et al., 2011), to ensure the quality and concentration of the starting sample, which can greatly affect results. Contamination with salt, ethanol, or proteins can strongly influence the performance of the downstream application.

Reverse transcription primers can be five repetitions of the oligonucleotide CCCTAA, random hexamers, or different set of primers. Poly-T, which is frequently used for reverse transcription of mRNA, is unsuitable due to the lack of TERRA transcript polyadenylation. GAPDH, U6snRNA, 36B4, GUSB, actin, and 18S have been described as suitable reference genes.

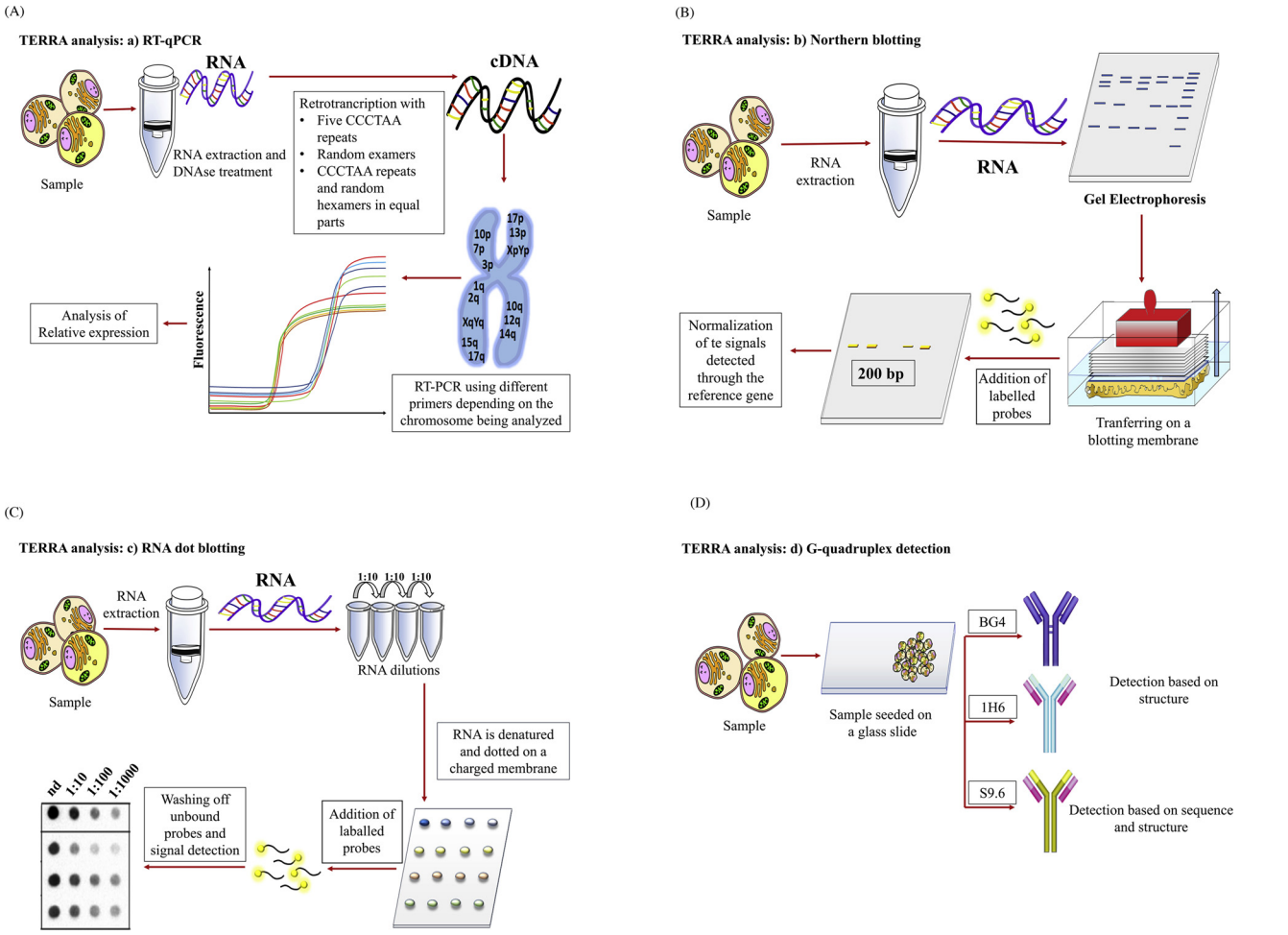

Fig. 3. Most commonly used techniques employed to quantify TERRA sequences.
Schematic representation of the three most common techniques employed to measure TERRA: 3a) RT-PCR; 3b) Northern blotting; 3c) RNA dot blotting (a simplification of Northern blotting that does not require gel electrophoresis); 3d) G-quadruplex detection with specific antibodies. G-quadruplex can be detected using engineered antibodies, such as clones 1H6 and BG4, which have specificity for the structure, or S9.6, which has specificity for structure and sequence.

5.1.2. Northern blotting

Northern blotting can detect the overall amount of TERRA transcripts, but unlike RT-qPCR it cannot measure minor changes in transcription or quantify TERRA levels in single chromosomes (Feretzaki and Lingner, 2017).

RNA extracted from samples is denatured and electrophoresed on agarose formamide gel, since the size of cf-TERRA is about 200 bp. Next, RNA can be transferred onto a blotting membrane and cross-linked to it using UV radiation. For RNA detection, the blot is hybridized using labeled probes specific for TERRA sense and antisense strands; 18S and U6 RNA have been used for normalization (Wang et al., 2015).

5.1.3. RNA dot blotting

RNA dot blotting is a simplification of Northern blotting. It does not require gel electrophoresis and it makes it possible to analyze different samples with different concentrations in a single test.

Extracted RNA is denatured using high temperatures or denaturing solutions, dotted on a charged nylon transfer membrane, and cross-linked to it by UV radiation. Subsequent steps involve a radiolabeled probe, washes in buffer to remove excess probe, and RNAse A treatment to eliminate single-strand RNA. The most common probes for TERRA detection are CCCTAA repeats labeled at their 5′ end with ^{32}P-γ-ATP by T4 polynucleotide kinase (Koskas et al., 2017).

5.1.4. RNA-FISH

RNA-FISH is used to analyze the cellular localization of TERRA by hybridizing detergent-extracted nuclei with a fluorescently labeled probe. It can even be used after immunofluorescence. Different probes, including C-rich peptidonucleic acid (PNA) coupled with a cyanine 3 fluorochrome, a fluorescently labeled probe containing CCCTAA repeats, or a light switching pyrene probe, can be used for hybridization to identify TERRA G4s in living cells (Koskas et al., 2017; Xu et al., 2010).

5.1.5. Detection of G-quadruplexes

G4s can be detected using engineered antibodies, such as clones 1H6 and BG4, which have specificity for the structure, not the sequence. These antibodies are used to detect the cellular localization of G4s by immunofluorescence. Since detection is based on structure, different types of G4s, *e.g.* DNA:RNA (hybrids), RNA-RNA, and DNA-DNA, can be identified.

Other critical aspects concern the labeling obtained with BG4 using different fixatives. Cytoplasmic TERRA is preferentially detected by fixation with PFA-Triton X-100, whereas nuclear quadruplexes (TERRA or DNA-DNA) can be detected by MeOH fixation (Laguerre et al., 2016). S9.6 is another monoclonal antibody with high affinity for DNA-RNA G4s formed at R-loops, because it is both structure- and sequence-specific. Maximum affinity is obtained with 52% of GC in the target sequence, whereas weak or no binding is obtained with amounts lower

than 25% or higher than 75% (König et al., 2017). Unfortunately, commercial kits including these antibodies are currently not available.

6. TA activity and aging

Telomerase is the only enzyme that can elongate a telomeric DNA chain to compensate for TS. It is different from other polymerases, because it involves a distinctive, reiterative reuse of an internal single-stranded telomeric template (Wu et al., 2017). Notably, the human TERT gene may be capable of autoregulation, because it is located very close to the telomere end of the chromosome, ˜ 1.2 Mb from the 5p end.

Most somatic cells lack TA; exceptions include embryonic tissue, stem cells, reproductive organs, and some rapidly regenerating tissues. Since TA is seen in 80–90% of tumor cells, its value as a diagnostic/prognostic tumor marker has prompted the development of reliable and standardized assays. As noted above, in somatic cells TA usually declines after birth; the successive cell divisions gradually lead to TS and trigger cellular senescence (Kim and Shay, 2018).

Most studies have investigated cells that express high levels of TERT, such as immortalized and cancer cells. However, TA regulation is a dynamic process also in normal human cells, suggesting that active telomere maintenance is required for the proliferation of normal cells (Masutomi et al., 2003). However, the role of telomerase in normal senescent cells has not been analyzed in depth. Reduced TERT protein levels and reduced TA have been described in senescent primary cultures of adult human dermal fibroblasts (HDFs) (Yehuda et al., 2017).

Telomerase activation/replacement has potential in treating patients with telomere maintenance deficiency syndrome as well as in tissue engineering approaches designed to treat degenerative conditions that are associated to normal aging. Telomerase-deficient mice have been proposed as a model to study the adverse cellular and organismal consequences of widespread DNA damage signaling activation *in vivo*. Telomerase reactivation in such mice extends TL, reduces DNA damage signaling, and eliminates degenerative phenotypes in multiple organs (Jaskelioff et al., 2011). Conversely, clinical research work is focusing on telomerase inhibition therapies to treat tumors, which induce telomerase overexpression by overcoming the short telomere barrier to unrestricted proliferation (Fleisig and Wong, 2007). Since telomerase-complex components are upregulated in most tumor cells, TERT restriction is a potential therapeutic option (Kim et al., 1994). Given that most somatic cells show low TA, selective inactivation of telomerase expression in cancer cells fails to influence most normal cells, suggesting that telomerase is a good target for cancer therapy (Sprouse et al., 2012).

TA is also considered as a biomarker for cardiovascular aging and CVD. Recent studies suggest a link between statins and telomere biology that may be explained by the anti-inflammatory actions of statins (Strazhesko et al., 2016).

Overall, TL and TA regulation is a complex and dynamic process that is impaired in patients with ARDs.

A greater understanding of the mechanisms underpinning telomerase regulation and the development of reliable TA assessment technologies is essential to help research in therapeutic strategies for telomerase modulation. A number of TA determination techniques, including those devised most recently, are described below. However, not all of them are suitable for epidemiological and clinical studies.

6.1. TA measurement: analytical caveats

TA detection assays can be divided into two main groups: those based on direct detection of telomerase products and those based on different systems of product amplification (Skvortsov et al., 2011). New bioanalytical methods based on direct detection of telomerase products, such as PCR-free assays, isothermal amplification, and Single Molecule Stochastic Binding assay, have recently been applied to TA detection not only in cells and tissues, but also in body fluids (Zhang et al., 2017a, 2017b; Su et al., 2017).

Multiple approaches have also been proposed to assess telomerase gene activity, including engagement of TERT alternative splicing, TERT gene amplification, and epigenetic changes (reviewed in Shay, 2016). Interestingly, some human TERT mutations/deletions have been associated to premature aging diseases, and patients carrying mutations in genes crucial for telomere maintenance show accelerated aging phenotypes (Chu et al., 2016). Recently, alterations in the gene encoding human TERT have been identified as points of interest for elucidating the oncogenic mechanism of several different cancer types (Bollam et al., 2018).

6.2. TA determination assays based on direct detection of telomerase products

6.2.1. TA detection using direct incorporation of a radioactively labeled substrate

The earliest TA detection method was based on the use of radioactive labeling without additional amplification (Blackburn et al., 1989). The method is still employed for qualitative determination of TA in cell line extracts. Since radioactive substances are complex and dangerous to use, new methods that do not use radioactive substances have been developed. Some of these approaches are briefly described in Table 1a.

6.3. TA detection assays based on telomerase product amplification

6.3.1. Telomere repeat amplification protocol (TRAP)

The Telomere Repeat Amplification Protocol (TRAP) is a widely used assay to determine TA in mammalian cells, tissues, and other biological samples (Kim et al., 1994). It involves three steps: extension, amplification, and detection of telomerase products. In the extension step, telomeric repeats are added to the telomerase substrate. In the amplification step, the extension products are amplified by PCR using specific primers (Wege et al., 2003). In the detection step, TA is estimated by electrophoretic analysis of the extension products. However, since amplification is often associated to poor reproducibility and high background, it is unsuitable for diagnostic applications. The main analytical challenges include throughput, the replacement of radioactive labels with non-labeled compounds, the reduction of the amount of side product, the elimination of primer-dimer artifacts and of false-positive amplification products, and the reduction of intra- and inter-sample variation (Wu et al., 2000; Skvortsov et al., 2011). Techniques employed to quantify telomerase activity (TA) were depicted in Fig. 4.

The main changes made to the basic TRAP protocol are summarized in Table 1b.

7. Biological variables related to TL, TERRA, and TA

Although TL is the area characterized by the largest number of applications, it is likely that similar biological, disease-mediated processes will be found to be relevant to TERRA and TA, which are interconnected.

Age, gender, and ethnicity have been found to be significantly associated to TL; for instance, the female gender and an African or Hispanic origin have been associated to a predisposition to have longer telomeres compared to the male gender and a European origin (Gardner et al., 2014; Hansen et al., 2016). Significant but weak correlations have also been described between LTL and hematological parameters (Meyer et al., 2016). A number of biomarkers related to a variety of physiological processes are also strongly associated to accelerated TS; however, the complex relationships between TL and the other chemical and clinical biomarkers are only beginning to be understood (Barrett et al., 2015).

The significant associations between inflammaging and telomere attrition, reported by several studies, suggest that TS is related to an

Table 1a
Some of the most relevant modification of TA detection assays based on direct detection of telomerase products.

Modifications of TA detection assays based on direct detection of telomerase products	Brief description of the protocol	References
Surface Plasmon Resonance ***(SPR)***	Surface Plasmon Resonance (SPR) can be applied to measure small local changes in refractive index on metal layers, linked directly to alterations in concentration on the surface. Biotin-conjugated oligonucleotides containing telomeric repeats can be immobilized on the surface of a sensor pretreated with streptavidin (). The oligomers associated with the telomerase extracts can be elongated and TA can be calculated by measuring the SPR signals. The main limiting factors are reaction time and sample concentration.	Maesawa et al., 2003
Detection of telomerase activity using oligo-modified magnetic particles and nuclear magnetic resonance ***(NMR)***	Another physical phenomenon employed for TA detection is nuclear magnetic resonance (NMR). Through a complementary interaction, the magnetic particles bind the telomeric sequences synthesized by telomerase. The spin-spin relaxation time is measured by a relaxometer. Since the formation of an organized nanoparticle ensemble involves a change in the magnetic relaxation time of surrounding water molecules, the magnetic field increases in presence of nanoparticle ensembles and decreases with non-ordered ones. Since the change reaches half of the maximum after 30 seconds and plateaus after 40-60 minutes, the analysis is fast, sensitive, and high-throughput.	Grimm et al., 2004
Quartz crystal microbalance technique (QCM)	This highly sensitive method involves microgravitometric analysis of TA based on the piezoelectric effect of quartz. The application of an alternating current promotes the oscillation of a quartz crystal, whose resonance frequency is then determined. Ligands on the crystal surface in a liquid environment can induce a reduction in resonance frequency. Telomerase induces oligonucleotide binding to the sensor's surface.	Pavlov et al., 2004.
Biobarcode assay	This approach uses magnetic particles, *i.e.* gold spheres, and two types of oligonucleotides, complementary and non complementary to telomerase-synthesized DNA. Binding of the electroactive complex $[Ru(NH_3)_6]^{3+}$ to the non-complementary telomerase-synthesized DNA chain permits quantitative detection. The method can measure TA in cell line extracts but is not used in tissues.	Li et al., 2010; Skvortsov et al., 2011
Optical biosensor assay	The assay is based on the change in the refraction index induced by the amount of telomerase products detected on the surface of the optical biosensor in real time. A three-oligonucleotide system, *i.e.* a "cassette system" including a sequence complementary to the RNA template of telomerase modifies the sensor surface to avoid steric impediments and to ensure process reversibility.	Buckle et al., 1996; Schmidt et al., 2002; Kulla and Katz, 2008
Quantum dots	Nanoparticles are conductor or semiconductor particles that represent quantum dots (QDs) in quantitative TA detection. Similar to the way a photon can be emitted during the transition of an atom between energy levels, a photon can be emitted during a transition in a quantum blot. In this system, photon absorption and emission occur at specific wavelengths that are related to QD size (smaller nanoparticles correspond to higher wavelengths). A modification involving a thio group at the end of the telomere oligonucleotide bound to the QD makes it capable of fluorescence when it absorbs a quantum with a wavelength of 400 nm and emits a quantum with wavelength of 560 nm. When a modified fluorescent oligonucleotide, TR-dUTP, is incorporated into telomerase DNA products bound to the QD, a fluorescence energy transfer occurs with a higher wavelength (610 nm). This method is not recommended for clinical materials.	Patolsky et al., 2003; Zavari-Nematabad et al., 2017; Li et al., 2018a, 2018b
Graphene oxide (GO)-based fluorescent nanosensor	A fluorescent DNA is adsorbed on a GO surface that can bind dye-labeled single-stranded DNA (ssDNA) complementary to the telomeric repeated sequence and efficiently quench the fluorescence of the dye *via* fluorescence resonance energy transfer (FRET). It is a rapid, sensitive and specific approach to detect telomerase activity.	Zhang et al., 2018

Brief description of NMR, SPR, QCM, Biobarcode assay, Optical biosensor assay, Quantum dots, Graphene oxide (GO)-based fluorescent nanosensor protocols.

enhanced susceptibility to the development and progression of ARDs, such as type 2 diabetes, CVD, and cancer (Bonfigli et al., 2016; Testa et al., 2011; Wang et al., 2016; Jose et al., 2017). With regard to cancer, long telomeres have been associated to an increased risk of several cancers; however, emerging data suggest that short telomeres might predict poor survival in cancer patients (Zhang et al., 2015; Rachakonda et al., 2018). Association studies of TL and cancer have identified significant, but not clinically relevant, differences in TL between cases and controls (Savage, 2018). A recent meta-analysis has highlighted that the inconsistent effect of TL on cancer outcomes may be due to different measurement methods (Adam et al., 2017; Wang et al., 2017b). Therefore, standardization of TL measurement and reporting has the potential to enhance the prognostic value of TL in human diseases.

A significant relationship, reported among exposure to factors promoting inflammation or oxidative stress (smoking) and shorter telomeres (Astuti et al., 2017), has been confirmed in the offspring of smoking mothers (Oerther and Lorenz, 2018). A recently described association between accelerated telomere attrition and marked weight gain in middle life suggests the importance of lifetime weight management to preserve functional telomeres (Hang et al., 2018). Nonetheless, the inconsistent effects of weight loss on TL and DNA repair indicate that interventions and assays should be reassessed (Himbert et al., 2017).

Different age-related telomere attrition trajectories and circulating inflammatory cytokine levels have been described in aging individuals (Lustig et al., 2017). This is not unexpected, since a number of stressors, including infectious agents, microbiota composition, cellular senescence, and misplaced nucleic acids (DNA/RNA), can promote TS in immune cells as well as in other somatic cells, fueling inflammation. These stressors are so closely interconnected that the respective effects are difficult to unravel. This could be one of the weakness of the studies exploring the relationship linking stressors, inflammaging, and TL: only the integrated analysis of a number of components in the same

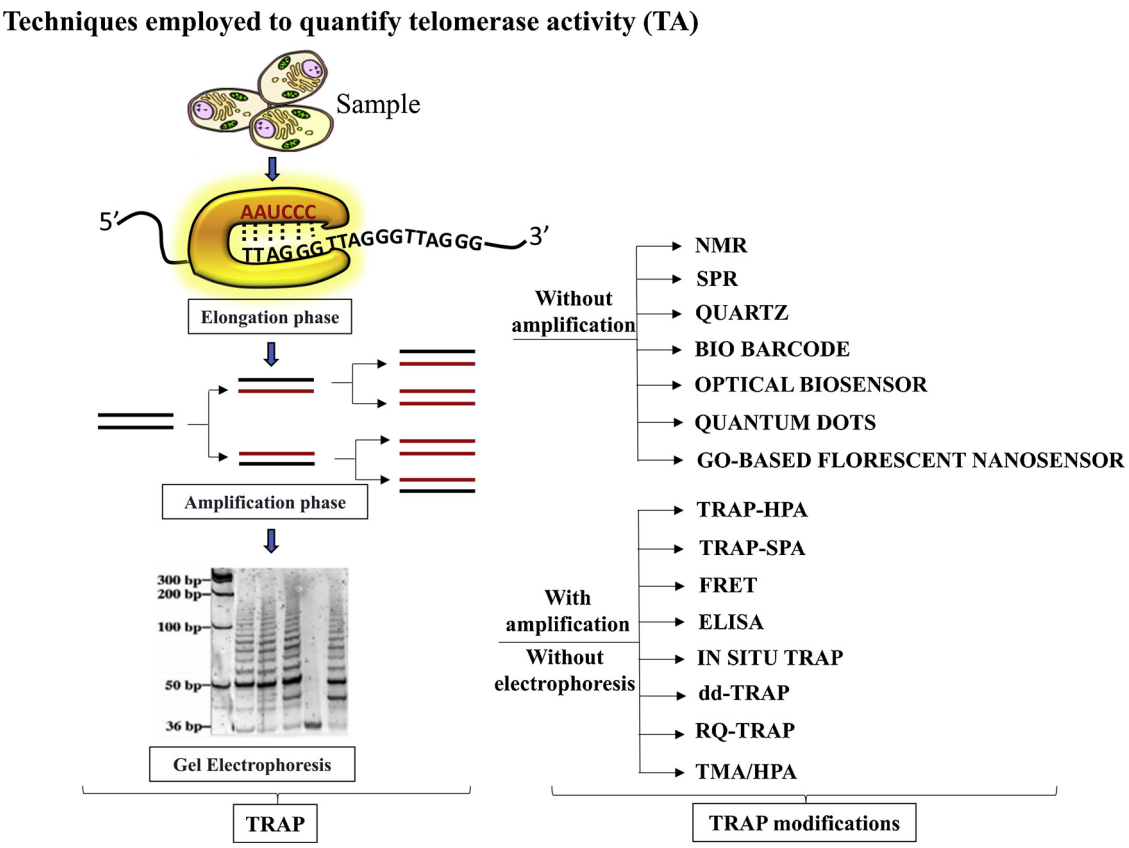

Fig. 4. Techniques employed to quantify telomerase activity (TA).
Schematic representation of the most common techniques employed to measure TA. The methods are grouped into two major categories: those based on direct detection of telomerase products and those based on different systems of amplification of these products (TRAP-based methods).

subjects/patients could clarify the issue. Moreover, the complex signaling affecting telomere balance during life requires multivariate analysis approaches to test for associations between TL and multiple biological variables; bias should be minimized especially in association studies involving TL and ARDs and TL and psychological and bio-behavioral variables.

TL measurement is also a useful approach to evaluate the pathogenicity of the genetic variants associated to telomere-related disorders. STSs are often caused by heritable gene mutations that result in decreased TL (Norberg et al., 2018). Their diverse clinical presentation – like bone marrow failure and idiopathic pulmonary fibrosis associated to gene mutations involving TERT, TERC, and other genes – make STSs a diagnostic challenge (Mangaonkar and Patnaik, 2018). Large-scale molecular epidemiological studies have uncovered novel associations between ARDs such as CVD, cancer, and impaired mental health, and both TL and common genetic variants in telomere biology genes (Savage, 2018).

Finally, it is conceivable that RNA-dependent factors will constitute additional biological variables for TERRA and TA measurement, both of which are RNA-dependent.

Advantages and disadvantages (sensitivity, specificity, number of samples that can be managed, ease to use and suitability for clinical studies) are reported in Table 2 for telomere length (TL), telomeric repeat-containing RNA (TERRA) and telomerase activity (TA) measurement techniques.

8. Conclusion

The outstanding challenge in telomere research is the development of accurate and reliable measurement methods ensuring simple and sensitive TL, TERRA, and TA detection. Reaching these goals requires guidelines for the development of standardized and automated measurement procedures. Studies of the reproducibility, accuracy, reliability, and sensitivity of the different TL, TERRA, and TA measurement methods at independent laboratories should be encouraged. Bench to bedside translation of biological metrics related to the telomere world requires the establishment of normal range values as well as critical values for interpretation. This is essential not only in studies of individual molecules, but also to shed light on the associations of TL, TERRA, and TA with physiological, psychological, and bio-behavioral phenomena and human pathological conditions. These tasks are complex and the data provided by the latest studies are not always clear and conclusive. For these reasons TL, TERRA, and TA are still not included in everyday clinical practice. Nevertheless, considerable progress has been made, and researchers are increasingly close to finding the solutions for better and faster measurement. Importantly, researchers undertaking the study of telomeres should be aware of the methodological problems involved in TL, TERRA, and TA analysis. Careful consideration is warranted when selecting measurement methods for research or clinical studies.

Notably, most of the sample material used for epidemiological studies is extracted banked DNA and/or RNA. Since the results of TL and TERRA measurement are affected by extraction methods and degradation, sample quality checks are critical for correct measurement and data interpretation.

Furthermore, RNA species detection in cells depends on metabolic activity, and although it may not be detectable in resting blood, it may be detected in tumor samples.

What is essential for future studies of the “telomere world” is that researchers publish full details of their methods and the quality control thresholds they employ. Notably, it is critical to be familiar with the relationships between telomeres and a number of other variables if

Table 1b
Some of the most relevant modifications made to the basic TRAP protocol.

Modifications of TRAP protocol	Brief description of the protocol	References
TRAP with a post-PCR hybridization protection protocol ***(TRAP-HPA)***	TRAP-HPA uses a probe labeled with covalently bound chemiluminescent acridine to detect DNA after amplification and provides high-throughput semi-quantitative determination of TA.	Hirose et al., 1997; Fajkus, 2006
Scintillation proximity assay ***(TRAP-SPA)***	TRAP-SPA enables detection of amplification products thought the conjugation of telomerase products with biotin and amplification in presence of [3 H] TTP. Semi-quantitative determination can be obtained in large series of tissue and cell line extracts. The main drawbacks are the use of tritium and PCR artifacts.	Savoysky et al., 1996; Fajkus,2006
TRAP with Fluorescence Resonance Energy Transfer ***(FRET)***	FRET uses two primers (amplifluors) whose hairpin structure contains a donor (fluorescein) and an acceptor (4'-dimethylaminophenyl-azobenzoic acid. Its main advantages include the absence of radioisotopes, the limited volume of the elongation products, the elimination of post-PCR processing, the reduction of carryover contamination risk, and fast analysis.	Uehara et al., 1999; Ding et al., 2010; Kawamura et al., 2014; Fajkus,2006
TRAP combined with Enzyme-Linked Immunosorbent Assay ***(ELISA)***	TRAP-ELISA is a colorimetric qualitative and semi-quantitative assay, where biotin conjugation of telomere-imitating oligonucleotide (TS) primers permits binding of amplified DNA to streptavidin-coated microplates. This step is followed by DNA denaturation and hybridization with digoxigenin (DIG)-labeled probes specific for telomeric sequences. The addition of polyclonal DIG antibodies conjugated to horseradish peroxidase prompts the colorimetric reaction and enables TA detection. Some commercial kits include positive and negative internal standards. Since TRAP-ELISA is fast and allows analyzing multiple samples in a single run, it is the most commonly used assay for TA determination in screening studies.	Fajkus, 2006; Wu et al., 2000; Sue et al., 2014
In situ TRAP	In *in situ* TRAP the cell suspensions are immobilized on silane-coated slides. PCR commonly uses FITC-labeled primers, and the final analysis is made under a fluorescence microscope. Fluorescence intensity and localization are employed to determine TA in individual cells (cancer cells usually show bright fluorescence). *In situ* TRAP can also be used to obtain a semi-quantitative determination of TA in tissue sections.	Skvortsov et al., 2011; Fajkus, 2006
Droplet Digital Telomere Repeat Amplification Protocol ***(ddTRAP)***	This is a two-step assay where cell lysates are analyzed by droplet digital PCR (ddPCR). It involves the same steps as a conventional TRAP assay, except that the PCR products are detected by ddPCR. This system has improved the throughput, sensitivity, and reproducibility of the TRAP assay. As a consequence, it can test a variety of cell types, including cell lines and primary adult human cells, without radioactive compounds but with comparable sensitivity.	Ludlow et al., 2018; Fajkus, 2006
Real-time Quantitative TRAP ***(RQ-TRAP)***	Real-time Quantitative TRAP (RQ-TRAP) uses fluorescent dyes (*e.g.* PicoGreen or SYBR Green) to quantify double-stranded DNA products in the PCR elongation and amplification steps. Its main advantage is that TA quantification is achieved without any additional time-consuming steps besides sample extraction and real-time cycling. The assay provides accurate TA measurement, hence highly effective TA monitoring in cultured cells, and can be used to analyze multiple samples. Its main disadvantages are the inhibitory effects of PCR contaminants, the possibility that PCR reaction saturation in the final step may level small TA differences compared to the results of conventional TRAP, and the risk of false-positive signals.	Wege et al., 2003; Gelmini et al., 1998; Hou et al., 2001; Saldanha et al., 2003; Hou et al., 2001; Skvortsov et al., 2011; Fajkus, 2006
TRAP with isothermic transcription-mediated amplification (TMA/HPA)	This approach provides a semi-quantitative determination of TA based on the presence of a polymerase that uses synthesized DNA as a matrix for RNA synthesis. Telomerase-synthesized DNA contains an additional sequence acting as a substrate for reverse primer hybridization. This tecnique also avoids the necessity of performing and evaluating polyacrylamide gel electrophoresis of reaction products and it is characterized by high sensitivity (1-1000 cells). Its main advantage is that it does not require sample heating. The assay is sensitive to the presence of RNase.	Saldanha et al., 2003; Skvortsov et al., 2011

Brief description of TRAP HPA, TRAP-SPA, FRET, ELISA, *in situ* TRAP, ddTRAP, RQ-TRAP and TMA/HPA protocols.

errors generated by confounding variables that are not controlled for are to be avoided.

Starting from the most recent evidence in telomere biology, we hypothesize that combined TL, TERRA, and TA analysis may provide highly reliable information to estimate the rate of cell, tissue and organismal aging and the risk of ARD development (Kim and Shay, 2018). TL, TERRA, and TA have been associated singly to aging and a number of common ARDs, yet no studies have evaluated them in an integrated way, either using cellular or organismal models.

Although red blood cells and platelets are a significant source of exosomes from blood, different cell types can release exosomes into human plasma/serum, including endothelial cells, monocytes and astrocytes (Goetzl et al., 2017; Goetzl et al., 2016; Halim et al., 2016). Plasma exosomes released by endothelial cells and monocytes should be extensively investigated for telomeres and TERRA content, especially in patients with ARDs.

9. Future perspective

A new geriatric medicine branch, geroscience, postulates that it should be possible to delay the aging process and the onset of the most common chronic ARDs (Vaiserman and Lushchak, 2017), and mounting evidence suggests that the human healthspan could be increased by nutraceutical or pharmaceuticals approaches (Gurău et al., 2018; Klimova et al., 2018). The hypothesis has prompted the organization of geroscience-guided therapeutic trials, *e.g.* TAME (Targeting Aging with

Table 2
Advantages and disadvantages of the most common TL, TERRA, and TA measurement techniques.

	Tecnique	Time efficient	Sensitivity	Specificity	Reproducibility	Easy to use	Suited for clinical studies	References
TL	**STELA/TeSLA**	No	High	High	High	No	No	Lai et al., 2018; Martin-Ruiz et al., 2015.
	(q)PCR	Yes	Low	Intermediate	Intermediate	Yes	Yes	Gutierrez-Rodrigues et al., 2014; Martin-Ruiz et al., 2015.
	Southern blot	No	Intermediate	High	High	Yes	No	Tarik et al., 2018; Martin-Ruiz et al., 2015.
	FISH-qFISH-Flow	No	Intermediate	Intermediate	Intermediate	Yes	No	Baerlocher et al., 2002
	FISH	Yes	High	High	High	Yes	Yes	Gutierrez-Rodrigues et al., 2014
	WGS	No	High	High	High	No	Yes	Lee et al., 2017
TERRA	**RT-qPCR**	Yes	High	Intermediate	–	Yes	Yes	Feretzaki and Lingner, 2017
	Northern Blot	No	Low	High	–	Yes	No	Feretzaki and Lingner, 2017
	RNA dot blotting	Yes	Low	High	–	Yes	No	Koskas et al., 2017
	RNA-FISH	Yes	High	Intermediate	–	Yes	No	Koskas et al., 2017; Xu et al., 2010
TA	**Classic**	No	Intermediate	Intermediate	Low	Yes	No	Ohuchida et al., 2005; Fajkus, 2006
	HPA	No	Intermediate	Intermediate	Low	Yes	No	Hirose et al., 1997; Fajkus, 2006
	SPA	No	Intermediate	Intermediate	Low	No	No	Savoysky et al., 1996; Fajkus,2006
		Yes	Intermediate	Intermediate	Intermediate	Yes	Yes	Uehara et al., 1999; Ding et al., 2010; Kawamura et al., 2014; Fajkus,2006
		Yes	High	High	Intermediate	Yes	Yes	Wu et al., 2000; Sue et al., 2014; Fajkus, 2006
		Yes	High	High	Intermediate	Yes	No	Skvortsov et al., 2011; Fajkus, 2006
		Yes	High	High	High	Yes	Yes	Ludlow et al., 2018; Fajkus, 2006
		Yes	High	Intermediate	High	Yes	Yes	Wege et al., 2003; Gelmini et al., 1998; Hou et al., 2001; Saldanha et al., 2003; Hou et al., 2001; Skvortsov et al., 2011; Fajkus, 2006
		Yes	High	High	–	Yes	No	Saldanha et al., 2003; Skvortsov et al., 2011
	SPR	Yes	Intermediate	Intermediate	High	Yes	No	Maesawa et al., 2003
	NMR	Yes	High	Intermediate	High	No	No	Grimm et al., 2004.
	QCM	Yes	High	Intermediate	High	No	No	Pavlov et al., 2004.
	Biobarcode	No	High	High	Intermediate	Yes	No	Li et al., 2010; Skvortsov et al., 2011
	Optical biosensor	Yes	High	High	High	Yes	No	Buckle et al., 1996; Schmidt et al., 2002; Kulla and Katz, 2008
	Quantum dots	No	High	High	–	Yes	No	Patolsky et al., 2003; Zavari-Nematabad et al., 2017; Li et al., 2018a, 2018b
	GO-based fluorescent nanosensor	Yes	High	High	–	Yes	Yes	Zhang et al., 2018

Advantages and disadvantages (sensitivity, specificity, number of samples that can be managed and ease to use) are reported for telomere length (TL), telomeric repeat-containing RNA (TERRA), and telomerase activity (TA) measurement techniques.
-Not yet addressed.

MEtformin) (Justice et al., 2018). However, ongoing studies highlight the scarcity of well-vetted "rate of aging" biomarkers for human studies and the need for such biomarkers to move from the assessment of chronological age to the evaluation of physiological age (Kohanski et al., 2016; Sierra and Kohanski, 2017).

Cutting-edge technologies for TL, TERRA, and TA measurement are still in their infancy, but they promise great future discoveries through method improvements and the multiplication of laboratories offering them. Technological advances are expected to provide fast, automated, and standardized measurement of TL, TERRA, and TA in the same sample not only in cells and tissues, but in all biological fluids and circulating vesicles. These new technologies are expected to provide more concordant data in association studies both with regard to aging *per se* and to a number of ARDs.

Conflicts of interest

None.

Authors' contributions

Emanuela Mensà, Silvia Latini, Deborah Ramini and Gianluca Storci wrote the paper, which was revised by Massimiliano Bonafè and Fabiola Olivieri.

Acknowledgment

This study was partially supported by grants from Università Politecnica delle Marche (UNIVPM), Ancona, Italy to FO.

References

Adam, R., Díez-González, L., Ocaña, A., Šeruga, B., Amir, E., Templeton, A.J., 2017. Prognostic role of telomere length in malignancies: a meta-analysis and meta-regression. Exp. Mol. Pathol. 102, 455–474. https://doi.org/10.1016/j.yexmp.2017.05.010.

Alder, J.K., Hanumanthu, V.S., Strong, M.A., DeZern, A.E., Stanley, S.E., Takemoto, C.M., Danilova, L., Applegate, C.D., Bolton, S.G., Mohr, D.W., Brodsky, R.A., Casella, J.F., Greider, C.W., Jackson, J.B., Armanios, M., 2018. Diagnostic utility of telomere length testing in a hospital-based setting. Proc. Natl. Acad. Sci. U. S. A. 115, E2358–E2365. https://doi.org/10.1073/pnas.1720427115.

Arora, R., Lee, Y., Wischnewski, H., Brun, C.M., Schwarz, T., Azzalin, C.M., 2014. RNaseH1 regulates TERRA-telomeric DNA hybrids and telomere maintenance in ALT tumour cells. Nat. Commun. 21, 5–5220.

Astuti, Y., Wardhana, A., Watkins, J., Wulaningsih, W., PILAR Research Network, 2017. Cigarette smoking and telomere length: a systematic review of 84 studies and meta-analysis. Environ. Res. 158, 480–489.

Baerlocher, G.M., Mak, J., Tien, T., Lansdorp, P.M., 2002. Telomere length measurement by fluorescence in situ hybridization and flow cytometry: tips and pitfalls. Cytometry 47, 89–99.

Balk, B., Dees, M., Bender, K., Luke, B., 2014. The differential processing of telomeres in response to increased telomeric transcription and RNA-DNA hybrid accumulation. RNA Biol. 11, 95–100.

Barrett, J.H., Iles, M.M., Dunning, A.M., Pooley, K.A., 2015. Telomere length and common disease: study design and analytical challenges. Hum. Genet. 134, 679–689.

Belsky, D.W., Caspi, A., Houts, R., Cohen, H.J., Corcoran, D.L., Danese, A., Harrington, H., Israel, S., Levine, M.E., Schaefer, J.D., Sugden, K., Williams, B., Yashin, A.I., Poulton, R., Moffitt, T.E., 2015. Quantification of biological aging in young adults. Proc. Natl. Acad. Sci. U. S. A. 112, E4104–10. https://doi.org/10.1073/pnas.1506264112.

Belsky, D.W., Moffitt, T.E., Cohen, A.A., Corcoran, D.L., Levine, M.E., Prinz, J.A., Schaefer, J., Sugden, K., Williams, B., Poulton, R., Caspi, A., 2018. Eleven telomere, epigenetic clock, and biomarker-composite quantifications of biological aging: do they measure the same thing? Am. J. Epidemiol. 187, 1220–1230.

Blackburn, E.H., 1990. Telomeres: structure and synthesis. J. Biol. Chem. 265,

5919–5921.
Blackburn, E.H., 2005. Telomeres and telomerase: their mechanisms of action and the effects of altering their functions. FEBS Lett. 579, 859–862.
Blackburn, E.H., Greider, C.W., Henderson, E., Lee, M.S., Shampay, J., Shippen-Lentz, D., 1989. Recognition and elongation of telomeres by telomerase. Genome 31, 553–560.
Blackburn, E.H., Epel, E.S., Lin, J., 2015. Human telomere biology: a contributory and interactive factor in aging, disease risks, and protection. Science 350, 1193–1198.
Blasco, M.A., Gasser, S.M., Lingner, J., 1999. Telomeres and telomerase. Genes Dev. 13, 2353–2359.
Bollam, S.R., Berens, M.E., Dhruv, H.D., 2018. When the ends are really the beginnings: targeting telomerase for treatment of GBM. Curr. Neurol. Neurosci. Rep. 18, 15.
Bonetti, D., Longhese, M.P., 2018. Analysis of de novo telomere addition by southern blot. Methods Mol. Biol. 1672, 363–373.
Bonfigli, A.R., Spazzafumo, L., Prattichizzo, F., Bonafè, M., Mensà, E., Micolucci, L., Giuliani, A., Fabbietti, P., Testa, R., Boemi, M., Lattanzio, F., Olivieri, F., 2016. Leukocyte telomere length and mortality risk in patients with type 2 diabetes. Oncotarget 7, 50835–50844. https://doi.org/10.18632/oncotarget.10615.
Brown, L., Zhang, Y., Mitchel, C., Ailshire, J., 2018. Does telomere length indicate biological, physical and cognitive health among older adults? Evidence from the health and retirement study. J. Gerontol. A Biol. Sci. Med. Sci. https://doi.org/10.1093/gerona/gly001.
Buckle, M., Williams, R.M., Negroni, M., Buc, H., 1996. Real time measurements of elongation by a reverse transcriptase using surface plasmon resonance. Proc. Natl. Acad. Sci. U. S. A. 93, 889–894.
Byrd, A.K., Zybailov, B.L., Maddukuri, L., Gao, J., Marecki, J.C., Jaiswal, M., Bell, M.R., Griffin, W.C., Reed, M.R., Chib, S., Mackintosh, S.G., MacNicol, A.M., Baldini, G., Eoff, R.L., Raney, K.D., 2016. Evidence that G-quadruplex DNA accumulates in the cytoplasm and participates in stress granule assembly in response to oxidative stress. J. Biol. Chem. 291, 18041–18057.
Cammas, A., Millevoi, S., 2017. RNA G-quadruplexes: emerging mechanisms in disease. Nucleic Acids Res. 45, 1584–1595.
Castle, J.C., Biery, M., Bouzek, H., Xie, T., Chen, R., Misura, K., Jackson, S., Armour, C.D., Johnson, J.M., Rohl, C.A., Raymond, C.K., 2010. DNA copy number, including telomeres and mitochondria, assayed using next-generation sequencing. BMC Genomics 11, 244.
Cawthon, R.M., 2009. Telomere length measurement by a novel monochrome multiplex quantitative PCR method. Nucleic Acids Res. 37, e21.
Cesare, A.J., Griffith, J.D., 2004. Telomeric DNA in ALT cells is characterized by free telomeric circles and heterogeneous t-loops. Mol. Cell. Biol. 24, 9948–9957.
Chen, W., Kimura, M., Kim, S., Cao, X., Srinivasan, S.R., Berenson, G.S., 2011. Longitudinal versus cross-sectional evaluations of leukocyte telomere length dynamics: age-dependent telomere shortening is the rule. J. Gerontol. A Biol. Sci. Med. Sci. 66, 312–319.
Chiang, Y.J., Calado, R.T., Hathcock, K.S., Lansdorp, P.M., Young, N.S., Hodes, R.J., 2010. Telomere length is inherited with resetting of the telomere set-point. Proc. Natl. Acad. Sci. U. S. A. 107, 10148–10153.
Chu, T.W., MacNeil, D.E., Autexier, C., 2016. Multiple mechanisms contribute to the cell growth defects imparted by human telomerase insertion in fingers domain mutations associated with premature aging diseases. J. Biol. Chem. 291, 8374–8386.
Cohen, S., Méchali, M., 2002. Formation of extrachromosomal circles from telomeric DNA in Xenopus laevis. EMBO Rep. 3, 1168–1174.
Cohen, S., Agmon, N., Sobol, O., Segal, D., 2010. Extrachromosomal circles of satellite repeats and 5S ribosomal DNA in human cells. Mob. DNA 1, 11.
Conklin, Q.A., King, B.G., Zanesco, A.P., Lin, J., Hamidi, A.B., Pokorny, J.J., Álvarez-López, M.J., Cosín-Tomás, M., Huang, C., Kaliman, P., Epel, E.S., Saron, C.D., 2018. Insight meditation and telomere biology: the effects of intensive retreat and the moderating role of personality. Brain Behav. Immun. 70, 233–245. https://doi.org/10.1016/j.bbi.2018.03.003.
Cusanelli, E., Romero, C.A., Chartrand, P., 2013. Telomeric noncoding RNA TERRA is induced by telomere shortening to nucleate telomerase molecules at short telomeres. Mol. Cell 51, 780–791.
d'Adda di Fagagna, F., Reaper, P.M., Clay-Farrace, L., Fiegler, H., Carr, P., Von Zglinicki, T., Saretzki, G., Carter, N.P., Jackson, S.P., 2003. A DNA damage checkpoint response in telomere-initiated senescence. Nature 426, 194–198.
Dahlgren, P.N., Bishop, K., Dey, S., Herbert, B.S., Tanaka, H., 2018. Development of a new monochrome multiplex qPCR method for relative telomere length measurement in Cancer. Neoplasia 20, 425–431.
Danese, E., Lippi, G., 2018. Telomere length: is the future in our "ends"? Ann. Transl. Med. 6, 280. https://doi.org/10.21037/atm.2018.06.24.
de Lange, T., 2002. Protection of mammalian telomeres. Oncogene 21, 532–540.
Diman, A., Decottignies, A., 2018. Genomic origin and nuclear localization of TERRA telomeric repeat-containing RNA: from Darkness to Dawn. FEBS J. 285, 1389–1398.
Ding, C., Li, X., Ge, Y., Zhang, S., 2010. Fluorescence detection of telomerase activity in cancer cells based on isothermal circular strand-displacement polymerization reaction. Anal. Chem. 82, 2850–2855.
Ding, Z., Mangino, M., Aviv, A., Spector, T., Durbin, R., UK10K Consortium, 2014. Estimating telomere length from whole genome sequence data. Nucleic Acids Res. 42, e75.
Fajkus, J., 2006. Detection of telomerase activity by the TRAP assay and its variants and alternatives. Clin. Chim. Acta 371, 25–31.
Farmery, J.H.R., Smith, M.L., NIHR BioResource - Rare Diseases, Lynch, A.G., 2018. Telomerecat: a ploidy-agnostic method for estimating telomere length from whole genome sequencing data. Sci. Rep. 8, 1300.
Feretzaki, M., Lingner, J., 2017. A practical qPCR approach to detect TERRA, the elusive telomeric repeat-containing RNA. Methods 114, 39–45.
Fernando, M.R., Jiang, C., Krzyzanowski, G.D., Ryan, W.L., 2017. New evidence that a large proportion of human blood plasma cell-free DNA is localized in exosomes. PLoS One 12, e0183915.
Fleisig, H.B., Wong, J.M., 2007. Telomerase as a clinical target: current strategies and potential applications. Exp. Gerontol. 42, 102–112.
Freitas-Simoes, T.M., Ros, E., Sala-Vila, A., 2018. Telomere length as a biomarker of accelerated aging: is it influenced by dietary intake? Curr. Opin. Clin. Nutr. Metab. Care 21, 430–436.
Gadalla, S.M., Khincha, P.P., Katki, H.A., Giri, N., Wong, J.Y., Spellman, S., Yanovski, J.A., Han, J.C., De Vivo, I., Alter, B.P., Savage, S.A., 2016. The limitations of qPCR telomere length measurement in diagnosing dyskeratosis congenital. Mol. Genet. Genomic Med. 4, 475–479.
Gao, X., Zhang, Y., Mons, U., Brenner, H., 2018. Leukocyte telomere length and epigenetic-based mortality risk score: associations with all-cause mortality among older adults. Epigenetics 13, 846–857. https://doi.org/10.1080/15592294.2018.1514853.
Garcia-Martin, I., Janssen, A.B., Jones, R.E., Grimstead, J.W., Penketh, R.J.A., Baird, D.M., John, R.M., 2017. Telomere length heterogeneity in placenta revealed with high-resolution telomere length analysis. Placenta 59, 61–68. https://doi.org/10.1016/j.placenta.2017.09.007.
Gardner, M., Bann, D., Wiley, L., Cooper, R., Hardy, R., Nitsch, D., Martin-Ruiz, C., Shiels, P., Sayer, A.A., Barbieri, M., Bekaert, S., Bischoff, C., Brooks-Wilson, A., Chen, W., Cooper, C., Christensen, K., De Meyer, T., Deary, I., Der, G., Diez Roux, A., Fitzpatrick, A., Hajat, A., Halaschek-Wiener, J., Harris, S., Hunt, S.C., Jagger, C., Jeon, H.S., Kaplan, R., Kimura, M., Lansdorp, P., Li, C., Maeda, T., Mangino, M., Nawrot, T.S., Nilsson, P., Nordfjall, K., Paolisso, G., Ren, F., Riabowol, K., Robertson, T., Roos, G., Staessen, J.A., Spector, T., Tang, N., Unryn, B., van der Harst, P., Woo, J., Xing, C., Yadegarfar, M.E., Park, J.Y., Young, N., Kuh, D., von Zglinicki, T., Ben-Shlomo, Y., Halcyon study team, 2014. Gender and telomere length: systematic review and meta-analysis. Exp. Gerontol. 51, 15–27.
Gelmini, S., Caldini, A., Becherini, L., Capaccioli, S., Pazzagli, M., Orlando, C., 1998. Rapid, quantitative nonisotopic assay for telomerase activity in human tumors. Clin. Chem. 44, 2133–2138.
Goetzl, E.J., Mustapic, M., Kapogiannis, D., Eitan, E., Lobach, I.V., Goetzl, L., Schwartz, J.B., Miller, B.L., 2016. Cargo proteins of plasma astrocyte-derived exosomes in Alzheimer's disease. FASEB J. 30, 3853–3859.
Goetzl, E.J., Schwartz, J.B., Mustapic, M., Lobach, I.V., Daneman, R., Abner, E.L., Jicha, G.A., 2017. Altered cargo proteins of human plasma endothelial cell-derived exosomes in atherosclerotic cerebrovascular disease. FASEB J. 31, 3689–3694.
Gomez, D.E., Armando, R.G., Farina, H.G., Menna, P.L., Cerrudo, C.S., Ghiringhelli, P.D., Alonso, D.F., 2012. Telomere structure and telomerase in health and disease (review). Int. J. Oncol. 41, 1561–1569. https://doi.org/10.3892/ijo.2012.1611.
Gorenjak, V., Akbar, S., Stathopoulou, M.G., Visvikis-Siest, S., 2018. The future of telomere length in personalized medicine. Front. Biosci. (Landmark Ed) 23, 1628–1654.
Graf, M., Bonetti, D., Lockhart, A., Serhal, K., Kellner, V., Maicher, A., Jolivet, P., Teixeira, M.T., Luke, B., 2017. Telomere length determines TERRA and R-Loop regulation through the cell cycle. Cell 170, 72–85.
Grimm, J., Perez, J.M., Josephson, L., Weissleder, R., 2004. Novel nanosensors for rapid analysis of telomerase activity. Cancer Res. 64, 639–643.
Gurău, F., Baldoni, S., Prattichizzo, F., Espinosa, E., Amenta, F., Procopio, A.D., Albertini, M.C., Bonafè, M., Olivieri, F., 2018. Anti-senescence compounds: a potential nutraceutical approach to healthy aging. Ageing Res. Rev. 46, 14–31. https://doi.org/10.1016/j.arr.2018.05.001.
Gursel, I., Gursel, M., Yamada, H., Ishii, K.J., Takeshita, F., Klinman, D.M., 2003. Repetitive elements in mammalian telomeres suppress bacterial DNA-induced immune activation. J. Immunol. 171, 1393–1400.
Gutierrez-Rodrigues, F., Santana-Lemos, B.A., Scheucher, P.S., Alves-Paiva, R.M., Calado, R.T., 2014. Direct comparison of Flow-FISH and qPCR as diagnostic tests for telomere length measurement in humans. PLoS One 9, e113747.
Haapanen, M.J., Perälä, M.M., Salonen, M.K., Guzzardi, M.A., Iozzo, P., Kajantie, E., Rantanen, T., Simonen, M., Pohjolainen, P., Eriksson, J.G., von Bonsdorff, M.B., 2018. Telomere length and frailty: the helsinki birth cohort study. J. Am. Med. Dir. Assoc. 19, 658–662. https://doi.org/10.1016/j.jamda.2018.05.011.
Halim, A.T., Ariffin, N.A., Azlan, M., 2016. Review: the multiple roles of monocytic microparticles. Inflammation 39, 1277–1284.
Hang, D., Nan, H., Kværner, A.S., De Vivo, I., Chan, A.T., Hu, Z., Shen, H., Giovannucci, E., Song, M., 2018. Longitudinal associations of lifetime adiposity with leukocyte telomere length and mitochondrial DNA copy number. Eur. J. Epidemiol. 33, 485–495.
Hansen, M.E., Hunt, S.C., Stone, R.C., Horvath, K., Herbig, U., Ranciaro, A., Hirbo, J., Beggs, W., Reiner, A.P., Wilson, J.G., Kimura, M., De Vivo, I., Chen, M.M., Kark, J.D., Levy, D., Nyambo, T., Tishkoff, S.A., Aviv, A., 2016. Shorter telomere length in Europeans than in Africans due to polygenetic adaptation. Hum. Mol. Genet. 25, 2324–2330.
Harley, C.B., Futcher, A.B., Greider, C.W., 1990. Telomeres shorten during ageing of human fibroblasts. Nature 345, 458–460.
Hastings, W.J., Shalev, I., Belsky, D.W., 2017. Translating Measures of Biological Aging to Test Effectiveness of Geroprotective Interventions: What Can We Learn from Research on Telomeres? Front. Genet. 8, 164.
Henson, J.D., Cao, Y., Huschtscha, L.I., Chang, A.C., Au, A.Y., Pickett, H.A., Reddel, R.R., 2009. DNA C-circles are specific and quantifiable markers of alternative-lengthening-of-telomeres activity. Nat. Biotechnol. 27, 1181–1185.
Henson, J.D., Lau, L.M., Koch, S., Martin La Rotta, N., Dagg, R.A., Reddel, R.R., 2017. The C-Circle assay for alternative-lengthening-of-telomeres activity. Methods 114, 74–84.
Himbert, C., Thompson, H., Ulrich, C.M., 2017. Effects of intentional weight loss on markers of oxidative stress, DNA repair and telomere length - a systematic review. Obes. Facts 10, 648–665.
Hirose, M., Abe-Hashimoto, J., Ogura, K., Tahara, H., Ide, T., Yoshimura, T., 1997. A

rapid, useful and quantitative method to measure telomerase activity by hybridization protection assay connected with a telomeric repeat amplification protocol. J. Cancer Res. Clin. Oncol. 123, 337–344.
Honig, L.S., Kang, M.S., Cheng, R., Eckfeldt, J.H., Thyagarajan, B., Leiendecker-Foster, C., Province, M.A., Sanders, J.L., Perls, T., Christensen, K., Lee, J.H., Mayeux, R., Schupf, N., 2015. Heritability of telomere length in a study of long-lived families. Neurobiol. Aging 36, 2785–2790.
Hou, M., Xu, D., Björkholm, M., Gruber, A., 2001. Real-time quantitative telomeric repeat amplification protocol assay for the detection of telomerase activity. Clin. Chem. 47, 519–524.
Hu, Y., Shi, G., Zhang, L., Li, F., Jiang, Y., Jiang, S., Ma, W., Zhao, Y., Songyang, Z., Huang, J., 2016. Switch telomerase to ALT mechanism by inducing telomeric DNA damages and dysfunction of ATRX and DAXX. Sci. Rep. 6, 32280.
Iglesias, N., Redon, S., Pfeiffer, V., Dees, M., Lingner, J., Luke, B., 2011. Subtelomeric repetitive elements determine TERRA regulation by Rap1/Rif and Rap1/Sir complexes in yeast. EMBO Rep. 12, 587–593.
Jaskelioff, M., Muller, F.L., Paik, J.H., Thomas, E., Jiang, S., Adams, A.C., Sahin, E., Kost-Alimova, M., Protopopov, A., Cadiñanos, J., Horner, J.W., Maratos-Flier, E., Depinho, R.A., 2011. Telomerase reactivation reverses tissue degeneration in aged telomerase-deficient mice. Nature 469, 102–106.
Jasmine, F., Shinkle, J., Sabarinathan, M., Ahsan, H., Pierce, B.L., Kibriya, M.G., 2018. A novel pooled-sample multiplex luminex assay for high-throughput measurement of relative telomere length. Am. J. Hum. Biol. 30, e23118. https://doi.org/10.1002/ajhb.23118.
Jiang, J., Wang, Y., Sušac, L., Chan, H., Basu, R., Zhou, Z.H., Feigon, J., 2018. Structure of telomerase with telomeric DNA. Cell 173, 1179–1190.
Jiménez, K.M., Forero, D.A., 2018. Effect of master mixes on the measurement of telomere length by qPCR. Mol. Biol. Rep. 45, 633–638.
Jose, S.S., Bendickova, K., Kepak, T., Krenova, Z., Fric, J., 2017. Chronic inflammation in immune aging: role of pattern recognition receptor crosstalk with the telomere complex? Front. Immunol. 8, 1078.
Justice, J.N., Ferrucci, L., Newman, A.B., Aroda, V.R., Bahnson, J.L., Divers, J., Espeland, M.A., Marcovina, S., Pollak, M.N., Kritchevsky, S.B., Barzilai, N., Kuchel, G.A., 2018. A framework for selection of blood-based biomarkers for geroscience-guided clinical trials: report from the TAME Biomarkers Workgroup. Geroscience. https://doi.org/10.1007/s11357-018-0042-y.
Jylhävä, J., Pedersen, N.L., Hägg, S., 2017. Biological age predictors. EBioMedicine 21, 29–36. https://doi.org/10.1016/j.ebiom.2017.03.046.
Karlseder, J., Broccoli, D., Dai, Y., Hardy, S., de Lange, T., 1999. p53- and ATM-dependent apoptosis induced by telomeres lacking TRF2. Science 283, 1321–1325.
Kaulage, M.H., Maji, B., Pasadi, S., Ali, A., Bhattacharya, S., Muniyappa, K., 2018. Targeting G-quadruplex DNA structures in the telomere and oncogene promoter regions by benzimidazole–carbazole ligands. Eur. J. Med. Chem. 148, 178–194.
Kawamura, K., Yaku, H., Miyoshi, D., Murashima, T., 2014. A simple "add and measure" FRET-based telomeric tandem repeat sequence detection and telomerase assay method. Org. Biomol. Chem. 12, 936–941.
Khan, S.S., Singer, B.D., Vaughan, D.E., 2017. Molecular and physiological manifestations and measurement of aging in humans. Aging Cell 16, 624–633. https://doi.org/10.1111/acel.12601.
Khincha, P.P., Dagnall, C.L., Hicks, B., Jones, K., Aviv, A., Kimura, M., Katki, H., Aubert, G., Giri, N., Alter, B.P., Savage, S.A., Gadalla, S.M., 2017. Correlation of leukocyte telomere length measurement methods in patients with dyskeratosis congenita and in their unaffected relatives. Int. J. Mol. Sci. 18 pii: E1765.
Kibriya, M.G., Jasmine, F., Roy, S., Ahsan, H., Pierce, B., 2014. Measurement of telomere length: a new assay using QuantiGene chemistry on a Luminex platform. Cancer Epidemiol. Biomarkers Prev. 23, 2667–2672.
Kim, W., Shay, J.W., 2018. Long-range telomere regulation of gene expression: telomere looping and telomere position effect over long distances (TPE-OLD). Differentiation 99, 1–9.
Kim, N.W., Piatyszek, M.A., Prowse, K.R., Harley, C.B., West, M.D., Ho, P.L., Coviello, G.M., Wright, W.E., Weinrich, S.L., Shay, J.W., 1994. Specific association of human telomerase activity with immortal cells and cancer. Science 266, 2011–2015.
Kimura, M., Stone, R.C., Hunt, S.C., Skurnick, J., Lu, X., Cao, X., Harley, C.B., Aviv, A., 2010. Measurement of telomere length by the Southern blot analysis of terminal restriction fragment lengths. Nat. Protoc. 5, 1596–1607. https://doi.org/10.1038/nprot.2010.124.
Klimova, B., Novotny, M., Kuca, K., 2018. Anti-aging drugs - prospect of longer life? Curr. Med. Chem. 25, 1946–1953. https://doi.org/10.2174/0929867325666171129215251.
Kohanski, R.A., Deeks, S.G., Gravekamp, C., Halter, J.B., High, K., Hurria, A., Fuldner, R., Green, P., Huebner, R., Macchiarini, F., Sierra, F., 2016. Reverse geroscience: how does exposure to early diseases accelerate the age-related decline in health? Ann. N. Y. Acad. Sci. 1386, 30–44. https://doi.org/10.1111/nyas.13297.
Komosa, M., Root, H., Meyn, M.S., 2015. Visualization and quantitative analysis of extrachromosomal telomere-repeat DNA in individual human cells by Halo-FISH. Nucleic Acids Res. 43, 2152–2163.
König, F., Schubert, T., Längst, G., 2017. The monoclonal S9.6 antibody exhibits highly variable binding affinities towards different R-loop sequences. PLoS One 12, e0178875.
Koskas, S., Decottignies, A., Dufour, S., Pezet, M., Verdel, A., Vourc'h, C., Faure, V., 2017. Heat shock factor 1 promotes TERRA transcription and telomere protection upon heat stress. Nucleic Acids Res. 45, 6321–6333.
Kulla, E., Katz, E., 2008. Biosensor techniques used for determination of telomerase activity in Cancer cells. Sensors (Basel) 8, 347–369.
Kuttler, F., Mai, S., 2007. Formation of non-random extrachromosomal elements during development, differentiation and oncogenesis. Semin. Cancer Biol. 17, 56–64.
Laguerre, A., Wong, J.M., Monchaud, D., 2016. Direct visualization of both DNA and RNA quadruplexes in human cells via an uncommon spectroscopic method. Sci. Rep. 6, 32141.
Lai, T.P., Zhang, N., Noh, J., Mender, I., Tedone, E., Huang, E., Wright, W.E., Danuser, G., Shay, J.W., 2017. A method for measuring the distribution of the shortest telomeres in cells and tissues. Nat. Commun. 8, 1356.
Lai, T.P., Wright, W.E., Shay, J.W., 2018. Comparison of telomere length measurement methods. Philos. Trans. R. Soc. Lond., B, Biol. Sci. 373, 20160451.
Lapham, K., Kvale, M.N., Lin, J., Connell, S., Croen, L.A., Dispensa, B.P., Fang, L., Hesselson, S., Hoffmann, T.J., Iribarren, C., Jorgenson, E., Kushi, L.H., Ludwig, D., Matsuguchi, T., McGuire, W.B., Miles, S., Quesenberry, C.P.Jr., Rowell, S., Sadler, M., Sakoda, L.C., Smethurst, D., Somkin, C.P., Van Den Eeden, S.K., Walter, L., Whitmer, R.A., Kwok, P.Y., Risch, N., Schaefer, C., Blackburn, E.H., 2015. Automated assay of telomere length measurement and informatics for 100,000 subjects in the genetic epidemiology research on adult health and aging (GERA) cohort. Genetics 200, 1061–1072. https://doi.org/10.1534/genetics.115.178624.
Lee, M., Napier, C.E., Yang, S.F., Arthur, J.W., Reddel, R.R., Pickett, H.A., 2017. Comparative analysis of whole genome sequencing-based telomere length measurement techniques. Methods 114, 4–15.
Li, B., Jog, S.P., Reddy, S., Comai, L., 2008. WRN controls formation of extrachromosomal telomeric circles and is required for TRF2DeltaB-mediated telomere shortening. Mol. Cell. Biol. 28, 1892–1904.
Li, Y., Liu, B., Li, X., Wei, Q., 2010. Highly sensitive electrochemical detection of human telomerase activity based on bio-barcode method. Biosens. Bioelectron. 25, 2543–2547.
Li, C.C., Hu, J., Lu, M., Zhang, C.Y., 2018a. Quantum dot-based electrochemical biosensor for stripping voltammetric detection of telomerase at the single-cell level. Biosens. Bioelectron. 122, 51–57. https://doi.org/10.1016/j.bios.2018.09.049.
Li, Y., Pan, G., Chen, Y., Yang, Q., Hao, T., Zhao, L., Zhao, L., Cong, Y., Diao, A., Yu, P., 2018b. Inhibitor of the human telomerase reverse trancriptase (hTERT) gene promoter induces cell apoptosis via a mitochondrial-dependent pathway. Eur. J. Med. Chem. 145, 370–378.
Lin, T.T., Norris, K., Heppel, N.H., Pratt, G., Allan, J.M., Allsup, D.J., Bailey, J., Cawkwell, L., Hills, R., Grimstead, J.W., Jones, R.E., Britt-Compton, B., Fegan, C., Baird, D.M., Pepper, C., 2014. Telomere dysfunction accurately predicts clinical outcome in chronic lymphocytic leukaemia, even in patients with early stage disease. Br. J. Haematol. 167, 214–223. https://doi.org/10.1111/bjh.13023.
Lin, Y., Damjanovic, A., Metter, E.J., Nguyen, H., Truong, T., Najarro, K., 2015. Age-associated telomere attrition of lymphocytes in vivo is co-ordinated with changes in telomerase activity, composition of lymphocyte subsets and health conditions. Clin. Sci. (Lond.) 128, 367–377.
Londoño-Vallejo, J.A., 2004. Telomere length heterogeneity and chromosome instability. Cancer Lett. 212, 135–144.
Lowsky, D.J., Olshansky, S.J., Bhattacharya, J., Goldman, D.P., 2014. Heterogeneity in healthy aging. J. Gerontol. A Biol. Sci. Med. Sci. 69, 640–649.
Ludlow, A.T., Shelton, D., Wright, W.E., Shay, J.W., 2018. ddTRAP: a method for sensitive and precise quantification of telomerase activity. Methods Mol. Biol. 1768, 513–529.
Lustig, A., Liu, H.B., Metter, E.J., An, Y., Swaby, M.A., Elango, P., Ferrucci, L., Hodes, R.J., Weng, N.P., 2017. Telomere shortening, inflammatory cytokines, and anti-cytomegalovirus antibody follow distinct age-associated trajectories in humans. Front. Immunol. 8, 1027.
Maesawa, C., Inaba, T., Sato, H., Iijima, S., Ishida, K., Terashima, M., Sato, R., Suzuki, M., Yashima, A., Ogasawara, S., Oikawa, H., Sato, N., Saito, K., Masuda, T., 2003. A rapid biosensor chip assay for measuring of telomerase activity using surface plasmon resonance. Nucleic Acids Res. 31 E4-4.
Mangaonkar, A.A., Patnaik, M.M., 2018. Short telomere syndromes in clinical practice: bridging bench and bedside. Mayo Clin. Proc. 93, 904–916.
Marchesini, M., Matocci, R., Tasselli, L., Cambiaghi, V., Orleth, A., Furia, L., Marinelli, C., Lombardi, S., Sammarelli, G., Aversa, F., Minucci, S., Faretta, M., Pelicci, P.G., Grignani, F., 2016. PML is required for telomere stability in non-neoplastic human cells. Oncogene 35, 1811–1821.
Martadinata, H., Heddi, B., Lim, K.W., Phan, A.T., 2011. Structure of long human telomeric RNA (TERRA): G-quadruplexes formed by four and eight UUAGGG repeats are stable building blocks. Biochemistry 50, 6455–6461.
Martin-Ruiz, C.M., Baird, D., Roger, L., Boukamp, P., Krunic, D., Cawthon, R., Dokter, M.M., van der Harst, P., Bekaert, S., de Meyer, T., Roos, G., Svenson, U., Codd, V., Samani, N.J., McGlynn, L., Shiels, P.G., Pooley, K.A., Dunning, A.M., Cooper, R., Wong, A., Kingston, A., von Zglinicki, T., 2015. Reproducibility of telomere length assessment: an international collaborative study. Int. J. Epidemiol. 44, 1673–1683. https://doi.org/10.1093/ije/dyu191.
Masutomi, K., Yu, E.Y., Khurts, S., Ben-Porath, I., Currier, J.L., Metz, G.B., Brooks, M.W., Kaneko, S., Murakami, S., DeCaprio, J.A., Weinberg, R.A., Stewart, S.A., Hahn, W.C., 2003. Telomerase maintains telomere structure in normal human cells. Cell 114, 241–253.
Meyer, A., Salewsky, B., Buchmann, N., Steinhagen-Thiessen, E., Demuth, I., 2016. Relative leukocyte telomere length, hematological parameters and Anemia - data from the Berlin aging study II (BASE-II). Gerontology 62, 330–336. https://doi.org/10.1159/000430950.
Mons, U., Müezzinler, A., Schöttker, B., Dieffenbach, A.K., Butterbach, K., Schick, M., Peasey, A., De Vivo, I., Trichopoulou, A., Boffetta, P., Brenner, H., 2017. Leukocyte telomere length and all-cause, cardiovascular disease, and Cancer mortality: results from individual-participant-Data meta-analysis of 2 large prospective cohort studies. Am. J. Epidemiol. 185, 1317–1326. https://doi.org/10.1093/aje/kww210.
Montero, J.J., López de Silanes, I., Graña, O., Blasco, M.A., 2016. Telomeric RNAs are essential to maintain telomeres. Nat. Commun. 7, 12534.
Montiel Rojas, D., Nilsson, A., Ponsot, E., Brummer, R.J., Fairweather-Tait, S., Jennings,

A., de Groot, L.C.P.G.M., Berendsen, A., Pietruszka, B., Madej, D., Caumon, E., Meunier, N., Malpuech-Brugère, C., Guidarelli, G., Santoro, A., Franceschi, C., Kadi, F., 2018. Short Telomere Length Is Related to Limitations in Physical Function in Elderly European Adults. Front. Physiol. 9, 1110. https://doi.org/10.3389/fphys.2018.01110. eCollection 2018.

Montpetit, A.J., Alhareeri, A.A., Montpetit, M., Starkweather, A.R., Elmore, L.W., Filler, K., Mohanraj, L., Burton, C.W., Menzies, V.S., Lyon, D.E., Jackson-Cook, C.K., 2014. Telomere length: a review of methods for measurement. Nurs. Res. 63, 289–299.

Moye, A.L., Porter, K.C., Cohen, S.B., Phan, T., Zyner, K.G., Sasaki, N., Lovrecz, G.O., Beck, J.L., Bryan, T.M., 2015. Telomeric G-quadruplexes are a substrate and site of localization for human telomerase. Nat. Commun. 6, 7643.

Müezzinler, A., Zaineddin, A.K., Brenner, H., 2013. A systematic review of leukocyte telomere length and age in adults. Ageing Res. Rev. 12, 509–519.

Müezzinler, A., Mons, U., Dieffenbach, A.K., Butterbach, K., Saum, K.U., Schick, M., Stammer, H., Boukamp, P., Holleczek, B., Stegmaier, C., Brenner, H., 2016. Body mass index and leukocyte telomere length dynamics among older adults: results from the ESTHER cohort. Exp. Gerontol. 74, 1–8. https://doi.org/10.1016/j.exger.2015.11.019.

Mundstock, E., Zatti, H., Louzada, F.M., Oliveira, S.G., Guma, F.T., Paris, M.M., Rueda, A.B., Machado, D.G., Stein, R.T., Jones, M.H., Sarria, E.E., Barbé-Tuana, F.M., Mattiello, R., 2015a. Effects of physical activity in telomere length: systematic review and meta-analysis. Ageing Res. Rev. 22, 72–80. https://doi.org/10.1016/j.arr.2015.02.004.

Mundstock, E., Sarria, E.E., Zatti, H., Mattos Louzada, F., Kich Grun, L., Herbert Jones, M., Guma, F.T., Mazzola In Memoriam, J., Epifanio, M., Stein, R.T., Barbé-Tuana, F.M., Mattiello, R., 2015b. Effect of obesity on telomere length: Systematic review and meta-analysis. Obesity 23 (Silver Spring), 2165–2174. https://doi.org/10.1002/oby.21183.

Nabetani, A., Ishikawa, F., 2011. Alternative lengthening of telomeres pathway: recombination-mediated telomere maintenance mechanism in human cells. J. Biochem. 149, 5–14. https://doi.org/10.1093/jb/mvq119.

Németh, A., Orgovan, N., Sódar, B.W., Osteikoetxea, X., Pálóczi, K., Szabó-Taylor, K.É., Vukman, K.V., Kittel, Á., Turiák, L., Wiener, Z., Tóth, S., Drahos, L., Vékey, K., Horvath, R., Buzás, E.I., 2017. Antibiotic-induced release of small extracellular vesicles (exosomes) with surface-associated DNA. Sci. Rep. 7, 8202.

Norberg, A., Rosén, A., Raaschou-Jensen, K., Kjeldsen, L., Moilanen, J.S., Paulsson-Karlsson, Y., Baliakas, P., Lohi, O., Ahmed, A., Kittang, A.O., Larsson, P., Roos, G., Degerman, S., Hultdin, M., 2018. Novel variants in Nordic patients referred for genetic testing of telomere-related disorders. Eur. J. Hum. Genet. 26, 858–867.

Nussey, D.H., Baird, D., Barrett, E., Boner, W., Fairlie, J., Gemmell, N., Hartmann, N., Horn, T., Haussmann, M., Olsson, M., Turbill, C., Verhulst, S., Zahn, S., Monaghan, P., 2014. Measuring telomere length and telomere dynamics in evolutionary biology and ecology. Methods Ecol. Evol. 5, 299–310.

Oerther, S., Lorenz, R., 2018. State of the science: using telomeres as biomarkers during the first 1,000 days of life. West. J. Nurs. Res. https://doi.org/10.1177/0193945918762806.

Ohuchida, K., Mizumoto, K., Ogura, Y., Ishikawa, N., Nagai, E., Yamaguchi, K., Tanaka, M., 2005. Quantitative assessment of telomerase activity and human telomerase reverse transcriptase messenger RNA levels in pancreatic juice samples for the diagnosis of pancreatic cancer. Clin. Cancer Res. 11, 2285–2292.

Oliva-Rico, D., Herrera, L.A., 2017. Regulated expression of the lncRNA TERRA and its impact on telomere biology. Mech. Ageing Dev. 167, 16–23.

Ouellette, M.M., Liao, M., Herbert, B.S., Johnson, M., Holt, S.E., Liss, H.S., Shay, J.W., Wright, W.E., 2000. Subsenescent telomere lengths in fibroblasts immortalized by limiting amounts of telomerase. J. Biol. Chem. 275, 10072–10076.

Parker, M., Chen, X., Bahrami, A., Dalton, J., Rusch, M., Wu, G., Easton, J., Cheung, N.K., Dyer, M., Mardis, E.R., Wilson, R.K., Mullighan, C., Gilbertson, R., Baker, S.J., Zambetti, G., Ellison, D.W., Downing, J.R., Zhang, J., Pediatric Cancer Genome Project, 2012. Assessing telomeric DNA content in pediatric cancers using whole-genome sequencing data. Genome Biol. 13, R113.

Patolsky, F., Gill, R., Weizmann, Y., Mokari, T., Banin, U., Willner, I., 2003. Lighting-up the dynamics of telomerization and DNA replication by CdSe-ZnS quantum dots. J. Am. Chem. Soc. 125, 13918–13919.

Pavlov, V., Xiao, Y., Gill, R., Dishon, A., Kotler, M., Willner, I., 2004. Amplified chemiluminescence surface detection of DNA and telomerase activity using catalytic nucleic acid labels. Anal. Chem. 76, 2152–2156.

Pérez, L.M., Amaral, M.A., Mundstock, E., Barbé-Tuana, F.M., Guma, F.T.C.R., Jones, M.H., Machado, D.C., Sarria, E.E., Marques E Marques, M., Preto, L.T., Epifanio, M., Meinem Garbin, J.G., Mattiello, R., 2017. Effects of diet on telomere length: systematic review and meta-analysis. Public Health Genomics 20, 286–292. https://doi.org/10.1159/000486586.

Perner, S., Brüderlein, S., Hasel, C., Waibel, I., Holdenried, A., Ciloglu, N., 2003. Quantifying telomere lengths of human individual chromosome arms by centromere-calibrated fluorescence in situ hybridization and digital imaging. Am. J. Pathol. 163, 1751–1756.

Pfeiffer, V., Lingner, J., 2012. TERRA promotes telomere shortening through exonuclease 1-mediated resection of chromosome ends. PLoS Genet. 8, e1002747.

Pickett, H.A., Cesare, A.J., Johnston, R.L., Neumann, A.A., Reddel, R.R., 2009. Control of telomere length by a trimming mechanism that involves generation of t-circles. EMBO J. 28, 799–809.

Rachakonda, S., Srinivas, N., Mahmoudpour, S.H., Garcia-Casado, Z., Requena, C., Traves, V., Soriano, V., Cardelli, M., Pajnova, D., Molven, A., Gruis, N., Nagore, E., Kumar, R., 2018. Telomere length and survival in primary cutaneous melanoma patients. Sci. Rep. 8, 10947. https://doi.org/10.1038/s41598-018-29322-9.

Raschenberger, J., Lamina, C., Haun, M., Kollerits, B., Coassin, S., Boes, E., Kedenko, L., Köttgen, A., Kronenberg, F., 2016. Influence of DNA extraction methods on relative telomere length measurements and its impact on epidemiological studies. Sci. Rep. 6, 25398. https://doi.org/10.1038/srep25398.

Rufer, N., Dragowska, W., Thornbury, G., Roosnek, E., Lansdorp, P.M., 1998. Telomere length dynamics in human lymphocyte subpopulations measured by flow cytometry. Nat. Biotechnol. 16, 743–747.

Saldanha, S.N., Andrews, L.G., Tollefsbol, T.O., 2003. Analysis of telomerase activity and detection of its catalytic subunit, hTERT. Anal. Biochem. 315, 1–21.

Savage, S.A., 2018. Beginning at the ends: telomeres and human disease. F1000Res. 7https://doi.org/10.12688/f1000research.14068.1. pii: F1000.

Savoysky, E., Akamatsu, K., Tsuchiya, M., Yamazaki, T., 1996. Detection of telomerase activity by combination of TRAP method and scintillation proximity assay (SPA). Nucleic Acids Res. 24, 1175–1176.

Schmidt, P.M., Matthes, E., Scheller, F.W., Bienert, M., Lehmann, C., Ehrlich, A., Bier, F.F., 2002. Real-time determination of telomerase activity in cell extracts using an optical biosensor. Biol. Chem. 383, 1659–1666.

Schvartzman, J.B., Martínez-Robles, M.L., Hernández, P., Krimer, D.B., 2013. Plasmid DNA topology assayed by two-dimensional agarose gel electrophoresis. Methods Mol. Biol. 1054, 121–132.

Shay, J.W., 2016. Role of telomeres and telomerase in aging and Cancer. Cancer Discov. 6, 584–593.

Shay, J.W., 2018. Telomeres and aging. Curr. Opin. Cell Biol. 52, 1–7. https://doi.org/10.1016/j.ceb.2017.12.001.

Sierra, F., Kohanski, R., 2017. Geroscience and the trans-NIH geroscience interest group, GSIG. Geroscience 39, 1–5. https://doi.org/10.1007/s11357-016-9954-6.

Skvortsov, D.A., Zvereva, M.E., Shpanchenko, O.V., Dontsova, O.A., 2011. Assays for detection of telomerase activity. Acta Naturae 3, 48–68.

Smith, E.D., Garza-Gongora, A.G., MacQuarrie, K.L., Kosak, S.T., 2018. Interstitial telomeric loops and implications of the interaction between TRF2 and lamin A/C. Differentiation 102, 19–26.

Sprouse, A.A., Steding, C.E., Herbert, B.S., 2012. Pharmaceutical regulation of telomerase and its clinical potential. J. Cell. Mol. Med. 16, 1–7. https://doi.org/10.1111/j.1582-4934.2011.01460.x.

Storci, G., De Carolis, S., Olivieri, F., Bonafè, M., 2018. Changes in the biochemical taste of cytoplasmic and cell-free DNA are major fuels for inflamm-aging. Semin. Immunol. https://doi.org/10.1016/j.smim.2018.08.003. pii: S1044-5323(18)30070-30078.

Stout, S.A., Lin, J., Hernandez, N., Davis, E.P., Blackburn, E., Carroll, J.E., Glynn, L.M., 2017. Validation of minimally-invasive sample collection methods for measurement of telomere length. Front. Aging Neurosci. 9, 397. https://doi.org/10.3389/fnagi.2017.00397.

Strazhesko, I.D., Tkacheva, O.N., Akasheva, D.U., Dudinskaya, E.N., Plokhova, E.V., Pykhtina, V.S., Kruglikova, A.S., Kokshagina, N.V., Sharashkina, N.V., Agaltsov, M.V., Kashtanova, D.A., Vygodin, V.A., Ozerova, I.N., Skvortsov, D.A., Vasilkova, D., Boytsov, S.A., 2016. Atorvastatin therapy modulates telomerase activity in patients free of atherosclerotic cardiovascular diseases. Front. Pharmacol. 7, 347.

Su, X., Li, Z., Yan, X., Wang, L., Zhou, X., Wei, L., Xiao, L., Yu, C., 2017. Telomerase activity detection with amplification-free single molecule stochastic binding assay. Anal. Chem. 89, 3576–3582.

Sue, M.J., Yeap, S.K., Omar, A.R., Tan, S.W., 2014. Application of PCR-ELISA in molecular diagnosis. Biomed Res. Int. 2014, 653014.

Takai, H., Smogorzewska, A., de Lange, T., 2003. DNA damage foci at dysfunctional telomeres. Curr. Biol. 13, 1549–1556.

Tarik, M., Ramakrishnan, L., Sachdev, H.S., Tandon, N., Roy, A., Bhargava, S.K., Pandey, R.M., 2018. Validation of quantitative polymerase chain reaction with Southern blot method for telomere length analysis. Future Sci. OA 4, FSO282.

Testa, R., Olivieri, F., Sirolla, C., Spazzafumo, L., Rippo, M.R., Marra, M., Bonfigli, A.R., Ceriello, A., Antonicelli, R., Franceschi, C., Castellucci, C., Testa, I., Procopio, A.D., 2011. Leukocyte telomere length is associated with complications of type 2 diabetes mellitus. Diabet. Med. 28, 1388–1394. https://doi.org/10.1111/j.1464-5491.2011.03370.x.

Tokutake, Y., Matsumoto, T., Watanabe, T., Maeda, S., Tahara, H., Sakamoto, S., Niida, H., Sugimoto, M., Ide, T., Furuichi, Y., 1998. Extra-chromosomal telomere repeat DNA in telomerase-negative immortalized cell lines. Biochem. Biophys. Res. Commun. 247, 765–772.

Tomaska, L., Nosek, J., Kramara, J., Griffith, J.D., 2009. Telomeric circles: universal players in telomere maintenance? Nat. Struct. Mol. Biol. 16, 1010–1015. https://doi.org/10.1038/nsmb.1660.

Toubiana, S., Selig, S., 2018. DNA:RNA hybrids at telomeres - when it is better to be out of the (R) loop. FEBS J. 285, 2552–2566. https://doi.org/10.1111/febs.14464.

Toupance, S., Labat, C., Temmar, M., Rossignol, P., Kimura, M., Aviv, A., Benetos, A., 2017. Short telomeres, but not telomere attrition rates, are associated with carotid atherosclerosis. Hypertension. 70, 420–425.

Uehara, H., Nardone, G., Nazarenko, I., Hohman, R.J., 1999. Detection of telomerase activity utilizing energy transfer primers: comparison with gel- and ELISA-based detection. Biotechniques. 26, 552–558.

Vaiserman, A., Lushchak, O., 2017. Implementation of longevity-promoting supplements and medications in public health practice: achievements, challenges and future perspectives. J. Transl. Med. 15, 160. https://doi.org/10.1186/s12967-017-1259-8.

Vetter, V.M., Antje, M., Karbasiyan, M., Steinhagen-Thiessen, E., Hopfenmüller, W., Demuth, 2018. Epigenetic clock and relative telomere length represent largely different aspects of aging in the Berlin Aging Study II (BASE-II). J. Gerontol. A Biol. Sci. Med. Sci. https://doi.org/10.1093/gerona/gly184.

Wang, Z., Lieberman, P.M., 2016. The crosstalk of telomere dysfunction and inflammation through cell-free TERRA containing exosomes. RNA Biol. 13, 690–695.

Wang, Y., Prosen, D.E., Mei, L., Sullivan, J.C., Finney, M., Vander Horn, P.B., 2004. A novel strategy to engineer DNA polymerases for enhanced processivity and improved performance in vitro. Nucleic Acids Res. 32, 1197–1207.

Wang, Z., Deng, Z., Dahmane, N., Tsai, K., Wang, P., Williams, D.R., Kossenkov, A.V., Showe, L.C., Zhang, R., Huang, Q., Conejo-Garcia, J.R., Lieberman, P.M., 2015. Telomeric repeat-containing RNA (TERRA) constitutes a nucleoprotein component of extracellular inflammatory exosomes. Proc. Natl. Acad. Sci. U. S. A. 112, E6293–300.

Wang, J., Dong, X., Cao, L., Sun, Y., Qiu, Y., Zhang, Y., Cao, R., Covasa, M., Zhong, L., 2016. Association between telomere length and diabetes mellitus: a meta-analysis. J. Int. Med. Res. 44, 1156–1173. https://doi.org/10.1177/0300060516667132.

Wang, H., Zhang, K., Liu, Y., Fu, Y., Gao, S., Gong, P., Wang, H., Zhou, Z., Zeng, M., Wu, Z., Sun, Y., Chen, T., Li, S., Liu, L., 2017a. Telomere heterogeneity linked to metabolism and pluripotency state revealed by simultaneous analysis of telomere length and RNA-seq in the same human embryonic stem cell. BMC Biol. 15, 114.

Wang, W., Zheng, L., Zhou, N., Li, N., Bulibu, G., Xu, C., Zhang, Y., Tang, Y., 2017b. Meta-analysis of associations between telomere length and colorectal cancer survival from observational studies. Oncotarget 8, 62500–62507. https://doi.org/10.18632/oncotarget.20055.

Wang, Z., Deng, Z., Tutton, S., Lieberman, P.M., 2017c. The telomeric response to viral infection. Viruses. 9https://doi.org/10.3390/v9080218. pii: E218.

Wang, Z., Li, J., Liu, J.P., 2018a. Effects of cation charges on the binding of stabilizers with human telomere and TERRA G-quadruplexes. J. Biomol. Struct. Dyn. https://doi.org/10.1080/07391102.2018.1471416.

Wang, Q., Zhan, Y., Pedersen, N.L., Fang, F., Hägg, S., 2018b. Telomere length and all-cause mortality: a meta-analysis. Ageing Res. Rev. 48, 11–20. https://doi.org/10.1016/j.arr.2018.09.002.

Wege, H., Chui, M.S., Le, H.T., Tran, J.M., Zern, M.A., 2003. SYBR Green real-time telomeric repeat amplification protocol for the rapid quantification of telomerase activity. Nucleic Acids Res. 31, E3–3.

Williams, J., Heppel, N.H., Britt-Compton, B., Grimstead, J.W., Jones, R.E., Tauro, S., Bowen, D.T., Knapper, S., Groves, M., Hills, R.K., Pepper, C., Baird, D.M., Fegan, C., 2017. Telomere length is an independent prognostic marker in MDS but not in de novo AML. Br. J. Haematol. 178, 240–249. https://doi.org/10.1111/bjh.14666.

Wu, Y.Y., Hruszkewycz, A.M., Delgado, R.M., Yang, A., Vortmeyer, A.O., Moon, Y.W., Weil, R.J., Zhuang, Z., Remaley, A.T., 2000. Limitations on the quantitative determination of telomerase activity by the electrophoretic and ELISA based TRAP assays. Clin. Chim. Acta 293, 199–212.

Wu, R.A., Upton, H.E., Vogan, J.M., Collins, K., 2017. Telomerase mechanism of telomere synthesis. Annu. Rev. Biochem. 86, 439–460.

Wulaningsih, W., Kuh, D., Wong, A., Hardy, R., 2018. Adiposity, telomere length, and telomere attrition in midlife: the 1946 british birth cohort. J. Gerontol. A Biol. Sci. Med. Sci. 73, 966–972. https://doi.org/10.1093/gerona/glx151.

Xu, Y., Suzuki, Y., Ito, K., Komiyama, M., 2010. Telomeric repeat-containing RNA structure in living cells. Proc. Natl. Acad. Sci. U. S. A. 107, 14579–14584.

Yehuda, S., Yanai, H., Priel, E., Fraifeld, V.E., 2017. Differential decrease in soluble and DNA-bound telomerase in senescent human fibroblasts. Biogerontology. 18, 525–533. https://doi.org/10.1007/s10522-017-9688-6.

Zavari-Nematabad, A., Alizadeh-Ghodsi, M., Hamishehkar, H., Alipour, E., Pilehvar-Soltanahmadi, Y., 2017. Development of quantum-dot-encapsulated liposome-based optical nanobiosensor for detection of telomerase activity without target amplification. Anal. Bioanal. Chem. 409, 1301–1310. https://doi.org/10.1007/s00216-016-0058-z.

Zhang, C., Chen, X., Li, L., Zhou, Y., Wang, C., Hou, S., 2015. The association between telomere length and Cancer prognosis: evidence from a meta-analysis. PLoS One 10, e0133174. https://doi.org/10.1371/journal.pone.0133174.

Zhang, T., Zhang, Z., Li, F., Hu, Q., Liu, H., Tang, M., Ma, W., Huang, J., Songyang, Z., Rong, Y., Zhang, S., Chen, B.P., Zhao, Y., 2017a. Looping-out mechanism for resolution of replicative stress at telomeres. EMBO Rep. 18, 1412–1428. https://doi.org/10.15252/embr.201643866.

Zhang, X., Lou, X., Xia, F., 2017b. Advances in the detection of telomerase activity using isothermal amplification. Theranostics. 7, 1847–1862.

Zhang, L., Peng, J., Hong, M.F., Chen, J.Q., Liang, R.P., Qiu, J.D., 2018. A facile graphene oxide-based fluorescent nanosensor for the in situ "turn-on" detection of telomerase activity. Analyst. 143, 2334–2341.

Zhu, Y., Liu, X., Ding, X., Wang, F., Geng, X., 2018. Telomere and its role in the aging pathways: telomere shortening, cell senescence and mitochondria dysfunction. Biogerontology. https://doi.org/10.1007/s10522-018-9769-1.

Zierer, J., Kastenmüller, G., Suhre, K., Gieger, C., Codd, V., Tsai, P.C., Bell, J., Peters, A., Strauch, K., Schulz, H., Weidinger, S., Mohney, R.P., Samani, N.J., Spector, T., Mangino, M., Menni, C., 2016. Metabolomics profiling reveals novel markers for leukocyte telomere length. Aging (Albany NY) 8, 77–94.

Zinkova, A., Brynychova, I., Svacina, A., Jirkovska, M., Korabecna, M., 2017. Cell-free DNA from human plasma and serum differs in content of telomeric sequences and its ability to promote immune response. Sci. Rep. 7, 2591.

Journal of Extracellular Vesicles

ISSN: (Print) (Online) Journal homepage: https://www.tandfonline.com/loi/zjev20

Small extracellular vesicles deliver miR-21 and miR-217 as pro-senescence effectors to endothelial cells

Emanuela Mensà , Michele Guescini , Angelica Giuliani , Maria Giulia Bacalini , Deborah Ramini , Giacomo Corleone , Manuela Ferracin , Gianluca Fulgenzi , Laura Graciotti , Francesco Prattichizzo , Leonardo Sorci , Michela Battistelli , Vladia Monsurrò , Anna Rita Bonfigli , Maurizio Cardelli , Rina Recchioni , Fiorella Marcheselli , Silvia Latini , Serena Maggio , Mirco Fanelli , Stefano Amatori , Gianluca Storci , Antonio Ceriello , Vilberto Stocchi , Maria De Luca , Luca Magnani , Maria Rita Rippo , Antonio Domenico Procopio , Claudia Sala , Iva Budimir , Cristian Bassi , Massimo Negrini , Paolo Garagnani , Claudio Franceschi , Jacopo Sabbatinelli , Massimiliano Bonafè & Fabiola Olivieri

To cite this article: Emanuela Mensà , Michele Guescini , Angelica Giuliani , Maria Giulia Bacalini , Deborah Ramini , Giacomo Corleone , Manuela Ferracin , Gianluca Fulgenzi , Laura Graciotti , Francesco Prattichizzo , Leonardo Sorci , Michela Battistelli , Vladia Monsurrò , Anna Rita Bonfigli , Maurizio Cardelli , Rina Recchioni , Fiorella Marcheselli , Silvia Latini , Serena Maggio , Mirco Fanelli , Stefano Amatori , Gianluca Storci , Antonio Ceriello , Vilberto Stocchi , Maria De Luca , Luca Magnani , Maria Rita Rippo , Antonio Domenico Procopio , Claudia Sala , Iva Budimir , Cristian Bassi , Massimo Negrini , Paolo Garagnani , Claudio Franceschi , Jacopo Sabbatinelli , Massimiliano Bonafè & Fabiola Olivieri (2020) Small extracellular vesicles deliver miR-21 and miR-217 as pro-senescence effectors to endothelial cells, Journal of Extracellular Vesicles, 9:1, 1725285, DOI: 10.1080/20013078.2020.1725285

To link to this article: https://doi.org/10.1080/20013078.2020.1725285

JOURNAL OF EXTRACELLULAR VESICLES
2020, VOL. 9, 1725285
https://doi.org/10.1080/20013078.2020.1725285

Taylor & Francis
Taylor & Francis Group

RESEARCH ARTICLE

OPEN ACCESS Check for updates

Small extracellular vesicles deliver miR-21 and miR-217 as pro-senescence effectors to endothelial cells

Emanuela Mensà [a*], Michele Guescini [b*], Angelica Giuliani [a*], Maria Giulia Bacalini [c], Deborah Ramini [a], Giacomo Corleone [d], Manuela Ferracin [e], Gianluca Fulgenzi [a], Laura Graciotti [a], Francesco Prattichizzo [f], Leonardo Sorci [g], Michela Battistelli [b], Vladia Monsurrò [h], Anna Rita Bonfigli [i], Maurizio Cardelli [j], Rina Recchioni [k], Fiorella Marcheselli [k], Silvia Latini [a], Serena Maggio [b], Mirco Fanelli [l], Stefano Amatori [l], Gianluca Storci [e], Antonio Ceriello [f], Vilberto Stocchi [b], Maria De Luca [m], Luca Magnani [d], Maria Rita Rippo [a], Antonio Domenico Procopio [a,k], Claudia Sala [n], Iva Budimir [n], Cristian Bassi [o], Massimo Negrini [o], Paolo Garagnani [e,p,q], Claudio Franceschi [c,r], Jacopo Sabbatinelli [a], Massimiliano Bonafè [e*] and Fabiola Olivieri [a,k*]

[a]Department of Clinical and Molecular Sciences, Università Politecnica delle Marche, Ancona, Italy; [b]Department of Biomolecular Sciences, University of Urbino Carlo Bo, Urbino, Italy; [c]IRCCS Istituto delle Scienze Neurologiche di Bologna, Bologna, Italy; [d]Department of Surgery and Cancer, Imperial College London, London, UK; [e]Department of Experimental, Diagnostic, and Specialty Medicine, University of Bologna, Bologna, Italy; [f]IRCCS MultiMedica, Milano, Italy; [g]Department of Materials, Environmental Sciences and Urban Planning, Università Politecnica delle Marche, Ancona, Italy; [h]Department of Medicine, University of Verona, Verona, Italy; [i]Scientific Direction, IRCCS INRCA, Ancona, Italy; [j]Advanced Technology Center for Aging Research, Scientific Technological Area, IRCCS INRCA, Ancona, Italy; [k]Center of Clinical Pathology and Innovative Therapy, IRCCS INRCA, Ancona, Italy; [l]Department of Biomolecular Sciences, Molecular Pathology Laboratory "Paola", University of Urbino Carlo Bo, Fano, Italy; [m]Department of Nutrition Sciences, University of Alabama at Birmingham, Birmingham, USA; [n]Department of Physics and Astronomy, University of Bologna, Bologna, Italy; [o]Department of Morphology, Surgery & Experimental Medicine, and Laboratory for the Technologies of Advanced Therapies, Tecnopolo, University of Ferrara, Ferrara, Italy; [p]Clinical Chemistry, Department of Laboratory Medicine, Karolinska Institutet at Huddinge University Hospital, Stockholm, Sweden; [q]Personal Genomics S.r.l., Verona, Italy; [r]Lobachevsky State University of Nizhny Novgorod, Nizhny Novgorod, Russia

ABSTRACT

The role of epigenetics in endothelial cell senescence is a cutting-edge topic in ageing research. However, little is known of the relative contribution to pro-senescence signal propagation provided by microRNAs shuttled by extracellular vesicles (EVs) released from senescent cells. Analysis of microRNA and DNA methylation profiles in non-senescent (control) and senescent (SEN) human umbilical vein endothelial cells (HUVECs), and microRNA profiling of their cognate small EVs (sEVs) and large EVs demonstrated that SEN cells released a significantly greater sEV number than control cells. sEVs were enriched in miR-21-5p and miR-217, which target DNMT1 and SIRT1. Treatment of control cells with SEN sEVs induced a miR-21/miR-217-related impairment of DNMT1-SIRT1 expression, the reduction of proliferation markers, the acquisition of a senescent phenotype and a partial demethylation of the locus encoding for miR-21. MicroRNA profiling of sEVs from plasma of healthy subjects aged 40–100 years showed an inverse U-shaped age-related trend for miR-21-5p, consistent with senescence-associated biomarker profiles. Our findings suggest that miR-21-5p/miR-217 carried by SEN sEVs spread pro-senescence signals, affecting DNA methylation and cell replication.

ARTICLE HISTORY
Received 10 August 2019
Revised 26 January 2020
Accepted 29 January 2020

KEYWORDS
Cellular senescence; microRNAs; DNMT1; SIRT1; extracellular vesicles

Introduction

Cellular senescence is considered as a hallmark of ageing and a major risk factor for the development of the most common age-related diseases (ARDs) [1]. Senescent cells (SCs) are characterised by a significantly reduced replicative potential and by the acquisition of a pro-inflammatory senescence-associated secretory phenotype (SASP) [2], which involves the paracrine induction of a senescent state in younger cells through a "bystander effect" [3]. Since this effect fuels inflammaging – the systemic, low-grade, chronic inflammation that accompanies human ageing [4] – it appears to be a critical step in SC accumulation during organismal ageing [5]. The clinical relevance of inflammaging in ARD development and progression has become clearly established [6]. SC clearance and attenuation of the bystander effect have been proposed

CONTACT Jacopo Sabbatinelli j.sabbatinelli@pm.univpm.it Department of Clinical and Molecular Sciences, Università Politecnica Delle Marche, Via Tronto 10/A, Ancona, Italy

*These authors contributed equally

Supplemental data for this article can be accessed here.

as innovative therapeutic approaches to address, ameliorate or prevent a range of human disorders [7–10]. In this framework, unravelling the contribution of the epigenetic mechanisms involved in the senescence process would be a major step forward [11]. Considerable effort is being devoted to discriminating the effects of several epigenetic mechanisms, including DNA methylation and long and small non-coding RNA activity, on the modulation of the transcriptional programme leading to cellular senescence [12,13]. Senescence-associated (SA) genome-wide hypomethylation has been described in SCs, whereas the expression and activity of DNA methyltransferase 1 (DNMT1) decline with ageing [14]. DNMT1 is involved in maintaining the methylation pattern and works with Sirtuin 1 (SIRT1), an enzyme exerting mono-ADP ribosyltransferase or deacetylase activity, in ensuring genome integrity and in exerting pro-longevity effects [15,16]. As a result, DNMT and SIRT activators/inhibitors are being investigated as therapeutic agents against ARDs [17].

Senescence modulation by microRNAs (miRNAs) is a major senescence-related epigenetic mechanism. This has been suggested, among other findings, by the identification of discrete miRNA signatures associated with senescence in different cell types [18] and by the fact that living cells can actively release extracellular vesicles (EVs), which contain different species and amounts of non-coding RNAs. EVs comprise large particles (lEVs; also known as micro-vesicles) and small particles (sEVs or exosomes) and differ both in their intra-cellular origin and in the cargo they transport [19]. lEVs and sEVs seem to reflect the molecular characteristics of their cells of origin and to modulate the phenotype of recipient cells both in a paracrine and in a systemic manner [20,21]. Despite the major contribution to organismal ageing demonstrated for EVs and their miRNA cargo [22,23], too little is known of the effect of ageing on human EV content, on the miRNA repertoire shuttled by SCs and their cognate EVs, and on circulating EVs. Evidence from a variety of cellular models suggests that the senescence phenotype is characterised by increased EV secretion [24–26], although circulating EV concentrations seem to decline with age, possibly as a consequence of increased internalisation by immune cells [27]. Notably, the pro-inflammatory effects of EVs released from SCs seem to be related to their DNA/RNA cargo, which suggests that EVs belong to the SC secretome [25,26,28]. Recently, the effects of EVs have been explored in relation to vascular ageing [28]. EVs from the plasma of elderly subjects and from senescent endothelial cells (ECs) promote vascular calcification [29], reduce the bone formation rate [30] and reprogram monocytes towards a pro-inflammatory phenotype [31].

Altogether, our knowledge of the *in vivo* effects of cellular senescence is quite limited. Moreover, the heterogeneous senescence phenotypes characterising living animals entail that there are currently no wholly reliable universal markers to identify senescent ECs *in vivo* [32].

This study was devised to unravel the relative contribution of EVs released from senescent ECs in spreading pro-senescence signals to proliferating cells via their miRNA cargo. Based on the evidence that the *in vitro* replicative senescence of ECs substantially mimics the progressive age-related impairment of endothelial function described *in vivo* [33], we set out to identify the miRNAs that are differentially expressed in senescent and non-senescent human umbilical vein endothelial cells (HUVECs) and their cognate EVs (lEVs and sEVs). We then correlated the miRNA levels with the methylation state of their genetic loci and assessed their interactions with the enzymes involved in the maintenance of the methylation pattern during ageing. Finally, we compared the SA-miRNAs isolated from EVs released from senescent HUVECs with the miRNAs showing a differential expression in circulating EVs obtained from subjects of different ages.

Materials and methods

Cell lines and cell culture

An *in vitro* model of replicative cell senescence was established using long-term cultured HUVECs and human aortic endothelial cells (HAECs). Cryopreserved HUVECs and HAECs obtained from pool of donors were purchased from Clonetics (Lonza, Switzerland) and cultured in endothelial basal medium (EBM-2, CC-3156, Lonza) supplemented with SingleQuot Bullet Kit (CC-4176, Lonza) containing 0.1% human recombinant epidermal growth factor (rh-EGF), 0.04% hydrocortisone, 0.1% vascular endothelial growth factor (VEGF), 0.4% human recombinant fibroblast growth factor (rh-FGF-B), 0.1% insulin-like growth factor-1 with the substitution of arginine for glutamic acid at position 3 (R3-IGF-1), 0.1% ascorbic acid, 0.1% heparin, 0.1% gentamicin and amphotericin-B (GA-1000) and 2% foetal bovine serum (FBS). Cells were seeded at a density of 5000/cm^2, sub-cultured when they reached 70–80% confluence, and maintained in a humidified atmosphere of 5% CO_2 at 37°C. All cells tested negative for mycoplasma infection. Before replating, harvested cells were counted using a haemocytometer. Population doublings (PDs) were calculated by the formula: $(\log_{10}F - \log_{10}I)/\log_{10}2$, where F is the number of

cells at the end of the passage and *I* is the number of seeded cells. Cumulative population doubling (cPD) was calculated as the sum of PD changes. Cells were cultured until the arrest of replication and classified based on SA β-Gal activity into control (CON, SA β-Gal < 5%) and senescent (SEN, SA β-Gal > 60%) cells. For the drug-induced senescence model, HUVECs and HAECs were treated with doxorubicin hydrochloride (Sigma Aldrich, Italy) at 50 nM for 24 h and were harvested following a 72-h recovery period with fresh medium.

Biomarkers of the HUVEC and HAEC senescent phenotype

SA β-galactosidase staining

SA β-galactosidase (β-gal) activity was assessed using Senescence Detection Kit (cat. no. K320, BioVision Inc., USA) as described previously [34].

Telomere length

Telomere length was analysed by quantitative PCR using Cawthon's method [35]. Genomic DNA was isolated from young and senescent HUVECs using Norgen's RNA/DNA Purification Kit (cat. no. 48,700, Norgen Biotek Corporation, Canada).

p16, IL-1β, IL-6, IL-8, DNMT1 and SIRT1 mRNA expression level

For mRNA gene expression, 1 µg of purified RNA was reverse-transcribed with OneScript® cDNA Synthesis Kit (Applied Biological Materials Inc., Canada) according to the manufacturer's instructions. qPCR reactions were conducted in a Rotor Gene Q 5plex HRM apparatus (Qiagen, Germany) in a 10 µl total reaction volume using TB Green Premix Ex Taq II (Clontech Laboratories, USA) according to the manufacturer's instructions. Each reaction was run in triplicate and always included a no-template control. The mRNA expression of the genes of interest was calculated using *GAPDH* as the reference gene.

mRNA expression levels were analysed by the $2^{-\Delta Ct}$ method. The value of the relative expression of the genes of interest is given as mean ± standard deviation (SD) of three independent experiments.

The primers sequences (written 5′-3′) were: p16, Fw: CATAGATGCCGCGGAAGGT, Rv: CTAAGTTTCCC GAGGTTTCTCAGA; IL-1β, Fw: CCAGCTACGAATC TCCGACC, Rv: TGGGGTGGAAAGGTTTGGA; IL-6, Fw: CCAGCTACGAATCTCCGACC, Rv: CATGGCC ACAACAATGACG; IL-8, Fw: TCTGCAGCTCTGTG TGTGAAGG, Rv: TGGGGTGGAAAGGTTTGGA; β-a ctin, Fw: TGCTATCCCTGTACGCCTCT, Rv: GTGGTGGTGAAGCTGTAGCC; DNMT1, Fw: AGA ACGCCTTTAAGCGCCG; Rv: CCGTCCACTGCCAC CAAAT; SIRT1, Fw: AGGCCACGGATAGGTCCATA; Rv: GTGGAGGTATTGTTTCCGGC. Primer concentration was 200 nM.

p16, DNMT1 and SIRT1 protein quantification

In HUVECs, total proteins were purified using RIPA buffer (150 mM NaCl, 10 mM Tris, pH 7.2, 0.1% SDS, 1.0% Triton X-100, 5 mM EDTA, pH 8.0) containing a protease inhibitor cocktail (Roche Applied Science, USA). Protein concentration was determined using the Bradford method (Sigma-Aldrich, Italy). Total protein extracts (30 µg) were separated by SDS-PAGE and transferred to nitrocellulose membranes (Whatman, Germany). Membranes were blocked in phosphate-buffered saline (PBS) with 0.1% Tween 20 (PBS-T) containing 5% fat-free dry milk for 1 h and then incubated overnight at 4°C with primary antibodies targeting p16(Ink4a) (1:200; sc-377,412, Santa Cruz Biotechnology, USA), pH2AX (1:1000; #9718, Cell Signaling, USA), DNMT1 (1:1000; ab19905; Abcam, UK) and SIRT1 (1:1000; ab12193, Abcam), using β-actin (1:10,000; Santa Cruz Biotechnology) or α-tubulin (1:1000; #2144, Cell Signaling) as normalizers. All primary antibodies were probed with a secondary horseradish peroxidase (HRP)-conjugated antibody (Vector, USA). A chemiluminescence assay (ECL, Amersham, USA) was used for detection; the autoradiographic films thus obtained were quantified using ImageJ2 software [36]. Independent samples *t*-test was used to analyse the differences between samples. p values < 0.05 were considered significant.

Genome-wide DNA methylation analysis

Genomic DNA was extracted in triplicate from CON and SEN HUVECs using Qiagen's QiAmp mini kit following the manufacturer's recommendations.

Accordingly, 1 µg DNA was bisulphite-converted using EZ DNA Methylation (Zymo Research, USA) and analysed by the Infinium HumanMethylationEPIC BeadChip (Illumina Inc., USA) according to the manufacturer's instructions. The DNA methylation levels from the EPIC kit [37] were quantified by applying the workflow described for EPIC array analysis in the Minfi v1.28.3 vignette [38]. The IlluminaHumanMethylationEPICanno.ilm10b2.hg19_0.6.0.tar.gz manifest was employed to annotate the EPIC probes.

Quality control of raw and normalised data was performed with the ShinyMethyl v1.18 package, available in Bioconductor 3.8 [39]. Data normalisation included noob background correction [40] followed by functional normalisation implemented in the Minfi

function "preprocess Funnorm" [41]. Probes matching single nucleotide polymorphism (SNP) loci were not deployed for downstream analysis and were removed by running the Minfi function "dropLociWithSnps".

DNA methylation polymorphisms (DMPs) were assigned to a genomic category following the annotation available in the IlluminaHumanMethylationEPIC manifest under the column "UCSC_RefGene_Group". Probes not assigned to any category were classified as "others". DMPs were split into hyper- and hypomethylated sites and plotted using an in-house-developed R script.

The methylation state of differentially expressed miRNAs (see below "Small RNAseq analysis [NGS] of cells and EVs") was inferred by evaluating the probes within −2 kb of the miRNA annotation start and +2 kb of their end in the hg19 genome assembly. DMPs associated with each miRNA were deployed to build a methylation state heatmap and linked to the miRNA expression state using an in-house-developed R script.

The methylation landscape of the *DNMT1* and *SIRT1* genes was characterised by estimating the normalised beta values of all probes occurring within −2 kb of the TSS of the gene and +2 kb of the gene end coordinate. Probes were classified by the "UCSC_RefGene_Group". Probes matching each genomic window were then plotted in boxplot format using an in-house-developed R script.

Electron microscopy analysis

HUVECs were plated on Aclar film (Ted Pella Inc., USA), sectioned tangential to the substrate and examined by TEM. HUVECs were fixed for 1 h at room temperature in 2.5 glutaraldehyde solution in 0.1 M cacodylate buffer (pH 7.4), post-fixed in 1% osmium tetroxide in the same buffer for 30 min at room temperature, dehydrated in an acetone series and embedded in epoxy resin (cat. no. 43,359, Sigma-Aldrich, Italy). Ultrathin (40 nm) sections were stained with lead citrate and uranyl acetate and examined in a Philips CM12 transmission electron microscope (Philips, Netherlands) at 100 kV. Scanning electron microscopy analysis was performed on HUVECs plated on Aclar film fixed and dehydrated as described above, critical point-dried (Balzers union cpd 020), gold-coated and imaged using a Philips XL20 microscope at 15 kV. The release of multi-vesicular bodies (MVBs) was evaluated by counting their number/μm^2 of cytoplasmic area in 24 CON and 22 SEN cells.

For TEM analysis of lEVs and sEVs, EVs were adsorbed to formvar carbon-coated 200 mesh grids (Agar Scientific Ltd., UK) for 2 min, gently washed with filtered PBS and immediately fixed on the grids with 2.5% glutaraldehyde for 1 min. The grids were incubated with 2% (w/v) sodium phosphotungstate for 1 min and observed in a Philips CM10 transmission electron microscope.

EV purification and characterisation (Nanosight tracking analysis and western blotting)

When CON and SEN HUVECs reached 70% confluence in T75 flasks, they were thoroughly washed with PBS and incubated in EGM-2 containing exosome-depleted FBS (cat. no. A2720801, Thermo Fisher Scientific, USA). Conditioned medium from 8′000′000 ± 1′000′000 cells was collected after 18 h and EVs (lEVs and sEVs) were purified by ultracentrifugation [42].

EVs released from SEN and CON cells were characterised according to the Minimal Information for Studies of Extracellular Vesicles guidelines, which were developed by the International Society for Extracellular Vesicles (ISEV) in 2018 [43]. Specifically, we (i) adopted the EV nomenclature suggested by the ISEV position papers; (ii) performed basic characterisation of the EV-releasing cells before the collection of conditioned medium (culturing condition details such as passage number, seeding density, confluence at harvest have been reported); (iii) employed a variety of techniques such as size-exclusion chromatography (SEC), serial ultracentrifugation or a combination of ultracentrifugation and density gradient separation to isolate EVs; (iv) characterised and quantified isolated EVs using nanoparticle tracking assay, transmission electron microscopy and western blot analysis using well-established markers (CD63, TSG101, calnexin).

EVs were purified by centrifugation at 1′000*g* for 15 min and then at 2′000*g* for 15 min to eliminate cell debris. Supernatants were further centrifuged at 18′000*g* for 30 min to obtain the lEV pellet. The resulting supernatant was pelleted by ultracentrifugation at 110′000*g* for 70 min. The sEV pellet was washed in 3 ml PBS, centrifuged again and resuspended in PBS.

EV amount and size was measured by NanoSight tracking analysis (NTA). sEVs and lEVs were loaded into the sample chamber of an LM10 unit (NanoSight, Malvern Instruments Ltd, UK). Three 30 or 60 s videos were recorded for each sample and analysed with NanoSight NTA 3.1 software. Data were expressed as mean ± SD of the three recordings. Samples containing a large number of particles were diluted before the analysis and the relative sEV and lEV concentration was calculated according to the dilution factor. Control beads (100 and 400 nm) were supplied by Malvern Instruments. EV lysates were prepared in RIPA buffer

containing a protease inhibitor cocktail (Roche Applied Science) and quantified using the Bradford method. Next, the lysates were subjected to SDS-PAGE and transferred to nitrocellulose membranes (Whatman). Membranes were then incubated with the primary antibodies overnight at 4°C. The following primary antibodies were used: calnexin (clone C4731, Sigma-Aldrich; 1:2000 dilution), TSG101 (ab125011, Abcam; 1:1000 dilution) and CD63 (ab59479, Abcam; 1:1000 dilution). After incubation with the specific HRP-conjugated antibody (Vector; 1:10,000 dilution), the chemiluminescent signal was detected using Clarity and/or Clarity Max (Bio-Rad, Italy). The autoradiographic films thus obtained were quantified using ImageJ2 software.

In order to exclude that protein-miRNA complexes could co-precipitate with EVs during the isolation procedure, we used a combination of density gradient separation and treatment of isolated vesicles with proteinase K 20 μg/ml to confirm that miR-21-5p is truly loaded into EVs. MiR-21-5p levels were not significantly different between the two conditions (miR-21-5p relative expression; control = 0.383 ± 0.050; proteinase K = 0.259 ± 0.063; n = 3; p = 0.185), confirming the intra-vesicular presence of the miRNAs.

Data regarding the EV-related aspects of the experiments conducted on HUVECs have been deposited to the EV-TRACK knowledge base (http://evtrack.org) [44] under accession number EV190105.

RNA extraction from HUVECs and EVs

Small RNAs (< 200 nucleotides) were extracted from HUVECs and sEV and lEV pellets using, respectively Norgen's total RNA Purification Kit and Total Exosome RNA & Protein Isolation Kit (Thermo Fisher Scientific) according to the manufacturer's protocol. Purified RNA was stored at −80°C until use.

Small RNA sequencing analysis (NGS) of HUVECs and EVs

CON and SEN cells, their EVs (lEVs and sEVs) and 12 samples of sEVs purified from plasma of four young, four elderly and four centenarian subjects were subjected to small RNA sequencing. RNA for the analysis was obtained from 6 ml of media from the culture of 2.000.000 CON cells and 1.600.000 SEN cells, in triplicate. TruSeq Small RNA Library PrepKit v2 (Illumina; RS-200-0012/24/36/48) was used for library preparation according to the manufacturer's indications. Briefly, 35 ng purified RNA was linked to RNA 3′ and 5′ adapters, converted to cDNA, and amplified using Illumina primers containing unique indexes for each sample. Each library was quantified using Agilent Bioanalyzer and High Sensitivity DNA Kit (cat. no. 5067-4626, Agilent Technologies, USA) and equal amounts of libraries were pooled together. Size selection allowed keeping 130–160 bp fragments. After ethanol precipitation, the library pool was quantified with Agilent High Sensitivity DNA Kit, diluted to 1.8 pM and sequenced using NextSeq® 500/550 High Output Kit v2 (75 cycles) (Illumina; FC-404-2005) on the Illumina NextSeq500 platform.

Raw base-call data generated by the Illumina NextSeq 500 system were demultiplexed using Illumina BaseSpace Sequence Hub (https://basespace.illumina.com/home/index) and converted to FASTQ format. After a quality check with FastQC (https://www.bioinformatics.babraham.ac.uk/projects/fastqc/), the adapter sequences were trimmed using Cutadapt (http://cutadapt.readthedocs.io/en/stable/index.html), which also removed sequences < 10 nucleotides. Reads were mapped using the STAR algorithm (https://www.ncbi.nlm.nih.gov/pubmed/23104886). The reference genome consisted of human miRNA sequences from the miRbase 21 database [45]. Raw counts from mapped reads were obtained using the htseq-count script from the HTSeq tools (http://www-huber.embl.de/HTSeq/doc/overview.html).

Raw counts were further normalised using DESeq2 bioconductor package (http://bioconductor.org/packages/release/bioc/html/DESeq2.html). NGS raw data are available through European Nucleotide Archive (http://www.ebi.ac.uk/) under accession number PRJEB33703.

MiRNAs expressed in SEN cells and their EVs were identified to obtain a normalised expression above the 40th percentile in at least one sample of the group.

Statistical analysis of NGS data

NGS data were analysed using Genespring GX software v14.8 (Agilent Technologies). The miRNAs showing a differential expression were identified by comparing SEN and CON cells using a fold change ≥ 1.5 filter and FDR 5% at moderated *t*-test with Benjamini-Hochberg correction. A fold change ≥ 1.3 with FDR 20% or 30% was used in lEV and sEV analysis, respectively. Cluster analysis was performed using GeneSpring GX software with Manhattan correlation as a similarity measure.

Quantitative PCR of mature miRNAs

MiRNA expression was measured by qPCR using the TaqMan miRNA assay (Catalogue #4427012 Thermo Fisher Scientific) as previously described [46].

Methylome analysis of loci coding for SA miRNAs

The sequences and genomic coordinates (GRCh38) of predicted hairpin precursor miRNAs were retrieved from miRbase 21 (Supplementary Table 7). The CpG nucleotide clusters (CpG islands) associated with miRNA genes within a distance of 2 kb were identified by visual inspection of the miRNA gene neighbourhood using the University of California Santa Cruz (UCSC) Genome Browser. Putative proximal promoter regions within 2 kb of the TSS were obtained from the database http://bicresources.jcbose.ac.in/zhumur/pirnaquest/.

Computational prediction of SA miRNA targets

To gain further insights into the relationship between SA miRNAs and the DNA methylation pattern of SEN cells, we explored the ability of SA miRNAs to target DNMT1 and/or SIRT1 using the StarBase v3.0 public platform (http://starbase.sysu.edu.cn) [47]. TargetScan, starBase and miRTarBase were used to predict potential miRNA-DNMT1/SIRT1 interactions. DIANA-mirPath v3 and Ingenuity Pathway Analysis (IPA) were used to identify the pathways targeted by SA miRNAs.

Uptake of sevs released from SEN HUVECs

An amount of 2×10^{11} sEVs has been collected from 6′000′000 of SEN HUVECs. sEVs released from SEN HUVECs were fluorescently labelled using PKH67 membrane dye (Sigma-Aldrich). Labelled sEVs were washed in 10 ml PBS, collected by ultracentrifugation and resuspended in PBS. Next, 10^9 sEVs were incubated with 5×10^4 recipient CON HUVECs for 4, 12, 18 and 24 h. An incubation time of 18 h was established to be optimal for sEV uptake by CON cells. Then, 10^9 sEVs released from SEN cells were incubated with 5×10^4 recipient CON HUVECs.

CON HUVECs were also treated for 18 h with sEVs transfected with miR-217 and miR-21-5p inhibitors (respectively, MH12774 and MH10206, Thermo Fisher Scientific). The transfection process was promoted by Exo-Fect kit (System Bio, USA) according to the manufacturer's recommendations. Briefly, sEVs were prepared for transfection by combining Exo-Fect solution, miRNA inhibitors, PBS and purified sEVs. The transfection solution was incubated at 37°C for 10 min and then put on ice. To stop the reaction, the EXoQuick-TC reagent supplied in the kit was added. After centrifuging for 3 min at 140,000 rpm, the supernatant was removed. The transfected sEVs pellet was suspended in 300 µl PBS and 150 µl of transfected sEVs were added to each well. The same method was used to load non-human cel-mir-39 into sEVs to assess the possibility of delivering miRNAs and their inhibitors through sEVs.

Assessment of the effects induced by SEN sEVs on CON cells

Immunofluorescence and western blot analysis of SIRT1 and DNMT1

CON HUVECs were seeded in BD Falcon chamber slides (cat. no. 354104; Falcon, USA) and treated with SEN sEVs and SEN sEVs transfected with miR-217 and miR-21-5p inhibitors as described above. Cells were washed twice with PBS and then fixed in 4% paraformaldehyde in PBS for 15 min at room temperature. After three washes in PBS they were incubated with 0.3% Triton X-100 in 2.5% bovine serum albumin (BSA) for 1 h at room temperature and then with KI67 antibody (dilution 1:150; Dako, Denmark), in 2.5% BSA overnight at 4°C. Cells were washed in PBS and incubated with secondary anti-rabbit Alexa Fluor 488 antibody (cat. no. 111-545-003, Jackson Laboratories, USA; dilution 1:200), at room temperature in 2% BSA for 1 h. After a wash in PBS, cells were stained with nuclear HOECHST 33,342 (cat. no. H-3570; Molecular Probes, USA) at 1:10,000 dilution in PBS for 5 min, coverslipped with Vectashield mounting medium (H-1200, Vector Laboratories) and viewed in a fluorescence microscope. Omission of the primary antibody resulted in lack of labelling, confirming the specificity of the antibody. The presence of senescence-associated heterochromatin foci (SAHF) was assessed by measuring the coefficient of variation (CV) of the HOECHST staining intensity in each nucleus. At least 200 nuclei have been assessed for each condition and each replicate using the using the CellProfiler image analysis software, version 3.1.9 [48].

The Ki67 proliferative index was expressed as a percentage based on the number of Ki67-positive cells.

Expression levels of PCNA and cyclins A, B1, D1

OneScript® cDNA Synthesis Kit was used to reverse-transcribe 1 µg of purified RNA according to the manufacturer's instructions. qPCR reactions were conducted on the Rotor Gene Q 5plex HRM apparatus in a 10 µl total reaction volume using TB Green Premix Ex Taq II (Clontech Laboratories) according to the manufacturer's recommendations. Each reaction was run in triplicate and included no-template controls. The mRNA expression of the genes of interest was calculated using *GAPDH* as the reference gene.

Relative mRNA levels were calculated with the $2^{-\Delta Ct}$ method. Relative expression values were reported as mean ± SD of three independent experiments.

Primer sequences (written 5′-3′) were: PCNA, Fw: CGGATACCTTGGCGCTAGTA, Rv: CACAGCTGT ACTCCTGTTCTGG; Cyclin D1, Fw: CCCTCGGT GTCCTACTTCAA, Rv: AGGAAGCGGTCCAGGTAG TT; Cyclin A, Fw: TTGAAGAAATATACCCCCCAG, Rv: AATGATTCAGGCCAGCTTTG; Cyclin B1, Fw: TTGGTGTCACTGCCATGTTT, Rv: TAAGCAAAAA GCTCCTGCTG.

Annexin V assay

Apoptosis was evaluated by annexin V staining followed by flow cytometry. Briefly, CON cells and CON cells treated with 10^9 SEN sEVs were plated in a 12-well plate at a density of 2×10^5 cells/well. Apoptosis was evaluated by staining cells with Annexin V and 7-AAD followed by fluorescence flow cytometry as described in Giuliani et al. [46]. The results were expressed as percentage of apoptotic cells out of total live cells.

Methylation status of MIR21 locus

Quantitative analysis of DNA methylation of the *MIR21* TSS200 region was performed using the EpiTYPER assay (Agena). Briefly, genomic DNA was bisulphite converted and the region chr17:57,918,197-57,918,709 (GRCh37/hg19 assembly) was amplified using the following primers: Fwd: aggaagagagTTTATATAAGTGAAAGGATATTGG AGAGA; Rev: cagtaatacgactcactatagggagaaggctAAATAC CAAAATATCAAACAACCCA. PCR products were then processed according to standard EpiTYPER protocol. Each sample was analysed in triplicate.

Plasma samples and EV isolation

Plasma samples were obtained from 12 healthy subjects enrolled for the study. Subjects were considered healthy if they did not present type 1 or 2 diabetes, liver diseases, renal failure, history of cancer, neurodegenerative disorders, infectious or autoimmune diseases. Samples were collected at IRCCS INRCA (Ancona) and at Sant'Orsola University Hospital (Bologna). The procedure was approved by the respective ethics boards (Prot. no. 2006061707, amended on 08/11/2011). Written informed consent was collected from all participants. EVs were purified from 500 µl of plasma by qEVoriginal column (IZON, USA) according to the manufacturer's indications.

Statistical analysis

Principal component analysis (PCA) with varimax orthogonal rotation and Kaiser normalisation was performed to investigate possible common trends in the miRNAs contained in circulating EVs. Only miRNAs that were detected in at least one subject were included in the analysis. Scree plots and the Kaiser-Meyer-Olkin (KMO) test were applied to evaluate the suitability of the correlation matrix. Anti-image-correlation was assumed as adequate for KMO > 0.5. The number of factors to be retained was determined by examining the scree plots. Each retained factor was assigned a score, determined as the linear combination of each miRNA weighted by its respective PCA loading. Factor scores were tested for normality using the Shapiro-Wilk test and compared by one-way ANOVA followed by Tukey's multiple comparison test for pairwise comparisons. p values < 0.05 were deemed significant.

Results

Characterisation of the senescence status of HUVECs

HUVEC senescence was characterised by analysing a number of well-established senescence biomarkers in non-senescent (control, CON) and senescent (SEN) HUVECs.

Compared with CON cells, SEN cells were characterised by growth arrest, which was documented by reduced cumulative population doublings (cPDs) (Figure 1(a)), progressive telomere shortening (Figure 1(b)), increased SA β-gal activity (Figure 1(c)), up-regulation of the cell cycle regulator p16 (INK4a) both at the transcriptional and the protein level (Figure 1(d,d')); up-regulation of phospho-histone H2AX (pH2AX), a biomarker of persistent DNA damage [49] (Figure 1(e)) and significantly increased mRNA transcription of the pro-inflammatory SASP components interleukin (IL)-1β, IL-6 and IL-8 (Figure 1(f–h)). A similar model of replicative senescence was replicated also in HAECs. Moreover, we established a model of drug-induced senescence by treating HUVECs and HAECs with 50 nM doxorubicin for 24 h. The characterisation of these additional models is reported in Supplementary Figure 1.

Human cell senescence is also marked by progressive, widespread genomic hypomethylation and focal hypermethylation at specific CpG sites [50]. Further characterisation and comparison of the epigenetic profile of SEN and CON cells demonstrated a differential methylation state at 335′495 CpG sites; in particular,

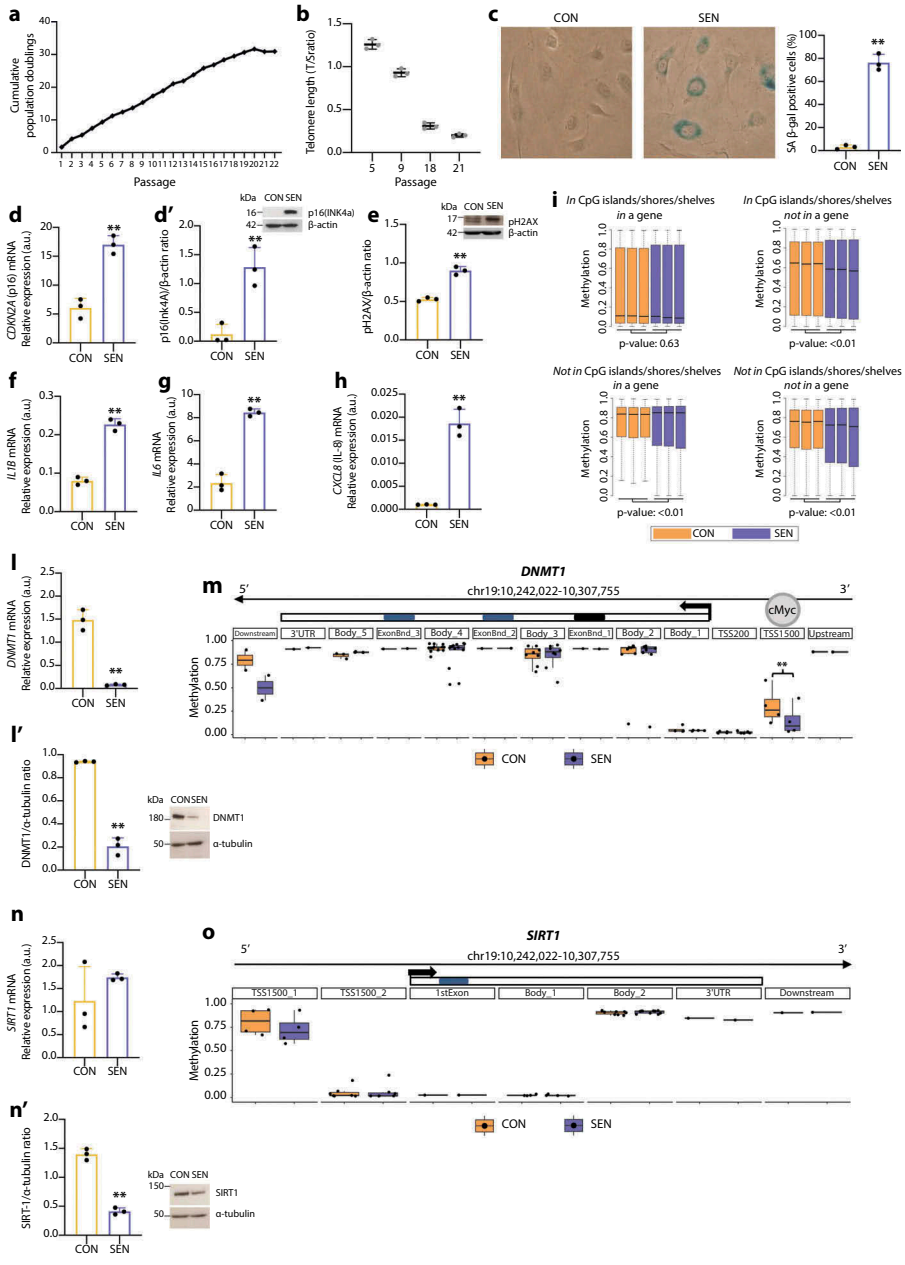

Figure 1. Characterisation of replicative senescence in human umbilical vein endothelial cells (HUVECs). (a) Cumulative population doubling (cPD) curves. (b) Telomere/single copy gene ratio (T/S) in DNA from HUVECs at different passages. (c) Representative positivity and quantification of the SA β-Gal staining in control (CON, < 10%) and senescent (SEN, > 60%) cells. (d) mRNA relative expression. (d') Western blot and densitometric analysis of p16(Ink4a) in CON and SEN cells. Protein expression values are reported as p16(Ink4)/β-actin ratio. (e) Western blot and densitometric analysis phospho-histone H2AX (pH2AX) in CON and SEN cells. Protein expression values are reported as pH2AX/β-actin ratio. (f) mRNA relative expression of interleukin (IL)-1β, (g) IL-6, (h) IL-8. (i) Boxplots of DNA methylation values of InfiniumEPIC probes in CON and SEN triplicates. The probes were divided in four groups according to their genomic location and *t*-test was applied to each group in order to compare mean beta values between CON and SEN. (l) mRNA relative expression. (l') Western blot and densitometric analysis of DNMT1 in CON and SEN cells. Protein expression values are reported as DNMT1/α-tubulin ratio. (m) Methylation status of CpGs among a genomic region covering the DNMT1 gene ± 2kb. The region is split in multiple windows based on Illumina Infinium annotation assigned to each CpG as reported in the Methods section. Methylation status of each window is represented with a boxplot. Each dot corresponds to the mean B value of an annotated CpG across the three replicates. Blue: SEN cells; Orange: CON cells. **, *q*-val < 0.01. Scale of the Methylation status corresponds to the B value. (n) mRNA relative expression. (n') Western blot and densitometric analysis of SIRT1 in CON and SEN cells. Protein expression values are reported as SIRT1/α-tubulin ratio. (**o**) Methylation status of CpGs among a genomic region covering the SIRT1 gene ± 2kb. The region is split in multiple windows based on Illumina Infinium annotation assigned to each CpG as reported in the Methods section. Methylation status of each window is represented with a boxplot. Each dot corresponds to an annotated CpG. Methylation status expressed in B value. Blue: SEN cells; Orange: CON cells. **, *q*-val < 0.01. For qPCR and western blot analysis data from three independent experiments are represented as mean ± SD. **, $p < 0.01$ from paired *t*-tests.

SEN cells showed significant hypomethylation in CpG island/shore/shelf regions located in intergenic regions and significant hypermethylation of non-CpG sites inside genes (Figure 1(i)).

Since DNMT1 and SIRT1 co-operate in maintaining the methylation pattern [15], we analysed their mRNA and protein levels and the methylation state of their loci in SEN and CON cells. We found that DNMT1 mRNA and protein levels were down-regulated in SEN cells (Figure 1(l,l')), even though methylation analysis disclosed significant loss of methylation at the *DNMT1* transcription start site (TSS)-1500 promoter region, which according to the ENCODE ChIP-Seq data binds the transcription factor c-MYC (Figure 1(m)). SIRT1 mRNA levels were similar in CON and SEN cells (Figure 1(n)); in contrast, the SIRT1 protein level was significantly reduced in SEN compared with CON cells (Figure 1(n')), despite the similar methylation state of SEN and CON cells (Figure 1(o)). These data suggest that during HUVEC replicative senescence DNMT1 and SIRT1 protein levels are modulated by post-transcriptional regulatory mechanisms.

Analysis of the senescence biomarkers confirmed that HUVECs aged in culture exhibit a senescent phenotype characterised by most of the established hallmarks of ageing [51]. This model can, therefore, be considered as an archetypal "*in vitro* model" of cellular senescence.

Senescent HUVECs release more sEVs than control cells

We characterised the structure and content of EVs released from SEN and CON cells according to Minimal Information for Studies of Extracellular Vesicles guidelines, which were proposed by the International Society for Extracellular Vesicles (ISEV) in 2018 [43]. Scanning electron micrograph analysis of EVs released from SEN and CON cells demonstrated a significantly greater number of vesicular bodies emerging from the cell surface of SEN cells (Figure 2(a,b)). To purify these small (sEVs) and large (lEVs) EV fractions, sEVs and lEVs were collected after ultracentrifugation and further characterised by Nanoparticle Tracking Analysis (NTA), transmission electron microscopy (TEM) and western blot analysis of some relevant biomarkers. Representative distribution plots of sEVs and lEVs released from CON (Figure 2(c,d)) and SEN cells (Figure 2(c',d')) indicated that sEVs and lEVs had a different size distribution. Representative TEM images of sEVs and lEVs purified from CON and SEN (Figure 2(e)) confirm their different size. Analysis of calnexin, TSG101 and CD63 membrane protein expression by western blotting demonstrated the efficient separation of supernatant-derived EV sub-populations: sEVs were positive for the exosomal markers CD63 and TSG101, whereas lEVs were positive for the endoplasmic reticulum marker calnexin (Figure 2(e')). Comparison of their number demonstrated that SEN and CON cells released more sEVs than lEVs. Moreover, NTA assay revealed that SEN cells released a threefold, significantly greater amount of sEVs (*t*-test for unpaired samples, $p < 0.01$) but a similar number of lEVs (Figure 2(f)) compared with CON cells. Notably, the size of sEVs and lEVs released from either cell type was not significantly different (Figure 2(g)). The increased release of sEVs from SEN cells was confirmed also in HUVECs undergoing drug-induced senescence following treatment with doxorubicin, and in HAECs undergoing both replicative and drug-induced senescence (Supplementary Figure 1d and 1d').

To further substantiate these data, multi-vesicular bodies (MVBs), a specialised subset of endosomes that contain sEVs, were identified and quantified in TEM images of SEN and CON HUVECs (Figure 2(h)). A significantly greater number of MVBs at different stages of maturation was detected in SEN compared to CON cells (*t*-test for unpaired samples, $p < 0.01$) (Figure 2(i)).

MiRNome analysis of CON and SEN HUVECs and their cognate EVs

The expression of the whole miRNome was analysed in triplicate in SEN and CON cells and cognate lEVs and sEVs from different pools of donors. The list of all miRNAs thus detected is reported in Supplementary Table 1. The miRNAs showing a significant differential expression in sEVs and lEVs released from SEN cells and in SEN compared with CON cells are listed in Figure 3(a–c), respectively. The miRNAs showing a differential expression in sEVs, lEVs and their parental SEN cells, the relevant fold changes, Benjamini-Hochberg adjusted *p* values and the normalised expression in SEN and CON are reported in Supplementary Tables 2–4. The miRNAs showing a differential expression were used to cluster miRNAs and samples. The resulting heatmaps – of the miRNAs showing significant de-regulation in sEVs released from SEN cells, of the miRNAs showing significant de-regulation in lEVs released from SEN cells, and of the miRNAs showing significant de-regulation in SEN cells – are reported in Supplementary Figure 2a, 2b and 2c, respectively. Supplementary Tables 5 and 6 report miRNAs showing differential expression between SEN cells and their cognate sEVs and lEVs, respectively. As previously

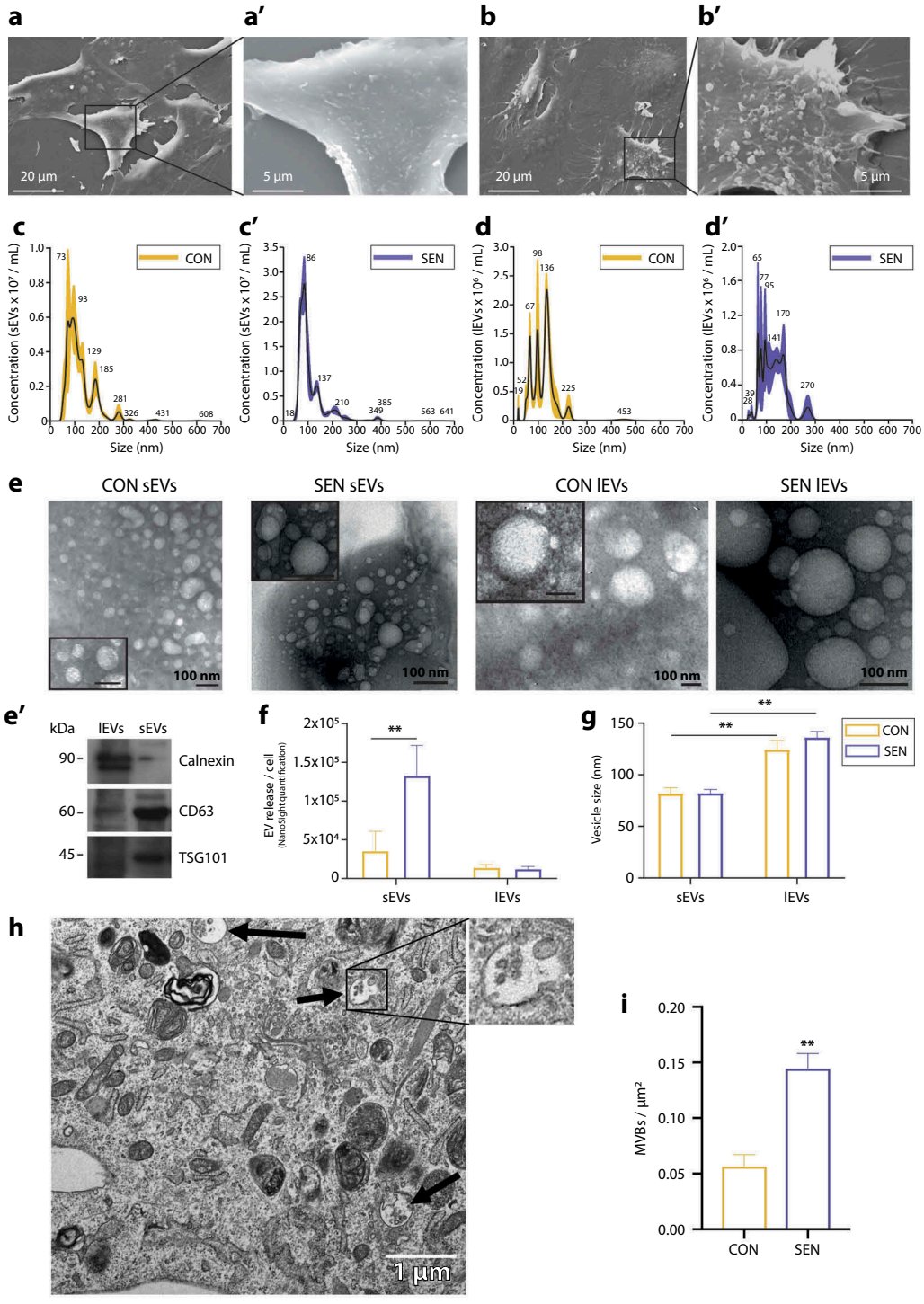

Figure 2. Characterisation of sEVs and lEVs released from CON and SEN cells. (a,a') SEM analysis of extracellular vesicles emerging from the CON cell plasmalemma. (b,b') SEM analysis of extracellular vesicles emerging from the SEN cell plasmalemma. Scale bars of 20 and 5 µm are applied for low and high magnification, respectively. (c) Average size distribution curve of sEVs released from (c) CON and (c') SEN cells. (d) Average size distribution curve of lEVs released from (d) CON and (d') SEN cells. EVs size was determined by NTA Nanoparticle Tracking Assay (NTA). Three 60 s videos were recorded for each sample, and NTA analysis settings kept constant between samples. The average concentration of vesicles was plotted against their size, with the black lines and the colour areas representing the fitting curve and the error bar, respectively. (e) Representative TEM analysis of sEVs and lEVs released into the culture media by CON and SEN cells with a scale bar of 100 nm. (e') Representative western blot analysis of calnexin, TSG101 and CD63 in isolated lEVs and sEVs. (f) Comparison of the number of sEVs and lEVs released per cell in CON and SEN cells as determined by NTA. (g) Comparison of the size of sEVs and lEVs released from CON and SEN cells as determined by NTA. Data from three independent experiments are represented as mean ± SD. **, $p < 0.01$ from paired *t*-tests. (h) Representative TEM photomicrograph of multi-vesicular bodies (MVBs) of SEN cells with a scale bar of 1 µm. (i) Comparison of the number of MVBs per µm^2 measured in $n = 24$ TEM images of CON and SEN cells. Data are represented as mean ± SD. **, $p < 0.01$ from unpaired *t*-test.

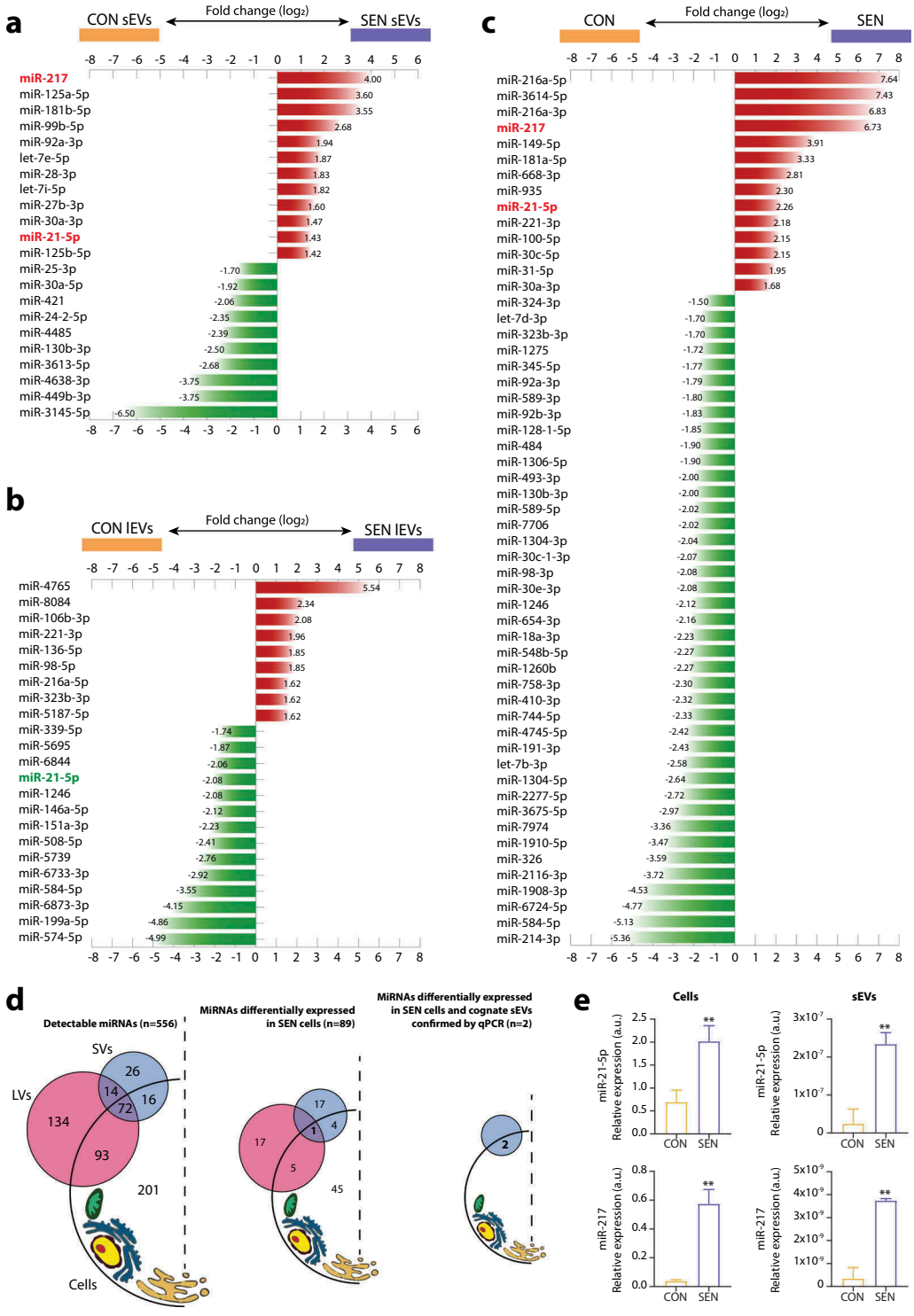

Figure 3. MiRNAs showing differential expression in SEN cells and cognate sEVs and lEVs. Bar charts reporting the (log_2) fold changes of the miRNAs showing a differential expression (a) in sEVs released from SEN cells, (b) in lEVs released from SEN cells and (c) in SEN cells. The miRNA de-regulation trend is indicated by bar colour; red, over-expression; green, under-expression in SEN sEVs/SEN lEVs/SEN cells compared with CON sEVs/CON lEVs/CON cells, respectively. Only miR-21-5p (highlighted in red) showed significant SA de-regulation in SEN cells and cognate sEVs and lEVs. Data from small RNAseq of $n = 3$ independent replicates for each condition. MiRNAs showing a differential expression were identified by comparing SEN and CON cells using a fold change ≥ 1.5 filter and FDR 5% at moderated *t*-test with Benjamini-Hochberg correction. A fold change ≥ 1.3 with FDR 20% or 30% was used in lEV and sEV analysis, respectively. (d) Summary of the results of small RNAseq analysis on CON and SEN cells and cognate sEVs and lEVs. Briefly, 556 miRNAs were detected in at least one compartment (cells, sEVs and lEVs). Of the 355 miRNAs carried by EVs, only 42 (12%) were selectively packaged in sEVs; 86 (24%) were carried by both lEVs and sEVs and 227 (64%) were found only in lEVs. None of the miRNAs shared a common SA modulation trend in lEVs and sEVs. Only miR-21-5p was significantly de-regulated in both sEVs and lEVs released from SEN cells; however, it was over-expressed in sEVs and under-expressed in lEVs from the same SEN cell pool. (e) qPCR validation analysis of miR-21-5p and miR-217 in different pools of SEN cells and their cognate sEVs. Data from $n = 3$ independent experiments are represented as mean ± SD. **, $p < 0.01$ from unpaired *t*-test.

Table 1. MiRNAs commonly de-regulated in SEN cells and their EVs.

				CON normalised expression (log2)			SEN normalised expression (log2)		
miRNA	Cells	sEVs	lEVs	Cells	sEVs	lEVs	Cells	sEVs	lEVs
hsa-miR-21-5p	**+**	**+**	-	9.70	4.78	5.03	11.60	7.33	4.40
hsa-miR-217	**+**	**+**		5.88	2.11	0.95	9.38	5.47	0.31
hsa-miR-30a-3p	+	+		4.13	0.00	0.00	4.89	0.56	0.40
hsa-miR-130b-3p	-	-		7.05	1.82	1.11	6.06	0.50	0.82
hsa-miR-92a-3p	-	+		11.19	2.44	4.56	10.35	3.40	4.70
hsa-miR-221-3p	+		+	8.76	3.64	3.19	9.89	3.20	1.17
hsa-miR-216a-5p	+		+	2.09	0.98	0.00	5.02	0.07	0.70
hsa-miR-323b-3p	-		+	3.68	0.00	0.00	2.92	0.00	0.70
hsa-miR-584-5p	-		-	7.99	1.18	2.32	5.63	0.00	0.49
hsa-miR-1246	-		-	2.41	0.00	1.06	1.33	0.00	0.00

For each miRNA and condition, the log2 normalised expression values are reported for cells, sEVs, and lEVs. The reader is referred to Supplementary Tables 2–6 for detailed data on miRNAs differentially regulated across the various sample types. sEVs, small extracellular vesicles; lEVs, large extracellular vesicles; (+) over-expressed; (-) under-expressed.

reported [52], the levels of miRNAs loaded onto EVs are significantly lower compared to their parent cells.

Overall, 22 miRNAs were differentially expressed in sEVs released from SEN cells; of these, 12 (55%) were up-regulated and 10 (45%) were down-regulated (Figure 3(a)). Of the 55 miRNAs that were significantly modulated in SEN compared with CON cells 14 were up-regulated (25%) and 41 (75%) were down-regulated (Figure 3(c)). Only five miRNAs – miR-21-5p, miR-217, miR-30a-3p, miR-130b-3p and miR-92a-3p – were differentially expressed in sEVs and parental SEN cells (Table 1 and Figure 3(d)). Their analysis in a different batch of cells from a different pool of donors confirmed these findings. qPCR analysis confirmed the NGS data for miR-21-5p and miR-217 in cells and their sEVs (Figure 3(e)), whereas no differential expression was detected for miR-30a-3p, -92a-3p and -130b-3p (data not shown). The up-regulation of miR-21-5p and miR-217 in SEN cells and their cognate sEVs was confirmed also in HAECs undergoing replicative senescence, as well as in the model of drug-induced senescence established in both HUVECs and HAECs (Supplementary Figure 1(e,f,e',f')).

The results of miRNome analysis of SEN cells and cognate sEVs and lEVs are summarised in Figure 3(d).

miRNAs capable of targeting DNMT1 and SIRT1 and showing a differential expression in SEN cells and cognate EVs

To unravel the complex interaction between miRNA expression and methylation state in cells with the senescent phenotype we tried to establish which miRNAs capable of targeting DNMT1 and SIRT1 were significantly de-regulated in SEN cells and cognate EVs. Of the 12 miRNAs that were up-regulated in SEN sEVs, 4 – including miR-21-5p and miR-217 (Figure 4(a)) – were capable of targeting DNMT1 and/or SIRT1, whereas none of the nine miRNAs up-regulated in SEN lEVs were able to target DNMT1 and/or SIRT1 (Figure 4(b)). Five of the 14 miRNAs showing up-regulation in SEN cells were able to target DNMT1 and/or SIRT1; of them, only miR-21-5p and miR-217 were also up-regulated in SEN sEVs (Figure 4(c)).

Surprisingly, SEN lEVs carried no up-regulated SA miRNAs targeting DNMT1 and/or SIRT1.

Altogether, these data suggest that miR-21-5p and miR-217 are the only miRNAs shuttled by SEN sEVs that are also expressed in SEN cells and are capable of targeting DNMT1 and SIRT1. This observation, coupled with the finding that SEN cells released three times more sEVs than CON cells, prompted further investigation on the effects of SEN sEVs on CON cells.

Methylation state of the loci coding for miRNAs showing differential expression in SEN and CON cells

To clarify whether miRNA expression in SEN cells was epigenetically regulated, we analysed the methylation state of the genetic loci encoding the miRNAs showing differential expression in SEN and CON cells. The genomic locations and sequences of the miRNAs showing significant down- or up-regulation in SEN cells are reported in Supplementary Table 5.

The methylation state was obtained by conducting a global methylation analysis, assessing CpG site methylation within 2000 bp upstream and downstream of each miRNA transcription start site (TSS).

The methylation changes observed at the loci encoding the 55 miRNAs showing significant de-regulation in SEN cells are reported in Figure 5(a). Principal component analysis (PCA) revealed significantly different methylation profiles of the miRNA genes that were differentially expressed in SEN compared with CON cells (Figure 5(b)); however, only about 50% showed SA methylation consistent with

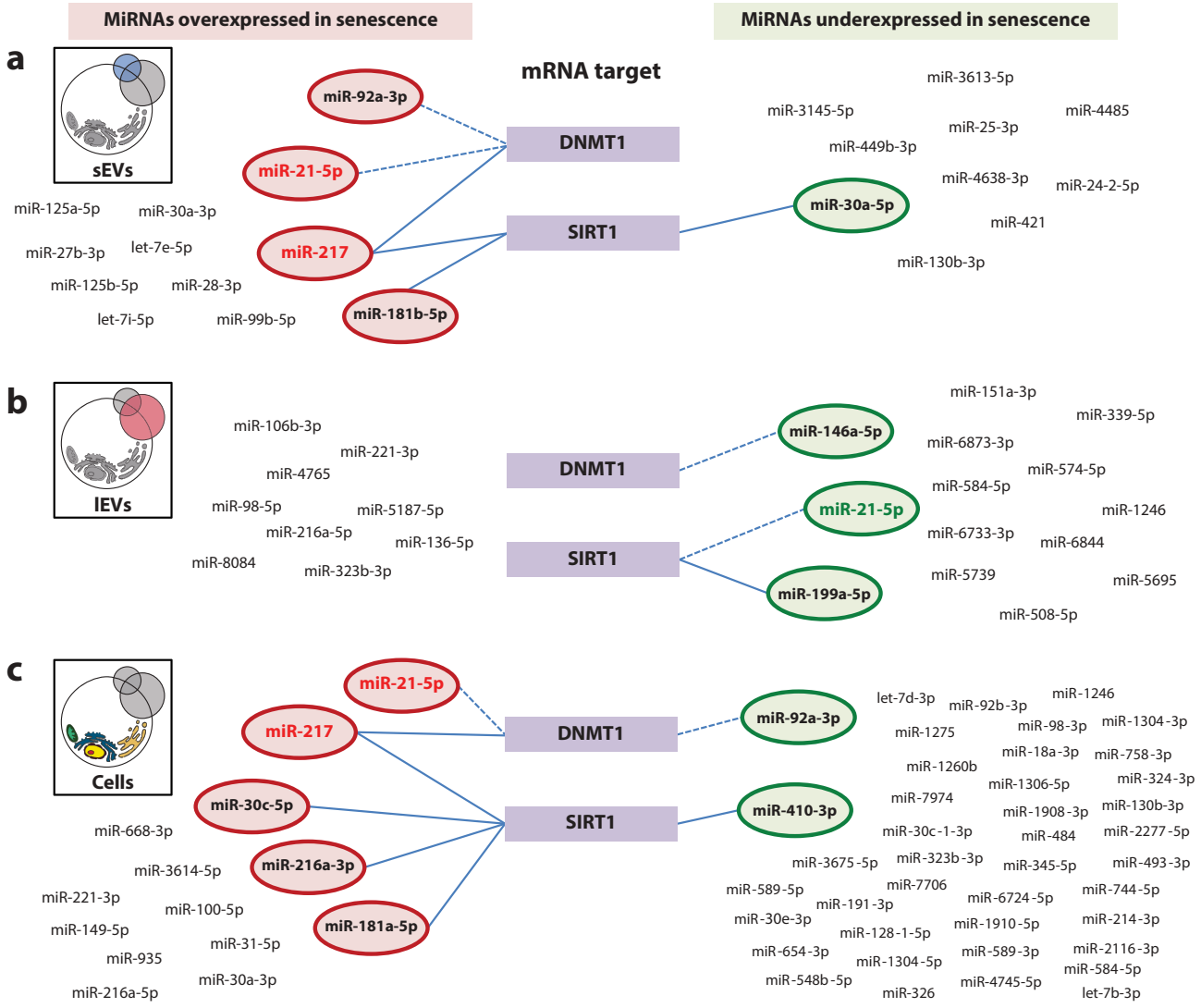

Figure 4. MiRNAs showing differential expression in SEN cells and their cognate sEVs and lEVs targeting DNMT1 and/or SIRT1. (a) MiRNAs showing over and under-expression in SEN sEVs compared with CON sEVs, (b) in SEN lEVs compared with CON lEVs, (c) and in SEN compared with CON cells targeting DNMT1 and/or SIRT1. Straight lines represent miRNA-mRNA interaction based on bioinformatic prediction from three different algorithms. Dotted lines represent miRNAs reducing DNMT1 activity by binding to its catalytic site, according to the report from Zhang et al. [54].

SA expression changes (Figure 5(c)). Of the miRNAs that exhibited differential methylation in SEN and CON cells, only miR-21-5p showed concordant DNA demethylation and RNA over-expression both in SEN cells and SEN sEVs (Figure 5(c)). The methylation state of miR-217 was not evaluated, because no CpG in the neighbourhood of its locus was covered by genome-wide methylome analysis.

Overall, in half of the loci encoding the miRNAs showing differential expression in SEN cells, the gene methylation and expression data were not consistent, suggesting that additional post-transcriptional regulation mechanisms are involved in the modulation of SA miRNAs. These data support the hypothesis of a complex interaction among different epigenetic mechanisms in inducing and maintaining a senescent phenotype.

SEN sEVs significantly reduce CON cell DNMT1 and SIRT1 levels and proliferation markers

Previous work has shown that miR-21-5p directly targets SIRT1 and indirectly down-regulates DNMT1 by targeting the *RASGRP1* gene, an upstream component of the Ras-MAPK pathway that regulates DNMT1 expression [53]. MiR-21-5p has also been demonstrated to inhibit DNMT1 activity by binding to its catalytic site [54]. As regards miR-217, it directly

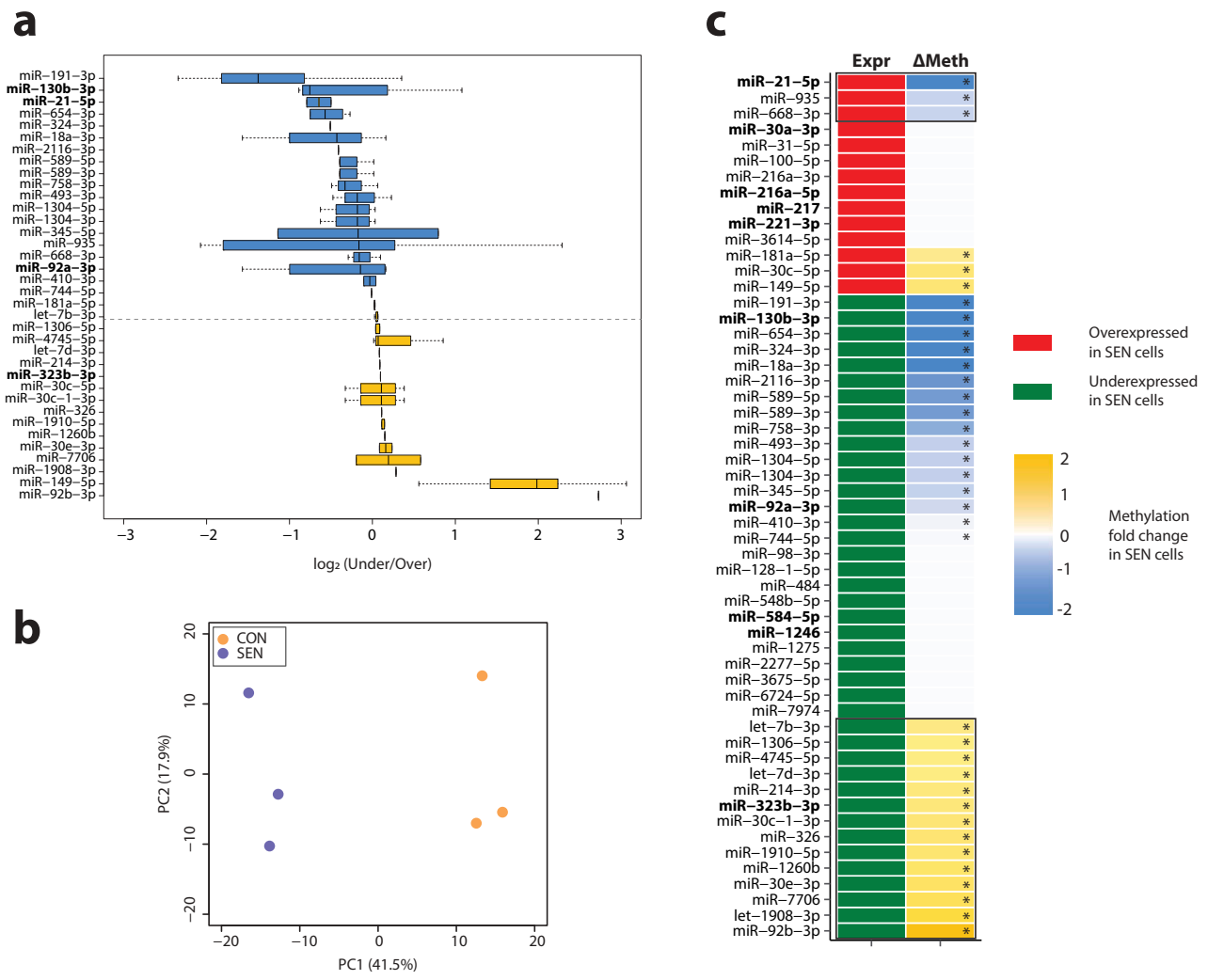

Figure 5. Methylation state of the loci encoding miRNAs showing a differential expression in SEN compared with CON cells. (a) Box plots showing the log2 B value fold change in SEN vs CON cells at CpG loci located within the coding regions of selected miRNA. Yellow: over-methylated CpG sites (median value); Blue: under-methylated CpG sites (median value). (b) PCA of DNA methylation values in CON and SEN triplicates, considering only the InfiniumEPIC probes mapping within 2000 bp upstream and downstream the miRNAs differentially expressed in SEN vs CON. The percentage of variance explained by the first and the second principal components is reported in brackets. (c) Figure summarising expression levels and methylation state of miRNAs showing a differential expression in SEN cells. MiRNAs showing expression concordant with the methylation state are enclosed in black lines. MiRNAs commonly de-regulated in SEN cells and their cognate sEVs and lEVs are highlighted in bold. Significantly methylated or unmethylated miRNAs are marked with (*).

targets DNMT1 in fibroblasts [55] and SIRT1 in endothelial cells [56].

Based on these findings, we assessed the functional potential of sEVs released from SEN cells to modulate DNMT1 and/or SIRT1 in CON cells. To do this, CON cells were treated with sEVs released from SEN cells. Their uptake was demonstrated by tracking sEVs with a fluorescent, membrane-permeable dye (Figure 6(a)). The possibility of delivering small RNAs through sEVs was further tested by loading non-human cel-miR-39 onto sEVs released from SEN cells. The latter treatment resulted in qPCR-detectable levels of cel-miR-39 in CON cells, confirming the delivery of a considerable amount of cargo in this setting (Figure 6(b)). Treatment of CON cells with sEVs from SEN cells resulted in a significantly increased expression of miR-21-5p and miR-217 (Figure 6(c)). To evaluate whether this observation was related to the intracellular delivery of the copies of miR-21-5p and miR-217 loaded onto SEN sEVs or to the induction of the transcription of the two miRNAs in the recipient cells, we assessed the levels of pri-miR-21 using SEN cells as a positive control. Treatment of CON cells with SEN sEVs was not able to induce the up-regulation of pri-miR-21 (Figure 6(d)).

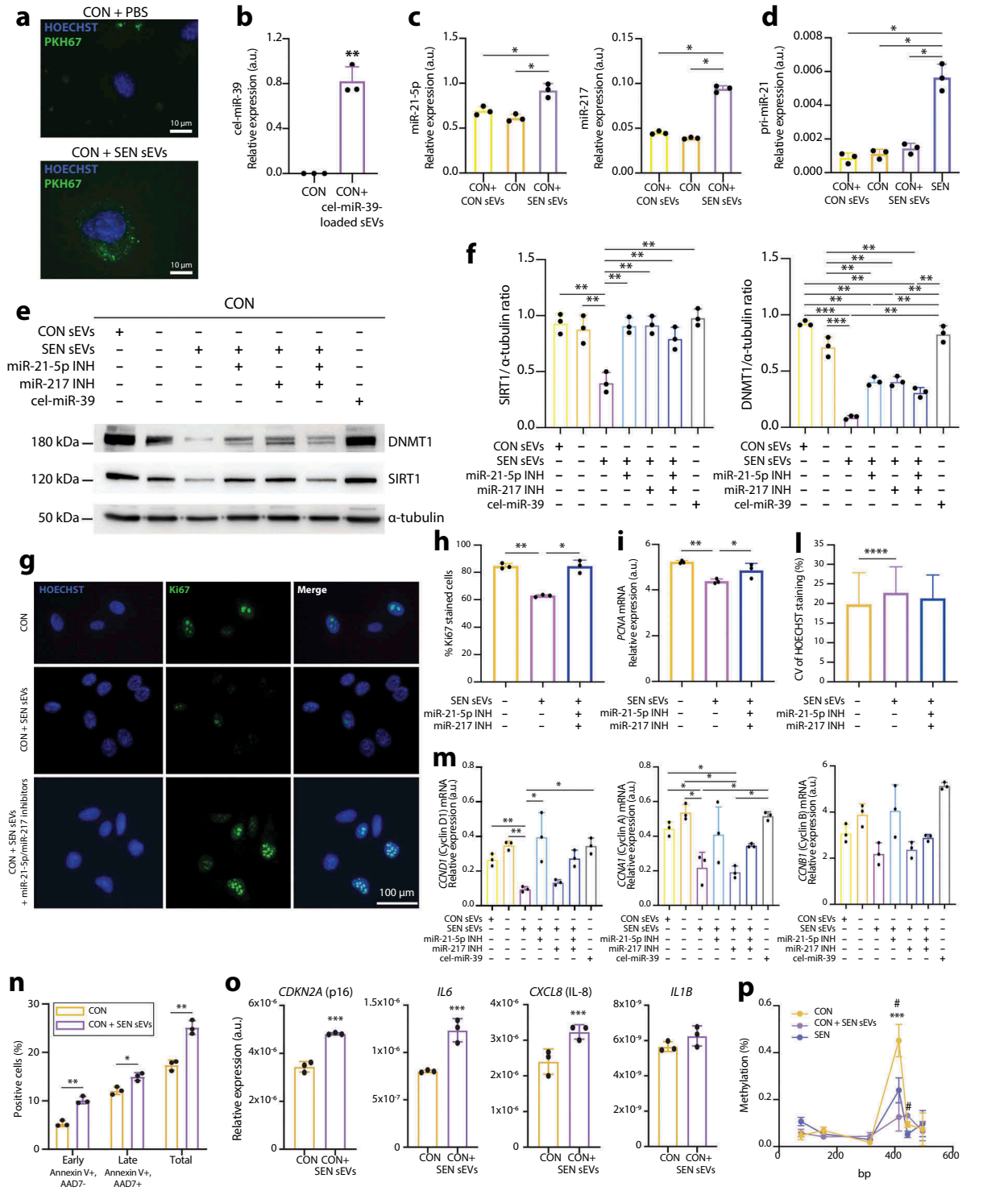

Figure 6. Modulation of DNMT1/SIRT1 and of replicative rate biomarkers induced in CON cells by treatment with sEVs released from SEN cells. (a) Immunofluorescence staining showing effective uptake in CON of sEVs released from SEN cells. sEVs were labelled with PKH67 green fluorescent dye. Scale bars of 10 µm are applied. (b) qPCR analysis of cel-miR-39 in CON cells treated with sEVs loaded with cel-miR-39. (c) qPCR analysis of miR-21-5p and miR-217 in CON cells treated with sEVs from SEN and with sEVs from CON. (d) qPCR analysis of pri-miR-21 in CON cells treated with sEVs from SEN and with sEVs from CON, and in SEN cells. (e) Western blots showing modulation of DNMT1 and SIRT1 protein levels in CON cells treated with sEVs released from SEN without and with miR-217 and miR-21 inhibitors. CON sEVs and cel-miR-39 were used as negative controls to exclude non-specific effects due to the treatment with sEVs and miRNAs, respectively. (f) Densitometric analysis of SIRT1 and DNMT1 protein level modulation in CON cells treated with sEVs released from SEN without and with miR-217 and miR-21 inhibitors. The effects of sEVs on SIRT1 and DNMT1 appear to be miR-21-5p- and miR-217-dependent. Protein expression values are reported as SIRT1/α-tubulin and SIRT1/α-tubulin ratios. (g) Immunofluorescence Ki67 staining of CON cells CON cells treated with sEVs released from SEN without and with miR-217 and

Treatment of CON cells with SEN sEVs also significantly reduced the expression of DNMT1 and SIRT1 (Figure 6(e,f)). This effect was not reproducible by treating CON cells with CON sEVs and was significantly rescued when SEN sEVs were loaded with miR-21-5p and miR-217 inhibitors, alone or combined (Figure 6(e,f)). This suggests that both miRNAs are involved in DNMT1 and SIRT1 modulation.

A reduction in CON cell replication ability, demonstrated by reduced Ki67 staining, was observed during the 18-h treatment with SEN sEVs (Figure 6(g, h)) and was associated with reduced PCNA (Figure 6 (i)), cyclin D1 and cyclin A (Figure 6(m)) expression. Importantly, the effects of SEN sEV uptake in CON cells appeared to be miR-21-5p-dependent. A trend towards the reduction of cyclin B mRNA was observed in treated CON cells, even if it did not reach statistical significance (Figure 6(m)). Notably, CON cells treated with SEN sEVs showed an increased formation of SAHF, as confirmed by the increased CV of the HOECHST staining intensity. This effect was not rescued by the addition of miR-21-5p/miR-217 inhibitors (Figure 6(l)).

We then performed Annexin V and 7-AAD staining and flow cytometry to quantify the rate of apoptosis in CON cells after treatment with SEN sEVs. As shown in Figure 6(n), the percentage of cells undergoing early (Annexin V+/7-AAD-) and late (Annexin V+/7-AAD +) apoptosis was significantly increased in CON cells treated with SEN sEVs compared with CON cells, demonstrating that SEN sEVs are able to induce apoptosis in CON cells after 18-h treatment.

Next, we evaluated whether treatment with SEN sEVs was capable of inducing a senescent phenotype in CON cells. A significant increase in the expression of p16, IL-6 and IL-8 mRNAs was observed, whereas no significant up-regulation of IL-1β mRNA was reported (Figure 6(o)).

As a final experiment, we assessed the methylation level of *MIR21* locus in CON and SEN cells, and in CON cells treated with SEN sEVs using the quantitative EpiTYPER assay. Treatment of CON cells with SEN sEVs was able to induce a significant demethylation of the fourth CpG site of the amplicon (corresponding to the microarray probe cg02515217, located in the TSS200 region), resulting in methylation levels comparable to those observed in SEN cells (Figure 6(p)).

Overall, SEN sEVs proved capable of modulating apoptosis and a number of key senescence features, i.e. cellular proliferation, SASP acquisition and DNMT1/SIRT1 expression. The effects on proliferation appear to be at least partly miR-21-5p-dependent, whereas those on DNMT1-SIRT1 expression appear to be dependent on miR-21-5p as well as miR-217. The down-regulation of DNMT1 in CON cells treated with SEN sEVs induced a partial demethylation of the *MIR21* locus which, however, was not associated to an increased transcription of miR-21-5p in treated cells.

miRNA profiling in circulating EVs from healthy adults of different ages

The finding that SEN cells can spread pro-senescence signals via miRNAs carried by their sEVs suggested a further experiment, where EVs purified from plasma of 12 healthy adult donors of different ages were subjected to NGS analysis. Donors were grouped into three gender-matched age groups, young (n = 4), elderly (n = 4) and centenarians (n = 4), whose mean age was 50 ± 8 years, 74 ± 9 years and 102 ± 1 year, respectively. The demographic and clinical characteristics of the 12 donors are reported in Supplementary Table 8. There were no age-related differences in the number of sEVs purified from plasma among the groups (p = 0.873, data not shown). Of the 1186 miRNAs detected by the

miR-21 inhibitors. Scale bars of 100 μm are applied. (h) Quantification of Ki67-positive cells. (i) PCNA, (m) cyclin D1, cyclin A, cyclin B1 mRNA relative expression in CON cells treated with sEVs released from SEN cells without and with miR-217 and miR-21 inhibitors. (l) Evaluation of senescence-associated heterochromatin foci (SAHF) based on the calculation of the CV of the HOECHST staining in at least 200 nuclei of CON cells treated with sEVs without and with miR-217 and miR-21 inhibitors. Treatment of CON cells with sEVs released from SEN cells induced significant reduction of proliferation markers and the formation of SAHF. These effects were significantly reduced by treatment with sEVs released from SEN cells loaded with miR-21-5p inhibitor, suggesting that the effects of SEN sEVs on CON cell replication are, at least partly, miR-21-5p-dependent. (n) Assessment of apoptosis rate in CON cells treated with sEVs released from SEN cells. Annexin V+/AAD7- and annexin V+/7AAD + cells were respectively considered to be early- and late-apoptotic cells. (o) p16, IL-6, IL-8, IL-1β mRNA relative expression in CON cells treated with sEVs released from SEN cells. (p) Methylation status of the *MIR21* locus in SEN cells and in CON cells treated with sEVs released from SEN cells. The microarray probe cg02515217 is significantly under-methylated in SEN cells and in CON cells treated with SEN sEVs compared to CON cells. *, CON vs CON + SEN sEVs; #, CON vs SEN. Data from n = 3 independent experiments are represented as mean ± SD. */#, $p < 0.05$; **, $p < 0.01$; ***, $p < 0.001$ from one-way ANOVA followed by Tukey's multiple comparison test for pairwise comparisons.

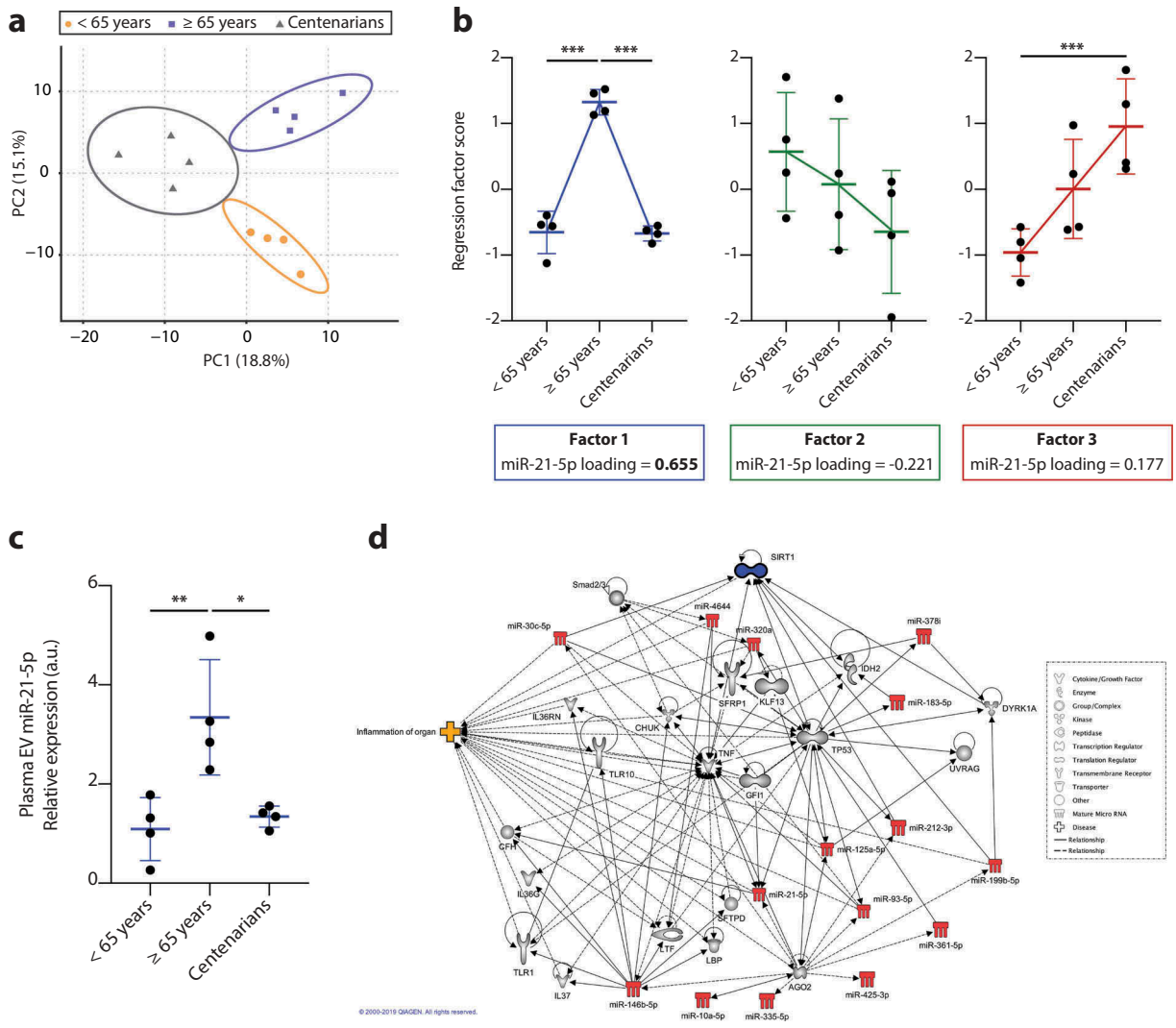

Figure 7. Profiling of miRNAs identified in circulating EVs purified from plasma of healthy adult subjects of different ages. (a) PCA factor analysis with varimax rotation of 360 miRNAs detectable in at least two samples of at least one group of healthy donors. Rotation converged after 11 iterations and yielded 11 components with an eigenvalue > 1.0. Three components explaining more than 45% of the total variance were retained. PC1 and PC2, explaining respectively 18.8% and 15.1% of the total variance, are represented. Circles represent 95% confidence intervals. (b) Line plots showing the estimated marginal means for factors 1, 2 and 3 regression scores across the three age groups (<65 years, ≥65 years and centenarians). (c) qPCR validation of miR-21-5p levels in EVs from healthy donors. Data from four subjects in each age group are displayed as mean ± SD. *, $p < 0.05$; **, $p < 0.01$; ***, $p < 0.001$ from one-way ANOVA followed by Tukey's multiple comparison test for pairwise comparisons. (d) Ingenuity Pathway Analysis (IPA) on miRNAs loading on factor 1 with a score > 0.60 or < −0.60. Association of this dataset with the "diseases and disorders" IPA database revealed a significant enrichment of the subcategory "inflammation of organ".

analysis, 360 were expressed in EVs from at least two subjects in at least one group. These were included in the subsequent analysis. Age-related trends were identified by applying PCA with varimax rotation converging after 11 iterations and yielding 11 components with an eigenvalue > 1.0. Three components explaining more than 45% of the total variance were retained. The PCA plot (Figure 7(a)) indicates that PC1 and PC2 enable clear separation of the miRNA expression profiles of the three groups of subjects, explaining respectively 18.8% and 15.1% of the total variance. The component loading for each miRNA is reported in Supplementary Table 9. Analysis of the factor scores reflecting the weighted level of the miRNAs expressed in the three groups identified an inverted U-shape distribution for factor 1, a slightly declining trend for factor 2 and a rising trend for factor 3 (Figure 7(b)). MiR-21-5p showed a strong loading on factor 1 (loading score = 0.655) (Figure 7(b)), whereas miR-217 was not detected in circulating EVs. We further validated

miR-21-5p levels in plasma EVs from the same subjects by qPCR and confirmed that miR-21-5p levels follow the same age-related inverted U-shaped trend observed for factor 1 (Figure 7(c)).

These data showed that in elderly people circulating EVs are characterised by increased miR-21-5p levels compared with either younger adults and healthy centenarians, suggesting that the EV miR-21-5p content can be a marker of cellular senescence and inflammaging. This finding lends support to our group's earlier report of an inverse U-shaped age-related trend of miR-21-5p purified from total plasma [57].

According to IPA, SIRT1 and miR-21-5p are spokes in a network that includes miRNA loading on factor 1 with a score > 0.60 or < −0.60. *TNF* and *TP53* can be considered as hubs. The association of the miRNAs loaded on factor 1 with the IPA database "diseases and disorders" revealed a significant enrichment of the sub-category "inflammation of organ", confirming the hypothesis that an inverse U-shaped trend reflects high circulating levels of the biomarkers of inflammaging in elderly individuals (Figure 7(d)).

Putative SA loop involving miR-21-5p and miR-217

The main results of the study are reported in Figure 8, which depicts a putative SA loop encompassing miR-21-5p and miR-217. In particular, the miR-21 locus is demethylated in SEN cells, resulting in miR-21-5p over-expression in these cells, which are marked by low levels of DNMT1 and SIRT1. sEVs released from SEN cells are enriched in miR-21-5p and miR-217 and can contribute to reduce DNMT1 and SIRT1 expression in younger recipient cells, promoting demethylation of the locus encoding miR-21 and increasing its transcription. This vicious circle could be critical in the maintenance of the epigenetic "senescence program" that propagates senescence signals from SEN to CON cells through sEVs. The inverse U-shaped age-related trend of miR-21-5p carried by circulating sEVs suggests a potential role for it as a circulating biomarker associated with senescence and inflammaging.

Discussion

Emerging evidence strongly supports the hypothesis that EVs mediate the effects of senescent cells on their micro-environment and that they do so at least partly through their miRNA cargo [23,58–61]. We set out to establish the relative contribution of the miRNAs carried by EVs released from senescent ECs in spreading pro-senescence signals to younger cells. The first relevant finding was that senescent cells release a significantly greater number of sEVs than control cells, a finding that was corroborated by the detection in senescent cells of a significantly increased number of MVBs, the endocytic organelles that generate sEVs. These data agree with recent studies of a mouse model of oncogene-induced senescence and human lung fibrotic lesions enriched in senescent cells [62], bone marrow stromal cells [63], human prostate cancer cells [24] and chondrocytes [64].

Another major question was whether EVs contained the same miRNA repertoire as the cells that had released them. Global miRNA profiling of SEN and CON cells and their cognate EVs (sEVs and lEVs) showed that cells and their EVs shared about 33% of the miRNAs. Surprisingly, lEVs and sEVs shared only 24%, supporting the hypothesis that different EVs shuttle different cargo [65,66]. Since SEN cells released significantly more sEVs than CON cells, we focused on the miRNAs showing concordant modulation in sEVs and their parental SEN cells. This, we reasoned, would also help reduce the risk of potential contamination from the EVs contained in the FBS serum supplement used in the culture medium [67].

Analysis of SEN sEVs showed that they were enriched in miR-21-5p and miR-217, both of which were over-expressed in SEN cells and were capable of targeting DNMT1 and SIRT1, two key enzymes in methylation pattern maintenance. Our data are in line with previous reports associating miR-21-5p and miR-217 with cellular senescence. MiR-21-5p over-expression has been seen to reduce EC replicative lifespan, whereas its stable knockdown by sponges has been reported to extend it [68,69]. MiR-21-5p over-expression has also been related to the development of cardiac fibrosis [70], T-cell subset alteration [71] and imbalances in platelet function [72], all functions that are affected by ageing. An intriguing mechanism has also been described, where DNMT1 inhibition was induced by miR-21-5p binding the DNMT1 catalytic site rather than its mRNA [54]. As regards miR-217 over-expression, it has been related to a premature senescence-like phenotype both in EC models (through impaired angiogenesis via SIRT1 inhibition [56]) and in fibroblasts (through direct suppression of DNMT1-mediated methylation of p16 and pRb [55]).

Notably, we were able to replicate the same observations in another EC lineage undergoing replicative senescence, and in a model of drug-induced senescence. The expression levels of cellular and sEV miR-21-5p and miR-217 in drug-induced senescence were comparable to those obtained in the replicative senescence models. The variations of the miRNA pool according to the different mechanisms of

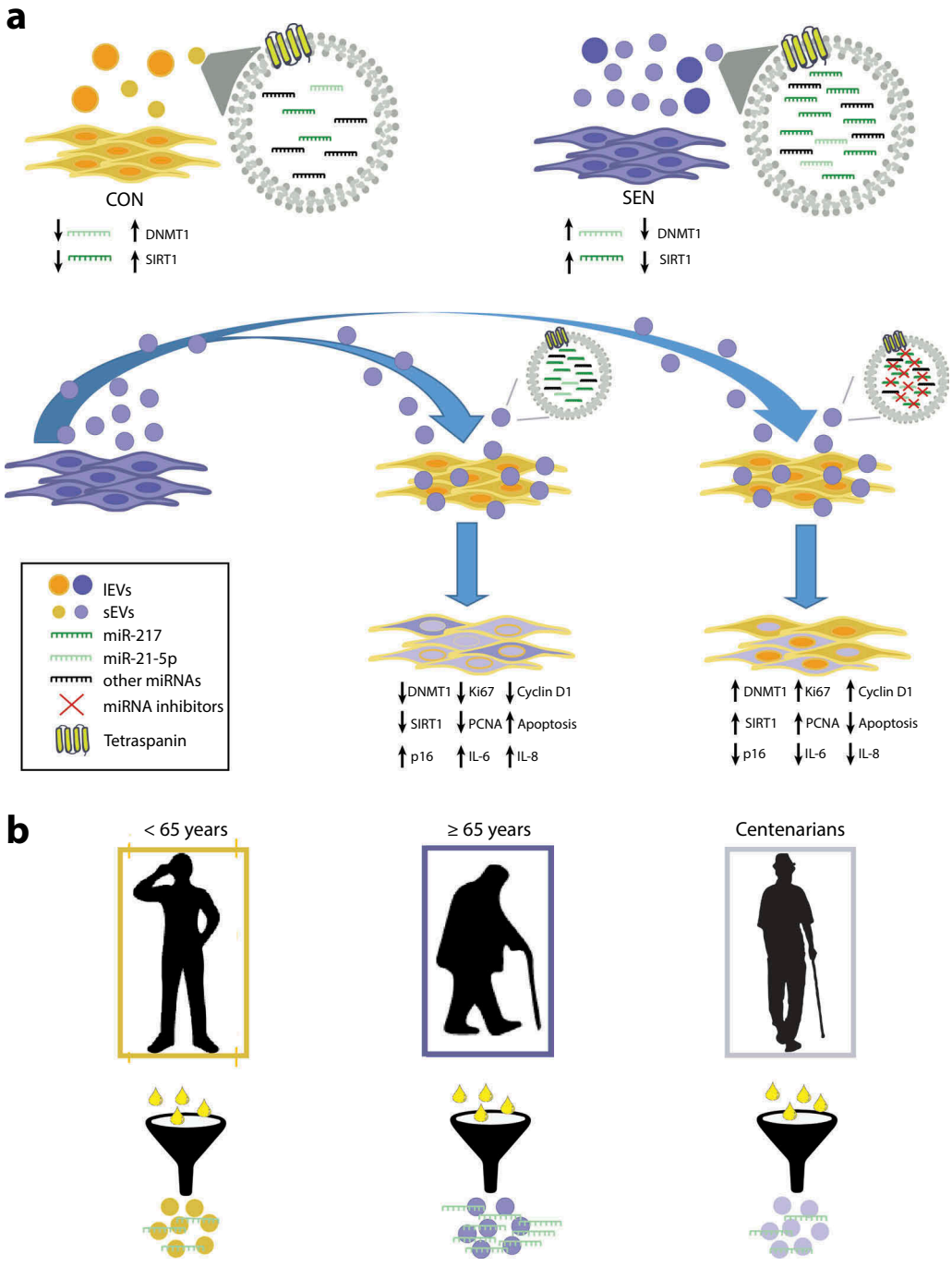

Figure 8. Overview of the SA effects of miR-21-5p and miR-217 carried by SEN sEVs into CON cells. (a) Graphic representation of the SA loop involving miR-21-5p. The miR-21 locus is de-methylated in SEN cells; the resulting miR-21-5p over-expression can contribute to reduce DNMT1/SIRT1 expression in SEN cells. sEVs released from SEN cells are enriched in miR-21-5p; their delivery to CON cells modulates DNMT1/SIRT1 and impairs their replication rate. This vicious cycle may be critical in maintaining the epigenetic "senescence program" through the spread of pro-senescence signals to younger cells through an increased sEV release. (b) MiR-21-5p in sEVs purified from plasma of healthy young, elderly and centenarian individuals showed an inverse U-shaped age-related trend, suggesting that miR-21-5p loaded on sEVs could be a systemic biomarker of senescence and inflammaging.

senescence are under-investigated. In this context, our results support the hypothesis that senescence-associated miRNAs participate in the control of a core set of senescence genes regardless of the pro-senescence stimulus [73].

When we explored the biological effects of SEN sEVs on younger cells, treatment of CON cells with SEN sEVs induced a significant reduction in DNMT1 and SIRT1 expression, which was associated with a reduction in cell replicative rate, with the acquisition

of a senescent phenotype, and with a partial demethylation of the locus encoding for miR-21. The demethylation of the *MIR21* locus was not coupled with the enhanced transcription of the miR-21-5p precursor pri-miR-21 in recipient cells. This suggests that (i) the increased levels of miR-21-5p and miR-217 in CON cells treated with SEN sEVs are related to the intracellular delivery of the sEV cargo, and (ii) a prolonged exposure to SEN sEVs could be required to establish the vicious cycle leading to miR-21-5p transcription in cells treated with CON sEVs. The most striking finding in this context was that miR-21-5p and miR-217 loaded on sEVs played a key role in DNMT1-SIRT1 modulation, with miR-21-5p being the major factor inducing replicative rate reduction in recipient cells. The underexpression of DNMT1 and SIRT1 detected in SEN HUVECs is not induced by changes in the methylation state of their loci, but by fine regulation by miR-21-5p and miR-217. These findings shed new light on the mechanisms promoting the spread of senescence via the bystander effect. Notably, miR-21-5p shuttling through sEVs has been associated with different biological functions depending on donors and recipient cell types [74,75]. While miR-21-5p has been extensively designated as an oncomiR [76], its role on the proliferative rate of non-cancer and replicative senescent cells is still debated. Our findings are in agreement with previous reports showing an anti-proliferative role of miR-21 on endothelial cells [68,77]. We can hypothesise that these effects could be related to the different transcriptional landscape between normal and cancer cells. In the latter, the inhibitory effects of miR-21 on many cell cycle regulators are potentially overwhelmed by gain-of-function somatic mutations.

As a final experiment, we set out to find *in vivo* evidence to compare with our *in vitro* data. Analysis of the miRNome profile of EVs purified from plasma of healthy subjects of different ages demonstrated for the first time that miR-21-5p shuttled by circulating EVs shows an inverse U-shaped trend, and that the trend becomes apparent only when centenarians are included in the analysis. We previously described an inverse U-shaped age-related trend for miR-21-5p during normal ageing and significantly increased miR-21-5p plasma levels in patients with ARDs such as cardiovascular disease and type 2 diabetes [57,61,78].

Notably, non-monotonic age-related trends have first been described for genetic determinants of human longevity; these studies suggested that the effects of mortality trends for different genotypes observed in cross-sectional studies could depend on interactions between genetic and epigenetic factors [79]. Experimental data about such interactions have begun to emerge only in recent years [80].

Our findings strongly support the hypothesis that circulating miR-21-5p may be an archetypal "inflamma-miR" related to cellular senescence and inflammaging, and that its non-monotonic age-related trend may be the result of the complex adaptive/selective remodelling that occurs during ageing. Crucially, therapies targeting miR-21 are already progressing to the clinical trial phase [81,82].

Interestingly, DNMT1 levels in circulating cells from healthy subjects of different ages exhibit a U-shaped pattern that mirrors the expression of miR-21-5p carried by circulating EVs [83].

Altogether, we provide proof of principle that senescent endothelial cells can spread their miRNA signature, thus contributing to the development of a pro-ageing environment, and that these miRNAs can be selectively packaged in and delivered through sEVs. Critically, the results obtained *in vivo* for miR-21-5p lend strong support to the *in vitro* observations and to the notion that cellular senescence is, at least partly, fractal of the ageing process; they also indicate that circulating factors derived from senescent cells can be used as biomarkers to depict and track ageing trajectories [84]. Even though senescence has been described as a terminal process, mounting evidence supports the view that the adverse effects of the senescence program can be attenuated or delayed [85] and that sEVs could play a critical anti-senescence role [86–88].

In conclusion, our findings pave the way for further research, in particular to work out how circulating pro-senescence signals carried by vesicles can become druggable targets that can help modulate the ageing process and delay ARD development. The discovery of several drugs targeting DNMT1 and SIRT1 and the possibility to modulate miRNA expression are making this ambitious goal easier to reach.

Acknowledgments

We wish to thank all the donors and their families. We gratefully acknowledge infrastructure support from the IRCCS INRCA Institute and Università Politecnica delle Marche. We are grateful to Word Designs for text editing (www.silviamodena.com).

Disclosure statement

The authors report no conflicts of interest.

Funding

This study was supported by grants from Marche Region, Italy (POR Marche FESR 2014-2020, project PrInTAGE 10439 to F.O.); Università Politecnica delle Marche (Scientific research grant, years 2017-2018-2019 and MIR-

AGE - Multidisciplinary Innovative Research Actions on AGE to F.O., A.D.P., and M.R.R.); Italian Ministry of Health ("Ricerca corrente" grant to IRCCS MultiMedica and IRCCS INRCA); European Union (H2020 grant IMforFuture, contract #721815 to I.B.) and Fondazione Umberto Veronesi (Fellowship 2017 and 2018 to E.M.).

ORCID

Emanuela Mensà http://orcid.org/0000-0002-3284-6161
Michele Guescini http://orcid.org/0000-0001-9372-7038
Angelica Giuliani http://orcid.org/0000-0002-8477-8519
Maria Giulia Bacalini http://orcid.org/0000-0003-1618-2673
Deborah Ramini http://orcid.org/0000-0001-8925-8195
Giacomo Corleone http://orcid.org/0000-0002-6170-9780
Manuela Ferracin http://orcid.org/0000-0002-1595-6887
Gianluca Fulgenzi http://orcid.org/0000-0003-2646-7728
Laura Graciotti http://orcid.org/0000-0002-1874-5217
Francesco Prattichizzo http://orcid.org/0000-0002-2959-2658
Leonardo Sorci http://orcid.org/0000-0002-4356-8873
Michela Battistelli http://orcid.org/0000-0003-4028-0652
Vladia Monsurrò http://orcid.org/0000-0002-9653-8432
Anna Rita Bonfigli http://orcid.org/0000-0002-9619-0181
Maurizio Cardelli http://orcid.org/0000-0002-4480-2473
Rina Recchioni http://orcid.org/0000-0002-7596-3077
Fiorella Marcheselli http://orcid.org/0000-0003-1188-1651
Silvia Latini http://orcid.org/0000-0002-8344-2220
Serena Maggio http://orcid.org/0000-0001-8778-6576
Mirco Fanelli http://orcid.org/0000-0002-9649-8661
Stefano Amatori http://orcid.org/0000-0001-7497-755X
Gianluca Storci http://orcid.org/0000-0001-5145-3091
Antonio Ceriello http://orcid.org/0000-0001-8122-3203
Vilberto Stocchi http://orcid.org/0000-0003-3269-9410
Maria De Luca http://orcid.org/0000-0001-6345-7508
Luca Magnani http://orcid.org/0000-0002-7534-0785
Maria Rita Rippo http://orcid.org/0000-0003-3024-3495
Antonio Domenico Procopio http://orcid.org/0000-0001-9909-2838
Claudia Sala http://orcid.org/0000-0002-4889-1047
Iva Budimir http://orcid.org/0000-0002-5297-8903
Cristian Bassi http://orcid.org/0000-0002-5823-709X
Massimo Negrini http://orcid.org/0000-0002-0007-1920
Paolo Garagnani http://orcid.org/0000-0002-4161-3626
Claudio Franceschi http://orcid.org/0000-0001-9841-6386
Jacopo Sabbatinelli http://orcid.org/0000-0001-9947-6778
Massimiliano Bonafè http://orcid.org/0000-0002-5218-6551
Fabiola Olivieri http://orcid.org/0000-0002-9606-1144

References

[1] Childs BG, Durik M, Baker DJ, et al. Cellular senescence in aging and age-related disease: from mechanisms to therapy. Nat Med. 2015;21(12):1424–1435.
[2] Acosta JC, Banito A, Wuestefeld T, et al. A complex secretory program orchestrated by the inflammasome controls paracrine senescence. Nat Cell Biol. 2013;15(8):978–990.
[3] McHugh D, Gil J. Senescence and aging: causes, consequences, and therapeutic avenues. J Cell Biol. 2018;217(1):65–77.
[4] Franceschi C, Bonafe M, Valensin S, et al. Inflamm-aging. An evolutionary perspective on immunosenescence. Ann N Y Acad Sci. 2000;908:244–254.
[5] da Silva PFL, Ogrodnik M, Kucheryavenko O, et al. The bystander effect contributes to the accumulation of senescent cells in vivo. Aging Cell. 2019;18(1):e12848.
[6] Fulop T, Witkowski JM, Olivieri F, et al. The integration of inflammaging in age-related diseases. Semin Immunol. 2018;40:17–35.
[7] Baker DJ, Childs BG, Durik M, et al. Naturally occurring p16(Ink4a)-positive cells shorten healthy lifespan. Nature. 2016;530(7589):184–189.
[8] Bussian TJ, Aziz A, Meyer CF, et al. Clearance of senescent glial cells prevents tau-dependent pathology and cognitive decline. Nature. 2018;562(7728):578–582.
[9] Childs BG, Gluscevic M, Baker DJ, et al. Senescent cells: an emerging target for diseases of ageing. Nat Rev Drug Discov. 2017;16(10):718–735.
[10] Prata L, Ovsyannikova IG, Tchkonia T, Kirkland JL. Senescent cell clearance by the immune system: emerging therapeutic opportunities. Semin Immunol. 2018;40:101275.
[11] Watroba M, Dudek I, Skoda M, et al. Sirtuins, epigenetics and longevity. Ageing Res Rev. 2017;40:11–19.
[12] Munk R, Panda AC, Grammatikakis I, et al. Senescence-associated microRNAs. Int Rev Cell Mol Biol. 2017;334:177–205.
[13] Hekmatimoghaddam S, Dehghani Firoozabadi A, Zare-Khormizi MR, et al. Sirt1 and Parp1 as epigenome safeguards and microRNAs as SASP-associated signals, in cellular senescence and aging. Ageing Res Rev. 2017;40:120–141.
[14] Wagner W, Weidner CI, Lin Q. Do age-associated DNA methylation changes increase the risk of malignant transformation? Bioessays. 2015;37(1):20–24.
[15] Lee SH, Lee JH, Lee HY, et al. Sirtuin signaling in cellular senescence and aging. BMB Rep. 2019;52(1):24–34.
[16] Wakeling LA, Ions LJ, Escolme SM, et al. SIRT1 affects DNA methylation of polycomb group protein target genes, a hotspot of the epigenetic shift observed in ageing. Hum Genomics. 2015;9:14.
[17] Zwergel C, Romanelli A, Stazi G, et al. Application of small epigenetic modulators in pediatric medulloblastoma. Front Pediatr. 2018;6:370.
[18] Williams J, Smith F, Kumar S, et al. Are microRNAs true sensors of ageing and cellular senescence? Ageing Res Rev. 2017;35:350–363.
[19] Chanda D, Otoupalova E, Hough KP, et al. Fibronectin on the surface of extracellular vesicles mediates fibroblast invasion. Am J Respir Cell Mol Biol. 2019;60(3):279–288.
[20] de Jong OG, Verhaar MC, Chen Y, et al. Cellular stress conditions are reflected in the protein and RNA content of endothelial cell-derived exosomes. J Extracell Vesicles. 2012;1(1):18396.
[21] Alexander M, Hu R, Runtsch MC, et al. Exosome-delivered microRNAs modulate the inflammatory response to endotoxin. Nat Commun. 2015;6:7321.

[22] Zhang Y, Kim MS, Jia B, et al. Hypothalamic stem cells control ageing speed partly through exosomal miRNAs. Nature. 2017;548(7665):52–57.
[23] Terlecki-Zaniewicz L, Pils V, Bobbili MR, et al. Extracellular vesicles in human skin: cross-talk from senescent fibroblasts to keratinocytes by miRNAs. J Invest Dermatol. 2019;139:2425–2436.e5.
[24] Lehmann BD, Paine MS, Brooks AM, et al. Senescence-associated exosome release from human prostate cancer cells. Cancer Res. 2008;68(19):7864–7871.
[25] Takahashi A, Okada R, Nagao K, et al. Exosomes maintain cellular homeostasis by excreting harmful DNA from cells. Nat Commun. 2017;8:15287.
[26] Takasugi M, Okada R, Takahashi A, et al. Small extracellular vesicles secreted from senescent cells promote cancer cell proliferation through EphA2. Nat Commun. 2017;8:15729.
[27] Eitan E, Green J, Bodogai M, et al. Age-related changes in plasma extracellular vesicle characteristics and internalization by leukocytes. Sci Rep. 2017;7(1):1342.
[28] Takasugi M. Emerging roles of extracellular vesicles in cellular senescence and aging. Aging Cell. 2018;17:2.
[29] Alique M, Ruiz-Torres MP, Bodega G, et al. Microvesicles from the plasma of elderly subjects and from senescent endothelial cells promote vascular calcification. Aging (Albany NY). 2017;9(3):778–789.
[30] Weilner S, Schraml E, Wieser M, et al. Secreted microvesicular miR-31 inhibits osteogenic differentiation of mesenchymal stem cells. Aging Cell. 2016;15(4):744–754.
[31] Hosseinkhani B, Kuypers S, van den Akker NMS, et al. Extracellular vesicles work as a functional inflammatory mediator between vascular endothelial cells and immune cells. Front Immunol. 2018;9:1789.
[32] Liu JY, Souroullas GP, Diekman BO, et al. Cells exhibiting strong p16 (INK4a) promoter activation in vivo display features of senescence. Proc Natl Acad Sci U S A. 2019;116(7):2603–2611.
[33] Regina C, Panatta E, Candi E, et al. Vascular ageing and endothelial cell senescence: molecular mechanisms of physiology and diseases. Mech Ageing Dev. 2016;159:14–21.
[34] Olivieri F, Lazzarini R, Recchioni R, et al. MiR-146a as marker of senescence-associated pro-inflammatory status in cells involved in vascular remodelling. Age (Dordr). 2013;35(4):1157–1172.
[35] Cawthon RM. Telomere measurement by quantitative PCR. Nucleic Acids Res. 2002;30(10):e47.
[36] Rueden CT, Schindelin J, Hiner MC, et al. ImageJ2: imageJ for the next generation of scientific image data. BMC Bioinformatics. 2017;18(1):529.
[37] Riboli E, Hunt KJ, Slimani N, et al. European prospective Investigation into cancer and nutrition (EPIC): study populations and data collection. Public Health Nutr. 2002;5(6B):1113–1124.
[38] Aryee MJ, Jaffe AE, Corrada-Bravo H, et al. Minfi: a flexible and comprehensive Bioconductor package for the analysis of Infinium DNA methylation microarrays. Bioinformatics. 2014;30(10):1363–1369.
[39] Huber W, Carey VJ, Gentleman R, et al. Orchestrating high-throughput genomic analysis with bioconductor. Nat Methods. 2015;12(2):115–121.
[40] Triche TJ Jr., Weisenberger DJ, Van Den Berg D, et al. Low-level processing of illumina infinium DNA methylation bead arrays. Nucleic Acids Res. 2013;41(7):e90.
[41] Fortin JP, Labbe A, Lemire M, et al. Functional normalization of 450k methylation array data improves replication in large cancer studies. Genome Biol. 2014;15(12):503.
[42] Guescini M, Maggio S, Ceccaroli P, et al. Extracellular vesicles released by oxidatively injured or intact C2C12 myotubes promote distinct responses converging toward myogenesis. Int J Mol Sci. 2017;18:11.
[43] Thery C, Witwer KW, Aikawa E, et al. Minimal information for studies of extracellular vesicles 2018 (MISEV2018): a position statement of the International Society for Extracellular Vesicles and update of the MISEV2014 guidelines. J Extracell Vesicles. 2018;7(1):1535750.
[44] Consortium E-T, Van Deun J, Mestdagh P, et al. EV-TRACK: transparent reporting and centralizing knowledge in extracellular vesicle research. Nat Methods. 2017;14(3):228–232.
[45] Kozomara A, Birgaoanu M, Griffiths-Jones S. miRBase: from microRNA sequences to function. Nucleic Acids Res. 2019;47(D1):D155–D162.
[46] Giuliani A, Cirilli I, Prattichizzo F, et al. The mitomiR/Bcl-2 axis affects mitochondrial function and autophagic vacuole formation in senescent endothelial cells. Aging (Albany NY). 2018;10(10):2855–2873.
[47] Li JH, S L, Zhou H, et al. starBase v2.0: decoding miRNA-ceRNA, miRNA-ncRNA and protein-RNA interaction networks from large-scale CLIP-Seq data. Nucleic Acids Res. 2014;42(Database issue):D92–97.
[48] McQuin C, Goodman A, Chernyshev V, et al. CellProfiler 3.0: next-generation image processing for biology. PLoS Biol. 2018;16(7):e2005970.
[49] Sharma A, Singh K, Almasan A. Histone H2AX phosphorylation: a marker for DNA damage. Methods Mol Biol. 2012;920:613–626.
[50] Cruickshanks HA, McBryan T, Nelson DM, et al. Senescent cells harbour features of the cancer epigenome. Nat Cell Biol. 2013;15(12):1495–1506.
[51] Lopez-Otin C, Blasco MA, Partridge L, et al. The hallmarks of aging. Cell. 2013;153(6):1194–1217.
[52] Turchinovich A, Drapkina O, Tonevitsky A. Transcriptome of extracellular vesicles: state-of-the-art. Front Immunol. 2019;10:202.
[53] Pan W, Zhu S, Yuan M, et al. MicroRNA-21 and microRNA-148a contribute to DNA hypomethylation in lupus CD4+ T cells by directly and indirectly targeting DNA methyltransferase 1. J Immunol. 2010;184(12):6773–6781.
[54] Zhang G, Esteve PO, Chin HG, et al. Small RNA-mediated DNA (cytosine-5) methyltransferase 1 inhibition leads to aberrant DNA methylation. Nucleic Acids Res. 2015;43(12):6112–6124.
[55] Wang B, Du R, Xiao X, et al. Microrna-217 modulates human skin fibroblast senescence by directly targeting DNA methyltransferase 1. Oncotarget. 2017;8(20):33475–33486.
[56] Menghini R, Casagrande V, Cardellini M, et al. MicroRNA 217 modulates endothelial cell senescence via silent information regulator 1. Circulation. 2009;120(15):1524–1532.
[57] Olivieri F, Spazzafumo L, Santini G, et al. Age-related differences in the expression of circulating microRNAs:

miR-21 as a new circulating marker of inflammaging. Mech Ageing Dev. 2012;133(11–12):675–685.
[58] Urbanelli L, Buratta S, Sagini K, et al. Extracellular vesicles as new players in cellular senescence. Int J Mol Sci. 2016;17:9.
[59] Xu D, Tahara H. The role of exosomes and microRNAs in senescence and aging. Adv Drug Deliv Rev. 2013;65 (3):368–375.
[60] Kim KM, Abdelmohsen K, Mustapic M, et al. RNA in extracellular vesicles. Wiley Interdiscip Rev RNA. 2017;8:4.
[61] Dluzen DF, Noren Hooten N, Evans MK. Extracellular RNA in aging. Wiley Interdiscip Rev RNA. 2017;8:2.
[62] Borghesan M, Fafian-Labora J, Eleftheriadou O, et al. Small extracellular vesicles are key regulators of non-cell autonomous intercellular communication in senescence via the interferon protein IFITM3. Cell Rep. 2019;27 (13):3956–3971 e3956.
[63] Umezu T, Imanishi S, Azuma K, et al. Replenishing exosomes from older bone marrow stromal cells with miR-340 inhibits myeloma-related angiogenesis. Blood Adv. 2017;1(13):812–823.
[64] Jeon OH, Wilson DR, Clement CC, et al. Senescence cell-associated extracellular vesicles serve as osteoarthritis disease and therapeutic markers. JCI Insight. 2019;4:7.
[65] Villarroya-Beltri C, Gutierrez-Vazquez C, Sanchez-Cabo F, et al. Sumoylated hnRNPA2B1 controls the sorting of miRNAs into exosomes through binding to specific motifs. Nat Commun. 2013;4:2980.
[66] Murillo OD, Thistlethwaite W, Rozowsky J. exRNA atlas analysis reveals distinct extracellular RNA cargo types and their carriers present across human biofluids. Cell. 2019;177(2):463–477 e415.
[67] Lehrich BM, Liang Y, Khosravi P, et al. Fetal bovine serum-derived extracellular vesicles persist within vesicle-depleted culture media. Int J Mol Sci. 2018;19:11.
[68] Dellago H, Preschitz-Kammerhofer B, Terlecki-Zaniewicz L, et al. High levels of oncomiR-21 contribute to the senescence-induced growth arrest in normal human cells and its knock-down increases the replicative lifespan. Aging Cell. 2013;12(3):446–458.
[69] Zhu S, Deng S, Ma Q, et al. MicroRNA-10A* and microRNA-21 modulate endothelial progenitor cell senescence via suppressing high-mobility group A2. Circ Res. 2013;112(1):152–164.
[70] Thum T, Gross C, Fiedler J, et al. MicroRNA-21 contributes to myocardial disease by stimulating MAP kinase signalling in fibroblasts. Nature. 2008;456 (7224):980–984.
[71] Kim C, Hu B, Jadhav RR, et al. Activation of miR-21-regulated pathways in immune aging selects against signatures characteristic of memory T cells. Cell Rep. 2018;25(8):2148–2162 e2145.
[72] Barwari T, Eminaga S, Mayr U, et al. Inhibition of profibrotic microRNA-21 affects platelets and their releasate. JCI Insight. 2018;3:21.
[73] Lafferty-Whyte K, Cairney CJ, Jamieson NB, et al. Pathway analysis of senescence-associated miRNA targets reveals common processes to different senescence induction mechanisms. Biochim Biophys Acta. 2009;1792(4):341–352.
[74] Hu Y, Rao SS, Wang ZX, et al. Exosomes from human umbilical cord blood accelerate cutaneous wound healing through miR-21-3p-mediated promotion of angiogenesis and fibroblast function. Theranostics. 2018;8(1):169–184.
[75] Mayourian J, Ceholski DK, Gorski PA, et al. Exosomal microRNA-21-5p mediates mesenchymal stem cell paracrine effects on human cardiac tissue contractility. Circ Res. 2018;122(7):933–944.
[76] Ge Y, Zhang L, Nikolova M, et al. Strand-specific in vivo screen of cancer-associated miRNAs unveils a role for miR-21(*) in SCC progression. Nat Cell Biol. 2016;18(1):111–121.
[77] Sabatel C, Malvaux L, Bovy N, et al. MicroRNA-21 exhibits antiangiogenic function by targeting RhoB expression in endothelial cells. PLoS One. 2011;6(2):e16979.
[78] Prattichizzo F, Micolucci L, Cricca M, et al. Exosome-based immunomodulation during aging: A nano-perspective on inflamm-aging. Mech Ageing Dev. 2017;168:44–53.
[79] Yashin AI, De Benedictis G, Vaupel JW, et al. Genes, demography, and life span: the contribution of demographic data in genetic studies on aging and longevity. Am J Hum Genet. 1999;65(4):1178–1193.
[80] Benayoun BA, Pollina EA, Brunet A. Epigenetic regulation of ageing: linking environmental inputs to genomic stability. Nat Rev Mol Cell Biol. 2015;16(10):593–610.
[81] Gomez IG, MacKenna DA, Johnson BG, et al. Anti-microRNA-21 oligonucleotides prevent Alport nephropathy progression by stimulating metabolic pathways. J Clin Invest. 2015;125(1):141–156.
[82] Wang D, Deuse T, Stubbendorff M, et al. Local microRNA modulation using a novel anti-miR-21-eluting stent effectively prevents experimental in-stent restenosis. Arterioscler Thromb Vasc Biol. 2015;35(9):1945–1953.
[83] Ciccarone F, Malavolta M, Calabrese R, et al. Age-dependent expression of DNMT1 and DNMT3B in PBMCs from a large European population enrolled in the MARK-AGE study. Aging Cell. 2016;15(4):755–765.
[84] Olivieri F, Capri M, Bonafe M, et al. Circulating miRNAs and miRNA shuttles as biomarkers: perspective trajectories of healthy and unhealthy aging. Mech Ageing Dev. 2017;165(Pt B):162–170.
[85] Shao Y, Lv C, Wu C, et al. Mir-217 promotes inflammation and fibrosis in high glucose cultured rat glomerular mesangial cells via Sirt1/HIF-1alpha signaling pathway. Diabetes Metab Res Rev. 2016;32(6):534–543.
[86] Yoshida M, Satoh A, Lin JB, et al. Extracellular vesicle-contained eNAMPT delays aging and extends lifespan in mice. Cell Metab. 2019;30(2):329–342 e325.
[87] Hu W, Ru Z, Zhou Y, et al. Lung cancer-derived extracellular vesicles induced myotube atrophy and adipocyte lipolysis via the extracellular IL-6-mediated STAT3 pathway. Biochim Biophys Acta Mol Cell Biol Lipids. 2019;1864(8):1091–1102.
[88] Prattichizzo F, Giuliani A, Sabbatinelli J, et al. Extracellular vesicles circulating in young organisms promote healthy longevity. J Extracell Vesicles. 2019;8 (1):1656044.

Received: 26 March 2020 | Revised: 25 April 2020 | Accepted: 4 May 2020

DOI: 10.1111/dom.14081

WILEY

BRIEF REPORT

Prevalence of residual inflammatory risk and associated clinical variables in patients with type 2 diabetes

Francesco Prattichizzo PhD[1] | Angelica Giuliani PhD[2] | Jacopo Sabbatinelli MD[2] | Giulia Matacchione PhD[2] | Deborah Ramini PhD[2] | Anna Rita Bonfigli PhD[3] | Maria Rita Rippo PhD[2] | Paola de Candia PhD[1] | Antonio Domenico Procopio MD[2,4] | Fabiola Olivieri PhD[2,4] | Antonio Ceriello MD[1]

[1]IRCCS MultiMedica, Milan, Italy

[2]Department of Clinical and Molecular Sciences (DISCLIMO), Università Politecnica delle Marche, Ancona, Italy

[3]Scientific Direction, IRCCS INRCA, National Institute, Ancona, Italy

[4]Center of Clinical Pathology and Innovative Therapy, IRCCS INRCA, Ancona, Italy

Correspondence
Francesco Prattichizzo, IRCCS MultiMedica, Polo Scientifico e Tecnologico, Via Fantoli 16/15, 20138 Milano, Italy.
Email: francesco.prattichizzo@multimedica.it

Funding information
Italian Ministry of Health, Grant/Award Number: Ricerca Corrente to IRCCS MultiMedica

Peer Review
The peer review history for this article is available at https://publons.com/publon/10.1111/dom.14081.

Abstract

Residual inflammatory risk (RIR) is defined as persistent circulating levels of high sensitivity C-reactive protein (hs-CRP) >2 mg/L despite an optimal (<70 mg/dL) control of LDL-cholesterol (LDL-C) and represents an emerging risk factor for the development of cardiovascular events in patients at high risk of atherosclerosis. Sparse data are available regarding the prevalence of RIR in patients with type 2 diabetes (T2D) and the clinical variables associated with hs-CRP elevation. Here, we report data from a well-characterized cohort of patients with T2D (n = 511) stratified for statins use, LDL-C goal attainment and prevalent T2D complications. Statins use and having at-target LDL-C partially affect the number of patients with inflammatory risk when compared with the whole T2D population, with an RIR prevalence of 39.2%. Among the spectra of complications, only patients with nephropathy had a higher prevalence of inflammatory risk. Total cholesterol, non-HDL-cholesterol, triglycerides, body mass index and waist-hip ratio were associated with hs-CRP, with an increased magnitude in at-target patients. Conversely, glucose-related variables were strongly associated with hs-CRP only in at-target patients, overall suggesting glycaemic control, insulin resistance, non-LDL-C lipid variables and especially central obesity as possible contributors to RIR in patients with T2D and LDL-C <70 mg/dL.

KEYWORDS

body mass index, cardiovascular diseases, c-reactive protein, diabetes complications, ischaemic heart disease, LDL-cholesterol, obesity, residual inflammatory risk, type 2 diabetes, waist-hip ratio

1 | INTRODUCTION

Residual inflammatory risk (RIR) is defined as persistently elevated circulating levels of high-sensitivity C-reactive protein (hs-CRP) despite optimal attainment of the LDL-cholesterol (LDL-C) goal.[1–3] Indeed, among the patients with a previous cardiovascular (CV) event enrolled in multiple trials of high-dose statin therapy, those who achieved LDL-C levels of <70 mg/dL and hs-CRP levels of <2 mg/L had substantially lower rates of recurrent CV events when compared with those who achieved only one or neither of these independent treatment targets, suggesting that the residual vascular risk observed in CV patients could be attributed to both a residual cholesterol risk and to RIR.[1–3] The inflammatory hypothesis driving ischaemic events has

This work was supported by the Italian Ministry of Health (Ricerca Corrente) to IRCCS MultiMedica.

been further substantiated by the results of the CANTOS trial. Indeed, treatment with an anti-IL-1β antibody reduced the incidence of CV events in a population with high CV risk, a cohort that includes 40% of diabetic patients.[4] In particular, the intervention was effective in those patients who had an hs-CRP of >2 mg/L at baseline and below this threshold at the end of the intervention, suggesting the tangible contribution of RIR to CV events.[5]

The prevalence of RIR in cohorts of patients with high CV risk ranges from 43% in the PROVE-IT trial to 61% in the VIRGO registry, a large database providing data from young adults with a previous myocardial infarction.[2,6] A recent publication also evidenced a high prevalence of RIR in patients with type 2 diabetes (T2D), as shown in the cohort of the EXAMINE trial, where patients with the highest values of hs-CRP had an increased incidence of CV events, an association independent of, and additive to, achieved LDL-C levels.[7] However, less data are available regarding the prevalence of RIR in patients with T2D from real-world cohorts. In addition, little information has been reported regarding the impact of statins and LDL-C goal attainment on RIR prevalence, as well as regarding the clinical variables associated with higher hs-CRP values in patients with T2D.

Here, we explored the impact of statins use, attainment of LDL-C goal and pre-existing T2D complications on the resulting prevalence of RIR in a well-characterized retrospective cohort (n = 511) of patients with T2D. In addition, we analysed the correlation between major clinical variables and hs-CRP among the different subgroups of patients. In order to better disentangle the effect of all these possible contributors, we used data from patients studied before 2009, when statins use and an LDL-C goal of <70 mg/dL were considered optional in subjects with T2D.[8]

2 | METHODS

2.1 | Cohort description

Samples were derived from a previously published cohort composed of 511 patients with T2D.[9] The study was approved by local institutional ethics committees. Written informed consent was obtained from each subject in accordance with the principles of the Declaration of Helsinki. T2D was diagnosed according to American Diabetes Association criteria, i.e. patients with an HbA1c of ≥6.5% or fasting blood glucose of ≥126 mg/dL or 2-hour blood glucose levels of ≥200 mg/dL after oral glucose tolerance test, or random blood glucose ≥200 mg/dL when severe diabetes symptoms are present.[10] Inclusion criteria for patients with diabetes were body mass index (BMI) <40 kg/m^2, age 35-85 years, and the ability and willingness to give written informed consent. Information collected included data on vital signs, anthropometric factors, medical history and behaviours. The presence/absence of diabetic complications was established as follows: diabetic retinopathy by fundoscopy through dilated pupils and/or fluorescence angiography; incipient nephropathy, defined as a urinary albumin excretion rate of >30 mg per 24 hours and a normal creatinine clearance; renal failure, defined as an estimated glomerular filtration rate (eGFR) of <60 mL/min per 1.73 m^2; neuropathy established by electromyography; ischaemic heart disease defined by clinical history and/or ischaemic electrocardiographic alterations; peripheral vascular disease, including atherosclerosis obliterans and cerebrovascular disease based on history, physical examinations and Doppler velocimetry. Among the 511 patients, 90 were affected by neuropathy, 120 by peripheral vascular disease, 75 by major adverse cardiovascular events (MACE), 62 by nephropathy or renal failure and 144 by retinopathy. Fasting blood samples of all subjects were processed to obtain EDTA plasma that was stored at −80°C. Concentrations of presented analytes were measured by standard procedures.

2.2 | Statistical analysis

Continuous variables were tested for normality using the Shapiro Wilk's test and reported as mean ± SD. Student's t test was used to evaluate differences in continuous variables between two groups, while the chi square test was used for dichotomous variables. Pearson's correlation was used for continuous variables. Spearman's coefficient was used to estimate the correlation between hs-CRP and the number of T2D complications. A stepwise logistic regression model with forward conditional method was used to identify factors associated with inflammatory risk in T2D. All variables showing a significant linear correlation with hs-CRP in T2D subjects with LDL-C ≤70 mg/dL were entered into the model. Model fit was assessed using the Hosmer-Lemeshow goodness-of-fit test. The analyses were carried out using IBM SPSS Statistics version 26 (IBM, Armonk, NY, USA) and R version 3.6.1. Statistical significance was defined as a two-tailed *P*-value of <.05.

3 | RESULTS

Clinical variables of patients with T2D categorized according to the presence/absence of inflammatory risk (i.e. hs-CRP ≥ or <2 mg/L) are shown in Table 1, while Table **S1** displays the clinical characteristics of the entire cohort. Subjects with inflammatory risk had a higher mean value of BMI, waist-hip ratio, total cholesterol, triglycerides, fasting glucose, insulin, homeostatic model assessment (HOMA) index and uric acid, while HDL-cholesterol (HDL-C) and mean diabetes duration were lower in this group. In addition, they were more probable to have a diagnosis of hypertension and less probable to be on treatment with sulphonylureas (Table 1).

When considering all patients with T2D, the prevalence of inflammatory risk was 51.9%, while a slightly lower prevalence (46.9%) was observed when considering only patients on stable (>1 year) statin therapy. When considering only patients with the currently recommended LDL-C goal of 70 mg/dL, i.e. those at target, the prevalence of RIR was 39.2% (Figure 1A).

Regarding the spectra of possible complications, only among patients with nephropathy was there a higher prevalence of

TABLE 1 Clinical variables of patients categorized according to the presence/absence of residual inflammatory risk (i.e. hs-CRP < or ≥2 mg/L).

Variable	High-sensitivity C-reactive protein stratification		
	Hs-CRP <2 mg/L (N = 246)	Hs-CRP ≥2 mg/L (N = 265)	*P*-value
Hs-CRP (mg/L)	1.06 (0.55)	5.91 (3.59)	**<.0001**
Age (y)	65.8 (8.6)	65.6 (7.7)	.796
Gender (males, %)	150 (61%)	132 (49.8%)	**.011**
Diabetes duration (y, SD)	16.3 (11.4)	13.25 (11.5)	**.005**
Body mass index (kg/m^2)	27.3 (3.8)	29.7 (4.3)	**<.0001**
Waist-hip ratio	0.92 (0.07)	0.94 (0.07)	**.001**
Total cholesterol (mg/dL)	202.0 (38.7)	210.7 (37.4)	**.010**
LDL-cholesterol (mg/dL)	114.2 (32.2)	117.8 (31.1)	.202
HDL-cholesterol (mg/dL)	54.9 (15.4)	50.3 (16.0)	**<.0001**
Triglycerides (mg/dL)	112.4 (58.1)	160.5 (134.4)	**<.0001**
Fasting glucose (mg/dL)	155.8 (42.7)	167.4 (51.2)	**.005**
HbA1c (%)	7.30 (1.13)	7.50 (1.31)	.062
Insulin (UI/mL)	6.30 (9.26)	7.69 (5.70)	**.043**
HOMA index	2.39 (3.35)	3.29 (7.24)	**.002**
WBC (n/mm^3)	6.29 (1.49)	6.87 (1.59)	**<.0001**
Platelets (n/mm^3)	212.4 (82.1)	221.4 (55.6)	.147
Creatinine (mg/dL)	0.89 (0.25)	0.92 (0.33)	.224
Azotemia (mg/dL)	40.6 (11.3)	39.7 (12.2)	.356
eGFR (mL/min)	80.9 (18.8)	73.2 (22.2)	.069
Uric acid (mg/dL)	4.62 (1.11)	4.94 (1.24)	**.002**
Hypertension (N, %)	140 (56.9%)	180 (67.9%)	**.010**
Smokers (N, %)	37 (15%)	42 (15.8%)	.800
Medication (N, %)			
Metformin	84 (34.1%)	100 (37.7%)	.398
Sulphonylureas	136 (55.3%)	113 (42.6%)	**.004**
Glinides	4 (1.6%)	7 (2.6%)	.429
Insulin	44 (17.9%)	46 (17.4%)	.876
Statins (N, %)	51 (20.8%)	45 (17%)	.278

Abbreviations: eGFR, estimated glomerular filtration rate; HOMA, homeostatic model assessment; WBC, white blood count
Data are expressed as mean (SD) and *P*-values refer to Student's t test for continuous variables or to chi square test for dichotomous variables. Significant differences ($P < .05$) are highlighted in bold.

inflammatory risk (66.1%), while patients with a previous MACE showed the same prevalence as the general T2D cohort (50.6%) (Figure 1B).

Pearson's correlations among variables in different subgroups revealed that total-C, non-HDL-C, triglycerides, apolipoprotein B, BMI and waist-hip ratio were positively associated with hs-CRP, while eGFR displayed a negative correlation. These associations were not significant in patients treated with statins, while the attainment of the goal of LDL-C <70 mg/dL markedly increased the magnitude of these correlations. On the other hand, HbA1c, fasting insulin, HOMA index, serum creatinine, platelets count and the number of complications were strongly associated with hs-CRP only in patients with LDL-C <70 mg/dL (Figure 1C and Table S2). The progressive nature of the association was particularly apparent for non-HDL-C, HbA1c and HOMA index, as evidenced by linear correlation graphs (Figure S1). Among other variables, fasting glucose and age were not associated with hs-CRP in the at-target group (Figure 1C and Table S2), despite the known proinflammatory effect of these two variables.[11] Among immune-related variables, monocytes and lymphocytes counts were positively associated with hs-CRP in at-target patients, possibly suggesting both innate and acquired immunity as potential contributors to RIR (Figure 1C and Table S2).

To gain further insights into the variable associated with inflammatory risk in T2D, we built a binary logistic regression model predicting the likelihood of hs-CRP levels of ≥2 mg/L. The logistic regression model with forward conditional selection was statistically significant ($\chi^2[14] = 59.120$, $P < .001$) and included four variables as significant predictors, i.e. waist-hip ratio, triglycerides, non-HDL-C and neutrophils (Table S3).

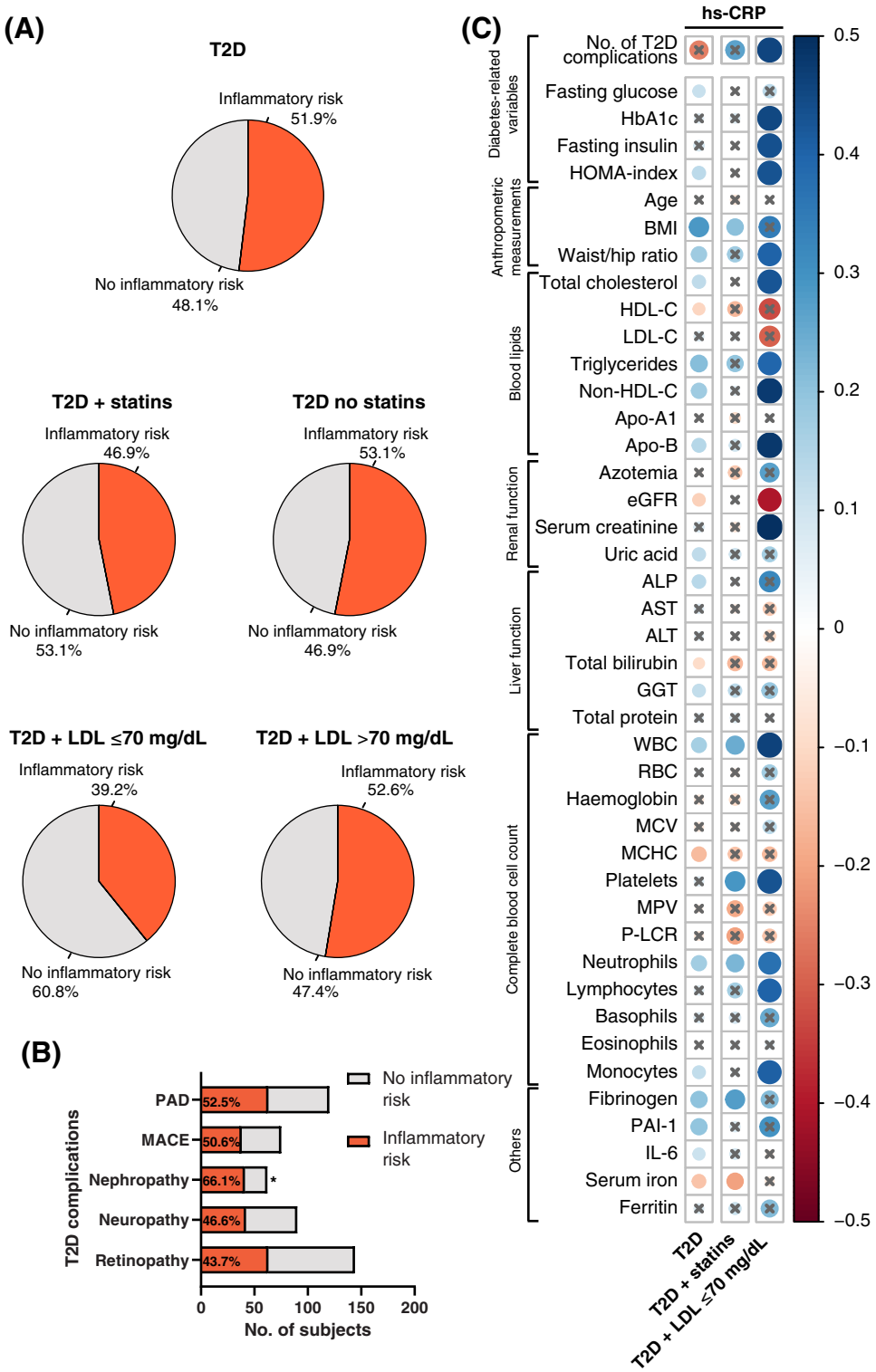

FIGURE 1 (A) Prevalence of inflammatory risk (hs-CRP ≥ 2 mg/L) in all patients with type 2 diabetes (T2D), only in those treated or not with statins, and only in patients with at-target (<70 mg/dL) or not at-target LDL-cholesterol (LDL-C). (B) Prevalence of residual inflammatory risk (RIR) in patients affected by different complications. (C) Correlation plot showing the significant correlations among the different variables and hs-CRP in the whole population (left), in patients on statin therapy (middle), and in patients with at-target LDL-C (right). The intensity of the colour and the size of the circles depend on the magnitude of the correlation, while the symbol X indicates a non-significant correlation. ALP, alkaline phosphatase; AST, aspartate transaminase; ALT, alanine transaminase; BMI, body mass index; GGT, gamma-glutamyltransferase; HDL-C, high density lipoprotein cholesterol; IL-6, interleukin 6; LDL-C, low density lipoprotein cholesterol; eGFR, estimated glomerular filtration rate; blue = positive correlation; red = negative correlation; MACE, major adverse cardiovascular events; MCV, mean corpuscular volume; MCHC, mean corpuscular haemoglobin concentration; MPV, mean platelet volume; P-LCR, platelet large cell ratio; PAI-1, plasminogen activator inhibitor-1; PAD, peripheral artery disease; RBC, red blood cells; WBC, white blood cells. *P <0.05 chi square test

4 | DISCUSSION

Our results evidence a high prevalence of RIR among patients with T2D, comparable with observations in previous cohorts of patients with CV diseases or in those at high risk.[2,6,12] To our knowledge, this is the first study showing the prevalence of RIR in a cohort with T2D, although many previous reports have described hs-CRP elevation in T2D.[7,13] These findings also highlight a limited effect of statins use and LDL-C goal attainment on RIR prevalence in T2D. Accordingly, lipid- and obesity-related variables were associated with hs-CRP in the whole T2D population, but more consistently in patients achieving the LDL-C target. Notably, glucose-related variables were associated with hs-CRP only in at-target patients, overall suggesting that RIR might be, at least in part, attributable to non-LDL-C dyslipidaemia,

central obesity, insulin resistance, and lack of glycaemic control in T2D.[13] In particular, waist-hip ratio, triglycerides and non-HDL-C appear to be the most probable variables explaining the burden of RIR in patients with T2D. It is worth noting, that among the range of different T2D complications, only patients with nephropathy have an increased prevalence of inflammatory risk. Consistently, diabetic nephropathy is accompanied by a complex proinflammatory remodelling promoting the development and progression of this complication, as evidenced by both prospective and cross-sectional studies.[14]

An inherent limitation to this study design is that none of the patients were treated with the recently introduced glucose-lowering drugs,[15] some of which have been suggested as also targeting the inflammatory process[16]; nor were any patients treated with recently introduced LDL-C-lowering drugs such as proprotein convertase subtilisin/kexin type 9 (PCSK9) inhibitors. In addition, other factors beyond the large range of common variables presented here may influence RIR.

Overall, these observations suggest that an effective targeting of modifiable risk factors, for example, central obesity and triglycerides, may reduce the burden of RIR in patients with T2D, as recently suggested for patients with prevalent CV diseases.[17] This hypothesis warrants further exploration, especially considering that an aggressive, multidimensional reduction of risk factors is already known to reduce the incidence of CV events in patients with T2D.[18]

CONFLICT OF INTEREST

None of the authors have any competing interests.

AUTHOR CONTRIBUTIONS

FP, FO and AC contributed to the conception and design of the study and drafted the manuscript. AG and JS contributed to acquisition and interpretation of data and drafted figures. GM, DR, ARB, MRR, PdC and ADP critically revised the manuscript. All of the authors gave their final approval.

ORCID

Francesco Prattichizzo https://orcid.org/0000-0002-2959-2658
Jacopo Sabbatinelli https://orcid.org/0000-0001-9947-6778

REFERENCES

1. Ridker PM. Residual inflammatory risk: addressing the obverse side of the atherosclerosis prevention coin. *Eur Heart J*. 2016;37(22):1720-1722.
2. Ridker PM. How common is residual inflammatory risk? *Circ Res*. 2017;120(4):617-619.
3. Aday AW, Ridker PM. Antiinflammatory therapy in clinical care: the CANTOS trial and beyond. *Front Cardiovasc Med*. 2018;5:62.
4. Ridker PM, Everett BM, Thuren T, et al. Antiinflammatory therapy with Canakinumab for atherosclerotic disease. *N Engl J Med*. 2017;377(12):1119-1131.
5. Ridker PM, MacFadyen JG, Everett BM, et al. Relationship of C-reactive protein reduction to cardiovascular event reduction following treatment with canakinumab: a secondary analysis from the CANTOS randomised controlled trial. *Lancet*. 2018;391(10118):319-328.
6. Lu Y, Zhou S, Dreyer RP, Spatz ES, et al. Sex differences in inflammatory markers and health status among young adults with acute myocardial infarction: results from the VIRGO (variation in recovery: role of gender on outcomes of young acute myocardial infarction patients) study. *Circ Cardiovasc Qual Outcomes*. 2017;10(2):e003470.
7. Hwang YC, Morrow DA, Cannon CP, et al. High-sensitivity C-reactive protein, low-density lipoprotein cholesterol and cardiovascular outcomes in patients with type 2 diabetes in the EXAMINE (examination of cardiovascular outcomes with Alogliptin versus standard of care) trial. *Diabetes Obes Metab*. 2018;20(3):654-659.
8. Kamari Y, Bitzur R, Cohen H, Shaish A, Harats D. Should all diabetic patients be treated with a statin? *Diabetes Care*. 2009;32((Suppl 2)):S378-S383.
9. Testa R, Olivieri F, Sirolla C, et al. Leukocyte telomere length is associated with complications of type 2 diabetes mellitus. *Diabet Med*. 2011;28(11):1388-1394.
10. American Diabetes Association. Classification and diagnosis of diabetes: standards of medical care in diabetes—2020. *Diabetes Care*. 2020;43(Suppl. 1):S14-S31.
11. Prattichizzo F, Giuliani A, Mensà E, et al. Pleiotropic effects of metformin: shaping the microbiome to manage type 2 diabetes and postpone ageing. *Ageing Res Rev*. 2018;48:87-98.
12. Kalkman DN, Aquino M, Claessen BE, et al. Residual inflammatory risk and the impact on clinical outcomes in patients after percutaneous coronary interventions. *Eur Heart J*. 2018;39(46):4101-4108.
13. Kahn SE, Zinman B, Haffner SM, et al. Obesity is a major determinant of the association of C-reactive protein levels and the metabolic syndrome in type 2 diabetes. *Diabetes*. 2006;55(8):2357-2364.
14. Sinha SK, Nicholas SB, Sung JH, et al. Hs-CRP is associated with incident diabetic nephropathy: findings from the Jackson heart study. *Diabetes Care*. 2019;42(11):2083-2089.
15. Prattichizzo F, La Sala L, Rydén L, et al. Glucose- lowering therapies in patients with type 2 diabetes and cardiovascular diseases. *Eur J Prev Cardiol*. 2019;26((suppl 2)):73-80.
16. Prattichizzo F, De Nigris V, Micheloni S, La Sala L, Ceriello A. Increases in circulating levels of ketone bodies and cardiovascular protection with SGLT2 inhibitors: is low-grade inflammation the neglected component? *Diabetes Obes Metab*. 2018;20(11):2515-2522.
17. Blaum C, Brunner FJ, Kröger F, et al. Modifiable lifestyle risk factors and C-reactive protein in patients with coronary artery disease: implications for an anti-inflammatory treatment target population. *Eur J Prev Cardiol*. 2019;10. [Epub ahead of print]
18. Gaede P, Lund-Andersen H, Parving HH, Pedersen O. Effect of a multifactorial intervention on mortality in type 2 diabetes. *N Engl J Med*. 2008;358(6):580-591.

SUPPORTING INFORMATION

Additional supporting information may be found online in the Supporting Information section at the end of this article.

How to cite this article: Prattichizzo F, Giuliani A, Sabbatinelli J, et al. Prevalence of residual inflammatory risk and associated clinical variables in patients with type 2 diabetes. *Diabetes Obes Metab*. 2020;22:1696–1700. https://doi.org/10.1111/dom.14081

Pre-eclampsia predictive ability of maternal miR-125b: a clinical and experimental study

CATERINA LICINI, CHIARA AVELLINI, ELENA PICCHIASSI, EMANUELA MENSÀ, SONIA FANTONE, DEBORAH RAMINI, CHIARA TERSIGNI, GIOVANNI TOSSETTA, CLARA CASTELLUCCI, FEDERICA TARQUINI, GIULIANA COATA, IRENE GIARDINA, ANDREA CIAVATTINI, GIOVANNI SCAMBIA, GIAN CARLO DI RENZO, NICOLETTA DI SIMONE, ROSARIA GESUITA, STEFANO R. GIANNUBILO, FABIOLA OLIVIERI[A], and DANIELA MARZIONI[A]

ANCONA, PERUGIA, ROMA, AND ITALY; AND MOSCOW, RUSSIA

Pre-eclampsia (PE) is a systemic maternal syndrome affecting 2-8% of pregnancies worldwide and involving poor placental perfusion and impaired blood supply to the foetus. It manifests after the 20th week of pregnancy as new-onset hypertension and substantial proteinuria and is responsible for severe maternal and newborn morbidity and mortality. Identifying biomarkers that predict PE onset prior to its establishment would critically help treatment and attenuate outcome severity. MicroRNAs are ubiquitous gene expression modulators found in blood and tissues. Trophoblast cell surface antigen (Trop)-2 promotes cell growth and is involved in several cancers. We assessed the PE predictive ability of maternal miR-125b in the first trimester of pregnancy by measuring its plasma levels in women with normal pregnancies and with pregnancies complicated by PE on the 12th week of gestation. To gain insight into PE pathogenesis we investigated whether Trop-2 is targeted by miR-125b in placental tissue. Data analysis demonstrated a significant association between plasma miR-125b levels and PE, which together with maternal body mass index before pregnancy provided a predictive model with an area under the curve of 0.85 (95% confidence interval, 0.70-1.00). We also found that Trop-2 is a target of miR-125b in placental cells; its localization in the basal part of the syncytiotrophoblast plasma membrane suggests a role for it in the early onset of PE. Altogether, maternal miR-125b proved a promising early biomarker of PE, suggesting that it may be involved in placental development through its action on Trop-2 well before the clinical manifestations of PE. (Translational Research 2021; 228:13–27)

Abbreviations: PE = pre-eclampsia; Trop-2 = Trophoblast cell surface antigen-2; miR-125b = microRNA-125b

[a]F.O. and D.M. contributed equally to this work.

From the Department of Experimental and Clinical Medicine, Università Politecnica delle Marche, 60126 Ancona, Italy; Department of Biomedical and Surgical Science, Clinic of Obstetrics and Gynaecology, University of Perugia, 06132 Perugia, Italy; Department of Clinical and Molecular Sciences, Università Politecnica delle Marche, 60126 Ancona, Italy; Fondazione Policlinico Universitario A. Gemelli IRCCS, U.O.C. di Ostetricia e Patologia Ostetrica, Dipartimento di Scienze della Salute della Donna, del Bambino e di Sanità Pubblica, 00168 Roma, Italy; Centre of Perinatal and Reproductive Medicine, University of Perugia, Italy; Department of Clinical Sciences, Università Politecnica delle Marche, Salesi Hospital, 60123 Ancona, Italy; Università Cattolica del Sacro Cuore, Istituto di Clinica Ostetrica e Ginecologica, 00168 Roma, Italy; Department of Obstetrics and Gynaecology I.M. Sechenov First State University, Moscow, Russia; Centre of Epidemiology and Biostatistics, Università Politecnica delle Marche, 60126 Ancona, Italy; Center of Clinical Pathology and Innovative Therapy, IRCCS INRCA National Institute, 60100 Ancona, Italy.

Submitted for Publication February 3, 2020; received submitted July 20, 2020; accepted for publication July 23, 2020.

Corresponding author. E-mail address: d.marzioni@staff.univpm.it.

1931-5244/$ - see front matter

https://doi.org/10.1016/j.trsl.2020.07.011

AT A GLANCE COMMENTARY

Licini C, et al

Background

This is a multidisciplinary study on the role of miR-125b on the development of preeclampsia. This study was undertaken to assess the preeclampsia predictive ability of maternal plasma miR-125b at 12 weeks of gestation and to establish whether miR-125b targets Trophoblast cell surface antigen-2 protein. We propose that maternal plasma miR-125b overexpression at 12 weeks of gestation inhibits placental Trophoblast cell surface antigen-2 protein and can directly favour preeclampsia onset by causing placental maldevelopment.

Translational Significance

These data advance our mechanistic understanding of preeclampsia complications and provide insights to develop new prevention strategies.

INTRODUCTION

PE is a maternal pregnancy disorder arising after the 20th week of gestation and characterized by new-onset hypertension and substantial proteinuria. It involves multiple organs including kidney, liver and brain (1-4) and affects 2−8% of pregnancies worldwide, causing severe maternal and newborn morbidity and mortality (5,6). According to the "two-stage model" of PE, inadequate trophoblast invasion of the placental bed in early pregnancy results in insufficient remodelling of uteroplacental spiral arteries (first stage of PE) (7). Poor placental perfusion may become clinically relevant at different times of gestation by affecting the blood supply to the foetal-placental unit; oxidative stress then induces the release into the maternal circulation of factors like Flt-1 and s-Endoglin, which induce the clinical features of PE, where hypertension (blood pressure $\geq$ 140/90 mm Hg) and proteinuria ($\geq$ 300 mg in 24 h) combine with clotting and liver dysfunction (second stage of PE) (8-11). Since a normal syncytiotrophoblast is critical for the establishment and maintenance of a healthy pregnancy, its impaired function directly affects foetal development and maternal adaptation to pregnancy. Syncytiotrophoblast necrosis, an extreme condition, involves a significantly higher release of syncytiotrophoblast extracellular vesicles into the maternal circulation, particularly in early-onset PE (12-15). However, the key mechanisms underlying placental pathophysiology remain to be elucidated. Investigation of the molecules regulating placental adaptation processes is therefore critical to gain a greater understanding of PE pathogenesis.

MicroRNAs (miRNAs), small non-coding RNAs that regulate the translation and degradation of specific mRNA targets, play a critical role in cellular functions such as proliferation, apoptosis, death, stress response, differentiation and development (16,18). Dysregulation of tissue and/or circulating miRNAs has been described in a variety of disorders (16-18). At least 500 miRNAs are known to be expressed in placental trophoblasts (19,20). After the early study by Pineles et al. in 2007 (21), mounting evidence has been suggesting a potential association between some miRNAs and PE pathogenesis (21-26). Although several miRNAs have been tested for their ability to predict PE onset (27-31), results have been inconclusive.

Among the miRNAs implicated in pregnancy disorders (32), miR-125b is especially interesting because it is involved in angiogenesis (33) and cell migration/remodelling (34) and is highly conserved in several species (35).

Trophoblast cell surface antigen (Trop)-2, also known as tumour-associated calcium signal transducer (TACSTD2), is a 35-49 kDa transmembrane glycoprotein (36) involved in the regulation of cell-cell adhesion, cell proliferation and maintenance of basement membrane integrity (37-39); it can function as a cell surface receptor for specific ligands to increase intracellular calcium levels (39) and plays a role in cell growth (38,40). Trop-2 was first identified by Lipinski et al. (41) as a marker of trophoblast and choriocarcinoma cell lines and has since been described as a major tumorigenic factor in several cancers (42-47). Interestingly, Trop-2 mRNA has been identified as a miR-125b target in breast, head and neck, and urothelial cancer (48-50), whereas no data are available for placental tissue.

Based on these considerations, a clinical, biomolecular and morphological study was devised i) to evaluate the ability of maternal miR-125b plasma levels measured at 12 weeks of pregnancy to predict PE onset; ii) to investigate whether Trop-2 protein is a miR-125b target in placental tissue; and iii) to elucidate the functional role of miR-125b in modulating Trop-2 in human trophoblasts.

MATERIALS AND METHODS

Study design. The participants who provided the blood samples were prospectively recruited from women attending a routine antenatal care visit at

Table 1. Characteristic of placental tissue from healthy pregnancies and pregnancies complicated by pre-eclampsia

	1st trimester (n=10)	3rd trimester (n=10)	Pre-eclampsia (n=10)	p value
Maternal age (years) (mean±SD)	30.2 ± 7.59	32.6 ± 4.05	36.9 ± 5.25	0.07
Gestational age (weeks) (mean±SD)	8.43 ± 1.95	37.25 ± 3.48	32.71 ± 3.85	0.0001

Obstetrics and Gynaecology outpatient clinic of Hospital 'S. Maria della Misericordia' (University of Perugia, Italy) from 2014 to 2016 and followed until delivery (Table 1).

This is a case-control study nested in a cohort study where 158 plasma samples from women with healthy pregnancies (n=144) or with pregnancy complicated by PE (n=14) had been analysed. The present case-control study involved 31 samples, 18 from women with healthy pregnancies and 13 from gestational age-matched women whose pregnancy was complicated by PE (the 14th sample was no longer available because it had been used for other tests).

Placenta samples were collected from 30 women, 20 with a healthy pregnancy and 10 whose pregnancy was complicated by PE. The former 20 samples were collected from women who had had voluntary terminations in the 1st trimester of gestation (n=10, Gynaecology and Obstetrics Unit, Department of Clinical Sciences, Università Politecnica delle Marche, Ancona, Italy) or who had had an uneventful term delivery (n=10, Department of Obstetrics and Gynaecology, Catholic University of the Sacred Heart, Roma, Italy). The 10 samples from pregnancies complicated by PE were collected at delivery at the Department of Obstetrics and Gynaecology, Catholic University of the Sacred Heart (Table 1).

The eligibility criteria were those described by Gesuita et al. (51). Briefly, women aged 18 to 45 years with a singleton pregnancy and no genetic diseases (*e.g.* aneuploidy) who gave their written informed consent to participate were considered eligible. Exclusion criteria were multiparity, multiple gestation, a history of hypertension, renal or cardiac disease, diabetes mellitus, thyroid and immune diseases and congenital or acquired thrombophilia.

Baseline demographics and information on the mother's medical (including obstetric) history and current and earlier lifestyle factors (smoking, diet and physical activity) was collected through an interview. The body mass index (BMI) was calculated based on the data obtained during the interview. The gestational age was calculated from the last menstrual period and was confirmed by ultrasound crown-rump-length measurement.

Newborn data included gender, health and birth weight. Placenta samples were not collected from stillbirths or from live births where the newborn suffered from chromosomal or other foetal abnormalities.

The study was approved by the institutional Ethics Board of the University of Perugia.

Healthy pregnancies were normotensive pregnancies with normal uterine and umbilical Doppler flow velocimetry during gestation and where the foetus was appropriate for the gestational age (newborns $\geq 10^{th} \leq 90^{th}$ percentile for gender and gestational age according to Italian charts [52]).

PE was diagnosed after the 20th week based on two blood pressure readings ≥ 140/90 mmHg taken at least 4 h apart and on proteinuria ≥ 300 mg in 24 h (or 2 dipstick readings of at least +2 of midstream or catheter urine specimens if 24-hour urine collection was not available) in previously normotensive patients (1).

Sample collection. ***Blood samples for the clinical study.*** Venous blood was collected on the 12th week of pregnancy in EDTA-containing VACUETTE® tubes and centrifuged at 1500 g for 15 min at 4°C. Plasma was aliquoted in 500 μl tubes and stored at -80°C until processing within 2 years of collection. To avoid bias in miRNA dosage, samples were thawed only once.

Placenta samples for the biomolecular and morphological study. Six tissue blocks were collected from each placental sample. Three blocks were immediately frozen at -80°C for use in Western blot analysis; the other 3 blocks were immediately fixed in 4% neutral buffered formalin for 8-12 h at 4°C and paraffin-embedded at a temperature not exceeding 56°C (44), to obtain sections for immunohistochemistry (2 μm), immunofluorescence and RT-PCR analysis of miR-125b (10 μm).

Analysis of tissue and plasma miR-125b for the clinical study. MiRNA-125b was measured in placental samples and plasma using Total RNA Purification Kit (Norgen Biotek Corp., Thorold, Canada). Synthetic *Caenorhabditis elegans* cel-miR-39 (Spike-In Kit, Norgen Biotek Corp.) was spiked into 100 μl of plasma before RNA extraction. Total RNA was stored at -80°C until use. Reverse transcription was performed using TaqMan microRNA Reverse Transcription kit a miR-125b-specific probe (cat. # 4427975 Assay ID 000449, both from Applied Biosystem, Life Technologies, Monza, Italy). Normalization of miR-125b values in placenta and plasma was also performed by reverse transcription with primers for RNU48 (cat. # 4427975 Assay ID 001006), a constituent siRNA, and for cel-miR-39 (cat. # 4427975 Assay ID 000200, both from Applied Biosystem, Life Technologies), respectively.

The conditions for reverse transcription were as follows: 16˚C for 30 min, 42˚C for 30 min, and 85˚C for 5 min. The temperature was then reduced to 4˚C.

MiRNA expression was quantified using TaqMan Fast Universal PCR Master Mix and probes for miR-125b, RNU48, and cel-miR-39 (all from Applied Biosystem, Life Technologies). The RT-PCR reaction conditions involved one cycle at 95˚C for 10 min, 40 cycles at 95˚C for 15 sec and 60˚C for 1 min. The threshold cycle (Ct) value was defined as the cycle number at which the signal exceeded a predetermined threshold. The relative amount of miR-125b to RNU48 and to cel-miR-39 was calculated by the equation $2^{-\Delta Ct}$, where $\Delta Ct = Ct$ miR − 125b − Ct RNU48 (placenta) and $\Delta Ct = Ct$ miR-125b − Ct cel-miR-39 (plasma) (28).

Statistical analysis for the clinical study. MiR-125b expression was analysed after log transformation. We used a non-parametric approach, because the Shapiro test demonstrated that the quantitative variables had a non-normal distribution. The quantitative variables were summarized using median and interquartile range (IQR, 1st-3rd quartiles), respectively, as a measure of centrality and variability; the qualitative variables were expressed as absolute and percent frequency. Between-group comparisons were performed using Wilcoxon's rank sum test and Fisher's exact test for quantitative and qualitative variables, respectively.

Multiple logistic regression was applied to estimate the independent effect of women' characteristics and log miR-125b on the probability of developing PE, and 95% confidence intervals (95% CI) were calculated. The most parsimonious model was obtained by including the variables that were significant on the likelihood ratio test. The model's goodness of fit was assessed with the Hosmer-Lemeshow test. The accuracy of the model in predicting PE was analysed using a ROC plot, the Area Under the Curve (AUC) and 95% CIs. The R statistical program was used for the analyses; a probability of 0.05 was set as the threshold for statistical significance.

***In vitro* cultures to establish whether placental Trop-2 protein is a miR-125b target.** To investigate Trop-2 localization, the first-trimester cytotrophoblast cell line HTR-8/SVneo (kindly provided by C. H. Graham, Queen's University, Kingston, ON, Canada) and the BeWo human placental cell line derived from choriocarcinoma (kindly provided by S. Alberti, Laboratory of Cancer Pathology, CeSI-MeT, University 'G. d'Annunzio', Chieti, Italy) were used as *in vitro* cytotrophoblast and syncytiotrophoblast models, respectively (53).

HTR-8/SVneo cells were cultured in RPMI-1640 medium (Euroclone S.p.A., Pero, Italy) with 10% foetal bovine serum (FBS; Gibco, Life Technologies, Waltham, MA, USA), 1% penicillin, 1% streptomycin, 1% L-glutamine at 37˚C, 20% O_2 and 5% CO_2. BeWo cells were cultured in Dulbecco's Modified Eagle Medium (DMEM) and Ham's F12 (both from Euroclone S.p.A.) 1:1 supplemented with 10% FBS, 1% penicillin, 1% streptomycin at 37˚C, 20% O_2 and 5% CO_2.

The BeWo cell line was used as a model to study Trop-2 expression in hypoxic conditions, to mimic PE. To mimic hypoxia, BeWo cells were incubated at 37˚C with 3% O_2, 92% N_2 and 5% CO_2 for 48 h. To demonstrate whether Trop-2 is a miR-125b target, BeWo cells (2.5×10^5) incubated at 37˚C with 20% O_2 and 5% CO_2 were seeded in 6-well plates and transfected with a complex containing X-tremeGene 9 DNA Transfection Reagent (Roche Applied Science, Penzberg, Germany) and mirVana miRNA mimic (cat. # MC10148 MIMAT0000423) or mirVana miRNA inhibitor (cat. # MH10148 MIMAT0000423, both from Ambion, Life Technologies, Monza, Italy). The ratio of transfecting agent to mimic or inhibitor was 6:1; the final oligonucleotide concentration was 30 nM. Cells were incubated for 48 h. The experiments were performed 3 times with two biological replicates each time. MG63 cells and placental

Table 2. Primary antibodies used

Antibody	Specificity	Catalogue #	Application	Concentration	Source
Mouse mAb	Human Trop-2	sc-376746	IHC, IF, WB	1:50 (IHC, IF) 1:250 (WB)	Santa Cruz Biotechnology, Santa Cruz, CA, USA
Rabbit pAb	Human CD138	PA5-16918	IF	1:100	Thermo Fisher Scientific, Rockford, IL, USA
Mouse mAb	Human Bcl-2	M0887	IF	1:50	Dako, Glostrup, Denmark
Rabbit pAb	Human RKIP	07-137	IF	1:400	Upstate Biotechnology, Lake Placid, NY, USA
Goat pAb	Human β-actin	sc-1616	WB	1:200	Santa Cruz Biotechnology, Santa Cruz, CA, USA
Rabbit pAb	Human GAPDH	A300-641A-T	WB	1:1000	Bethyl Laboratories, Montgomery, TX, USA

mAb: monoclonal antibody; pAb: polyclonal antibody; IHC: immunohistochemistry; IF: immunofluorescence; WB: western blotting.

tissue from women in the 3rd trimester of gestation were used as positive controls for Trop-2 (54).

Western blot analysis of Trop-2 in HTR-8/SVneo and BeWo cells. For protein extraction, cell pellets were collected and incubated with lysis buffer in ice for 30 min and centrifuged at 14,000 g for 20 min at 4˚C. Supernatants were aliquoted and stored at -80˚C until use. Protein concentration was determined by the Bradford assay (Bio-Rad Protein Assay Dye Reagent Concentrate; Bio-Rad Laboratories, Milano, Italy). Protein samples (50 μg each) were fractionated in 15% SDS-PAGE gel and electrophoretically transferred to Trans-Blot Turbo Mini Nitrocellulose membranes with Trans-Blot Turbo Transfer System (all from Bio-Rad Laboratories).

Membranes were incubated with 5% milk in distilled water to block non-specific sites and then with monoclonal mouse Trop-2 antibody (Table 2) in TBS with 0.05% Tween 20 (TBS-T) at 4˚C overnight. After washing with TBS-T, membranes were incubated with the secondary anti-mouse antibody conjugated to horseradish peroxidase (Santa Cruz Biotechnology) at 1:1500 dilution. Antibody binding was detected with Clarity Western ECL Substrate and images were acquired with Chemidoc (both from Bio-Rad Laboratories). Densitometric analysis was performed with ImageJ software (https://imagej.nih.gov/ij/download.html). The housekeeping genes *GAPDH* and β-actin were used to normalize cell and tissue values, respectively (see antibodies in Table 2). HTR-8/SVneo cells were negative for Trop-2.

Trop-2 immunohistochemistry and immunofluorescence in placental tissue. Trop-2 localization in normal and PE samples from 1st- and 3rd-trimester placenta was investigated by immunohistochemistry.

Paraffin sections were deparaffinized and rehydrated with xylene and a graded ethyl alcohol series. To inhibit endogenous peroxidase activity, sections were incubated with 3% hydrogen peroxide in methanol and treated with 0.3% Tween 20 in phosphate-buffered saline (PBS) 1X for 20 min at room temperature for antigen retrieval. To block non-specific background, sections were incubated with normal horse serum (Vector Laboratories, Burlingame, CA, USA) diluted 1:75 in PBS. Sections were incubated with mouse monoclonal Trop-2 antibody (Table 2) overnight at 4˚C. After washing in PBS, sections were incubated with horse anti-mouse biotinylated antibody diluted 1:200 (Vector Laboratories) for 30 min. The avidin-biotin-peroxidase complex (ABC) method (Vector Laboratories) was performed using 3′,3′-diaminobenzidine hydrochloride (Sigma-Aldrich, St. Louis, MO, USA) as the chromogen. Sections were counterstained with Mayer's haematoxylin, dehydrated and mounted with Eukitt solution (Kindler GmbH and Co., Freiburg, Germany). Negative controls involved omitting the primary antibody; normal human skin was the positive control (55,56).

Trop-2 protein localization was investigated by immunofluorescence and confocal microscopy. Two double reactions were performed using Bcl-2 as a syncytiotrophoblast (57) and Trop-2 marker and RKIP as a cytotrophoblast (58) and Trop-2 marker, to establish whether Trop-2 is localized in one or the other cell type.

Tissue samples were deparaffinized and hydrated with xylene and a graded alcohol series. To reduce autofluorescence, samples were incubated with 0.1% Sudan Black B (Sigma-Aldrich) in 70% ethanol for 30 min then washed with PBS 1X with 0.03% Tween 20. In double-staining reactions, sections for antigen retrieval were incubated i) with Tris-EDTA buffer pH 9.0 at 95˚C for 30 min (Trop-2/Bcl-2) or ii) with 0.3% Tween 20 in PBS for 20 min at room temperature (Trop-2/RKIP). Sections were then washed twice with PBS 1X. Non-specific sites were blocked with 3% bovine serum albumin in PBS 1X for 30 min, then sections were incubated with mouse monoclonal Trop-2 antibody (Table 2) overnight at 4˚C. Sections were washed and incubated with anti-mouse secondary antibody (Alexa Fluor® 594, 1:400 dilution; Invitrogen, Carlsbad, CA, USA). After washing, they were incubated with mouse monoclonal Bcl-2 antibody as a syncytiotrophoblast marker (57) or with RKIP as a cytotrophoblast marker (58), both overnight at 4˚C (Table 2). Samples were washed and incubated with donkey anti-mouse (Bcl-2) or donkey anti-rabbit (RKIP) Alexa Fluor® 488 secondary antibody (1:400 dilution, Invitrogen) for 30 min. Slides were then incubated with TO-PRO-3® Iodide (1:3000 dilution, Invitrogen) for 10 min for nuclear staining, washed and mounted onto glass slides using Vectashield mounting medium (Vector Laboratories). Negative controls were performed by omitting the primary antibody.

Sections were analysed with a motorized Leica DM6000 microscope (Leica Microsystems srl, Milano, Italy) at different magnifications. Fluorescence was detected with a Leica TCS-SL spectral confocal microscope equipped with an Argon and a He/Ne mixed gas laser. Fluorophores were excited with the 488, 543 and 649 nm lines and imaged separately. Images (1024 × 1024 pixels) were obtained sequentially from two channels using a confocal pinhole of 1.1200 and stored as TIFF files.

Western blot analysis of placental tissue sections. For protein extraction, 1st- and 3rd-trimester placenta samples from healthy pregnancies and pregnancies complicated by PE were homogenized using an Ultra-Turrax T8 apparatus (IKA-WERKE, Lille, France) in lysis buffer containing PBS 1X, 0.1% SDS, 1% NONIDET-P40, 1 mM orthovanadate sodium, 12 mM deoxycholate

sodium, 1 mM phenylmethylsulfonyl fluoride (PMSF) and 1.7 μg/ml aprotinin and centrifuged at 16,000 g for 20 min at 4˚C. Pellets were discarded and supernatants were collected and stored at -80˚C until use. Western blot analysis was performed as described above.

Analysis of tissue miR-125b for the biomolecular and morphological study. Total RNA was extracted from formalin-fixed paraffin-embedded (FFPE) samples of 1st- and 3rd-trimester placenta from healthy and PE pregnancies using FFPE RNA/DNA Purification Kit (Norgen Biotek Corp.) according to the manufacturer's protocol. RT-PCR and miR-125b quantification were as described above.

Statistical analysis for the biomolecular and morphological study. Trop-2 levels were reported as mean ± standard deviation (SD) and represented as histograms. MiR-125b levels were analysed after log transformation. Median and IQR were used respectively as a measure of centrality and variability and graphically represented as boxplots. The Mann-Whitney test was applied to between-group comparisons and the Kruskal-Wallis test to comparisons among three groups.

GraphPad Prism 7 (https://www.graphpad.com/scientific-software/prism/) was used for the analyses; a probability of 0.05 was set as the threshold for statistical significance.

Table 3. Demographics, lifestyle factors, clinical characteristics and log miR-125b levels in relation to participant health status

	Healthy women	Women with pre-eclampsia	
Variables	n=18	n=13	P
Maternal age (years)#	30 (28;35)	33 (31;34)	0.199
Gestational age#	39 (38;40)	39 (38;39)	0.367
Smoking (yes/quit)§	3 (16.7)	1 (7.7)	0.621
Poor diet§	5 (27.8)	4 (30.8)	0.999
Physical activity (yes)§	13 (72.2)	7 (53.8)	0.114
BMI before pregnancy#	20 (19;22)	23 (21;28)	0.039
log miR-125b#	-8.14 (-9.04;-7.88)	-7.16 (-8.27;-6.1)	0.040
Birth weight (gg)#	3.175 (2.95;3.5)	3.1 (2.95;3.3)	0.410

BMI: body mass index; # median and interquartile range (1st-3rd quartiles); § absolute and percent frequencies
P values: # Wilcoxon rank sum test; § Fisher's exact test

Table 4. Effect estimate of the factors associated with pre-eclampsia. Results of multiple logistic regression analysis.

	Odd ratio	95% confidence interval
log miR-125b	2.17	1.11; 5.35
Maternal age (years)	1.15	0.94; 1.48
BMI before pregnancy (kg/m^2)	1.24	1.02; 1.68

Hosmer and Lemeshow goodness of fit test: χ^2 test with 8 df, χ^2=8.11,
p= 0.423 Likelihood ratio test: χ^2 test with 3 df, χ^2=13.01, p=0.004

RESULTS

Clinical study: PE prediction model based on miR-125b levels. The demographics, lifestyle factors, BMI values and log miRNA-125b plasma levels of women with a normal pregnancy and of those whose pregnancy was complicated by PE are reported in Table 3. Whereas healthy women and PE cases were similar in terms of age, smoking and dietary habits, physical activity, gestational age at delivery and newborn birth weight, PE cases had a significantly higher BMI before pregnancy and significantly higher log miR-125b levels at 12 weeks. The multiple logistic regression analysis (Table 4) showed that PE was significantly associated with log miR-125b (relative expression), maternal age and BMI before pregnancy. In particular, the likelihood of developing PE more than doubled with every additional log miR-125b unit and it increased by about 24% with every additional BMI unit.

The ROC plot showed that the model displayed a good accuracy in predicting PE, as demonstrated by an AUC of 0.85 (95%CI: 0.70-1.00) (Figure 1).

Trop-2 is a miR-125b target, as demonstrated by an* in vitro *placental model. An *in vitro* approach was devised to document whether Trop-2 is targeted by miR-125b. HTR8/SV-neo cells, used as a cytotrophoblast model, were negative for Trop-2 (Figure 2A), indicating that the protein is not found in villous cytotrophoblasts. Forskolin-induced syncytialization (58) demonstrated that BeWo cells could be used as an *in vitro* syncytiotrophoblast model and, as expected, they were positive for Trop-2 (Figure 2B). Syncytialized BeWo cells cultured in hypoxic conditions (3% O_2) to mimic the PE environment demonstrated significant (p=0.03) Trop-2 downregulation compared with control cells cultured in normal atmospheric conditions (20% O_2) (Figure 2C; quantification in Figure 2D). Their transfection with the miR-125b mimic also induced significant (p=0.0005) Trop-2 downregulation, as demonstrated by the Western blots (Figure 2D; quantification in Figure 2F), thus confirming that Trop-2 is targeted by miR-125b.

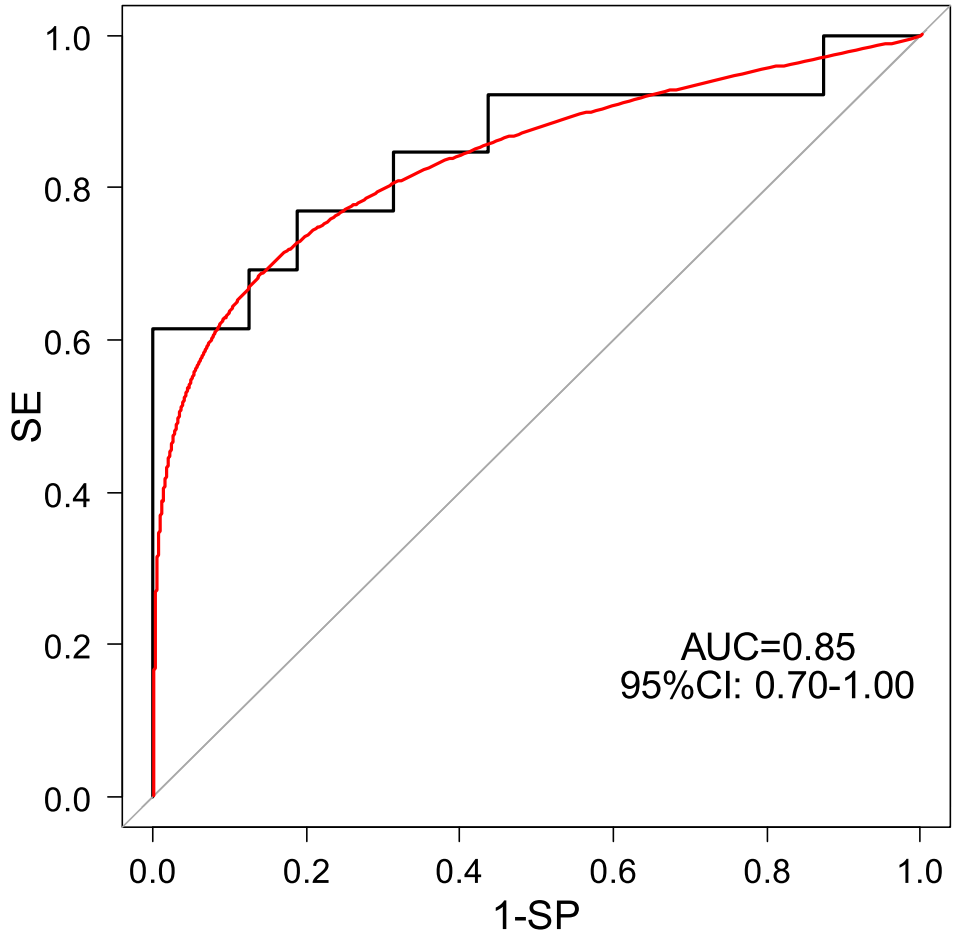

Figure 1. ROC curve for the predictiveness of pre-eclampsia (black curve=raw data; red curve=smoothed ROC curve). The ROC curve was estimated by entering in the model log miR-125b, BMI before pregnancy and gestational age at delivery (variables with $p < 0.10$). SE: Sensitivity; SP: Specificity; AUC: Area Under Curve; 95%CI: 95% Confidence Interval.

Trop-2 protein, a miR-125b target, is expressed in normal and PE placenta, as demonstrated by biomolecular and morphological analyses. Immunohistochemical analysis demonstrated Trop-2 protein (brown staining in Figure 3,A-F) in the syncytiotrophoblast basal plasma membrane in 1st-trimester (Figure 3A,B) and 3rd-trimester (Figure 3C,D) normal and PE placenta (Figure 3E,F). Trop-2 localization in the syncytiotrophoblast was demonstrated by double immunofluorescence in first trimester placenta (Figure 4a e 4b). In fact, yellow staining (merged image, yellow arrows) showed that Trop-2 (red) co-localized with the syncytiotrophoblast marker Bcl-2 (green) (Figure 4a), whereas the absence of yellow staining demonstrated that Trop-2 (red) did not co-localize with the cytotrophoblast marker RKIP (green) (Figure 4b).

Western blot analysis demonstrated a significant increase in Trop-2 from the 1st to the 3rd trimester in placenta from normal pregnancies (Figure 5A) and a significantly decreased in gestational age-matched PE placenta (Figure 5B).

MiR-125b is expressed in normal and PE placental tissue, as demonstrated by biomolecular analysis. From the 1st to the 3rd trimester, miR-125b levels in normal placenta (Figure 6A) showed a significantly greater increase compared to gestational age-matched PE placenta (Figure 6B).

DISCUSSION

This study describes how an early PE prediction model based on plasma miR-125b levels, maternal age and BMI before pregnancy was developed and tested. Since the experimental work also established that Trop-2 is a miR-125b target, we also found that miR-125b may be involved in PE development through

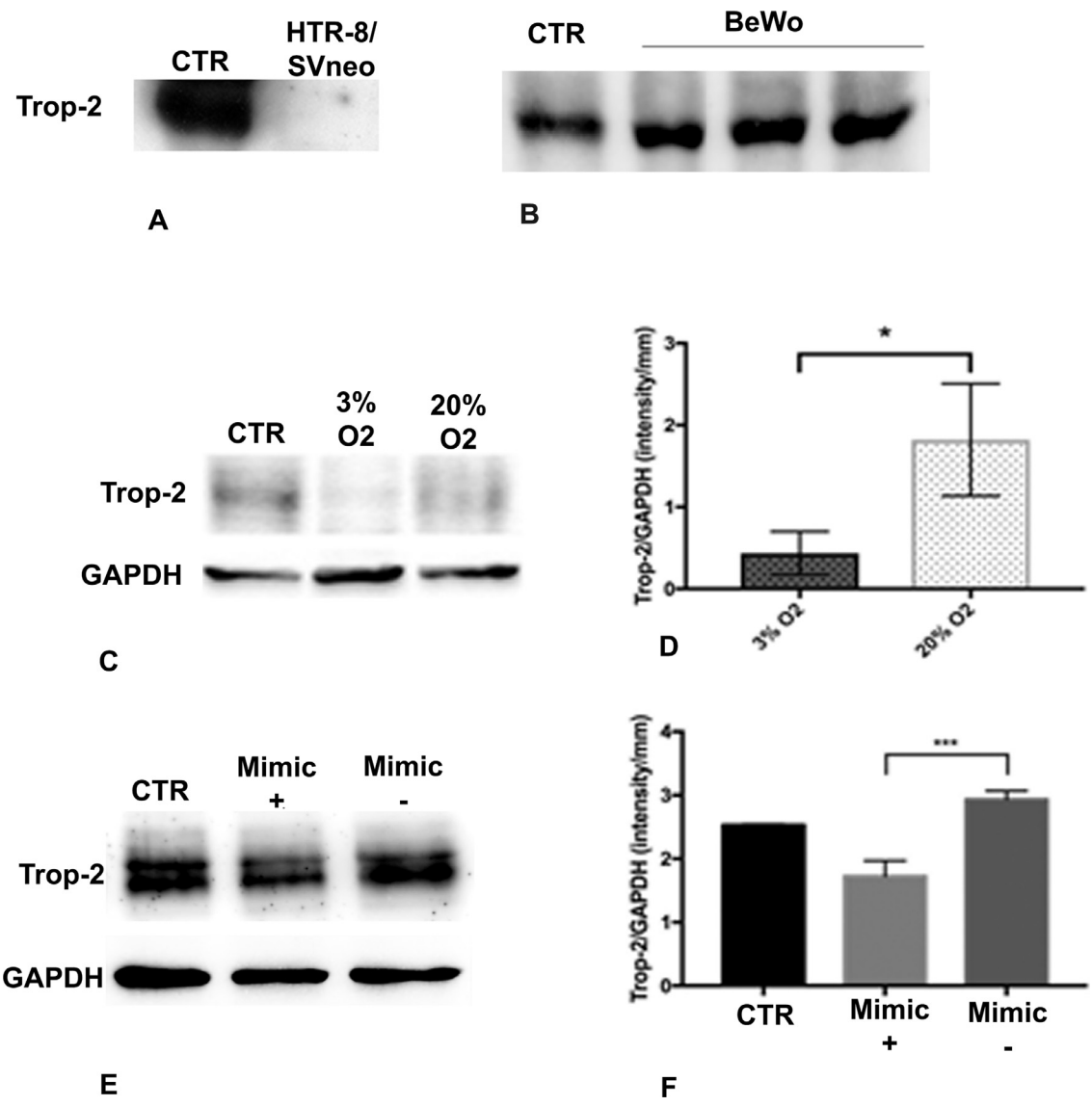

Figure 2. *In vitro* model of Trop-2 protein, a miR-125b target. A) HTR-8/SVneo cells were negative for Trop-2 whereas BeWo cells (B, shown in triplicate) with forskolin-induced syncytialization were positive for Trop-2. The MG63 cell line was used as a positive control. C) Representative Western blot of BeWo cells with forskolin-induced syncytialization cultured at 3% O_2 and 20% O_2 and histogram representing band quantification (D). Representative blot (E) and histogram (F) of BeWo cells treated with forskolin and transfected with miR-125b mimic and negative mimic (*: p = 0.03; ***: p = 0.0005). CTR: control placental tissue in the 3rd trimester of gestation.

modulation of Trop-2 expression in the syncytiotrophoblast. Our findings therefore have clear clinical implications.

Although the key pathological changes related to PE arise well before the 20th week of gestation, its clinical symptoms do not manifest before this time (1). From a clinical point of view, pregnant women who are at high risk of developing PE seem to benefit from prophylactic treatment; for instance, low-dose aspirin administered before the 16th week has been seen to reduce the risk and attenuate the severity of the maternal and foetal outcomes, not to mention the social, economic and healthcare impacts of PE (60,61).

Early detection would of course be more effective. However, although several promising predictors have been identified – *e.g.* uterine artery ultrasonography, maternal serum/urinary levels of human chorionic gonadotropin, inhibin A and activin A, pregnancy-associated plasma protein A, sex hormone-binding globulin, placental growth factor, soluble fms-like tyrosine kinase 1 and serum placental protein 13 (62-65) – PE screening in early pregnancy is still poorly

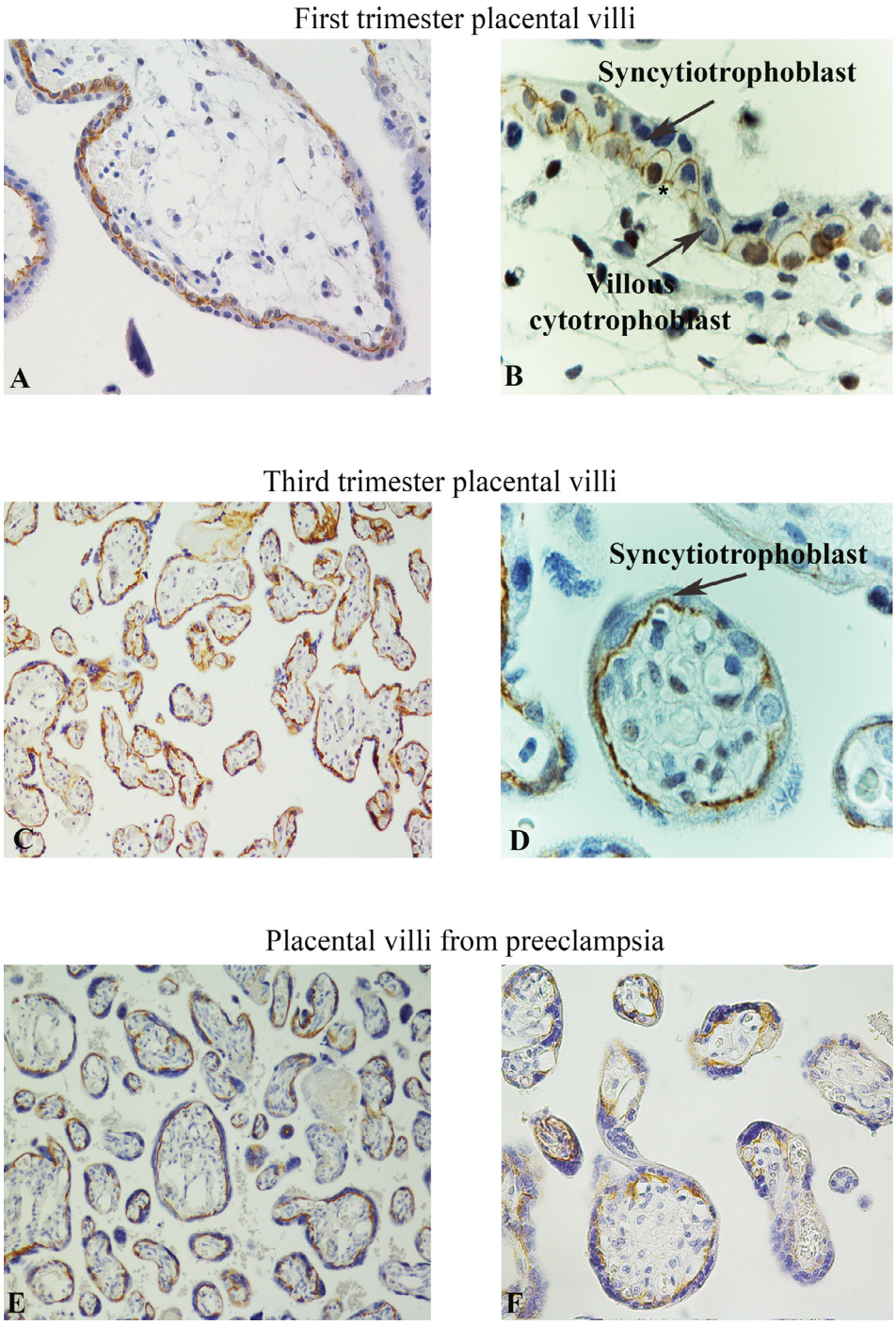

Figure 3. Trop-2 expression in normal placenta and placenta from pregnancies complicated by PE by immunohistochemistry. Trop-2 expression in 1st-trimester placenta (A, B), 3rd-trimester placenta (C, D) and in placental samples from pregnancies complicated by PE (E,F). The brown Trop-2 staining is localized in the basal part of the syncytiotrophoblast in all samples. B) Note the brown immunostaining of the syncytiotrophoblast between two villous cytotrophoblast cells (*).

effective. Several stable miRNAs with important regulatory roles in proliferation, apoptosis and cell-cell communication have been identified and quantified during pregnancy (27-29,66-79). Some are expressed in the 3rd trimester whereas for some miRNAs identified in the 1st trimester a target protein has not yet been identified. MiR-125b overexpression in the 1st trimester has been reported in women who went on to

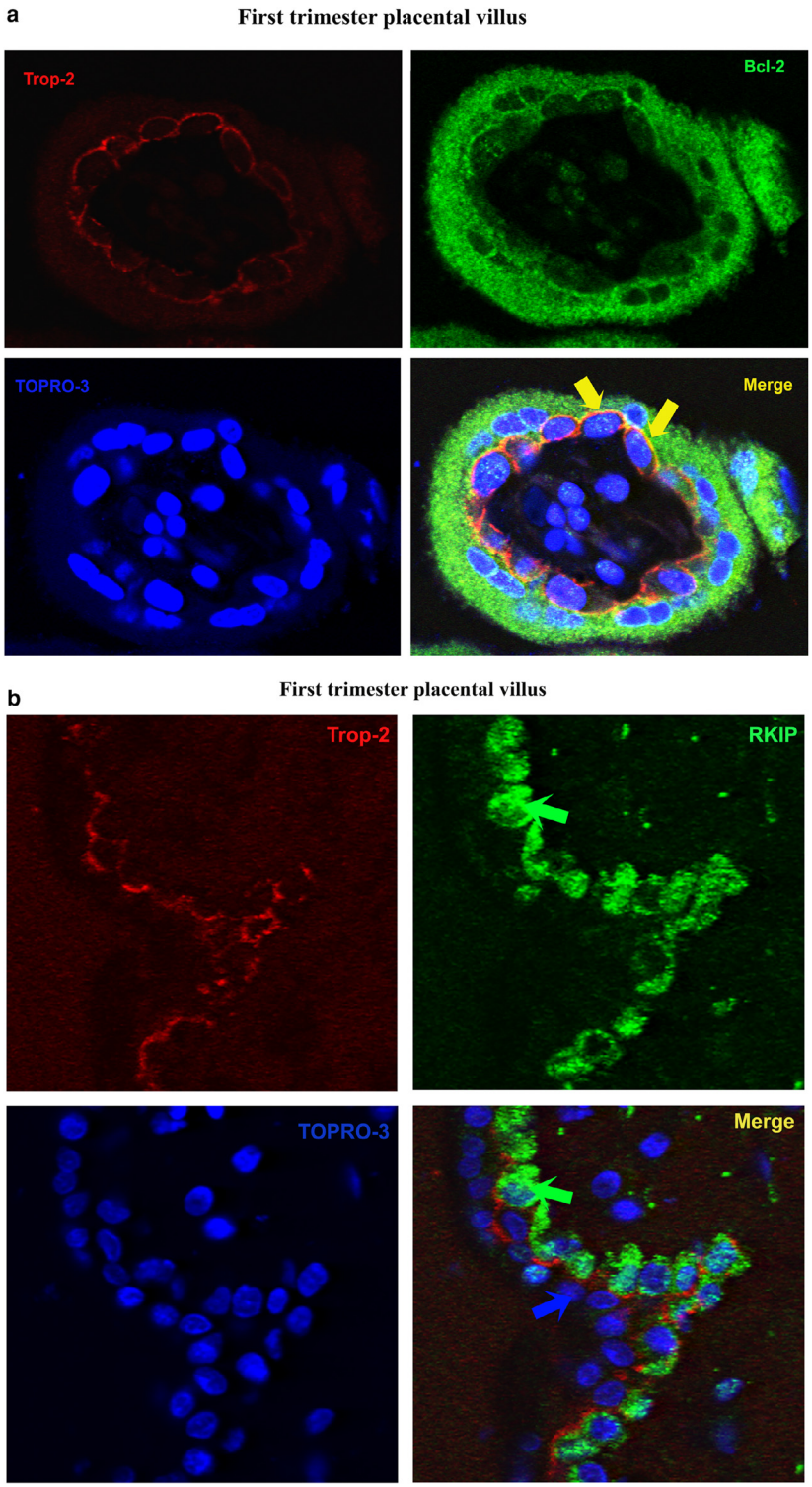

Figure 4. a) Double staining detected by confocal microscopy in a 1st-trimester placental villus showing Trop-2 and Bcl-2 colocalization in the syncytiotrophoblast. Trop-2 stained red whereas Bcl-2, a syncytiotrophoblast marker, stained green. The nuclei are blue. Merge (yellow) shows that Trop-2 and Bcl-2 are colocalized in the basal part of the syncytiotrophoblast (yellow arrows). 100X magnification. b) Double staining detected by confocal microscopy in a 1st-trimester placental villus showing no Trop-2/RKIP colocalization. Trop-2 stained red; RKIP, a villous cytotrophoblast marker, stained green (green arrows). Trop-2 and RKIP are not colocalized in the villous cytotrophoblast. Blue arrow points at syncytiotrophoblast nuclei. No yellow staining is detected in Merge. 40X magnification.

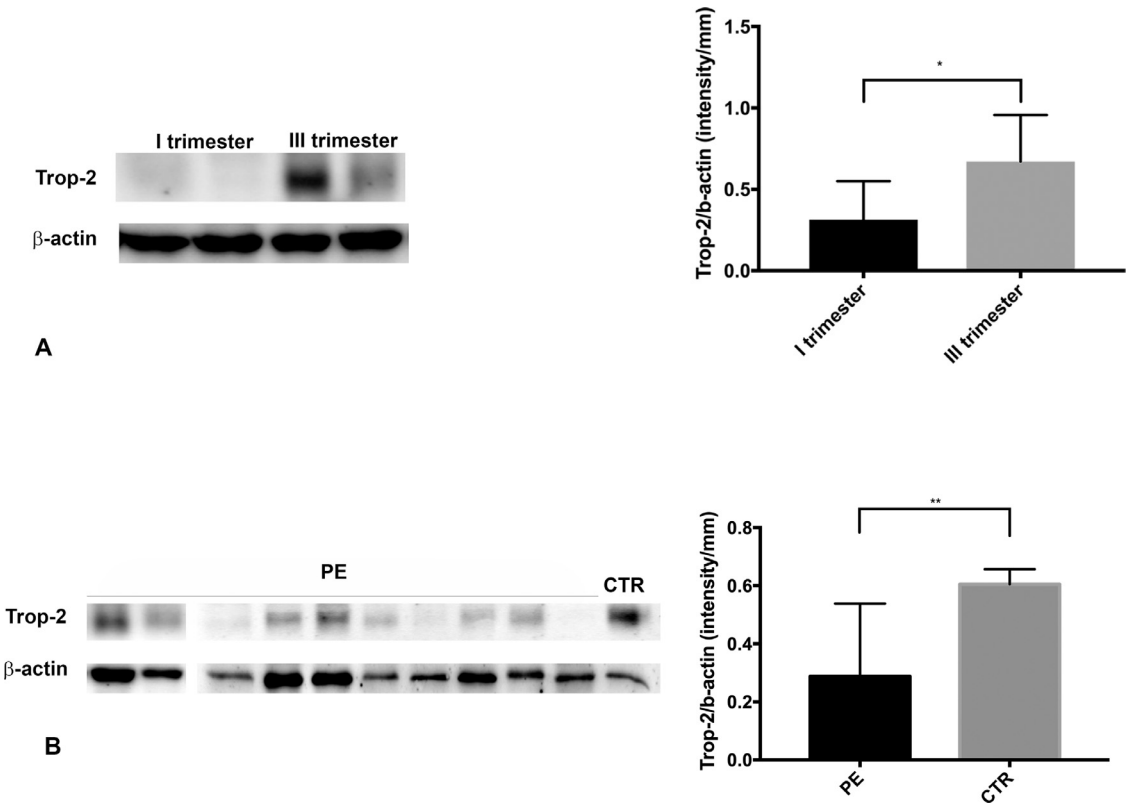

Figure 5. Western blot analysis of Trop-2 in placental tissue. A) Trop-2 increased significantly from the 1st to the 3rd trimester; B) Trop-2 protein decreased significantly in PE placenta (*: $p \leq 0.05$; **: $p \leq 0.01$; ***; $p \leq 0.001$). CTR: normal gestational age-matched placenta. PE=pre-eclampsia.

develop PE, as also documented in our study. The results of randomized controlled trials of a number of biomarkers, tested to identify high-risk women, have also been disappointing, possibly because the sensitivity of most of them is highest in the 2nd trimester, long after PE has become clinically manifest. A recent study of the ability of a miRNA panel to predict PE (27) has found that none showed a good performance (*i.e.* greater than 0.70). Some studies have denied a PE predictive value for miRNAs in 1st trimester maternal serum/plasma. However, the population investigated by Luque et al (80) included only early PE and no late PE cases; other studies evaluated miR-125b only in the 3rd trimester (81) or compared only two cases to two controls (82,83). However, in 2013 Gu et al. (20) described miR-125b localization in trophoblasts during gestation (20), whereas two interesting papers have described an association between miR-125b and PE, suggesting a possible role for this miRNA in PE onset (66,67). The present study found significant plasma miR-125b overexpression in 1st-trimester plasma from women who went on to develop PE. Since according to multiple regression analysis BMI before pregnancy and maternal age are associated with PE development, these three factors were entered in a model for PE prediction. Testing of the model demonstrated that it showed a good performance, with an AUC equal to 0.85.

As regards the biomolecular and morphological study, data analysis also demonstrated that miR-125b was underexpressed and Trop-2 was downregulated in PE placenta compared with control samples. These data suggest that maternal miR-125b is involved in Trop-2 modulation in placental tissue. Combined with the *in vitro* demonstration that Trop-2 is targeted by miR-125b, which reduces its expression, our findings suggest that maternal miR-125b overexpression at 12 weeks of gestation could be involved in the early onset of PE through an action on Trop-2 concentrations from the earliest phases of placental development.

We feel that this paper has a number of strengths: i) a complex and rigorous design, involving the prospective collection of 1st-trimester plasma samples, the collection of healthy placenta at two different time points and the collection of gestational-age-matched normal and PE placenta; ii) biomolecular and morphological analyses to establish that placental Trop-2 is targeted by miR-125b and to identify its site of action, which

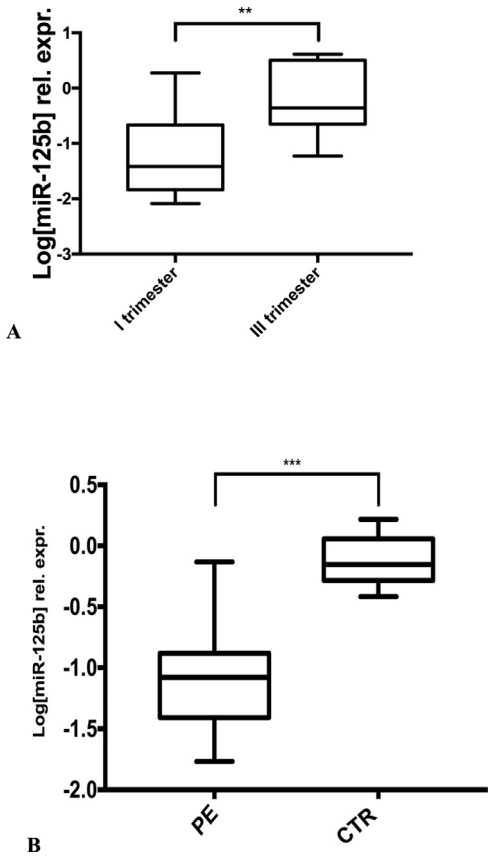

Figure 6. Relative miR-125b expression in 1st- and 3rd-trimester normal placenta and in placenta from pregnancies complicated by PE. A) Boxplot of relative miR-125b expression (RT-PCR) in 1st- and 3rd-trimester placenta showing miR-125b overexpression in placental tissue at term; B) Boxplot of relative miR-125b expression (RT-PCR) in PE placenta showing a significant reduction of miR-125b (**: $p \leq 0.01$; ***: $p \leq 0.001$). CRT: normal gestational age-matched placenta. PE=pre-eclampsia.

has implications for diagnostic and treatment strategies; and iii) the development of an accurate PE prediction model based on easily measurable parameters, *i.e.* BMI before pregnancy and maternal age.

Its limitations include the facts that we did not investigate other miRNAs that may be involved in Trop-2 modulation; that the overexpression of plasma miR-125b at 12 weeks of gestation in women who will eventually develop PE could be the effect, rather than the cause of PE, with Trop-2 downregulation being the downstream effect; and the limited sample size used to evaluate the prognostic role of miR-125b. However, PE is a rare condition, and the size of the sample was determined by the number of women who developed PE in the cohort study (51) in which this case-control study was nested. Moreover, our analysis demonstrated a significant and accurate predictive role for miR-125b. Further research is clearly needed to confirm its role and to elucidate the contributions of other differentially expressed miRNAs in the placenta of PE patients; a more powerful, large-scale, multicentre study is required to validate the model.

In conclusion, the practical, non-invasive and efficient screening method to identify women at risk of developing PE described herein can contribute to its prevention and early treatment, whereas the identification of a protein target of miR-125b in placental tissue and its downregulation in PE placenta advances our mechanistic understanding of the complications of PE and provide insights for PE prevention strategies.

AUTHOR CONTRIBUTION

Provision of clinical specimens: Stefano Raffaele Giannubilo, Gian Carlo Di Renzo, Andrea Ciavattini, Nicoletta Di Simone, Irene Giardina, Chiara Tersigni; Study conception and design: Caterina Licini, Fabiola Olivieri, Daniela Marzioni; Experimental assays and data analysis: Caterina Licini, Emanuela Mensà, Giovanni Tossetta, Chiara Avellini, Elena Picchiassi, Deborah Ramini, Clara Castellucci, Giuliana Coata, Rosaria Gesuita Sonia Fantone and Federica Tarquini; Data interpretation, manuscript preparation and revision: Caterina Licini, Daniela Marzioni, Fabiola Olivieri, Rosaria Gesuita, Stefano Raffaele Giannubilo, Nicoletta Di Simone.

ACKNOWLEDGEMENTS

We are grateful to Dr Charles Graham (Queen's University, Kingston, ON, Canada) for his kind gift of HTR-8/SV-neo cells, to Prof Luca Tiano (Università Politecnica delle Marche, Ancona, Italy), to Prof Berthold Huppertz (Medical University of Graz, Graz, Austria), and to Prof Saverio Alberti and Dr Emanuela Guerra (Laboratory of Cancer Pathology, CeSI-MeT, University 'G. d'Annunzio', Chieti, Italy) for valuable advice, and to Dr. Martina Senzacqua for her technical assistance with the confocal microscope. All authors have read the journal's authorship agreement and policy on disclosure of potential conflicts of interest and they declare no conflict of interest. They have read, reviewed and approved the manuscript. **Financial support**: This work was supported partly by Italian Ministry of University and Research (PRIN 2010) to GCDR, SRG and by a Scientific Research Grant from Università Politecnica delle Marche (RSA 2016-2017-2018) to SRG, FO, DM.

REFERENCES

1. ACOG Committee on Obstetric Practice. Practice bulletin #33: diagnosis and management of preeclampsia and eclampsia. Obstetrics & Gynecology 2002;99(1):159–67.

2. Sibai B, Dekker G, Kupferminc M. Pre-eclampsia. The Lancet 2005;365(9461):785–99.
3. Brosens I, Brosens JJ, Muter J, Puttemans P, Benagiano G. Pre-eclampsia: the role of persistent endothelial cells in uteroplacental arteries. Am J Obstet Gynecol 2019;S0002-9378(19):30320–3.
4. Poon LC, Shennan A, Hyett JA, Kapur A, Hadar E, Divakar H, McAuliffe F, da Silva Costa F, von Dadelszen P, McIntyre HD, Kihara AB, Di Renzo GC, Romero R, D'Alton M, Berghella V, Nicolaides KH, Hod M. The International Federation of Gynecology and Obstetrics (FIGO) initiative on pre-eclampsia: A pragmatic guide for first-trimester screening and prevention. Int J Gynaecol Obstet 2019;145(Suppl 1):1–33.
5. Khan KS, Wojdyla D, Say L, Gülmezoglu AM, Look PFV. WHO analysis of causes of maternal death: a systematic review. The Lancet 2006;367(9516):1066–74.
6. Abalos E, Cuesta C, Carroli G, et al. Pre-eclampsia, eclampsia and adverse maternal and perinatal outcomes: a secondary analysis of the World Health Organization Multicountry Survey on Maternal and Newborn Health. BJOG 2014;121:14–24.
7. Redman CW, Sargent IL. Latest advances in understanding pre-eclampsia. Science 2005;308(5728):1592–4.
8. Chaiworapongsa T, Romero R, Erez O, Tarca AL, Conde-Agudelo A, Chaemsaithong P, et al. The prediction of fetal death with a simple maternal blood test at 20-24 weeks: a role for angiogenic index-1 (PlGF/sVEGFR-1 ratio). Am J Obstet Gynecol 2017;217:682., e1-682.e13.
9. Leaños-Miranda A, Navarro-Romero CS, Sillas-Pardo LJ, Ramírez-Valenzuela KL, Isordia-Salas I, Jiménez-Trejo LM. Soluble Endoglin As a Marker for Preeclampsia, Its Severity, and the Occurrence of Adverse Outcomes. Hypertension 2019;74(4):991–7.
10. Haram K, Mortensen JH, Myking O, Roald B, Magann EF, Morrison JC. Early development of the human placenta and pregnancy complications. J Matern Fetal Neonatal Med 2019;27:1–8.
11. Villar J, Carroli G, Wojdyla D, Abalos E, Giordano D, Ba'aqeel H, et al. Preeclampsia, gestational hypertension and intrauterine growth restriction, related or independent conditions? American Journal of Obstetrics & Gynecology 2006;194(4):921–31.
12. Labarrere CA, DiCarlo HL, Bammerlin E, Hardin JW, Kim YM, Chaemsaithong P, et al. Failure of physiologic transformation of spiral arteries, endothelial and trophoblast cell activation, and acute atherosis in the basal plate of the placenta. Am J Obstet Gynecol 2017;216(3):287., e1-287.e16.
13. Armant DR, Fritz R, Kilburn BA, Kim YM, Nien JK, Maihle NJ, et al. Reduced expression of the epidermal growth factor signaling system in preeclampsia. Placenta 2015;36(3):270–8.
14. Roland CS, Hu J, Ren C-E, Chen H, Li J, Varvoutis MS, et al. Morphological changes of placental syncytium and their implications for the pathogenesis of preeclampsia. Cell Mol Life Sci 2016;73(2):365–76.
15. Tannetta D, Collett G, Vatish M, Redman C, Sargent I. Syncytiotrophoblast extracellular vesicles - Circulating biopsies reflecting placental health. Placenta 2017;52:134–8.
16. Shah NR, Chen H. MicroRNAs in pathogenesis of breast cancer: Implications in diagnosis and treatment. World J Clin Oncol 2014;5(2):48–60.
17. Niu S, Ma X, Zhang Y, Liu Y-N, Chen X, Gong H, et al. MicroRNA-19a and microRNA-19b promote the malignancy of clear cell renal cell carcinoma through targeting the tumor suppressor RhoB. PLOS ONE 2018;13(2):e0192790.
18. Paul P, Chakraborty A, Sarkar D, Langthasa M, Rahman M, Bari M, et al. Interplay between miRNAs and human diseases. J Cell Physiol 2018;233(3):2007–18.
19. Forbes K, Farrokhnia F, Aplin JD, Westwood M. Dicer-dependent miRNAs provide an endogenous restraint on cytotrophoblast proliferation. Placenta 2012;33(7):581–5.
20. Gu Y, Sun J, Groome LJ, Wang Y. Differential miRNA expression profiles between the first and third trimester human placentas. Am J Physiol Endocrinol Metab 2013;304(8):E836–43.
21. Pineles BL, Romero R, Montenegro D, Tarca AL, Han YM, Kim YM, et al. Distinct subsets of microRNAs are expressed differentially in the human placentas of patients with preeclampsia. Am J Obstet Gynecol 2007;196(3):261., e1-6.
22. Laganà AS, Vitale SG, Sapia F, Valenti G, Corrado F, Padula F, Rapisarda AMC, D'Anna R. miRNA expression for early diagnosis of preeclampsia onset: hope or hype? J Matern Fetal Neonatal Med 2018;31(6):817–21.
23. Mouillet J-F, Ouyang Y, Coyne CB, Sadovsky Y. MicroRNAs in placental health and disease. Am J Obstet Gynecol 2015;213(4 Suppl):S163–72.
24. Devor E, Santillan D, Scroggins S, Warrier A, Santillan M. Trimester-specific plasma exosome microRNA expression profiles in preeclampsia. J Matern Fetal Neonatal Med 2019:1–9.
25. Gan L, Liu Z, Wei M, Chen Y, Yang X, Chen L, et al. MiR-210 and miR-155 as potential diagnostic markers for pre-eclampsia pregnancies. Medicine (Baltimore) 2017;96(28):e7515.
26. Timofeeva AV, Gusar VA, Kan NE, Prozorovskaya KN, Karapetyan AO, Bayev OR, Chagovets VV, Kliver SF, Iakovishina DY, Frankevich VE, Sukhikh GT. Identification of potential early biomarkers of preeclampsia. Placenta 2018;61:61–71.
27. Hromadnikova I, Kotlabova K, Ivankova K, Krofta L. First trimester screening of circulating C19MC microRNAs and the evaluation of their potential to predict the onset of preeclampsia and IUGR. PLoS One;12(2):e0171756.
28. Zhang Y, Diao Z, Su L, Sun H, Li R, Cui H, Hu Y. MicroRNA-155 contributes to preeclampsia by down-regulating CYR61. Am J Obstet Gynecol 2010;202(5):466e1–7.
29. Ura B, Feriotto G, Monasta L, Bilel S, Zweyer M, Celeghini C. Potential role of circulating microRNAs as early markers of preeclampsia. Taiwan J Obstet Gynecol 2014;53(2):232–4.
30. Zhang Y, Huang G, Zhang Y, Yang H, Long Y, Liang Q, Zheng Z. MiR-942 decreased before 20 weeks gestation in women with preeclampsia and was associated with the pathophysiology of preeclampsia in vitro. Clin Exp Hypertens 2017;39(2):108–13.
31. Salomon C, Guanzon D, Scholz-Romero K, Longo S, Correa P, Illanes SE, Rice GE. Placental Exosomes as Early Biomarker of Preeclampsia: Potential Role of Exosomal MicroRNAs Across Gestation. J Clin Endocrinol Metab 2017;102(9):3182–94.
32. Li JY, Yong TY, Michael MZ, Gleadle JM. MicroRNAs: are they the missing link between hypoxia and pre-eclampsia? Hypertens Pregnancy 2014;33(1):102–14.
33. He J, Jing Y, Li W, Qian X, Xu Q, Li FS, Liu LZ, Jiang BH, Jiang Y. Roles and mechanism of miR-199a and miR-125b in tumor angiogenesis. PLoS One 2013;8(2):e56647.
34. Li Y, Chao Y, Fang Y, Wang J, Wang M, Zhang H, Ying M, Zhu X, Wang H. MTA1 promotes the invasion and migration of non-small cell lung cancer cells by downregulating miR-125b. J Exp Clin Cancer Res 2013;29:32., 33.
35. Sun Y-M, Lin K-Y, Chen Y-Q. Diverse functions of miR-125 family in different cell contexts. Journal of Hematology & Oncology 2013;6:627.
36. McDougall AR, Tolcos M, Hooper SB, Cole TJ, Wallace MJ. Trop2: From development to disease. Dev Dyn 2015;244(2):99–109.
37. Nakatsukasa M, Kawasaki S, Yamasaki K, Fukuoka H, Matsuda A, Tsujikawa M, et al. Tumor-Associated Calcium Signal

Transducer 2 Is Required for the Proper Subcellular Localization of Claudin 1 and 7. Am J Pathol 2010;177(3):1344–55.
38. McDougall ARA, Hooper SB, Zahra VA, Sozo F, Lo CY, Cole TJ, et al. The oncogene Trop2 regulates fetal lung cell proliferation. American Journal of Physiology - Lung Cellular and Molecular Physiology 2011;301(4):L478–89.
39. Ripani E, Sacchetti A, Corda D, Alberti S. Human Trop-2 is a tumor-associated calcium signal transducer. Int J Cancer 1998;76(5):671–6.
40. Pavšič M, Ilc G, Vidmar T, Plavec J, Lenarčič B. The cytosolic tail of the tumor marker protein Trop2−a structural switch triggered by phosphorylation. Sci Rep 2015;5:10324.
41. Lipinski M, Parks DR, Rouse RV, Herzenberg LA. Human trophoblast cell-surface antigens defined by monoclonal antibodies. Proc Natl Acad Sci U S A 1981;78(8):5147–50.
42. Fong D, Moser P, Krammel C, Gostner JM, Margreiter R, Mitterer M, et al. High expression of TROP2 correlates with poor prognosis in pancreatic cancer. Br J Cancer 2008;99(8):1290–5.
43. Mühlmann G, Spizzo G, Gostner J, Zitt M, Maier H, Moser P, et al. TROP2 expression as prognostic marker for gastric carcinoma. J Clin Pathol 2009;62(2):152–8.
44. Bignotti E, Todeschini P, Calza S, Falchetti M, Ravanini M, Tassi RA, et al. Trop-2 overexpression as an independent marker for poor overall survival in ovarian carcinoma patients. European Journal of Cancer 2010;46(5):944–53.
45. Guerra E, Trerotola M, Aloisi AL, Tripaldi R, Vacca G, La Sorda R, et al. The Trop-2 signalling network in cancer growth. Oncogene 2013;32(12):1594–600.
46. Trerotola M, Jernigan DL, Liu Q, Siddiqui J, Fatatis A, Languino LR. Trop-2 promotes prostate cancer metastasis by modulating β1 integrin functions. Cancer Res 2013;73(10):3155–67.
47. Lin H, Zhang H, Wang J, Lu M, Zheng F, Wang C, et al. A novel human Fab antibody for Trop2 inhibits breast cancer growth in vitro and in vivo. Int J Cancer 2014;134(5):1239–49.
48. Lin H, Zhang H, Wang J, Lu M, Zheng F, Wang C, et al. A novel human Fab antibody for Trop2 inhibits breast cancer growth in vitro and in vivo. Int J Cancer 2014;134(5):1239–49.
49. Nakanishi H, Taccioli C, Palatini J, Fernandez-Cymering C, Cui R, Kim T, et al. Loss of miR-125b-1 contributes to head and neck cancer development by dysregulating TACSTD2 and MAPK pathway. Oncogene 2014;33(6):702–12.
50. Avellini C, Licini C, Lazzarini R, Gesuita R, Guerra E, Tossetta G, et al. The trophoblast cell surface antigen 2 and miR-125b axis in urothelial bladder cancer. Oncotarget 2017 Aug 29;8 (35):58642–53.
51. Gesuita R, Licini C, Picchiassi E, Tarquini F, Coata G, Fantone S, Tossetta G, Ciavattini A, Castellucci M, Di Renzo GC, Giannubilo SR, Marzioni D. Association between first trimester plasma htra1 level and subsequent preeclampsia: A possible early marker? Pregnancy Hypertens 2019;18:58–62.
52. Bertino E, Spada E, Occhi L, Coscia A, Giuliani F, Gagliardi L, et al. Neonatal anthropometric charts: the Italian neonatal study compared with other European studies. JPGN 2010;51:353–61.
53. Orendi K, Gauster M, Moser G, Meiri H, Huppertz B. The choriocarcinoma cell line BeWo: syncytial fusion and expression of syncytium-specific proteins. Reproduction 2010;140(5):759–66.
54. Gu QZ, Nijiati A, Gao X, Tao KL, Li CD, Fan XP, Tian Z. TROP2 Promotes Cell Proliferation and Migration in Osteosarcoma Through PI3K/AKT Signaling. Mol Med Rep 2018;18 (2):1782–8.
55. Stepan LP, Trueblood ES, Hale K, Babcook J, Borges L, Sutherland CL. Expression of Trop2 Cell Surface Glycoprotein in Normal and Tumor Tissues. J Histochem Cytochem 2011;59 (7):701–10.
56. Marzioni D, Quaranta A, Lorenzi T, Morroni M, Crescimanno C, De MN, et al. Expression pattern alterations of the serine protease HtrA1 in normal human placental tissues and in gestational trophoblastic diseases. Histol Histopathol 2009;24(10):1213–22.
57. Marzioni D, Mühlhauser J, Crescimanno C, Banita M, Pierleoni C, Castellucci M. Bcl-2 expression in the human placenta and its correlation with fibrin deposits. Hum Reprod 1998;13(6):1717–22.
58. Ciarmela P, Marzioni D, Islam MS, Gray PC, Terracciano L, Lorenzi T, et al. Possible role of RKIP in cytotrophoblast migration: immunohistochemical and in vitro studies. J Cell Physiol 2012 May 1;227(5):1821–8.
59. Prakash GJ, Suman P, Gupta SK. Relevance of Syndecan-1 in the Trophoblastic BeWo Cell Syncytialization. American Journal of Reproductive Immunology 2011 Nov 1;66(5):385–93.
60. Roberge S, Bujold E, Nicolaides KH. Aspirin for the prevention of preterm and term preeclampsia: systematic review and meta-analysis. Am J Obstet Gynecol 2018;218:287-293.e1.
61. Li R, Tsigas EZ, Callaghan WM. Health and economic burden of preeclampsia: no time for complacency. Am J Obstet Gynecol 2017;217:235–6.
62. Chafetz I, Kuhnreich I, Sammar M, Tal Y, Gibor Y, Meiri H, Cuckle H, Wolf M. First-trimester placental protein 13 screening for preeclampsia and intrauterine growth restriction. Am J Obstet Gynecol 2007;197:35.e1-7.
63. Gray KJ, Saxena R, Karumanchi SA. Genetic predisposition to preeclampsia is conferred by fetal DNA variants near FLT1, a gene involved in the regulation of angiogenesis. Am J Obstet Gynecol 2018;218:211–8.
64. Levine RJ, Thadhani R, Qian C, et al. Urinary placental growth factor and risk of preeclampsia. JAMA 2005;293:77–85.
65. Dugoff L, Hobbins JC, Malone FD, et al. for the FASTER Trial Research Consortium. First trimester maternal serum PAPP-A and free beta subunit human chorionic gonadotropin concentrations and nuchal translucency are associated with obstetric complications: a population-based screening study (the FASTER Trial). Am J Obstet Gynecol. 2004;191:1446–51.
66. Luque A, Farwati A, Crovetto F, Crispi F, Figueras F, Gratacós E, Aran JM. Usefulness of circulating microRNAs for the prediction of early preeclampsia at first−trimester of pregnancy. Sci Rep 2014;4:4882.
67. Yang M, Chen Y, Chen L, Wang K, Pan T, Liu X, Xu W. miR-15b-AGO2 play a critical role in HTR8/SVneo invasion and in a model of angiogenesis defects related to inflammation. Placenta 2016;41:62–73.
68. Wu L, Zhou H, Lin H, Qi J, Zhu C, Gao Z, Wang H. Circulating microRNAs are elevated in plasma from severe preeclamptic pregnancies. Reproduction 2012;143(3):389–97.
69. Li H, Ge Q, Guo L, Lu Z. Maternal plasma miRNAs expression in pre-eclamptic pregnancies. Biomed Res Int 2013;2013:970265.
70. Yang S, Li H, Ge Q, Guo L, Chen F. Deregulated microRNA species in the plasma and placenta of patients with preeclampsia. Mol Med Rep 2015;12(1):527–34.
71. Tang Q, Wu W, Xu X, Huang L, Gao Q, Chen H, Sun H, Xia Y, Sha J, Wang X, Chen D, Xu Q. miR-141 contributes to fetal growth restriction by regulating PLAG1 expression. PLoS One 2013;8(3):e58737.
72. Lykoudi A, Kolialexi A, Lambrou GI, Braoudaki M, Siristatidis C, Papaioanou GK, Papantoniou N. Dysregulated placental microRNAs in early and late onset pre−eclampsia. Placenta 2018;61:24–32.
73. Zhong W, Peng H, Tian A, Wei Y, Li H, Tian J, Zhao X. Expression of miRNA-1233 in placenta from patients with hypertensive disorder complicating pregnancy and its role in disease pathogenesis. Int J Clin Exp Med 2015;8(6):9121–7.

74. Xiao J, Tao T, Yin Y, Zhao L, Yang L, Hu L. miR-144 may regulate the proliferation, migration and invasion of trophoblastic cells through targeting PTEN in preeclampsia. Biomed Pharmacother 2017;94:341–53.
75. Poliseno L, Tuccoli A, Mariani L, Evangelista M, Citti L, Woods K, Mercatanti A, Hammond S, Rainaldi G. MicroRNAs modulate the angiogenic properties of HUVECs. Blood 2006;108 (9):3068–71.
76. Ito M, Sferruzzi-Perri AN, Edwards CA, Adalsteinsson BT, Allen SE, Loo TH, Kitazawa M, Kaneko-Ishino T, Ishino F, Stewart CL, Ferguson-Smith AC. A trans-homologue interaction between reciprocally imprinted miR−127 and Rtl1 regulates placenta development. Development 2015;142(14):2425–30.
77. Hong F, Li Y, Xu Y. Decreased placental miR-126 expression and vascular endothelial growth factor levels in patients with preeclampsia. J Int Med Res 2014;42(6):1243–51.
78. Manaster I, Goldman-Wohl D, Greenfield C, Nachmani D, Tsukerman P, Hamani Y, Yagel S, Mandelboim O. MiRNA-mediated control of HLA-G expression and function. PLoS One 2012;7(3):e33395.
79. Fu G, Ye G, Nadeem L, Ji L, Manchanda T, Wang Y, Zhao Y, Qiao J, Wang YL, Lye S, Yang BB, Peng C. MicroRNA−376c Impairs Transforming Growth Factor−β and Nodal Signaling to Promote Trophoblast Cell Proliferation and Invasion. Hypertension 2013;61(4):864–72.
80. Luque A, Farwati A, Crovetto F, Crispi F, Figueras F, Gratacós E, Aran JM. Usefulness of circulating microRNAs for the prediction of early preeclampsia at first-trimester of pregnancy. Sci Rep 2014;8(4):4882.
81. Gan L, Liu Z, Wei M, Chen Y, Yang X, Chen L, Xiao X. MiR-210 and miR-155 as potential diagnostic markers for preeclampsia pregnancies. Medicine (Baltimore) 2017;96(28): e7515.
82. Zhao Z, Moley KH, Gronowski AM. Diagnostic potential for miRNAs as biomarkers for pregnancy-specific diseases. Clin Biochem 2013;46(10-11):953–60.
83. Sheikh AM, Small HY, Currie G, Delles C. Systematic Review of Micro-RNA Expression in Pre-Eclampsia Identifies a Number of Common Pathways Associated with the Disease. PLoS One 2016 Aug 16;11(8):e0160808.

scientific reports

Check for updates

OPEN

Long-term exposure of human endothelial cells to metformin modulates miRNAs and isomiRs

Angelica Giuliani[1,6], Eric Londin[2,6], Manuela Ferracin[3], Emanuela Mensà[1], Francesco Prattichizzo[4], Deborah Ramini[1], Fiorella Marcheselli[5], Rina Recchioni[5], Maria Rita Rippo[1], Massimiliano Bonafè[3], Isidore Rigoutsos[2], Fabiola Olivieri[1,5]✉ & Jacopo Sabbatinelli[1]

Increasing evidence suggest that the glucose-lowering drug metformin exerts a valuable anti-senescence role. The ability of metformin to affect the biogenesis of selected microRNAs (miRNAs) was recently suggested. MicroRNA isoforms (isomiRs) are distinct variations of miRNA sequences, harboring addition or deletion of one or more nucleotides at the 5′ and/or 3′ ends of the canonical miRNA sequence. We performed a comprehensive analysis of miRNA and isomiR profile in human endothelial cells undergoing replicative senescence in presence of metformin. Metformin treatment was associated with the differential expression of 27 miRNAs (including miR-100-5p, -125b-5p, -654-3p, -217 and -216a-3p/5p). IsomiR analysis revealed that almost 40% of the total miRNA pool was composed by non-canonical sequences. Metformin significantly affects the relative abundance of 133 isomiRs, including the non-canonical forms of the aforementioned miRNAs. Pathway enrichment analysis suggested that pathways associated with proliferation and nutrient sensing are modulated by metformin-regulated miRNAs and that some of the regulated isomiRs (e.g. the 5′ miR-217 isomiR) are endowed with alternative seed sequences and share less than half of the predicted targets with the canonical form. Our results show that metformin reshapes the senescence-associated miRNA/isomiR patterns of endothelial cells, thus expanding our insight into the cell senescence molecular machinery.

Metformin is a hypoglycemic drug used as a first-line treatment for newly diagnosed type 2 diabetes patients[1]. Over the years, metformin has been shown to exert a geroprotective action, beyond its primary glucose-lowering effect[2]. In particular, recent metanalyses showed a significantly lower rate of all-cause mortality and age-related disease (ARD) incidence associated with metformin treatment, thus suggesting that this drug may extend lifespan and disease-free survival in diabetic subjects even compared with non-diabetic people[3,4].

These evidence prompted the launching of the controlled clinical trial Targeting Aging with Metformin (TAME), in order to test whether metformin can delay the onset of ARDs in healthy (non-diabetic) aged subjects[5]. However, although the clinical outcomes of metformin as a pharmacological intervention to achieve healthy longevity are currently being investigated, the exact mechanisms of action remain elusive[6]. At the cellular level, metformin acts on several pathways which are recognized as molecular pillars of cell senescence, including inflammation, autophagy, proteostasis and cellular survival[2,7,8]. While metformin has been shown to influence the cellular epigenetic machinery by modulating Sirtuin-1 (SIRT1)[9], i.e. the pro-longevity histone deacetylase[10], few studies have attempted to identify changes in expression profiles of microRNAs (miRNAs, miRs) induced by metformin treatment in the framework of cellular senescence, mainly showing a general increased abundance of multiple miRNAs after a short-term, high-dose treatment[11,12]. Due to their capability of preventing translation of specific messenger RNAs (mRNA), miRNAs, can impact many cellular processes, including cellular senescence[13]. The knowledge of miRNAs has significantly improved with the advent of next-generation sequencing (NGS) technologies. Indeed, small RNA sequencing (small RNA-seq) of miRNAs enables the analysis of the expression of thousands of miRNAs, the concurrent discovery of new miRNAs, and confirmation of known miRNAs[14]. Moreover, bioinformatic analyses of small RNA-seq data have shown that multiple miRNA isoforms, commonly

[1]Department of Clinical and Molecular Sciences, Università Politecnica Delle Marche, Via Tronto 10/A, 60126 Ancona, Italy. [2]Computational Medicine Center, Thomas Jefferson University, Philadelphia, PA, USA. [3]Department of Experimental, Diagnostic, and Specialty Medicine (DIMES), University of Bologna, Bologna, Italy. [4]IRCCS MultiMedica, Milan, Italy. [5]Center of Clinical Pathology and Innovative Therapy, IRCCS INRCA, Ancona, Italy. [6]These authors contributed equally: Angelica Giuliani and Eric Londin. ✉email: f.olivieri@univpm.it

named isomiRs, can be generated from the processing of each precursor miRNA[15]. IsomiRs present with the addition or deletion of one or more nucleotides at the 5′ and/or 3′ ends of the canonical miRNA sequence and are thought to be produced as distinct products rather than being transcription errors[16,17]. Beyond these genetically encoded variants, miRNAs can undergo post-transcriptional sequence modifications resulting in non-template uridylation at the 3′ end[18]. Growing evidence showed that these modifications can affect the stability of the RNA sequence, confer different targets compared the canonical mature form[19], or affect the subcellular compartmentalization of the miRNA[20]. However, their biological significance is still under discussion.

Based on the evidence that treatment with metformin can modulate in vitro cellular senescence, as well as the biogenesis of miRNAs[12], we performed for the first time a miR-seq analysis of human umbilical vein endothelial cells (HUVECs) undergoing replicative senescence in the presence of pharmacologically pertinent doses of metformin in order to identify senescence-associated (SA) miRNA and isomiR signatures affected by metformin treatment.

Results

Modulation of miRNA patterns induced by metformin treatment in senescent endothelial cells. To identify the pool of SA miRNAs modulated by metformin, we used a well-established model of human umbilical vein endothelial cells (HUVECs) undergoing replicative senescence[21,22]. When the proportion of SA β-gal positivity exceeded 10% in replicating cells (cPD = 9.83; Fig. 1a), 20 μM metformin was added at each medium replacement, and cells were cultured until complete growth arrest (SA β-gal positive cells > 80%). We selected this concentration since it falls within the range observed in plasma of patients treated with the lowest doses of metformin[6]. At passage 16, after approximately 60 days, senescent cells (SEN) and senescent cells treated with metformin (SEN + M) were harvested to perform small RNA-seq (Fig. 1a). Interestingly, SEN + M showed an increased population doubling rate (Fig. 1a), a reduced SA β-gal activity (Fig. 1b), and a decreased CDKN2A mRNA expression (Fig. 1c) compared to SEN.

Pair-wise correlation among normalized reads generated by three biological replicates for each condition gave Pearson correlation coefficients > 0.90 (Supplementary Fig. S1), indicating high correlation among replicates. Normalized miRNA expression data were compared via principal component analysis (PCA). A PCA plot based on principal components 1 and 2, explaining 27.2% and 22.4% of the total variance respectively, showed a clear separation between SEN and SEN + M (Fig. 2a). MiRNAs with a significant moderated *t* test (FDR < 0.05) and an absolute fold change ≥ 1.5 were considered as differentially regulated. The Volcano plot showed log2 fold change and − log10 p-values of all the detected miRNAs (Fig. 2b), while the normalized expressions of differentially expressed miRNAs were displayed in a heatmap (Fig. 2c). Of 1706 miRNAs detected in at least one sample, we identified 27 miRNAs whose expression was altered by metformin. In particular, 15 miRNAs were upregulated and 12 were downregulated in SEN + M (Fig. 2c).

Changes in the isomiR pattern associated with metformin treatment. Since studying miRNAs at the isomiR level could lend new insights into miRNA biology and function, we analysed isomiR modulation associated with metformin treatment of HUVECs during replicative senescence. IsomiRs result from a shift of the cutting site of Drosha/Dicer enzymatic activities during miRNA biogenesis[23,24] and can be classified into six categories according to the types of sequence modifications: (1) canonical miRNAs, (2) 3′ deletion isomiRs, (3) 3′ addition isomiRs, (4) 5′ deletion isomiRs, (5) 5′ addition isomiRs, and (6) mixed isomiRs, which represent a combination of the prior categories[25]. We also analysed the post-transcriptional addition of one or more uridines at the 3′ end of isomiRs and canonical miRNAs, namely uridylation. It has to be noted that the entire spectrum of isomiRs is covered by the standard miR-seq analysis.

Figure 3a shows the contribution of different sequence isoforms to the total miRNA pool in SEN + M. On a total of 3,632,423 reads, the 43.1% was mapped to non-canonical isoforms. No statistically significant difference in the proportion of isomiR variations between SEN and SEN + M was observed (p = 0.103).

The heatmap showed that 133 isomiRs, which are variants of a total of 73 individual miRNAs, were significantly deregulated in SEN + M vs SEN (Fig. 3b). Specifically, 43 isomiRs were isoforms of 14 miRNAs significantly deregulated by metformin treatment (miR-17-3p, -100-5p, -216a-3p, -216a-5p, -217-5p, -125b-5p, -143-3p, -493-3p, -493-5p, -92a-1-5p, -125b-1-3p, -424-3p, -654-3p, -98-3p) (Fig. 3b, red and blue highlights refer to up-/down-regulated miRNAs, respectively).

Among the remaining 90 deregulated isomiRs (related to a total of 59 miRNAs not significantly modulated by metformin), 48 were up-regulated and 42 were down-regulated in SEN + M cells (Fig. 3b, in black). These 59 miRNAs, though not modulated by the treatment as a whole group, encompass at least one isomiR that is differentially regulated by metformin. Notably, 3 miRNAs which were not differentially regulated between SEN + M and SEN, i.e. miR-92b-3p, -149-5p and -125b-2-3p, included isomiRs showing opposite regulations across the two different conditions. In addition, metformin induced the downregulation of isomiRs from 3 members of the miR-17/92 cluster, i.e. miR-17-3p, miR-18a-5p, and miR-92a-3p (Fig. 3b, right panel).

Of note, 39 of 133 metformin-modulated isomiRs showed a modification at the 5′ end (Fig. 3c), which leads to a shift of the seed sequence resulting in a change of the miRNA-target binding site[26]. Moreover, in some instances the seed sequence of the 5′ isomiR is identical to the seed sequence of another canonical microRNA. Indeed, miR-27b-3p|+3|0, miR-29a-3p|-1|-2, miR-34a-5p|+1|+1 and miR-423-5p|+2|0 share the same seed sequence of miR-5693, miR-5682, miR-6499-3p and miR-486-3p, respectively. Among the differentially regulated isomiRs, the most frequent modification was the 3′ deletion. Furthermore, 3′uridylation was extensively represented among all isomiR types, except those presenting a 5′ nucleotide addition (Fig. 3c). Interestingly, metformin affected the expression of 24 3′-uridylated miRNAs (Fig. 3b,c).

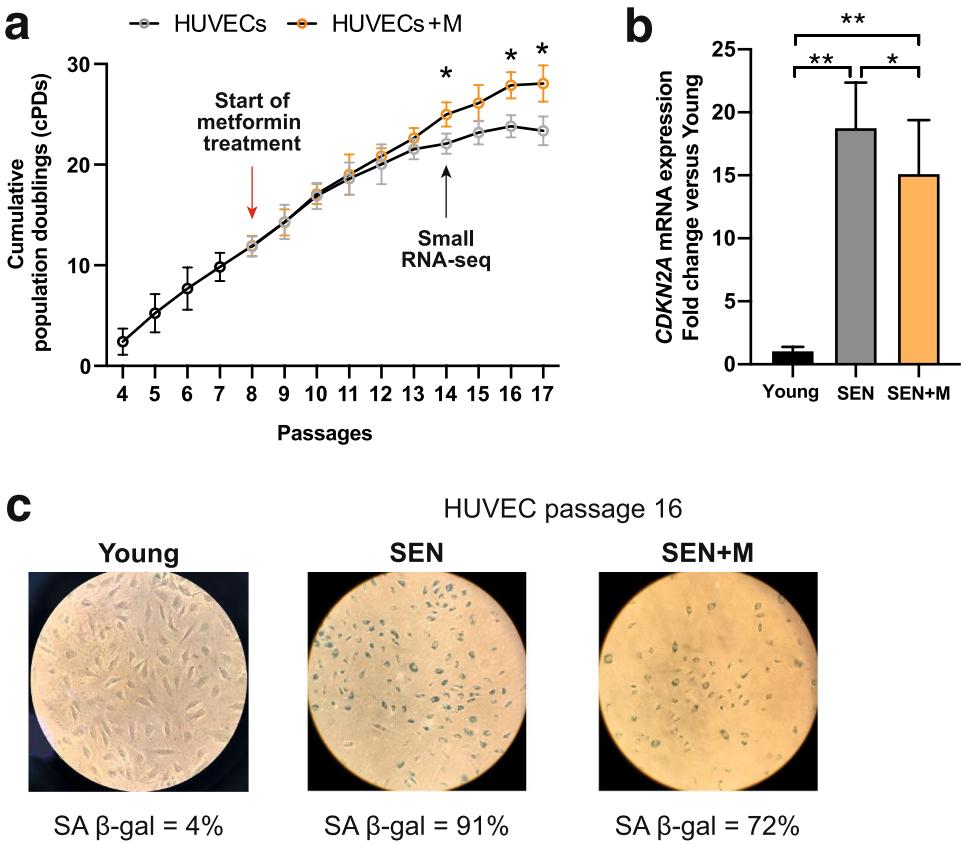

Figure 1. Characterization of replicative senescence in HUVECs. (**a**) Cumulative population doubling (cPD) curves. Metformin treatment was started after passage 7 (cPD = 9.83) and conducted at each medium replacement until complete growth arrest. (**b**) *CDKN2A* mRNA relative expression in young, SEN and SEN + M. Data are mean ± SD. *p < 0.05; **p < 0.01. (**c**) Representative positivity and quantification of the SA β-Gal staining in young, senescent (passage 16, SEN) and SEN HUVECs treated with metformin (SEN + M). *HUVECs* human umbilical vein endothelial cells, *SA* senescence-associated.

Figure 4a shows the expression of the different isomiR variants of the 73 miRNAs including at least one isomiR differentially regulated by metformin. Notably, we observed a high variability in the proportion of isomiR variants among the evaluated miRNAs. Indeed, the canonical form, i.e. the one reported in the miRBase database, is not always prevalent (e.g. in the miR-30 family) and some miRNAs included non-canonical variants.

Moreover, metformin induced a significant redistribution of the isomiR variant proportions within 6 out of the 27 differentially regulated miRNAs (Fig. 4b). Only one isoform was detected for 3 miRNAs (miR-17-3p, miR-98-3p, and miR-92–1-5p), whereas no isoforms were detected for the remaining 12 miRNAs. The proportions of the different isomiR variation types between SEN and SEN + M are reported in Table 1.

MiRNA/isomiR expression trends in endothelial cells during replicative senescence. To gain insight into the biological significance of miRNA/isomiR modulation induced by metformin treatment in senescent HUVECs (SEN, SEN + M) we used non-senescent HUVECs as control (Young, SA β-gal < 5%, Fig. 1b)[22]. This strategy allowed us to identify two different trends in miRNA modulation and to separate the 27 miRNAs according to their pattern of modulation. On one hand, 13 miRNAs were characterized by linear increasing or decreasing trend, when the Young/SEN/SEN + M sequence was examined (Fig. 5a, group 1). The most evident linear trends were observed for miR-100, -125b-5p, and -654-3p, showing the most abundant expression. Metformin treatment further increases the expression of these miRNAs in senescent cells. On the other hand, 14 miRNAs were characterized by a 'U-shaped'/ 'inverted U-shaped' trend of the Young/SEN/SEN + M sequence, suggesting that metformin induced a (partial) reversal of the miRNA expression induced by senescence (Fig. 5b, group 2). Among the 14 miRNAs belonging to this latter group, the 'U-shaped'/ 'inverted U-shaped' trend was confirmed by a significant likelihood ratio test (adjusted p value < 0.05) (in bold in Fig. 5b). The most relevant inverted U-shaped trends were observed for miR-217-5p, -216a-3p, and -216a-5p. Overall, metformin affected the expression of 18 SA miRNAs (Fig. 5c) and notably was able to rescue the miR-216a and miR-217-5p overexpression in senescent cells previously reported by our group[22].

A similar approach was carried out on the 133 differentially regulated isomiRs. Results of the likelihood ratio test performed on Young, SEN, and SEN + M samples revealed significant U-shaped/inverted U-shaped trends for 75 isomiRs and linear trends for 49 isomiRs, belonging to 52 and 20 individual miRNAs, respectively. Notably,

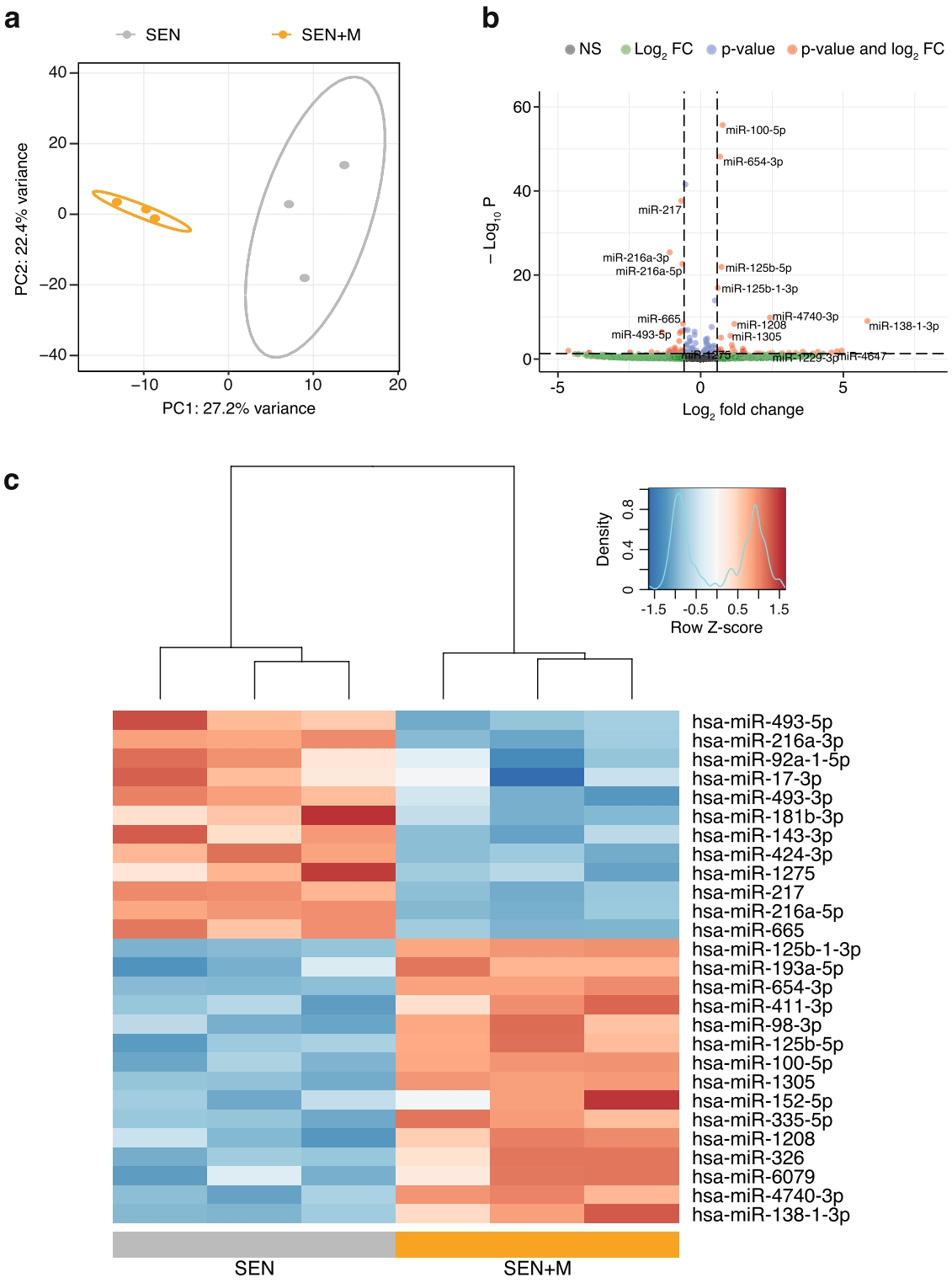

Figure 2. MiR-seq analysis of senescent HUVECs treated with metformin. (**a**) PCA plot of the first two principal components (PC1 and PC2) using transformed normalized miR-seq data. Circles represent 95% confidence intervals. (**b**) Volcano plot of $\log_2$ fold-changes (FC, SEN + M compared to SEN) vs. -$\log_{10}$ adjusted p-values using transformed normalized miR-seq data. MiRNAs with FC ≥ 1.5 (log2 FC ≥ 0.585) and FDR < 0.05 (− log10 p-value < 1.30) are highlighted in red. (**c**) Heatmap showing clustering of samples and miRNAs differentially expressed in SEN + M compared to SEN. Data is shown following Z-score transformation. Red color indicates Z-scores > 0 (above mean), blue colors indicate Z-scores < 0 (below mean). MiRNAs are ranked according to the lowest $\log_2$ FC.

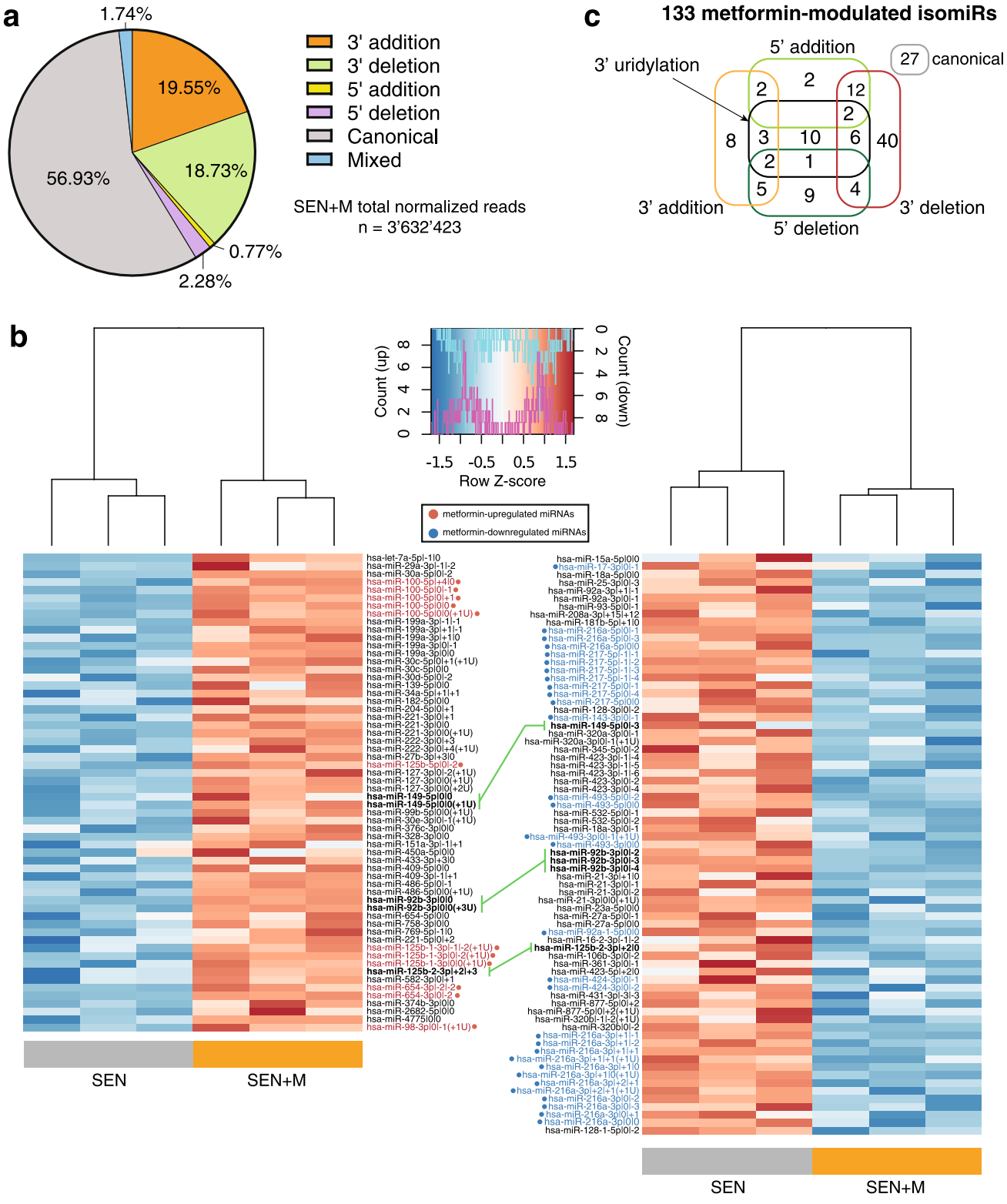

Figure 3. IsomiR analysis of senescent HUVECs treated with metformin. (**a**) Pie chart showing the proportion of isomiR variations in SEN + M samples. (**b**) Heatmaps showing clustering of samples, and isomiRs upregulated (left panel) and downregulated (right panel) in SEN + M compared to SEN, with a FC ≥ 1.5 and FDR < 0.05 cut-off. Data is shown following Z-score transformation. Red color indicates Z-scores > 0 (above mean), blue color indicates Z-scores < 0 (below mean). IsomiR labels are marked and colored in red or blue according to the upregulation or downregulation of their parent miRNA in SEN + M, respectively. Green lines connect variations of the same miRNA (labeled in bold) showing opposite modulation between SEN + M and SEN. IsomiRs are ordered by the MIMAT ID of the parent miRNA. For the isomiR nomenclature, the reader is referred to the Materials and Methods section. (**c**) Diagram reporting the frequencies of the different type of variations among isomiRs modulated by metformin treatment.

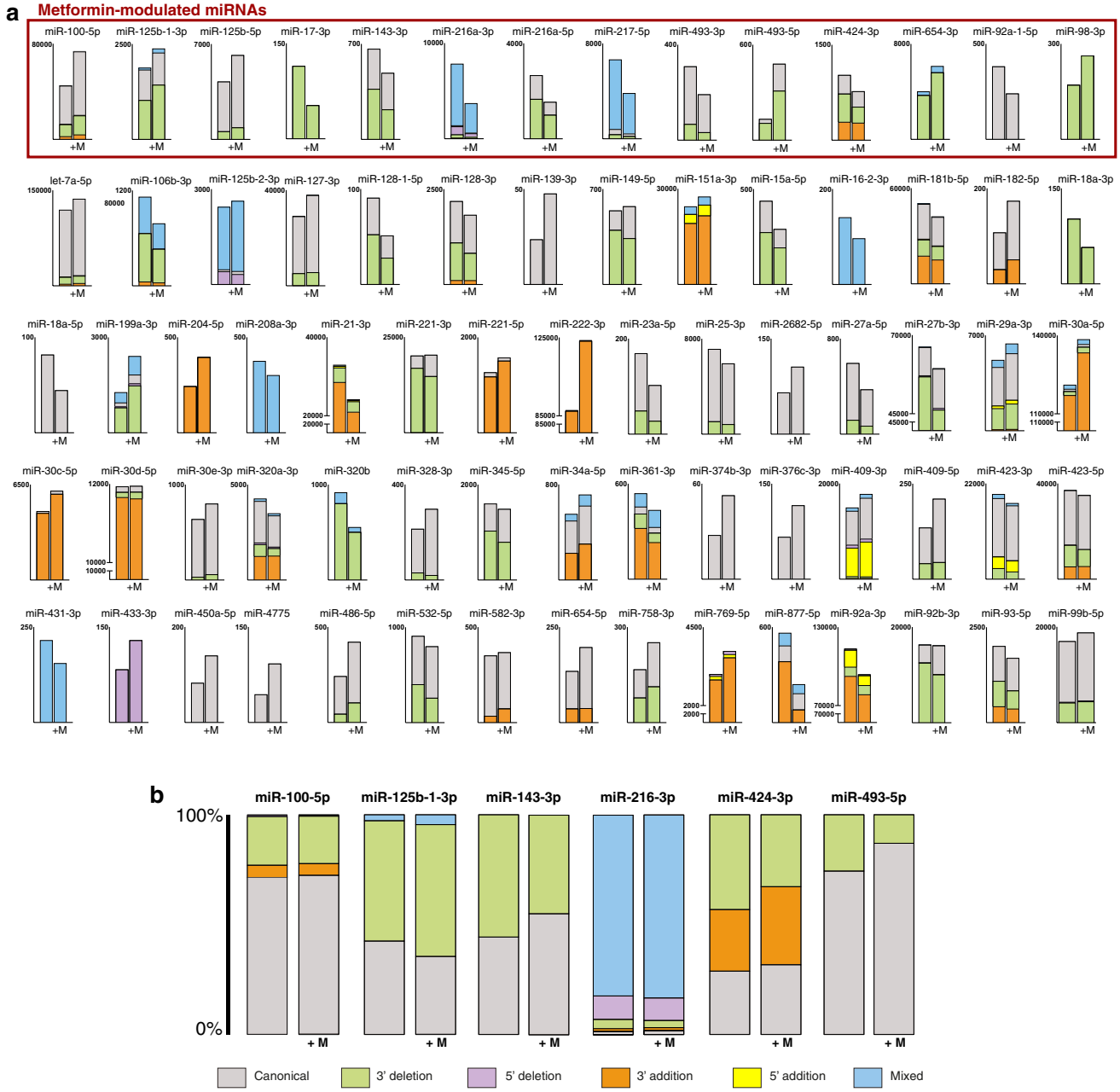

Figure 4. Proportions of isomiR variations within miRNAs modulated by metformin. (**a**) Comparison of normalized reads of the different types of isomiR variations of miRNAs including at least one isomiR differentially regulated by metformin. The 14 metformin-modulated miRNAs including at least one differentially regulated isomiR are highlighted. (**b**) Proportions of isomiR variation types within 6 out of the 27 miRNAs differentially regulated by metformin showing significant isomiR redistribution between SEN and SEN + M.

5 miRNAs, i.e. miR-92b-3p, -149-5p, -221-3p, -222-3p, 532-5p, included isomiRs following either U-shaped or linear trends (data not shown).

Metformin alters the miRNA and isomiR targetome of senescent endothelial cells. To explore target genes and pathways affected by the 11 miRNAs showing significant U-shaped or inverted U-shaped trends, pathway enrichment analysis was performed using the miRPath v.3/Diana tool. Figure 6a lists the involved KEGG pathways ($p < 0.01$) ranked by the significance of the enrichment. The proportion of targeted genes over total genes for each pathway is also reported. A considerable number of pathways related to cell proliferation, i.e. TGFβ, ErbB, Wnt and MAPK pathways, is significantly enriched. Notably, the PI3K-Akt-mTOR pathway is the one containing the greatest amount of targeted genes (72.3%), in agreement with the inhibitory effects of metformin on mTOR signaling[27].

microRNA	Condition	Canonical	Templated modifications				NTA
			3′ addition	3′ deletion	5′ deletion	Mixed	3′ uridylation
miR-17-3p	Sen			100			
	Sen + M			100			
	p-value			–			
miR-100-5p	Sen	71.27	5.63	22.21	0.63	0.26	0.81
	Sen + M	72.21	5.34	21.66	0.56	0.23	1.00
	p-value	0.007	0.033	0.026	0.126	0.308	0.001
miR-216a-5p	Sen	37.40		62.60			
	Sen + M	35.33		64.67			
	p-value	0.180		0.180			
miR-217-5p	Sen	6.80		5.33		87.87	7.16
	Sen + M	5.91		5.34		88.75	8.40
	p-value	0.075		0.984		0.180	0.021
miR-125b-5p	Sen	86.16		13.84			
	Sen + M	85.87		14.13			
	p-value	0.674		0.674			
miR-143-3p	Sen	44.29		55.71			
	Sen + M	55.05		44.95			
	p-value	< 0.001		< 0.001			
miR-493-5p	Sen	74.32		25.68			
	Sen + M	86.96		13.04			
	p-value	< 0.001		< 0.001			
miR-493-3p	Sen	78.20		21.80			21.80
	Sen + M	82.90		17.10			17.10
	p-value	0.201		0.201			0.201
miR-92a-1-5p	Sen	100					
	Sen + M	100					
	p-value	–					
miR-125b-1-3p	Sen	42.42		54.81		2.78	40.64
	Sen + M	35.38		60.08		4.54	50.11
	p-value	< 0.001		0.001		0.003	< 0.001
miR-193a-5p	Sen	43.38		56.62			11.79
	Sen + M	40.68		59.32			10.23
	p-value	0.596		0.596			0.638
miR-424-3p	Sen	28.77	27.99	43.23			
	Sen + M	31.70	35.53	32.77			
	p-value	0.180	0.001	< 0.001			
miR-654-3p	Sen			91.95		8.05	5.25
	Sen + M			91.29		8.71	4.45
	p-value			0.242		0.242	0.064
miR-98-3p	Sen			100			100
	Sen + M			100			100
	p-value			–			–
miR-216a-3p	Sen	1.44	1.27	4.32	10.70	82.27	9.46
	Sen + M	1.75	1.45	3.32	10.26	83.22	9.58
	p-value	0.208	0.430	0.010	0.472	0.208	0.834

Table 1. Proportions (expressed as %) of isomiR variations among 15 miRNAs differentially regulated by metformin with at least one detected isomiR. *M* metformin, *NTA* non-template addition, *Sen* senescent HUVECs. P-values for z test.

Among these miRNAs, we focused on the only two miRNAs showing detectable levels of at least one 5′ isoform, i.e. miR-217-5p and miR-216a-3p. Interestingly, the canonical/3′ and the 5′ miR-217-5p isomiRs share only half of the predicted targets, while the other half is exclusive to either seed sequence. Regarding miR-216a-3p, the deletion of one or two nucleotides at the 5′ end leads to the generation of two alternative seed sequences. The 3 different seed sequences shared only a small pool (35) of predicted targets (Fig. 6b). The target genes of canonical and 5′isomiR seed sequences were evaluated also for those miRNAs including at least one 5′isomiR presenting

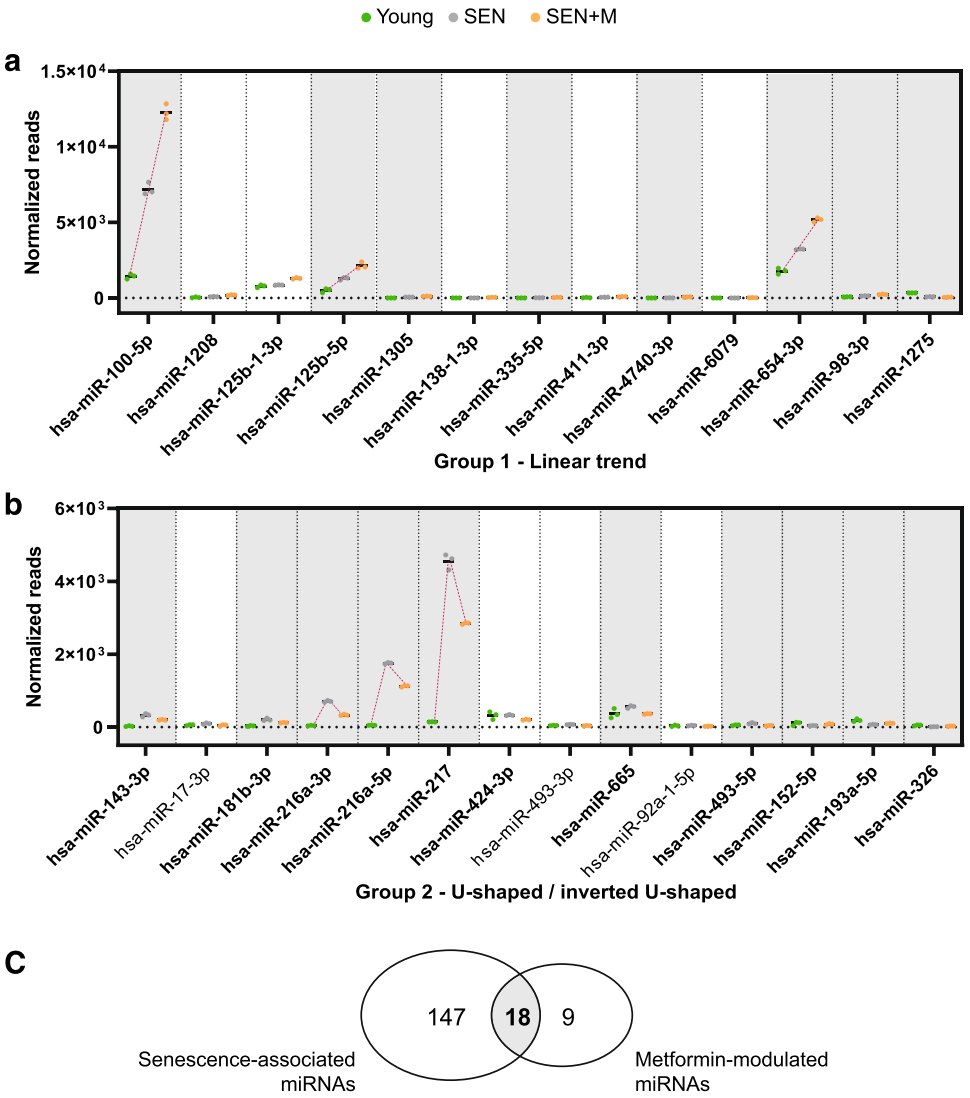

Figure 5. Influence of metformin treatment on senescence-associated miRNA modulation. Normalized reads of 27 miRNAs differentially modulated in Young (green), SEN (gray), and SEN + M (orange), grouped according to the linear (**a**) or U-shaped/inverted U-shaped (**b**) pattern of modulation. MiRNAs with a significant likelihood-ratio test are highlighted in bold. Senescence-associated miRNAs are highlighted with a gray background. (**c**) Venn diagram reporting the number of miRNAs differentially regulated in SEN compared to Young cells and in SEN + M compared to SEN.

a significant linear or U-shaped trend in Young, SEN, and SEN + M (Supplementary Figure S2). Notably, the canonical form and the 5′ isomiR of miR-100-5p shared no predicted target genes.

Discussion

In the present study, we investigated for the first time the miRNA landscape in endothelial cells (ECs) undergoing replicative senescence after a long-term treatment with metformin. Surprisingly, only 27 miRNAs on a total of 1706 detected by the small RNA-seq analysis were differentially regulated by metformin, despite the long duration of the exposure to a pharmacologically pertinent dose of the drug. To gain insight into the biological significance of these modulations, we used young proliferating HUVECs as reference group, in order to identify specific trends of modulation. We focused on the group of miRNAs characterized by a U-shaped/inverted U-shaped trend of expression in young vs. SEN vs. SEN + M, since this peculiar trend could reflect the ability of metformin to modulate the trajectories of senescence associated miRNAs (Fig. 7a). Increasing evidence suggests that a number of biomarkers of human aging followed non-linear trends when subjects representing the extreme phenotype of successful aging, i.e. the centenarians, are included in the analysis[28–32]. We therefore employed an in vitro cellular senescence model mimicking the gradual deterioration of endothelial function that accompanies human aging[33], to unravel the ability of metformin to affect the senescence-associated miRNA/isomiR modulation.

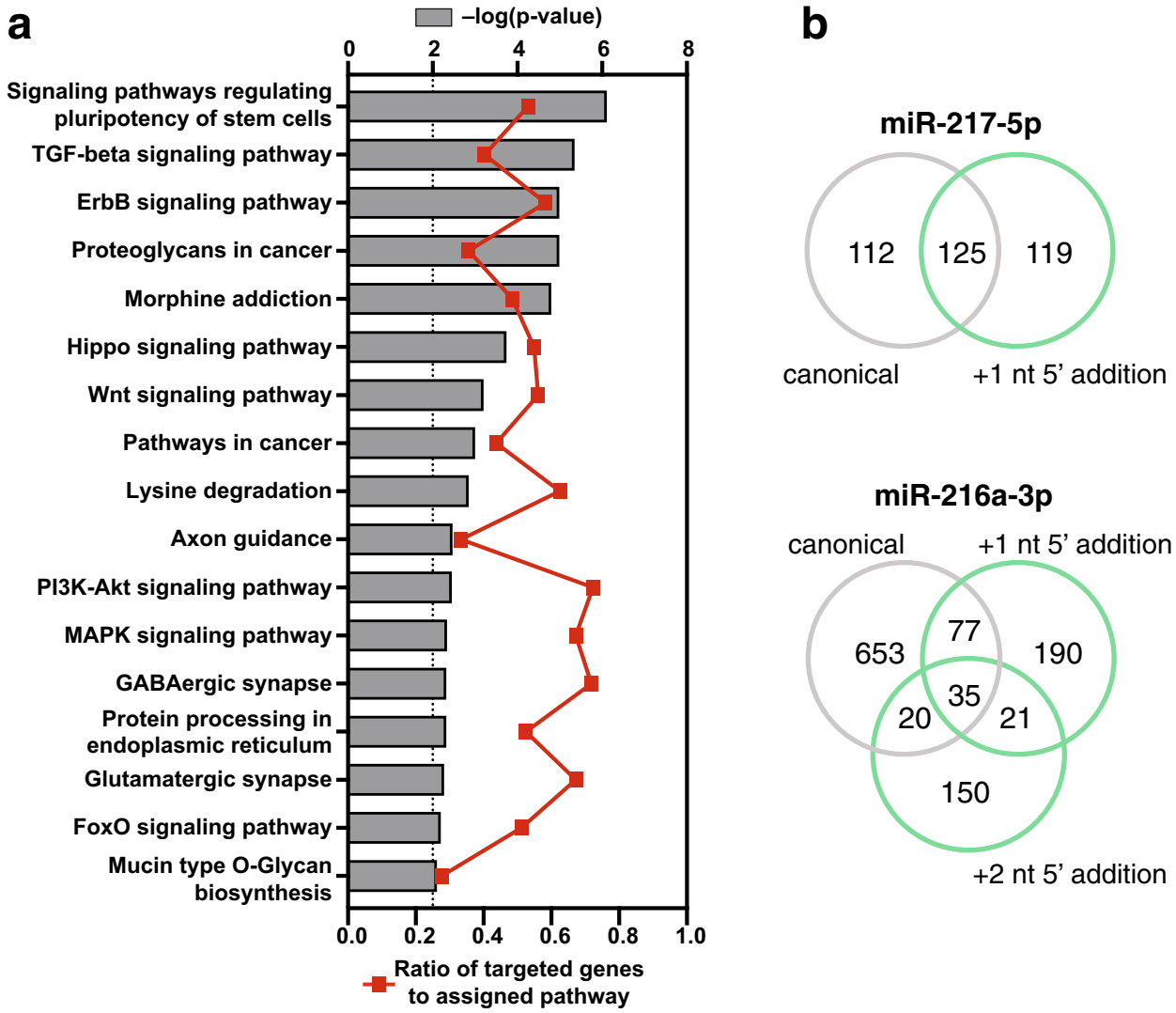

Figure 6. Target analysis of miRNAs and isomiRs affected by metformin. (**a**) KEGG pathways significantly enriched in predicted target genes of the 11 miRNAs showing a significant U-shaped/inverted U-shaped trend among Young/SEN/SEN + M samples. Pathways are ranked according to the significance of enrichment (grey bars, upper y-axis). Ratios referring to the proportion of targeted genes related to the total number of genes in each pathway are displayed (red line graph, bottom y-axis). (**b**) Results of the TargetScan custom analysis on the canonical and 5′ isomiR seed sequences of miR-217-5p and miR-216-3p.

This approach allowed us to show that metformin can revert the SA trend of a number of miRNAs that were extensively studied in the context of cellular aging, including miR-216-3p, -216-5p, and -217-5p, which we previously identified among the most upregulated miRNAs in senescent HUVECs[22]. MiR-217-5p was proved to be involved in EC and human fibroblast senescence by targeting SIRT1 and DNMT1, respectively[34,35]. Furthermore, we recently demonstrated that the same pro-senescence effects of miR-217 can be spread through the exchange of small extracellular vesicles[22]. Similarly, miR-216a was shown to be involved in EC aging, in atherosclerosis-related endothelial dysfunction by impairing the autophagy response to the accumulation of oxidized low-density lipoproteins[36], and in macrophage pro-inflammatory M1 polarization by boosting the NF-κB pathway[37,38]. Among miRNAs showing a linear trend in Young vs. SEN vs. SEN + M, miR-100-5p was previously shown to be upregulated in senescent HUVECs[22,39], while the metformin-mediated induction of miR-125-5p was consistent with previous reports on macrophages[40] and senescent ECs[12].

Regarding the analysis of isomiRs, this is the first deep sequencing assessment of isomiRs in senescent HUVECs. One miRNA gene can potentially produce multiple distinct isomiRs, differing in length, sequence, or both[26]. Our results proved that the assessment of isomiRs can unravel complex modulations of the miRNA pool not detectable with standard miRNA analysis. Indeed, isomiR analysis allowed us to fully uncover the downregulating effects of metformin on the miR-17/92 cluster, which has been previously shown to be over-represented in a wide range of cancers and cardiovascular diseases and downregulated in physiological aging[41]. Therefore, further developments of isomiR analysis are warranted to increase our knowledge on miRNA modulation in a number of physiological and pathological processes.

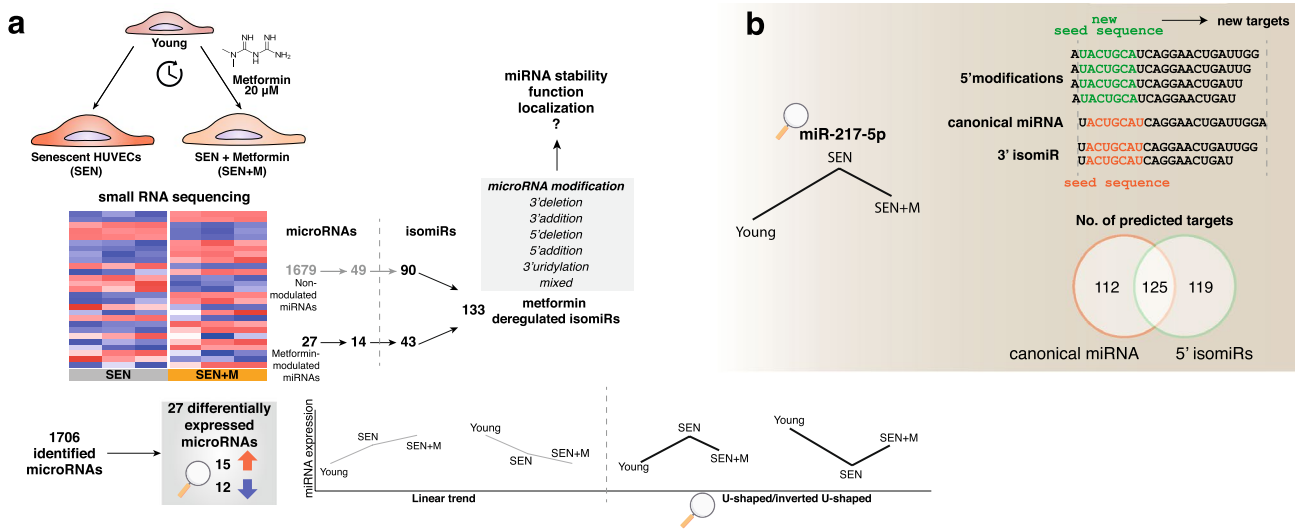

Figure 7. (**a**) Summary of the effects of metformin treatment on the miRNA/isomiR pool of HUVECs undergoing replicative senescence. Metformin differentially regulates the expression of 27 miRNAs. Two different trends in miRNA modulation were observed with reference to the Young/SEN/SEN + M sequence, i.e. a linear increasing/decreasing trend and a 'U-shaped'/'inverted U-shaped' trend. Moreover, metformin treatment altered the expression of 133 isomiRs, related to 14 differentially expressed miRNAs and 59 non differentially expressed miRNAs. (**b**) Metformin treatment induced a partial reversal of the senescence-associated expression of miR-217-5p, including its 5′ isomiRs, which are associated to a shifting of the seed sequence. The inclusion of these additional seed sequences into the targetome analysis yielded a considerably greater number of target genes, most of which were not shared with the canonical miRNAs.

In agreement with previous reports[25,42], we observed a considerable presence of 3′ isomiRs, while more than half of the total reads was mapped to canonical miRNAs. It has to be noted, however, that the term 'canonical' refers to the sequence annotated in miRBase and do not necessarily indicate the most abundant miRNA isoform in a specific cell type or tissue or the primary product of pre-miRNA cleavage[43].

On the other hand, only a small number of reads (about 3%) mapped to 5′ isomiRs, which are associated to a shifting of the seed sequence (Fig. 7b). For this reason, we evaluated the number of targets shared by the isoforms of miR-216a-3p and miR-217-5p, which were both modulated by metformin treatment and expressed 5′ isoforms. The inclusion of these additional seed sequences into the targetome analysis yielded a considerably greater number of target genes, most of which were not shared with the canonical miRNAs. As expected, the coexistence of more than one 5′ isomiR, as in the case of miR-216-3p, proportionally increased the amount of target genes. The ability of isomiRs of being loaded onto the RISC complex support their possible biological role[19,44]. Indeed, a previous report showed that the ratio between miR-411 and its 5′ isomiR in ECs is affected by acute ischemia and that only the 5′ isoform of miR-411 is capable of impairing angiogenesis by targeting a different subset of mRNAs[19].

The 3′ end miRNA modifications are mostly related to post transcriptional deletion of nucleotides, i.e. trimming, or the addition of one or more nucleotides, i.e. tailing[45]. It has to be noted, however, that is quite challenging to distinguish templated nucleotides added during miRNA maturation from those added post-transcriptionally to the mature miRNA. In our study, we assessed isomiRs resulting from the untemplated nucleotide addition to the 3′ end of pre-miRNA or mature miRNA[46]. While these modifications are not associated with a shifting of the seed sequence, it has been demonstrated that 3′ uridylation enhances base-pairing between tailed miRNA and targets, a phenomenon named as tail-U-mediated repression (TUMR). Therefore, TUMR expands the miRNA target repertoires by producing novel miRNA-target binding sites in the presence of an incomplete seed-pairing[18]. Moreover, 3′ post-transcriptional modifications were shown to affect miRNA stability[47], intracellular levels, and compartmentalization into extracellular vesicles[20]. Notably, miRNAs are not the sole substrates of the 3′ uridylation mediated by terminal uridyltransferases (TUTs). Indeed, 3′-terminal uridylation of viral RNAs in mammalian cells has been recently identified as a conserved antiviral defense mechanism[48]. Interestingly, metformin affected the expression of 22 3′-uridylated miRNAs; therefore, it is straightforward to conceive a framework in which metformin could impact cellular senescence through the modulation of miRNA function, stability, and localization.

Our in vitro results support the role of isomiR assessment in biological samples as a useful tool to improve our knowledge on the aging process or discover new biomarkers of biological aging.

Nevertheless, several limitations need to be acknowledged. The study design does not allow to draw any mechanistical conclusion on the role of metformin on ECs or cellular senescence. In addition, some of the mechanisms of isomiR biogenesis are still unclear, implying the intrinsic difficulty to assess whether 3′ nucleotide addition occurs during or after miRNA transcription. Finally, qPCR validation of NGS assessment of isomiRs is still hampered by analytical challenges, such as the absence of dedicated protocols and reagents, e.g. probes

and primers, and the relative inefficiency of the currently available techniques in differentiating highly similar sequences[49,50].

NGS studies on isomiRs paved the way to the exploration of novel non-canonical targets and allowed the identification of new regulatory mechanisms of miRNA expression and intracellular localization, adding an additional layer of complexity to the study of the epigenetic variations accompanying cell senescence, although further investigations are required to better understand the biological functions of the cellular isomiR pool.

Overall, we showed that long-term treatment with metformin is able to partly attenuate the complex miRNA/isomiR remodeling observed during cellular senescence in ECs, supporting further exploration of the impact of metformin on the cellular epigenetic landscape as a possible mediator of the putative beneficial effect of this drug on the aging process.

Materials and methods

Cell culture and treatment. An in vitro model of endothelial replicative cell senescence was established using long-term cultured HUVECs. Cryopreserved HUVECs obtained from pool of donors were purchased from Clonetics (Lonza, Switzerland) and cultured in EGM-2 (CC-3162, Lonza) at 37 °C in a humidified atmosphere containing 5% CO_2. Cells were seeded at a density of 5000/cm^2 and sub-cultured when they reached 70–80% confluence. All cells tested negative for mycoplasma infection. Before replating, harvested cells were counted using a hemocytometer. Population doublings (PDs) were calculated by the formula: $(\log_{10}F - \log_{10}I)/\log_{10}2$, where F is the number of cells at the end of the passage and I is the number of seeded cells. Cumulative population doubling (cPD) was calculated as the sum of PD changes. Cells were cultured until the arrest of replication and classified based on SA β-galactosidase (β-gal) activity into young (SA β-gal < 5%) and senescent (SEN, SA β-gal > 80%) cells using Senescence Detection Kit (cat. no. K320, BioVision Inc., USA) as described previously[21]. Cells were treated with 20 μM metformin (cat. D150959, Sigma Aldrich, Italy) added at each medium replacement.

RNA extraction. Total RNA, including small (< 200 nucleotides) RNAs, was extracted from HUVEC pellets using Norgen total RNA Purification Kit (cat. no. 37500, Norgen Biotek Corporation, Canada) according to the manufacturer's protocol. Purified RNA was stored at − 80 °C until analysis.

mRNA expression level. *CDKN2A* mRNA expression was assessed as previously described[22]. Primer sequences (written 5′-3′) were as follows: p16, Fw: CATAGATGCCGCGGAAGGT, Rv: CTAAGTTTCCCG AGGTTTCTCAGA; β-actin, Fw:TGCTATCCCTGTACGCCTCT, Rv: GTGGTGGTGAAGCTGTAGCC. Primer concentration was 200 nM. Delta delta Ct method was performed to analyze the results and Young cells were used as reference group.

Small RNA sequencing analysis. Small RNA sequencing was performed in triplicate on Young and SEN cells, and SEN cells treated with metformin. TruSeq Small RNA Library PrepKit v2 (Illumina; RS-200-0012/24/36/48) was used for library preparation according to the manufacturer's indications. Briefly, 35 ng purified RNA was linked to RNA 3′ and 5′ adapters, converted to cDNA, and amplified using Illumina primers containing unique indexes for each sample. Each library was quantified using Agilent Bioanalyzer and High Sensitivity DNA Kit (cat. no. 5067-4626, Agilent Technologies, USA) and equal amounts of libraries were pooled together. Size selection allowed keeping 130–160 bp fragments. After ethanol precipitation, the library pool was quantified with Agilent High Sensitivity DNA Kit, diluted to 1.8 pM, and sequenced using NextSeq 500/550 High Output Kit v2 (75 cycles) (Illumina; FC-404-2005) on the Illumina NextSeq500 platform.

Raw base-call data generated by the Illumina NextSeq 500 system were demultiplexed using Illumina BaseSpace Sequence Hub (https://basespace.illumina.com/home/index) and converted to FASTQ format. After a quality check with FastQC (https://www.bioinformatics.babraham.ac.uk/projects/fastqc/), sequence reads were quality trimmed using the cutadapt tool[51]. Sequence reads were aligned to the miRBase version 21.0 database[52] using the STAR algorithm[53]. Standard miRNA quantification (including the canonical form and all isoforms) was obtained as previously detailed[22].

Quantification of miRNA isoforms. Sequence reads were quality trimmed using the cutadapt tool, and mapped unambiguously using SHRIMP2[54] to the human genome assembly GRCh38. During the mapping, no insertions or deletions, and at most one mismatch was permitted. IsomiRs were identified as done previously[16,17,55–57]. The isomiR nomenclature used is based upon the one used previously in Loher et al.[17]. For example, the isomiR whose 5′ terminus begins one position to the right (+1) of the archetype's 5′ terminus and whose 3′ terminus ends two positions to the left (−2) of the archetype's 3′ terminus is labeled "+1|−2". The archetype isomiR, the sequence found in public databases, is labeled as "0|0".

IsomiR abundances were quantified in reads per million (RPM). Only reads that passed quality trimming and filtering and could be aligned exactly to miRNA arms were used in the denominator of this calculation. The abundance of a miRNA arm is calculated as the sum of normalized abundances of all isomiRs from the arm.

Raw and processed datasets have been deposited in NCBI's Gene Expression Omnibus (GEO) (https://www.ncbi.nlm.nih.gov/geo) with accession reference GSE149771.

Statistical analysis of small RNA-seq data. Data analysis was carried out using the DESeq2 1.26.0[58] Bioconductor package within the R version 3.6.1 environment. MiRNAs/isomiRs showing a differential expression between SEN and SEN + M were identified using a fold change ≥ 1.5 filter and an FDR < 5% cut-off at two-

tailed moderated *t*-test with Benjamini–Hochberg correction. A two-tailed likelihood ratio test (LRT) was used to compare miRNA/isomiR expression among Young, SEN, and SEN + M samples, with a Benjamini–Hochberg FDR < 5%. The significance of the differences between isomiR proportions within each miRNA was tested using z-test. The PCA plot and correlation matrix showing Pearson's correlations among samples were created using the pcaExplorer version 2.12.0 R/Bioconductor package[59]. Heatmaps were produced using the heatmap2 function from the R package gplots version 3.0.3 (https://cran.r-project.org/web/packages/gplots/) with row scaling and hierarchical clustering of the rLog transformed expression values.

MiRNA target prediction. Putative miRNA targets were individuated using the Diana mirPath v.3 platform and the tools TarBase v7.0 and microT-CDS v5.0, which allow the analysis of KEGG pathways enrichment[60,61] for experimentally validated and predicted target genes, respectively[62]. The analysis was carried out using the 'pathways union' option. P-values were calculated by the Fisher's exact test and the false discovery rate (FDR) was estimated using the Benjamini and Hochberg method. A p-value threshold of 0.01 was applied. Differential target genes of the canonical/3′ isomiRs and 5′ isomiRs were predicted using the TargetScan Custom tool v. 5.2 (http://www.targetscan.org/vert_50/seedmatch.html), which searches for a complementary 3′ UTR against a provided seed sequence.

Data availability

Raw and processed datasets have been deposited in NCBI's Gene Expression Omnibus (GEO) (https://www.ncbi.nlm.nih.gov/geo) with accession reference GSE149771.

Received: 23 June 2020; Accepted: 1 December 2020
Published online: 11 December 2020

References

1. 1American Diabetes Association. 9. Pharmacologic Approaches to Glycemic Treatment: Standards of Medical Care in Diabetes-2020. *Diabetes Care* **43**, S98-S110. doi:https://doi.org/10.2337/dc20-S009 (2020).
2. Salvatore, T. *et al.* Metformin: an old drug against old age and associated morbidities. *Diabetes Res. Clin. Pract.* **160**, 108025. https://doi.org/10.1016/j.diabres.2020.108025 (2020).
3. Han, Y. *et al.* Effect of metformin on all-cause and cardiovascular mortality in patients with coronary artery diseases: a systematic review and an updated meta-analysis. *Cardiovasc. Diabetol.* **18**, 96. https://doi.org/10.1186/s12933-019-0900-7 (2019).
4. Campbell, J. M., Bellman, S. M., Stephenson, M. D. & Lisy, K. Metformin reduces all-cause mortality and diseases of ageing independent of its effect on diabetes control: a systematic review and meta-analysis. *Ageing Res. Rev.* **40**, 31–44. https://doi.org/10.1016/j.arr.2017.08.003 (2017).
5. Barzilai, N., Crandall, J. P., Kritchevsky, S. B. & Espeland, M. A. Metformin as a tool to target aging. *Cell Metab.* **23**, 1060–1065. https://doi.org/10.1016/j.cmet.2016.05.011 (2016).
6. Prattichizzo, F. *et al.* Pleiotropic effects of metformin: Shaping the microbiome to manage type 2 diabetes and postpone ageing. *Ageing Res. Rev.* **48**, 87–98. https://doi.org/10.1016/j.arr.2018.10.003 (2018).
7. Moiseeva, O. *et al.* Metformin inhibits the senescence-associated secretory phenotype by interfering with IKK/NF-kappaB activation. *Aging Cell* **12**, 489–498. https://doi.org/10.1111/acel.12075 (2013).
8. Rena, G., Hardie, D. G. & Pearson, E. R. The mechanisms of action of metformin. *Diabetologia* **60**, 1577–1585. https://doi.org/10.1007/s00125-017-4342-z (2017).
9. Song, Y. M. *et al.* Metformin alleviates hepatosteatosis by restoring SIRT1-mediated autophagy induction via an AMP-activated protein kinase-independent pathway. *Autophagy* **11**, 46–59. https://doi.org/10.4161/15548627.2014.984271 (2015).
10. Giblin, W., Skinner, M. E. & Lombard, D. B. Sirtuins: guardians of mammalian healthspan. *Trends Genet.* **30**, 271–286. https://doi.org/10.1016/j.tig.2014.04.007 (2014).
11. Bridgeman, S. C., Ellison, G. C., Melton, P. E., Newsholme, P. & Mamotte, C. D. S. Epigenetic effects of metformin: from molecular mechanisms to clinical implications. *Diabetes Obes. Metab.* **20**, 1553–1562. https://doi.org/10.1111/dom.13262 (2018).
12. Noren Hooten, N. *et al.* Metformin-mediated increase in DICER1 regulates microRNA expression and cellular senescence. *Aging Cell* **15**, 572–581. https://doi.org/10.1111/acel.12469 (2016).
13. Williams, J., Smith, F., Kumar, S., Vijayan, M. & Reddy, P. H. Are microRNAs true sensors of ageing and cellular senescence?. *Ageing Res. Rev.* **35**, 350–363. https://doi.org/10.1016/j.arr.2016.11.008 (2017).
14. Tam, S., de Borja, R., Tsao, M. S. & McPherson, J. D. Robust global microRNA expression profiling using next-generation sequencing technologies. *Lab. Invest.* **94**, 350–358. https://doi.org/10.1038/labinvest.2013.157 (2014).
15. Morin, R. D. *et al.* Application of massively parallel sequencing to microRNA profiling and discovery in human embryonic stem cells. *Genome Res* **18**, 610–621. https://doi.org/10.1101/gr.7179508 (2008).
16. Telonis, A. G., Loher, P., Jing, Y., Londin, E. & Rigoutsos, I. Beyond the one-locus-one-miRNA paradigm: microRNA isoforms enable deeper insights into breast cancer heterogeneity. *Nucleic Acids Res* **43**, 9158–9175. https://doi.org/10.1093/nar/gkv922 (2015).
17. Loher, P., Londin, E. R. & Rigoutsos, I. IsomiR expression profiles in human lymphoblastoid cell lines exhibit population and gender dependencies. *Oncotarget* **5**, 8790–8802. https://doi.org/10.18632/oncotarget.2405 (2014).
18. Yang, A. *et al.* 3' uridylation confers miRNAs with non-canonical target repertoires. *Mol. Cell* **75**, 511–522. https://doi.org/10.1016/j.molcel.2019.05.014 (2019).
19. van der Kwast, R., Woudenberg, T., Quax, P. H. A. & Nossent, A. Y. MicroRNA-411 and its 5'-IsomiR have distinct targets and functions and are differentially regulated in the vasculature under ischemia. *Mol. Ther.* **28**, 157–170. https://doi.org/10.1016/j.ymthe.2019.10.002 (2020).
20. Koppers-Lalic, D. *et al.* Nontemplated nucleotide additions distinguish the small RNA composition in cells from exosomes. *Cell Rep.* **8**, 1649–1658. https://doi.org/10.1016/j.celrep.2014.08.027 (2014).
21. Giuliani, A. *et al.* The mitomiR/Bcl-2 axis affects mitochondrial function and autophagic vacuole formation in senescent endothelial cells. *Aging (Albany NY)* **10**, 2855–2873. https://doi.org/10.18632/aging.101591 (2018).
22. Mensà, E. *et al.* Small extracellular vesicles deliver miR-21 and miR-217 as pro-senescence effectors to endothelial cells. *J. Extracell. Vesic.* **9**, 1725285. https://doi.org/10.1080/20013078.2020.1725285 (2020).
23. Gu, S. *et al.* The loop position of shRNAs and pre-miRNAs is critical for the accuracy of dicer processing in vivo. *Cell* **151**, 900–911. https://doi.org/10.1016/j.cell.2012.09.042 (2012).
24. Bofill-De Ros, X. *et al.* Structural differences between Pri-miRNA Paralogs promote alternative drosha cleavage and expand target repertoires. *Cell Rep.* **26**, 447–459. https://doi.org/10.1016/j.celrep.2018.12.054 (2019).

25. Haseeb, A., Makki, M. S., Khan, N. M., Ahmad, I. & Haqqi, T. M. Deep sequencing and analyses of miRNAs, isomiRs and miRNA induced silencing complex (miRISC)-associated miRNome in primary human chondrocytes. *Sci. Rep.* **7**, 15178. https://doi.org/10.1038/s41598-017-15388-4 (2017).
26. Bofill-De Ros, X., Yang, A. & Gu, S. IsomiRs: expanding the miRNA repression toolbox beyond the seed. *Biochim. Biophys. Acta Gene Regul. Mech.* **1863**, 194373. https://doi.org/10.1016/j.bbagrm.2019.03.005 (2020).
27. Howell, J. J. *et al.* Metformin inhibits hepatic mTORC1 signaling via dose-dependent mechanisms involving AMPK and the TSC complex. *Cell Metab.* **25**, 463–471. https://doi.org/10.1016/j.cmet.2016.12.009 (2017).
28. Olivieri, F. *et al.* Circulating miRNAs and miRNA shuttles as biomarkers: Perspective trajectories of healthy and unhealthy aging. *Mech. Ageing Dev.* **165**, 162–170. https://doi.org/10.1016/j.mad.2016.12.004 (2017).
29. Fulop, T., Witkowski, J. M., Olivieri, F. & Larbi, A. The integration of inflammaging in age-related diseases. *Semin. Immunol.* **40**, 17–35. https://doi.org/10.1016/j.smim.2018.09.003 (2018).
30. Prattichizzo, F. *et al.* Endothelial cell senescence and inflammaging: MicroRNAs as biomarkers and innovative therapeutic tools. *Curr. Drug Targets* **17**, 388–397. https://doi.org/10.2174/1389450116666150804105659 (2016).
31. Mensà, E. *et al.* Circulating miR-146a in healthy aging and type 2 diabetes: age- and gender-specific trajectories. *Mech. Ageing Dev.* **180**, 1–10. https://doi.org/10.1016/j.mad.2019.03.001 (2019).
32. Olivieri, F., Prattichizzo, F., Grillari, J. & Balistreri, C. R. Cellular senescence and inflammaging in age-related diseases. *Mediat. Inflamm.* **2018**, 9076485. https://doi.org/10.1155/2018/9076485 (2018).
33. Sabbatinelli, J. *et al.* Where metabolism meets senescence: focus on endothelial cells. *Front. Physiol.* **10**, 1523. https://doi.org/10.3389/fphys.2019.01523 (2019).
34. Wang, B. *et al.* Microrna-217 modulates human skin fibroblast senescence by directly targeting DNA methyltransferase 1. *Oncotarget* **8**, 33475–33486. https://doi.org/10.18632/oncotarget.16509 (2017).
35. Menghini, R. *et al.* MicroRNA 217 modulates endothelial cell senescence via silent information regulator 1. *Circulation* **120**, 1524–1532. https://doi.org/10.1161/CIRCULATIONAHA.109.864629 (2009).
36. Menghini, R. *et al.* MiR-216a: a link between endothelial dysfunction and autophagy. *Cell Death Dis.* **5**, e1029. https://doi.org/10.1038/cddis.2013.556 (2014).
37. Yang, S. *et al.* MicroRNA-216a induces endothelial senescence and inflammation via Smad3/IkappaBalpha pathway. *J. Cell. Mol. Med.* **22**, 2739–2749. https://doi.org/10.1111/jcmm.13567 (2018).
38. Yang, S. *et al.* MicroRNA-216a promotes M1 macrophages polarization and atherosclerosis progression by activating telomerase via the Smad3/NF-kappaB pathway. *Biochim. Biophys. Acta Mol. Basis Dis.* **1772–1781**, 2019. https://doi.org/10.1016/j.bbadis.2018.06.016 (1865).
39. Kuosmanen, S. M., Sihvola, V., Kansanen, E., Kaikkonen, M. U. & Levonen, A. L. MicroRNAs mediate the senescence-associated decline of NRF2 in endothelial cells. *Redox. Biol.* **18**, 77–83. https://doi.org/10.1016/j.redox.2018.06.007 (2018).
40. Luo, X., Hu, R., Zheng, Y., Liu, S. & Zhou, Z. Metformin shows anti-inflammatory effects in murine macrophages through Dicer/microribonucleic acid-34a-5p and microribonucleic acid-125b-5p. *J. Diabetes Investig.* **11**, 101–109. https://doi.org/10.1111/jdi.13074 (2020).
41. Mogilyansky, E. & Rigoutsos, I. The miR-17/92 cluster: a comprehensive update on its genomics, genetics, functions and increasingly important and numerous roles in health and disease. *Cell Death Differ* **20**, 1603–1614. https://doi.org/10.1038/cdd.2013.125 (2013).
42. Gebert, L. F. R. & MacRae, I. J. Regulation of microRNA function in animals. *Nat. Rev. Mol. Cell Biol.* **20**, 21–37. https://doi.org/10.1038/s41580-018-0045-7 (2019).
43. Boele, J. *et al.* PAPD5-mediated 3' adenylation and subsequent degradation of miR-21 is disrupted in proliferative disease. *Proc. Natl. Acad. Sci. USA* **111**, 11467–11472. https://doi.org/10.1073/pnas.1317751111 (2014).
44. Ameres, S. L. & Zamore, P. D. Diversifying microRNA sequence and function. *Nat. Rev. Mol. Cell Biol.* **14**, 475–488. https://doi.org/10.1038/nrm3611 (2013).
45. Ameres, S. L. *et al.* Target RNA-directed trimming and tailing of small silencing RNAs. *Science* **328**, 1534–1539. https://doi.org/10.1126/science.1187058 (2010).
46. Ha, M. & Kim, V. N. Regulation of microRNA biogenesis. *Nat. Rev. Mol. Cell Biol.* **15**, 509–524. https://doi.org/10.1038/nrm3838 (2014).
47. Gutierrez-Vazquez, C. *et al.* 3' Uridylation controls mature microRNA turnover during CD4 T-cell activation. *RNA* **23**, 882–891. https://doi.org/10.1261/rna.060095.116 (2017).
48. Le Pen, J. *et al.* Terminal uridylyltransferases target RNA viruses as part of the innate immune system. *Nat. Struct. Mol. Biol.* **25**, 778–786. https://doi.org/10.1038/s41594-018-0106-9 (2018).
49. Magee, R., Telonis, A. G., Cherlin, T., Rigoutsos, I. & Londin, E. Assessment of isomiR discrimination using commercial qPCR methods. *Noncoding RNA* **3**, 1. https://doi.org/10.3390/ncrna3020018 (2017).
50. Wu, C. W. *et al.* A comprehensive approach to sequence-oriented IsomiR annotation (CASMIR): demonstration with IsomiR profiling in colorectal neoplasia. *BMC Genomics* **19**, 401. https://doi.org/10.1186/s12864-018-4794-7 (2018).
51. Martin, M. *Cutadapt removes adapter sequences from high-throughput sequencing reads.* **17**(3), 2011. https://doi.org/10.14806/ej.17.1.200 (2011).
52. Kozomara, A., Birgaoanu, M. & Griffiths-Jones, S. miRBase: from microRNA sequences to function. *Nucleic Acids Res* **47**, D155–D162. https://doi.org/10.1093/nar/gky1141 (2019).
53. Dobin, A. *et al.* STAR: ultrafast universal RNA-seq aligner. *Bioinformatics* **29**, 15–21. https://doi.org/10.1093/bioinformatics/bts635 (2013).
54. David, M., Dzamba, M., Lister, D., Ilie, L. & Brudno, M. SHRiMP2: sensitive yet practical SHort read mapping. *Bioinformatics* **27**, 1011–1012. https://doi.org/10.1093/bioinformatics/btr046 (2011).
55. Magee, R. G., Telonis, A. G., Loher, P., Londin, E. & Rigoutsos, I. Profiles of miRNA isoforms and tRNA fragments in prostate cancer. *Sci. Rep.* **8**, 5314. https://doi.org/10.1038/s41598-018-22488-2 (2018).
56. Londin, E. *et al.* IsomiRs and tRNA-derived fragments are associated with metastasis and patient survival in uveal melanoma. *Pigment Cell Melanoma Res.* **33**, 52–62. https://doi.org/10.1111/pcmr.12810 (2020).
57. Telonis, A. G. & Rigoutsos, I. Race disparities in the contribution of miRNA isoforms and tRNA-derived fragments to triple-negative breast cancer. *Cancer Res* **78**, 1140–1154. https://doi.org/10.1158/0008-5472.CAN-17-1947 (2018).
58. Love, M. I., Huber, W. & Anders, S. Moderated estimation of fold change and dispersion for RNA-seq data with DESeq2. *Genome Biol.* **15**, 550. https://doi.org/10.1186/s13059-014-0550-8 (2014).
59. Marini, F. & Binder, H. pcaExplorer: an R/Bioconductor package for interacting with RNA-seq principal components. *BMC Bioinformatics* **20**, 331. https://doi.org/10.1186/s12859-019-2879-1 (2019).
60. Kanehisa, M., Sato, Y., Furumichi, M., Morishima, K. & Tanabe, M. New approach for understanding genome variations in KEGG. *Nucleic Acids Res.* **47**, D590–D595. https://doi.org/10.1093/nar/gky962 (2019).
61. Kanehisa, M. & Goto, S. KEGG: kyoto encyclopedia of genes and genomes. *Nucleic Acids Res.* **28**, 27–30. https://doi.org/10.1093/nar/28.1.27 (2000).
62. Vlachos, I. S. *et al.* DIANA-miRPath v3.0: deciphering microRNA function with experimental support. *Nucleic Acids Res.* **43**, W460-466. https://doi.org/10.1093/nar/gkv403 (2015).

Acknowledgements
This work was supported by grants from Università Politecnica delle Marche [Scientific research grant, years 2017–2018–2019 to F.O. and M.R.R.] and by the Italian Ministry of Health ["Ricerca corrente" to IRCCS INRCA and IRCCS MultiMedica].

Author contributions
A.G., E.M., and D.R. performed cell culture and treatments. E.L. performed isomiR analysis and participated in the interpretation of results. M.F. performed small RNAseq analyses. M.F., F.M., and R.R. collaborated in data analysis. F.P., M.R.R., M.B., and I.R. critically commented on the results and reviewed the manuscript. A.G., F.O. and J.S. conceptualized the study, wrote the manuscript and prepared figures. All authors approve the submission of the final manuscript and agree to be responsible for all aspects of the work.

Competing interests
The authors declare no competing interests.

Additional information
Supplementary Information The online version contains supplementary material available at https://doi.org/10.1038/s41598-020-78871-5.

Correspondence and requests for materials should be addressed to F.O.

Reprints and permissions information is available at www.nature.com/reprints.

Publisher's note Springer Nature remains neutral with regard to jurisdictional claims in published maps and institutional affiliations.